

Development and Characterization of Environment Friendly Carbon Coating for Piston Ring Applications

A THESIS

Submitted in partial fulfilment of the requirements for the award of the Degree

Of

DOCTOR OF PHILOSOPHY

In

Mechanical Engineering

Submitted by

ANKIT TYAGI

ROLL NO-2K17/PhD/ME/39

Under the Supervision of

Prof. Qasim Murtaza

(Professor, DTU, Delhi)

Prof. R.S. Walia

(Professor, PEC, Chandigarh)



**DEPARTMENT OF MECHANICAL ENGINEERING
DELHI TECHNOLOGICAL UNIVERSITY
BAWANA ROAD, DELHI- 110042**



CERTIFICATE

This is to certify that the thesis entitled "**Development and Characterization of Environment Friendly Carbon Coating for Piston Ring Applications**" being submitted by **ANKIT TYAGI**, Roll No.2K17/PhD ME/39 to the Delhi Technological University, Delhi for the award of the degree of **Doctor of Philosophy** is a bonafide record of original research work carried out by him. He has worked under our guidance and supervision and has fulfilled the requirements for the submission of this thesis, which has reached the requisite standard.

The results contained in this thesis have not been submitted, in part or full, to any other University or Institute for the award of any degree.

Prof. Qasim Murtaza

Department of Mechanical Engineering

(Professor, DTU)

Prof. R.S. Walia

Department of production & Industrial Engineering

(Professor, PEC, Chandigarh)

ACKNOWLEDGEMENTS

I express my deep gratitude to my supervisors Prof. Qasim Murtaza and Prof R. S. Walia, for assisting me in identifying and formulating the research problem. Despite their busy schedule, they were always available for the advice and discussions. Their valuable comments and advice gave me the confidence to overcome the challenges in the formulation of this research work.

I express my special thanks to Prof. S.K Garg, Head of Mechanical Engineering department, DTU, for his continuation inspiration and support during this research work.

I would like to thank Dr. SM Pandey, Assistant Professor, NIT Patna, for his invaluable moral support, constant motivation, valuable feedback during my experimental and thesis work. I would like to thank Prof. Jai Gopal of DTU, Dr. Kumar Krishen, Lead Technologist, NASA Johnson Space Centre for his valuable feedback during my experimental and thesis work.

I would like to thank my friends, Kalpana Gupta, Rajesh Bohra, Virender Kumar, Ankit Kumar, and Krishan Kaushik, who have supported me through their encouragement, support and friendship during this period of research work. I would also like to thank all those who directly and indirectly supported me in carrying out this thesis work successfully.

Furthermore, I would like to express my sincere gratitude my parents, and every member of my family for their endless inspiration, support and guidance throughout my whole life.

Ankit Tyagi

(Roll No. 2K17/Ph.D.ME/39)

PREFACE

In this thesis, a newly developed environment friendly carbon coating is developed for piston ring application and it would help the researchers to enhance the tribological and mechanical properties. The contents of the thesis are as follows:

Chapter 1 In this chapter piston ring wear, surface engineering and thermal spray process techniques have been discussed. Later the details of different types of wear, wear mechanism, and surface modification techniques, for wear reduction of carbon coating have been elaborated.

Chapter 2 A comprehensive review of the literature has been discussed with different types of carbon coating, Protective coating, High temperature coating, Role of coating, HVOF process and deposition and tribological condition of HVOF based composite coating.

Chapter 3 In this chapter, after reviewing the literature critically, brainstorming with the supervisors and field expert, the research gap and the objectives of the present study have been formulated. The present investigation is mainly focused on the development and characterization of carbon coating for piston ring applications.

Chapter 4 This chapter contains a description of the experimental equipment used and the procedures adopted for deposition, characterizations and tribological investigation of the deposited coatings

Chapter 5 This chapter includes the characterization, residual stress, micro-hardness, surface roughness and high temperature tribological test of:

Part 1: Carbon coating for the piston rings application prepared by HVOF spray technique.

Part 2: Carbon based composite coating for the piston rings application prepared by HVOF spray technique.

Chapter 6 This chapter includes the comparative analysis of tribological and mechanical properties of carbon coating and carbon based composite coating for piston rings.

Chapter 7 This chapter contains salient conclusions. Important conclusions of the investigation regarding carbon and carbon based composite coating have been presented with significant findings have been drawn from performed experimentation followed by future scope of present work.

TABLE OF CONTENTS

Certificate	i
Acknowledgement	ii
Preface	iii
Table of contents	iv-vii
List of Figures	viii-xi
List of Tables	xii-xiii
Acronyms	xiv
Abstract	xv
1. CHAPTER 1 INTRODUCTION	1-22
1.1.PISTON RING WEAR	1-2
1.2.SURFACE ENGINEERING	3-7
1.3.THERMAL SPRAY PROCESS	7-12
1.3.1. High velocity Oxy fuel spray process	7-9
1.3.2. Atmospheric Plasma Arc Spray	9-10
1.3.3. Flame Spray Process	10
1.3.4. Wire Flame Spray	11
1.3.5. Detonation Flame Spray	11-12
1.3.6. Cold Spray Technique	12-13
1.4.TRIBOLOGY	13-20
1.4.1. Friction	13
1.4.2. Wear	13-20
1.4.2.1.Adhesive wear	15
1.4.2.2.Abrasive wear	16-17
1.4.2.3.Fatigue wear	17
1.4.2.4.Fretting wear	17-18
1.4.2.5.Impact wear	18-19
1.4.2.6.Erosion wear	19-20
1.5.Motivation of this research work	20-22
2. CHAPTER 2 LITERATURE REVIEW	23-48

2.1. MAJOR TYPES, PROPERTIES AND TRIBOLOGICAL BEHAVIOR OF CARBON BASED COATING	23-30
2.1.1. Diamond like carbon	23-27
2.1.2. Carbon Nanotubes	27-30
2.2. DEPOSITION PARAMETERS OF CARBON COATING	30-31
2.3. TRIBOLOGICAL CONDITIONS OF CARBON BASED COATING MATERIALS	31-32
2.4. HIGH TEMPERATURE COATINGS	32-34
2.5. ROLE OF THE COATING	34-36
2.6. HIGH VELOCITY OXY FUEL THERMAL SPRAY COATING	36-41
2.6.1. Pressure Blaster	37-38
2.6.2. Spray Booth	38
2.6.3. HIPOJET-2700M Gun	39
2.6.4. Control Panel	39-40
2.6.5. Powder feeder	40-41
2.7. HVOF BASED COMPOSITE COATING FOR WEAR RESISTANCE APPLICATIONS	41-47
2.8. RESEARCH GAP	48
3. CHAPTER 3 PROBLEM FORMULATION	49-51
3.1. SCOPE	49
3.2. RESEARCH OBJECTIVES	49-50
3.3. RESEARCH METHODOLOGY	50-51
4. CHAPTER 4 MATERIALS AND METHODS	52-65
4.1. SAMPLE CHARACTERIZATION	52-54
4.1.1. Field Emission Scanning electron microscopy	52
4.1.2. High resolution X-ray Diffraction	53
4.1.3. Raman Spectrum	53-54
4.2. MECHANICAL TESTING	54-57
4.2.1. Surface Roughness Measurement	55
4.2.2. Micro-hardness	55
4.2.3. Residual stress	55-57

4.3.TRIBOLOGICAL TEST	57-62
4.4.DESIGN OF EXPERIMENT	62-63
4.5.SAMPLE PREPARATION	63
4.6.CARBON POWDER PREPARATION	63-64
4.7.CARBON BASED COMPOSITE POWDER PREPARATION	64-65
4.8.COATING PREPARATION	65
5. CHAPTER 5 RESULTS AND DISCUSSION	66-124
5.1.SAMPLE CHARACTERIZATION	66-71
5.2.POWDER CHARACTERIZATION	71-77
PART 1:	77-100
5.3.CARBON COATING CHARACTERIZATION	77-81
5.3.1. FESEM+EDS results of carbon coating	77-79
5.3.2. HRXRD result of carbon coating	79-80
5.3.3. Raman spectrum result of carbon coating	80-81
5.4.MECHANICAL CHARACTERIZATION OF CARBON COATING	81-84
5.4.1. Surface Roughness	81-82
5.4.2. Micro-hardness	82-83
5.4.3. Residual stress	84
5.5.TRIBOLOGICAL CHARACTERIZATION OF CARBON COATING	85-100
5.5.1. COF & Wear behavior of carbon coating	85-87
5.5.2. Wear mechanism of carbon coating	87-89
5.5.3. Effects of parameters on Coefficient of friction (COF) for Carbon coating	89-95
5.5.4. Effects of parameters on Wear for Carbon coating	95-100
PART 2:	101-124
5.6.CARBON BASED COMPOSITE COATING CHARACTERIZATION	101-104
5.6.1. FESEM+EDS results of carbon based composite coating	101-103

5.6.2. HRXRD result of carbon based composite coating	103
5.6.3. Raman spectrum result of carbon based composite coating	104
5.7.MECHANICAL CHARACTERIZATION OF CARBON BASED COMPOSITE COATING	104-107
5.7.1. Surface Roughness	104-105
5.7.2. Micro-hardness	106
5.7.3. Residual stress	107
5.8.TRIBOLOGICAL CHARACTERIZATION OF CARBON BASED COMPOSITE COATING	108-124
5.8.1. COF & Wear behavior of carbon based composite coating	108-110
5.8.2. Wear mechanism of carbon based composite coating	110-112
5.8.3. Effect of Parameters on Coefficient of Friction	112-118
5.8.4. Effect of Parameters on Wear	119-124
6. CHAPTER 6 COMPARATIVE ANALYSIS	124-130
7. CHAPTER 7 CONCLUSIONS	131-133
8. SCOPE OF FUTURE WORK	134
9. APPENDIX	135-153
10. REFERENCES	154-172
11. RESEARCH PUBLICATIONS	173-174

LIST OF FIGURES

Figure 1.1	Systematic diagram of deposition techniques	4
Figure 1.1.1	Systematic diagram of (a) thermal spray deposition (b) working of thermal spray powder process	5
Figure 1.1.2	Systematic diagram of electro-deposition	6
Figure 1.1.3	Systematic diagram of physical vapor deposition	7
Figure 1.1.4	Systematic diagram of chemical vapor deposition	7
Figure 1.2	Schematic diagram of the (a) HVOF spray process (28) and (b) Thermal Spray Robot	9
Figure 1.3	Schematic diagram of the (a) plasma spray process (b) Plasma Spray System Layout (c) Plasma spray gun PSG100	10
Figure 1.4	Systematic diagram of wire flame spray process	11
Figure 1.5	Systematic diagram of cold spray process	12
Figure 1.6	Systematic sketch of types of wear	14
Figure 1.7	Systematic diagram of adhesive wear mechanism	15
Figure 1.8	Systematic diagram of two and three body abrasive wear mechanism	17
Figure 1.9	Systematic diagram of fatigues wear mechanism	17
Figure 1.10	Systematic diagram of fretting wear mechanisms	18
Figure 1.11	Schematic illustrations of the mechanisms of impact wear	19
Figure 1.12	Systematic diagram of erosion wear	20
Figure 1.13	Variation in Coefficient of friction of different coating material	21
Figure 2.1	SEM image for DLC coating surface morphology obtained by (a) PIID and (b) PEMS + PIID techniques	24
Figure 2.2	Variation in Friction coefficient value at different lubricating condition for (a) Multilayer DLC film (b) Hard DLC film (c) Soft DLC film	25

Figure 2.3	Variation in COF at different test condition of DLC coating (a) Effect of load and sliding velocity (b) Effect of sample aging	26-27
Figure 2.4	(a) SEM micrograph at 80°C (b) SEM micrograph at 120°C (c) EDX spectrum at 800°C (d) EDX spectrum at 120°C nanocomposite coating with overcoat of PFPE	29
Figure 2.5	Process of wear mechanism	32
Figure 2.6	Systematic diagram of HVOF thermal spray system	36
Figure 2.7	Systematic diagram of pressure blaster of HVOF thermal spray system	38
Figure 2.8	Systematic diagram of spray booth	38
Figure 2.9	HVOF spray gun HIPOJET® 2700	39
Figure 2.10	HVOF powder spray system	40
Figure 2.11	Systematic diagram of powder feeder of HVOF thermal spray system	41
Figure 3.1	Flow diagram of research methodology	51
Figure 4.1	Systematic diagram of FESEM attached with EDS	52
Figure 4.2	(a) systematic diagram of HRXRD (b) angle of diffraction angle from 10° to 120°	53
Figure 4.3	Systematic diagram of Raman Spectrum	54
Figure 4.4	Systematic diagram of Taylor Hobson precision machine used to measured surface roughness	54
Figure 4.5	Systematic diagram of Vickers's hardness tester.	55
Figure 4.6	Systematic representation of Bragg's law	56
Figure 4.7	Systematic diagram of residual stress of coating	56
Figure 4.8	Systematic diagram of residual stress analyzer	57
Figure 4.9	(a) Pin on disk tribometer (b) wear track (c) Tribometer, model of Coating	60-61

Figure 4.10	(a) wear disc & pin before test (b) wear disc & pin after test (c) wear behavior of developed coating.	61-62
Figure 4.11	Systematic diagram of carbon powder preparation	64
Figure 4.12	Systematic diagram of ball mill	64
Figure 5.1	(a-b) FESEM image (c) EDS result of uncoated samples	67-68
Figure 5.2	HRXRD result of uncoated samples	68
Figure 5.3	Raman spectrum result of uncoated samples	69
Figure 5.4	Surface roughness results of uncoated sample	69
Figure 5.5	Residual stress results of uncoated sample	69-70
Figure 5.6	Micro-hardness results of uncoated sample	71
Figure 5.7	(a-c) FESEM image of agricultural waste produced powder	72-73
Figure 5.8	HRXRD image of agricultural waste produced powder	73
Figure 5.9	(a-c) FESEM image of powder at 550°C	74-75
Figure 5.10	HRXRD image of powder at 550°C	75
Figure 5.11	(a-b) FESEM image of composite powder	76
Figure 5.12	HRXRD image of composite powder	77
Figure 5.13	(a-d) FESEM+ EDS image of carbon coating	78-79
Figure 5.14	HRXRD image of carbon coating	80
Figure 5.15	Raman Spectra of carbon coating	81
Figure 5.16	Surface roughness of carbon coating	82
Figure 5.17	Micro-hardness Vs carbon coating graph	83
Figure 5.18	Residual stress Vs carbon coating graph	84
Figure 5.19	(a-b) COF (c) Wear Vs sliding distance graph carbon coating	86-87
Figure 5.20	FESEM images of worn surfaces of carbon coating	88-89

Figure 5.21	Shows deviation of COF with parameters (a) Temperature ($^{\circ}\text{C}$) (b) Sliding velocity (m/s) (c) Load (N) of carbon coating	91-92
Figure 5.22	Shows deviation of Wear with parameters (a) Temperature ($^{\circ}\text{C}$) (b) Sliding velocity (m/s) (c) Load (N) of carbon coating	96-97
Figure 5.23	(a-d) FESEM images (c-d) EDS mapping result of composite coating	101-103
Figure 5.24	HRXRD of composite coating	103
Figure 5.25	Raman spectra of composite coating	104
Figure 5.26	Surface roughness result of composite coating	105
Figure 5.27	Micro-hardness Vs composite coating graph	106
Figure 5.28	Residual stress Vs composite coating graph	107
Figure 5.29	(a-b) COF (c) Wear Vs Sliding distance graph carbon coating	109-110
Figure 5.30	FESEM images of wear characteristics of composite coating	111
Figure 5.31	Stages of wear mechanism of carbon-based composite coating	112
Figure 5.32	Shows deviation of COF with parameters (a) Temperature ($^{\circ}\text{C}$) (b) Sliding velocity (m/s) (c) Load (N) of composite coating	114-115
Figure 5.33	Shows deviation of COF with parameters (a) Temperature ($^{\circ}\text{C}$) (b) Sliding velocity (m/s) (c) Load (N) of composite coating	120-121
Figure 6.1	Comparative analysis of (a) COF (b) Wear of developed Coatings	126-127
Figure 6.2	Comparative analysis of micro-hardness developed of Coatings	128
Figure 6.3	Comparative analysis of residual stress of developed Coatings	130

LIST OF TABLES

Table 1.1	Merits and demerits of deposition techniques	4
Table 1.2	Merits and demerits of thermal spray deposition techniques	12
Table 2.1	Comparison of carbon based material structure	23
Table 2.2	Deposition Parameters for CNT/DLC coating	135-139
Table 2.3	Tribological conditions of carbon based coating materials	140-147
Table 2.4	Deposition parameters of HVOF based coating	147-153
Table 4.1	Details of wear test experiments	60
Table 4.2	Design parameters and trial conditions chosen for the Taguchi's experiment	63
Table 4.3	Chemical composition, mechanical and tribological property of steel substrate	63
Table 4.4	Details of coating deposition	65
Table 5.1	EDS result of carbon coating	77
Table 5.2	Experimental results of Taguchi L9 OA of COF, and Wear for Carbon Coating	89
Table 5.3	Main Effects and average values of COF (S/N ratio and raw data) for carbon coating	90
Table 5.4	Pooled ANOVA for COF (S/N ratio and raw data) for carbon coating	93
Table 5.5	Average values of COF at optimal levels for carbon coating	94
Table 5.6	Main Effects and average values of wear (S/N ratio and raw data) for carbon coating	95
Table 5.7	Pooled ANOVA for wear (S/N ratio and raw data) for carbon coating	99
Table 5.8	Average values of wear at optimal levels for carbon coating	99
Table 5.9	Experimental results of Taguchi L9 OA of COF, and Wear for composite Coating	112-113

Table 5.10	Main Effects and average values of COF (S/N ratio and raw data) for composite coating	113
Table 5.11	Pooled ANOVA for COF (S/N ratio and raw data) for composite coating	117
Table 5.12	Average values of COF at optimal levels for composite coating	117
Table 5.13	Main Effects and average values of wear (S/N ratio and raw data) for composite coating	119
Table 5.14	Pooled ANOVA for wear (S/N ratio and raw data) for composite coating	122
Table 5.15	Average values of wear at optimal levels for composite coating	123

ACRONYMS

COF	Coefficient of Friction
IC engine	Internal Combustion Engine
PVD	Physical Vapour Deposition
CVD	Chemical Vapour Deposition
RF-MS	Radio Frequency Magnetron Sputtering
ED	Electro Deposition
HVOF	High Velocity Oxy-Fuel
SV	Sliding Velocity
Temp.	Temperature
2θ	2 theta
CC	Carbon coating
FESEM	Field Emission Scanning Electron Microscopy
EDS	Energy Dispersive Spectroscopy
HRXRD	High Resolution X-Ray Diffraction
N ₂	Nitrogen
SiC	Silicon Carbide
CNT	Carbon Nanotube
DLC	Diamond Like Carbon

ABSTRACT

To abate frictional loss, emission and optimization of advance coatings is vital for piston rings, thick low friction environment friendly carbon coatings have been successfully deposited by agriculture waste produced carbon and carbon based composite powder using HVOF process. The present work evaluates the microstructure, surface morphology, tribological and mechanical properties of carbon coating and carbon based composite coating for piston rings. The aim of present work is to optimize the COF and Wear behavior of carbon and carbon based composite coating using Taguchi L9 orthogonal array (OA). FESEM+EDS, HRXED & Raman spectra confirms deposition of coating which exhibits typical semi-molten, molten and un-melted grains of composite particles along with formation of lamellae.

The experimental results of COF for composite coating is almost 6.7% less than carbon coating, while the experimental results of wear for composite coating is almost 16-20% less than carbon coating at test condition of temperature ranging from 150 to 350°C, load 50 N and sliding velocity 1 m/s respectively. The experimental results of micro-hardness for composite coating is almost 8-12% greater than carbon coating, while the test results of residual stress for composite coating is almost 14-25% less than carbon coating at test condition of temperature ranging from 150 to 350°C, load 50 N and sliding velocity 1 m/s respectively.

The percentage contribution of sliding velocity (75.49 %) was highest followed by temperature (12.93 %) and load (8.09 %) for COF. The percentage contribution of sliding velocity (59.62 %) was highest followed by temperature (28.43 %) and load (9.36 %) for Wear. The percentage contribution of sliding velocity (74.76 %) was highest followed by load (12.85 %) and temperature (9.46 %) for COF. The percentage contribution of sliding velocity (64.004 %) was highest followed by temperature (24.01 %) and load (10.94 %) for wear.

Keywords: Coating; FESEM; HRXRD; Raman Spectra: COF; Wear; Taguchi L9 orthogonal array.

This chapter includes piston ring wear, surface engineering and thermal spray process techniques have been discussed. Later the details of different types of wear, wear mechanism, and surface modification techniques, for wear reduction of carbon coating have been elaborated.

1.1. PISTON RING WEAR

Many researchers and industry professionals have become interested over the years about improving and optimising tribological properties for future surface engineering applications. When contrasted to the environmental benefits, even a 20% reduction in friction can save a lot of money, according to a tribology research [1].

Fossil fuels accounted for nearly 85% of total energy use, regardless of their influence on climate change. According to a study, environmental change can be effectively mitigated or even reversed if harmful emissions are decreased by 60% by 2050 [2]. This is a significant challenge, given that up to 2040, 75% of the vehicle industry is expected to rely on IC engines [3]. For the time being, the sudden worry about emissions and fuel economy must be addressed properly. The performance of engines can be enhanced by adjusting fuel characteristics, operating circumstances, and mechanical design [4-6]. Modern engines are subjected to significant mechanical and thermal loads due to their high power-to-weight ratio [7]. In IC engines, friction consumes roughly 4-15 % of the fuel energy [8] with piston rings accounting for nearly 40-55% of these losses [9]. The inefficiency of piston rings has been the subject of a number of analytical and experimental studies. Surface geometry optimization, enhanced lubrication, and the employment of unique surface treatments are now directly linked to major improvements in IC engine tribological performance. Because friction loses 40-45 % of overall energy, piston rings are very important among engine components. The tribological performance of piston assemblies has a big impact on fuel economy, harmful exhaust emissions, and power loss. IC engine piston rings must maintain a dynamic seal under chemical, thermal, and tribological environments. For piston rings, the following needs have been identified:

1. Low frictions for higher power efficiency rate
2. Low wear for retaining surface texture of cylinder linear
3. Low wear for ensuring long operational life of piston ring
4. Good resistance against erosion, chemical attack and mechano-thermal fatigue.

5. Good emission suppression
6. Cost effectiveness and reliable operation for long life

Piston ring failure is common phenomenon even after constant research of piston cylinder assembly and failure may arise due to wear, fluctuation in temperature, operating environment, fatigue, corrosion and oxidation. The wear resistance of piston ring can either by surface modification or by lubrications.

The optimization of lubrication regime [10], surface topography [11, 12], and surface modification [13] are all mentioned in the literature as ways to improve piston component performance. Surface modification and engineering is one of the most important methods for minimizing friction and wear.

Manufacturers of lubricants and gasoline additives, as well as worldwide equipment manufacturers, are attempting to meet the requirement of customer, while the and new legislation are aiming towards environmental protection and energy conservation [14]. Fuel and energy efficient automobiles and lubricants are critical for reducing friction and wear in engines while also conserving natural resources [15]. According to Skjoedt et al., a 10% reduction in engine friction applied to all US passenger automobiles would save 3.4 billion gallons of fuel in 2007 [16]. Piston rings have a critical role for power loss, fuel consumption, and toxic exhaust emissions of IC engines tribological performance. According to a study, a piston ring with minimal power loss, minimal wear, and a noticeable sliding interface can greatly extend the component's life.

Higher efficiency in IC engines would mainly rely on improvements in innovative techniques such as surface texturing [17-18], after exhaust heat treatment [19-20], CDA [21] and advanced coatings. Coating technology for IC engine applications has been mostly investigated experimentally in numerous conditions & operation, accelerated wear, cold starts and hot scuffing [22-23].

To improve tribology in piston rings, researchers have advocated surface modification using nano HVOF, thermal and plasma spray, ceramic or metallic alloying, nitriding, and hard chrome plating. Thermal spray and HVOF deposition are two well-known coating processes for adjusting chemical, mechanical, and tribological properties while preserving the geometry of the piston ring. Coating technology is a novel strategy for reducing the environmental impact of IC engines. Using typical Chromium coatings as a baseline, tungsten doped carbon coatings improved friction, while bilayer and multilayer coatings improved wear resistance.

1.2. SURFACE ENGINEERING

Surface engineering is the process of designing a surface to improve and enhance a substance's functional qualities. Surface execution requires interdisciplinary effort, surface design, and planning, which ultimately leads to cost-effective surface augmentation. Engineering materials have a critical function in human growth. As a result, material engineers are always stumped when it comes to developing new materials and changing materials that are frequently utilised in engineering component design. Engineers can enhance and increase the qualities and life of existing engineered materials by surface modification. Several tribology systems are capable of delivering low COF, high wear resistance, and great mechanical properties. Coatings are a common way to adjust the surface morphology, wear performance, adhesion, and fatigue strength of substrate materials without changing their bulk properties. Coating deposition, ion beam deposition, thermal spray deposition, RF-M.S. and electro deposition are some of the most often used tribology processes [24]. Successful material deposition opens up new possibilities and stimulates scientists to develop novel coating materials with superior mechanical, wear, thermal, electrical, and frictional properties. Surface modification or coating deposition is used for customization of surface properties. Following are the keys points that significantly played a vital role in the development of coating techniques:

- Environment and sustainability
- Process robustness
- Smart layers and structure
- Education and training
- Cost effectiveness

Figure 1.1 depicts the various coating material deposition procedures. Table 1.1 lists the benefits and drawbacks of different deposition processes [24]. The commonly used deposition techniques are thermal spray deposition, electrodeposition, physical vapor deposition and chemical vapor deposition which are elaborated below:

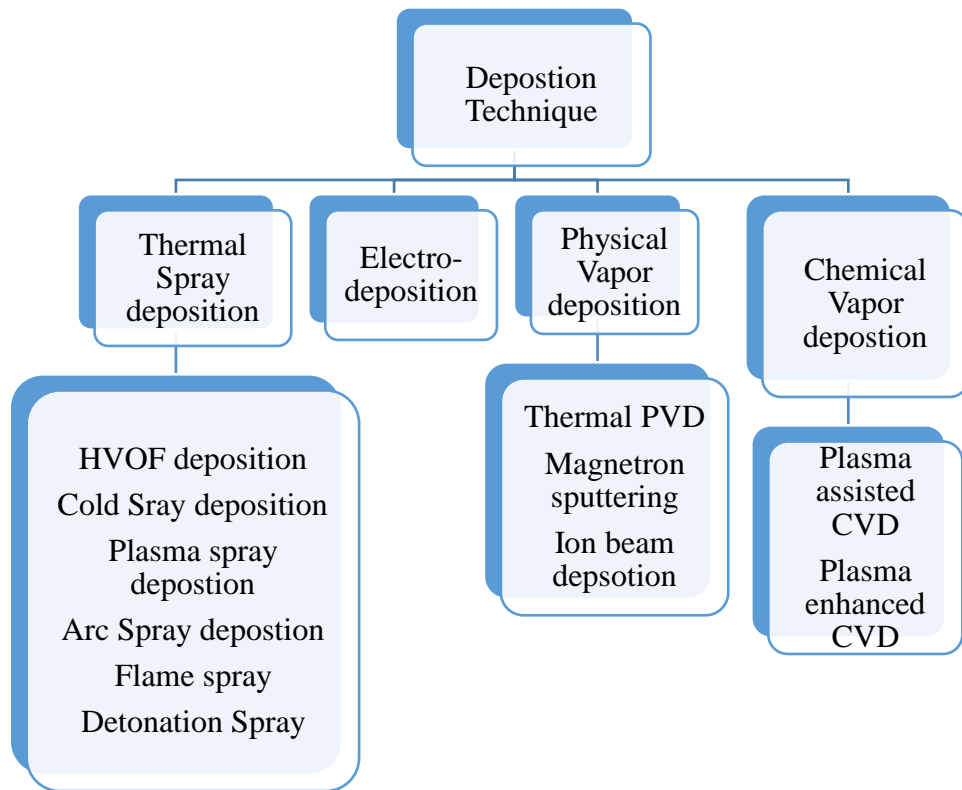


Figure 1.1 systematic diagram of deposition techniques [24]

Table 1.1 Merits and demerits of deposition techniques [24]

Process	Merits	Demerits
Thermal spray deposition	(i) Low cost (ii) High deposition rate (iii) Can be widely used for numerous coating material	(i) Residual stress concentration is high (ii) Difficulty in Nano porous coating.
Electro-deposition	(i) High deposition rate (ii) Ability to coat complex materials (iii) Controlled nano porous coating.	(i) Caustic waste
Physical vapor deposition	(i) Can coat complex materials. (ii) Dense coating of nano scale thickness	(i) Low deposition rate (ii) High initial cost
Chemical vapor deposition	(i) Uniform deposition on complex shape (ii) Can coat complex materials.	(i) Restricted to chemical composition and use of volatile gases (ii) Low deposition rate (iii) High initial cost

- **THERMAL SPRAY DEPOSITION**

It is a deposition technique in which powder metal is sprayed onto a substrate material. Thermal spray has high deposition rate and is used to coat thick coating with low cost. It has wide range of coating material like ceramic, plastic, composite, metal & alloy and temperature. Quality of deposition can be evaluated by determining its hardness, porosity, bond strength, oxide content and surface roughness. Thermal spray processes are mainly categorized as combustion spray, plasma spray and cold spray. Combustion spray techniques are detonation gun spraying and high-velocity oxy-fuel spray. Likewise, plasma spray processes are plasma transferred wire arc spray, radio frequency inductively coupled spray, and straight current blown arc spray [24]. Figure.1.1.1 shows a systematic representation of the thermal spray process in action.

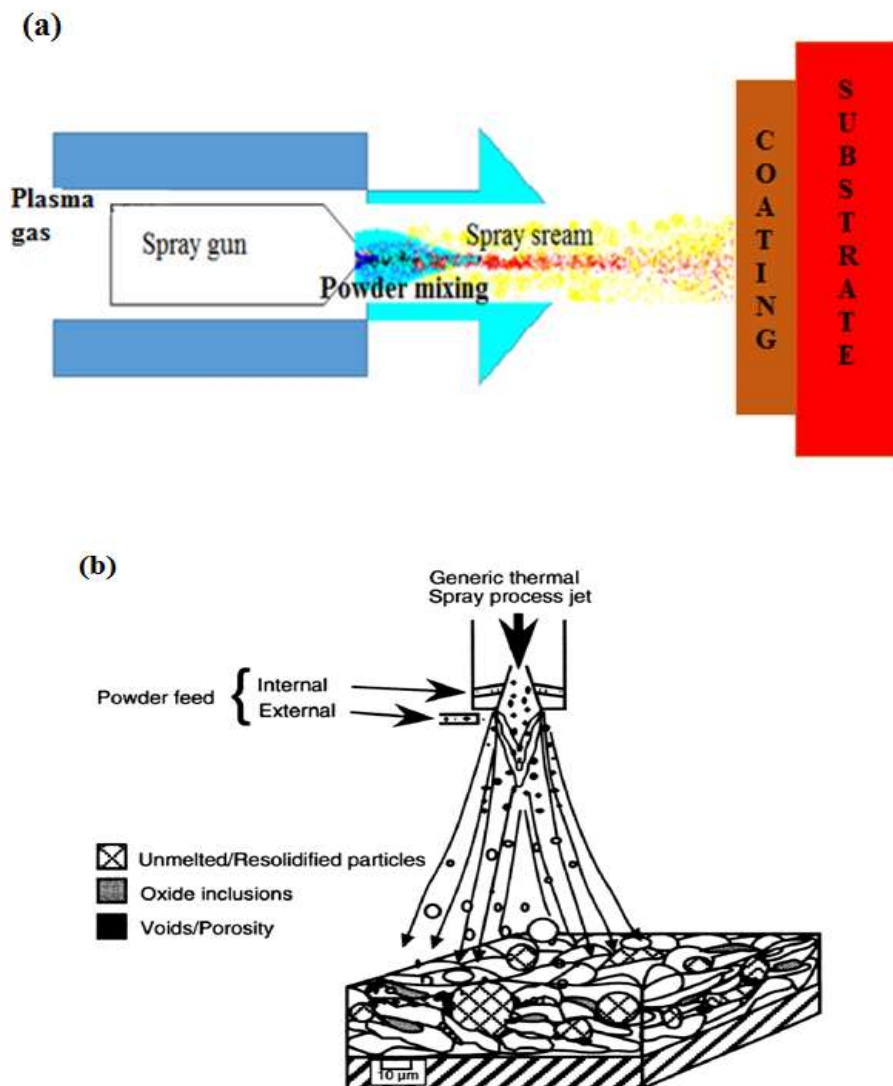


Figure 1.1.1 systematic diagram of (a) thermal spray deposition (b) working of thermal spray powder process [25]

- **ELECTRO-DEPOSITION**

It's a deposition technique that uses an electrolysis process to deposit a thin adherent layer onto a substrate material, as shown in figure 1.1.2. Electro-deposition process has high deposition rate with an ability to coat complex materials and controlled nanoporous coating. The ability to control the coating microstructure and nanostructure, as well as morphology and mineralization by varying parameters such as deposition potential/current, bath composition, temperature, and deposition time, made electrodeposition a novel method for producing coatings [24]. There are some notable disadvantages of electrodeposition. Process parameters must be optimized for each workpiece to obtain uniform thickness. Environmental concerns also arise from the process such as the acidic, alkaline, and cyanide discharge.

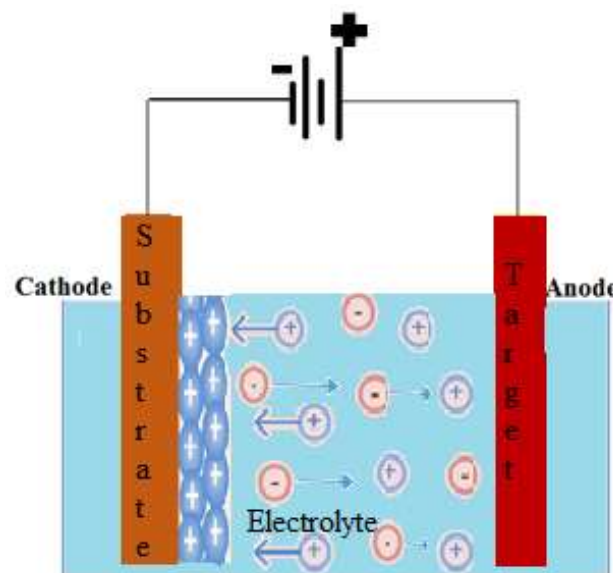


Figure 1.1.2 systematic diagram of electro-deposition [24]

- **PHYSICAL VAPOR DEPOSITION**

It is a deposition technique in which ions are bombarded on the substrate material, ions are mechanically ejected from target material as shown in figure 1.13. Physical vapor deposition technique is commonly used for thin film deposition. It has low deposition rate with high initial cost and is used to coat complex materials. Thermal evaporation PVD involves heating the coating metal to the point of evaporation by means of a resistance heat source, high-energy arc or electron beam. In the case of a coating metal with relatively low melting point, a resistance source can be used to heat a crucible containing a powdered form of the coating. This method does not allow the evaporation of metals with high melting temperatures, such as molybdenum and tungsten. Evaporation of refractory metals can be achieved by heating with an intense beam of electrons [24].

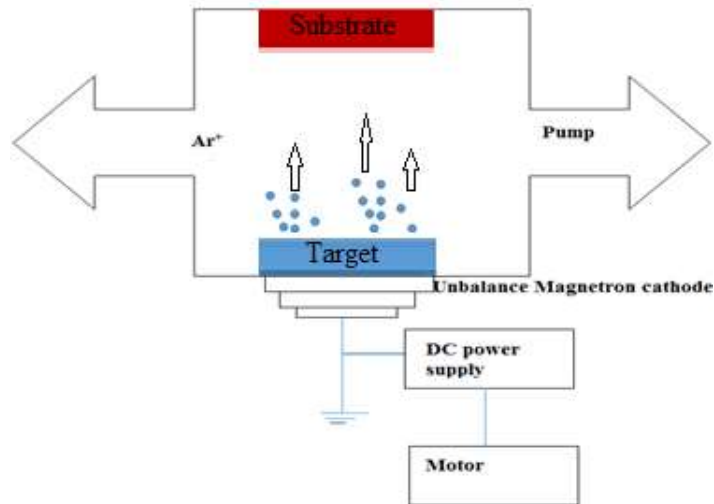


Figure 1.1.3 systematic diagram of physical vapor deposition [24]

- **CHEMICAL VAPOR DEPOSITION**

It is a deposition technique in which plasma arc is generated from power supply and used for deposition of complex shape uniformly but restricted to chemical composition. It has low deposition rate with high initial cost and usually used to coat thin film. As opposed to most PVD techniques, chemical vapor deposition (CVD) is desirable for the deposition of a coating on complex geometric work piece uniformity. At a rudimentary level, CVD utilizes chemical reactions of a precursor gas in a heated chamber containing the work piece. The products of this chemical reaction are deposited in thin layers on the surface of the substrate and the byproducts are exhausted from the system. CVD has been used to deposit TiO_2 on Ti machined implants [24]. Figure 1.1.4 depicts a systematic diagram of chemical vapour deposition.

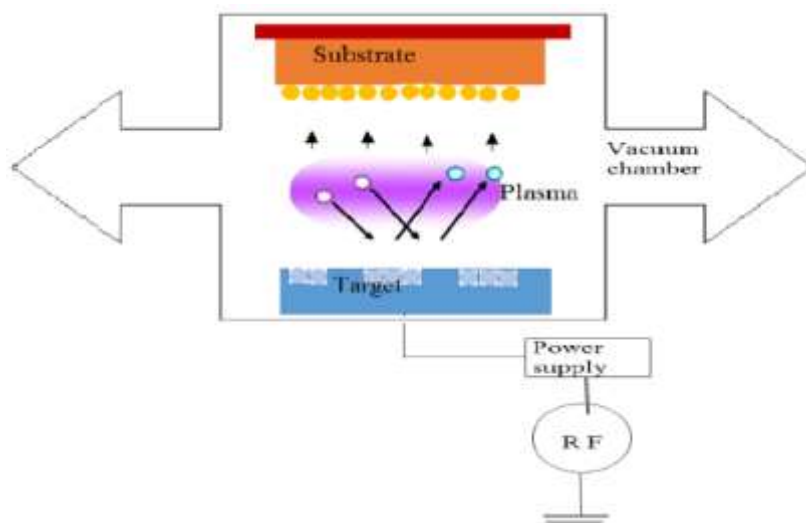


Figure 1.1.4 systematic diagram of chemical vapor deposition [24]

1.3.THERMAL SPRAY PROCESS

1.3.1. HIGH VELOCITY OXY-FUEL (HVOF) SPRAY PROCESS

HVOF spray is most popular thermal spray coating techniques which can approximately deposit 12 mm of thick layer and is having highest deposition rate on comparing with other techniques. HVOF spray works on supersonic gas speed with MACH no. greater than 5. In this process, large amount of fuel gas and air is supplied to combustion chamber. In combustion chamber, oxygen and spraying fuel are ignited. Gases flow through convergent-divergent nozzle with a speed greater than 1500m/s [25]. The commonly used fuel gases are propylene, acetylene, LPG, hydrogen and kerosene. A carrier gases such as argon, nitrogen and helium feeds the coating powder from feedstock to spraying nozzle. The powder particles impinges with huge force on the substrate and having spraying speed of 1000m/s at 3300⁰C temperature [27]. The coating produce are having excellent cohesive and adhesive strength, low oxide content and less porosity. Low particles temperature also ensures less thermal stresses and on optimized HVOF deposition condition will produce less than 1% porosity and more than 80MPa bond strength.

It has ability to provide high bond strength, good surface finish, improved toughness, improved hardness and higher thickness of coatings by varying deposition parameters like powder size, fuel rate velocity, deposition time, temperature, oxygen pressure and jet velocity, which made HVOF a novel techniques for generating sound coatings at low cost. Following are the advantages of HVOF technique:

- Effective heating of sprayed particles
- The mixing of air with sprayed particles is almost eliminated
- High particle speeds results in low exposure time which ultimately results in low particle oxidation
- Low particle temperature

The HVOF system used in present research work consist of spraying gun, hoses of suppling carrier and fuel gas, powder feeding system, air cooling circuit and gas regulator. The systematic diagram of HVOF spray process is shown in the figure 1.2.

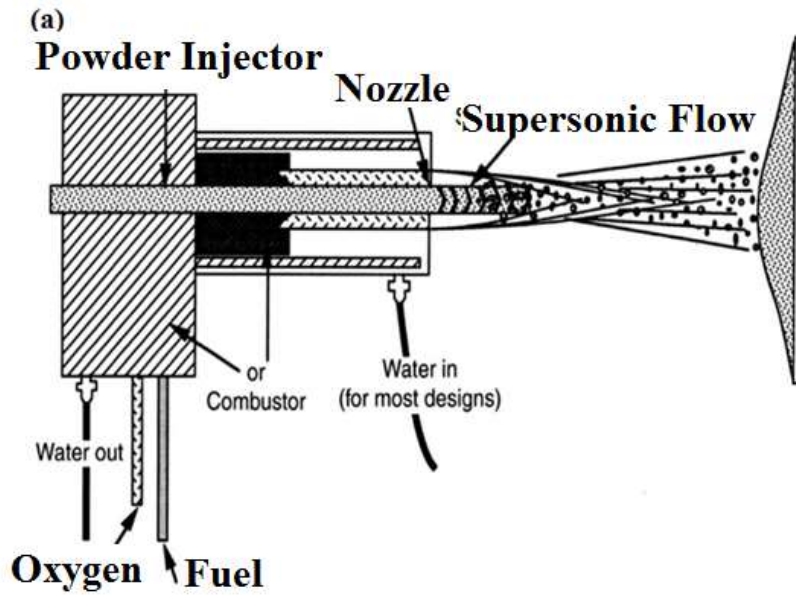


Figure 1.2 schematic diagram of the (a) HVOF spray process [25] and (b) Thermal Spray Robot [27]

1.3.2. ATMOSPHERIC PLASMA ARC SPRAY

It is the deposition techniques where the plasma arc are generated by high DC voltage and is used to ionize gases like helium, argon and nitrogen. Plasma spray is basically spraying technique in which molten metal or heated metal is sprayed onto surface of substrate at high temperature plasma flame to accelerated high velocity to provide coating [26]. The widely used materials includes metals, alloy, carbides, refractory oxides and ceramics. The tested bond strength of plasma spray technique may varies from 34 to 69 MPa. In plasma jet spray, due to the use of inert gases lesser in-flight oxidation is observed and some in-flight particles get oxidized and entrapped in splats, on comparing with other thermal spray techniques. To minimize inclusions of oxide, optimization of spraying distance, particles temperature and

particles velocity should be done. The systematic diagram of plasma spray process is shown in the figure 1.3.

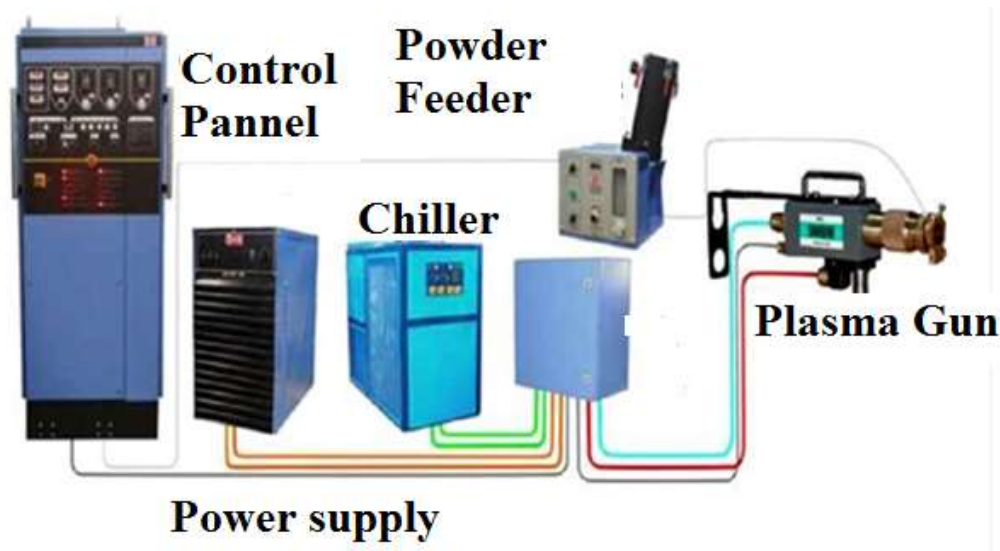


Figure 1.3 schematic diagram of the Plasma Spray System Layout [26]

1.3.3. FLAME SPRAY PROCESS

It is the oldest thermal spray deposition techniques in which wire and powder are used as a coating material with 1000°C flame temperature and 40m/s particle velocity. Coatings prepared by flame spray techniques are highly porous and low strength of deposition. The main characteristics of these coatings are its lamella structure, porosity, bond strength, surface roughness and oxides content [25]. The capability to restraint microstructure behavior of coatings as well as syllable structure by optimized parameters such as spraying nozzle distance, gas flow rate, spraying conditions, flame temperature and deposition time, made successfully generous process for producing defect less coatings at low capital cost. Flame spray process are having coarse structure with high porosity, due to low flame temperature and low spray velocity. Generally, inferior coating density of ranging 85% to 98% is achieved with different spraying parameters and coating materials [26]. For improving properties of flame spray process, spray and fuse technique is required and fusion can be carried out using laser or in furnace or by using spraying torch without powder.

1.3.4. WIRE FLAME SPRAY

It is the oldest thermal spray deposition techniques in which wire based materials are transferred at $<150\text{ m/s}$ particle spray, 4000°C temperature through spraying gun and feedstock is in the form of wire [27]. Wire flame processes are basically combustion process where oxygen and combustibile fuel i.e. propane and acetylene are used for generating flame and melt the wire metals .Molten metal formed by wire is atomizes by compressed air and project the

particles onto the substrate materials. Hydrogen, propane, natural gas and acetylene are the commonly use combustible gases which are used for producing heat during wire flame spraying. Wire flame spray can be used to deposit good strength coating with no cracks and are having coating thickness ranging from 20 microns to several millimeters, depending upon process parameters and feedstock materials [27]. It is used to provide good dimensional and morphological stability. The systematic diagram of wire flame pray process is shown in the figure 1.4.

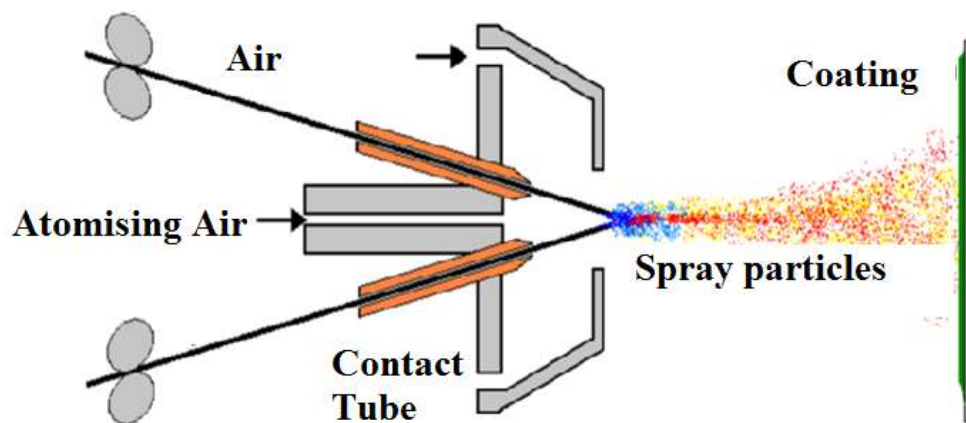


Figure 1.4 systematic diagram of wire flame spray process [27]

1.3.5. DETONATION FLAME SPRAY

It is a deposition technique in which combustible gases are used to melt the powder and sprayed at 3500m/s velocity and 4000⁰C. Detonation flame spray consist of long barrel type tube where mixture of coating powders is done along with feeding of oxygen and acetylene gas. The coating developed by detonation spray was dense and adherent layer having thickness of about 2.54 cm and can be used to coat hard materials. It can be used to produce less porous having low oxygen content, good wear resistance coating at low load condition. For coating deposition, the commonly used materials are hard materials, copper, iron etc.

1.3.6. COLD SPRAY TECHNIQUE

It is the deposition technique in which helium gas is used as a carrier gas to feed powder from feedstock to combustion chamber. It is in which powder particle of sizes ranging from 1 to 50 micrometres at 300 to 1200 m/s speed in a supersonic gas jet speed through de Laval nozzle [28]. Cold spray technique has high deposition rate, oxide free coating, less shrinkage, good bond strength and having an ability to coat different materials at lowest possible temperature. The commonly used materials for coating deposition are metals, nano crystalline,

polymers and ceramics. The systematic diagram of cold spray process is shown in the figure 1.5.

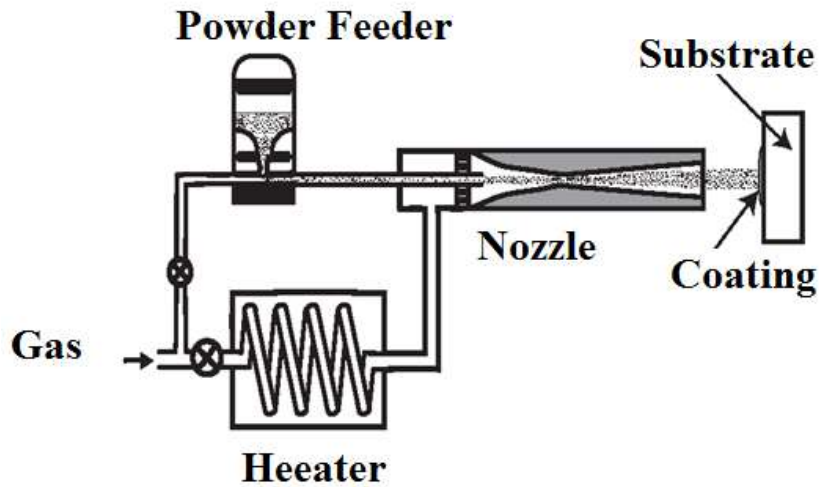


Figure 1.5 systematic diagram of cold spray process [28]

Table 1.2 shows the merits and demerits of thermal spray deposition techniques

Table 1.2 Merits and demerits of thermal spray deposition techniques [29]

Process	Merits	Demerits
HVOF	<ol style="list-style-type: none"> 1. Dense coating 2. Low oxide 3. Good wear resistance 4. Excellent impact resistance 	<ol style="list-style-type: none"> 1. Powder size restricted to 5-60 microns 2. Costly 3. Difficult to coating internal surface due to spray distance of 150-300mm from line sight.
Plasma arc Spray	<ol style="list-style-type: none"> 1. High temp plasma jet suitable for refractory materials 2. Larger powder size 5-100 microns 3. Ability to coat different materials 	<ol style="list-style-type: none"> 1. Very expensive 2. Excessive oxidation 3. Lower hardness
Flame Spray	<ol style="list-style-type: none"> 1. Low cost, 2. Wide range of materials can be used 3. Highly porous 4. Low deposition rate 	<ol style="list-style-type: none"> 1. Limited with higher melting points than flame 2. High porosity 3. Low density 4. High oxides formations
Cold Spray	<ol style="list-style-type: none"> 1. Low shrinkage capacity 2. Spray micro sized particles 3. Minimum surface penetration 4. Low energy consumption, 5. High deposition rate and efficiency 	<ol style="list-style-type: none"> 1. Hard and brittle cannot sprayed, 2. High gas consumption, 3. Expensive process

1.4. TRIBOLOGY

Tribology is a Greek word derived from the word tribos which means rub. It was coined by Jost in 1966 and the study of tribology is related to mate surfaces when they are in motion. Tribology has mainly three components namely friction, wear and lubrication. The main function of tribology is to improve performance and product life, lowering costs and saving energy.

1.4.1. FRICTION

Friction is defined as the resistive force that opposes the relative motion between two surfaces. It is represented by the dimensionless entity, coefficient of friction μ and is defined as the ration of frictional force to the normal force. Friction may be characterized into following parts:

- Fluid friction
- Static friction
- Rolling friction
- Sliding friction

Frictional force can be defined as the ratio of force exerted to the applied load and is independent of apparent contact area. Mathematically, it is represented as

$$F \leq \mu N$$

Where F is defined as the frictional force acting parallel to surface, N is normal force and μ is coefficient of friction.

For surface at rest, $\mu = \mu_s$, where μ_s , is coefficient of static friction

For surface at motion, $\mu = \mu_k$, where μ_k , is coefficient of kinetic friction

1.4.2. WEAR

In engineering wear is the one of the most vital problem occurs in manufacturing industries which leads to deteriorating the surface condition of components. It reduces the efficiency of components by increasing its oil consumption; power losses. It has been observed that only abrasion wear is responsible for the loss of 1.4% cost of the national gross income of industrialized based nations. Now in the present time wear is drawing considerably much attention of researchers in the field of tribology, in spite of that less research has been done in the field of corrosion, fatigue and cavitation's. Figure 1.6 shows systematic sketch of different types of wear.

Wear is the process in which two adjacent layers of solids surfaces slides and that causes the plastic deformation of materials. It is defined as the characteristic of material removal from the

mating surface. The removal of material occurs from softer surface to harder surface or from both the surfaces, in the form of debris. It is frequently expressed in terms of mass loss per unit distance.

According to Archard, wear is defined as the plastic deformation and fracture of asperities at contact due to localized pressure. It is directly proportional to normal load and is independent of contact area. Mathematically, it is represented as:

$$W = k \frac{P}{P_m} S$$

Where W is the volume of worn material, P_m is yielding strength, k is the wear constant, P is applied pressure and s is the sliding distance.

K is also used to compare the tribological behaviour of material tested under similar condition and mathematically, it is represented as:

$$k = \frac{W}{SP}$$

where K is wear ratio in mm^3/Nm , s is sliding distance in m, W is worn volume in mm^3 and P is normal load in N.

Wear may be classified as following:



Fig 1.6 systematic sketch of types of wear

1.4.2.1.ADHESIVE WEAR

It is a type of wear which occurs between the bodies that are in relative motion and material in the form of wear debris is removed when atomic bonding forces of one material are more than those of the other material. The reason for adhesive wear can be either due to localised bonding or due to solid phase welding at the contact point. In this process an eroded particle tends to be momentarily or completely attached from one surface to another surface. Adhesive wear may also be defined as the plastic deformation of minor asperities within the surfaces of two bodies when they are in relative motion with each other. Adhesion takes place in between the asperities and finally results in transfer of metal from one surface to another surface. Adhesive wear can be reduced, when contact area between the mated surfaces is reduced. During sample testing, high coefficient of friction was observed because of adhesive wear and on the other hand due to oxides and oil film, adhesive wear between two surfaces cannot be observed. The coefficient of adhesive wear in metals varies from 10^{-7} to 10^{-2} .

The adhesive wear mechanism can be distinguished from other wear mechanisms due to the characteristic feature of it, due to the transfer film formation of wear particles before the detachment of particles from the surface. The wear debris of the brass became too hard because of the work hardening. This wear debris was probably capable of wearing brass itself. Wear rate was critically affected by the formation of the transfer film. It's obvious from the figure that wear debris lifted the pin away from the other surface. This phenomenon may be the reason for negative wear rate [30]. Figure 1.7 shows the systematic diagram of adhesive wear mechanism

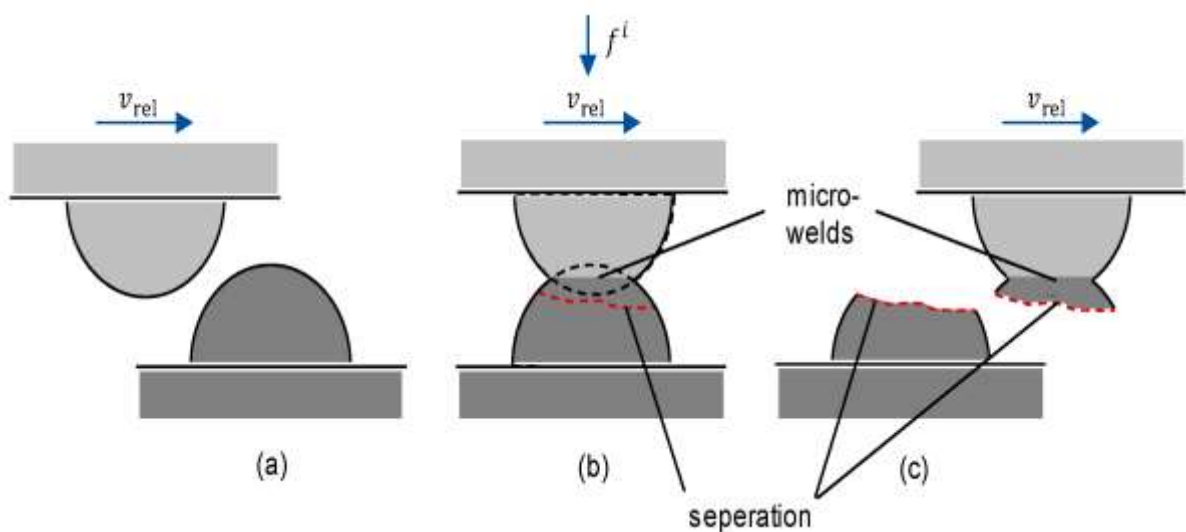


Figure 1.7 systematic diagram of adhesive wear mechanism [31]

1.4.2.2.ABRASIVE WEAR

It is a type of wear which occurs when a surface of higher hardness is rubbed or forced against the surface of lower or equal hardness. If a softer material is having a presence of hard particles, it may cause abrasive wear. For example, due to the presence of silica in sugarcane (organic material), it is responsible for abrasive wear in shredders and cane cutters. The wear mechanism of abrasive is difficult to control and prevent as it doesn't describe the mechanism precisely and all the wear mechanism occurs simultaneously with different characteristics. The various abrasive wear mechanism involved are grain pull out, fracture, cutting, and fatigue [32]. Ploughing wear occurs when grooves are formed and materials are displaced from the materials. Fragmentation occurs when material is removed from the surface by cutting action and due to the presence of indenting abrasive localised fracture. Material is imparted from the surface of material in the form of microchips, small debris with less or no material dislocate to the next side of the grooves.

Abrasive wear is process of friction and wear, in which wearing material should be softer than the abrasive material and abrasive resistant materials may combat wear by prevention of intrusion of hard grains, and change in design process. In abrasive wear, degree of penetration can be defined as the ratio of load on particles to the surface hardness of materials. Mathematically it can be expressed as:

$$p = \frac{W}{H_v}$$

where, p is the degree of penetration, H_v is the surface hardness of materials while W is the normal load on the particles.

$$V = \frac{W}{H_v} * A * L$$

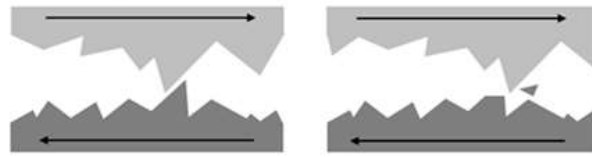
where, V is the wear volume, H_v is the surface hardness of materials, A is the area of groove cross section, L is the length of groove while W is the normal load on the particles.

Abrasive wear can be characterized into two different ways:

- Two body wear mechanism: Action of sandpaper on the surface and hard asperities and grit passes over the cutting tool.
- Three body wear mechanism: Due to loose bonding, grits are free to slide as well as roll over the surface.

Figure 1.8 shows the systematic diagram of two and three body abrasive wear mechanism.

Two Body Wear



Three Body Wear

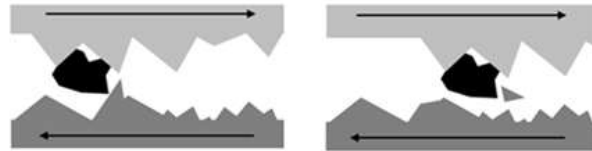


Figure 1.8 systematic diagram of two and three body abrasive wear mechanism [33]

1.4.2.3.FATIGUE WEAR

It is a type of wear which occurs due to deformation sustained by asperities of both the surfaces. Fatigue wear occurs when high local stresses are repeated no. of times during fatigue cracks propagation, in courses of rolling or sliding and wear particles. Wear mechanism during this process can be determined by crack initiation, crack growth and fracture. In fatigue wear process, very high plastic strains are generated on worn surfaces as compared to unworn surfaces and these strains along with surface consequent modifications have strong effect on wear process. Figure 1.9 shows the systematic diagram of fatigue wear

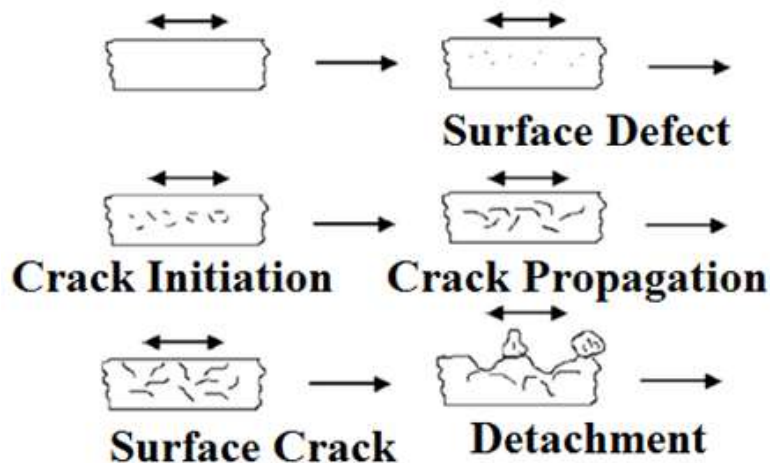


Figure 1.9 systematic diagram of fatigues wear mechanism [25]

1.4.2.4.FRETTING WEAR

The main characteristic of fretting is its reddish brown appearance on the surface of metal and a debris which often occurs to as “Cocoa” due to its small oscillatory amplitude motion i.e. 130 μm . It is destructive type of wear phenomena which occurs in between two mating

surfaces which is having oscillatory relative motion with small amplitude. The amplitude of the relative sliding motion is varies in order from micro-meters to millimetres, but can be low as three nanometres i.e about $0.1\text{mg per } 10^6 \text{ cycles, per } \text{MN m}^{-2}$. One of the characteristics features of fretting wear is that wear debris are retained within surface contact and may gradually separates the surface or may contribute to accelerate abrasion wear. It may also be accelerated by temperature, corrosion or other effects. Figure 1.10 shows the systematic diagram of fretting wear

The fretting wear occurs on three basic processes:

- Oxides are formed on the clean surface of strained steel and are disrupts by mechanical action and it would be reactive
- Usually mechanical grinding operation is to be used to remove the metal particles from the surface in the form of finely divided particles either by direct shearing action or by localized fatigue.
- The oxidation of surface particles in the existing atmosphere and the presence of abrasive powders are the reasons to formation of oxide debris.

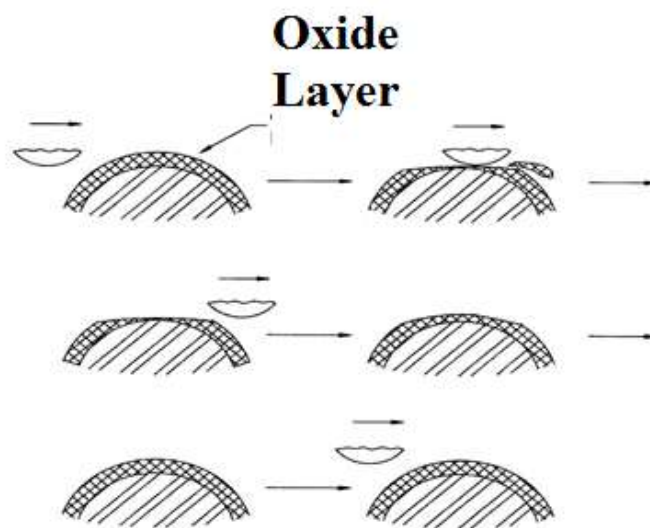


Figure 1.10 systematic diagram of fretting wear mechanisms [28]

1.4.2.5.IMPACT WEAR

It is a type of wear that occurs due to repetitive collision between two surfaces. An example of impact wear is found in heads of hammers. In this type of wear involves nearly flat surface with larger radius of curvature compared to wear scare size. This is the main distinguish feature of impact wear from erosion wear, in which sharp particles indents on flat surface. The impact

wear mechanism involves elastic and plastic deformation, occurs due to high impact energy [34]. Figure 1.11 shows the systematic diagram of impact wear

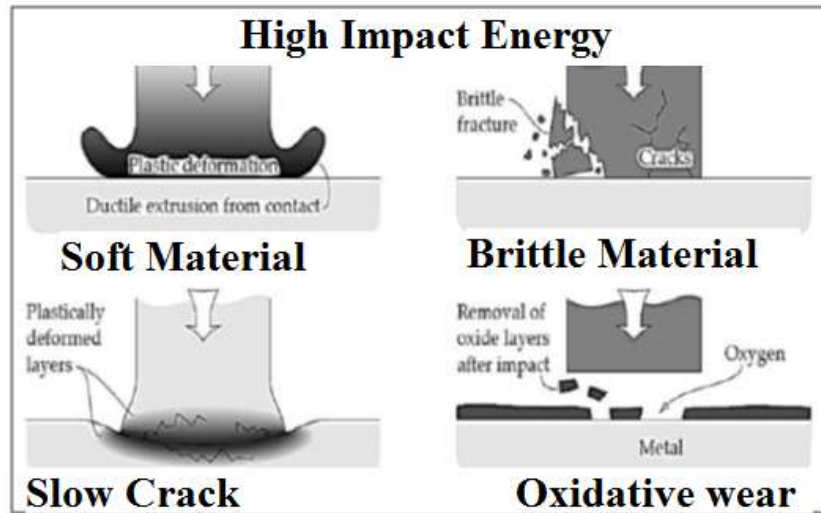


Figure 1.11 schematic illustrations of the mechanisms of impact wear [35]

1.4.2.6. EROSION WEAR

It is a type of wear mechanism which occurs when small particles impacts against the mechanical components. The commonly known erosion wear mechanisms are fatigue, abrasion, erosion and plastic deformation by melting, brittle fracture and superplastic flow. The wear mechanism involves particles materials, impacts velocity, particle size and angle of incidence as different controlling parameters. It is noted that if the erosion particles are hard then there may be a possibility of abrasive wear mechanism. Erosive is the form of abrasion wear in which the removal of materials occurs due to enforcement of solid particles having high kinetic energy on to surface. In this process, particles are generally treated in different medium such as fluids and slurry's. It has been observed that in erosive wear, stream impinges on the surface with certain impact angle that influences the removal of material from the surface, which directly affects the wear mechanism. It is noted that the hardness and cutting wear of surface wear resistance may prevails at smaller impact angles. It has been observed that the angle between the leading edge and wearing surface can be used to determine the whether there will be deformation of materials or cutting acting will take place between the particles. It can be calculated by using the following formula:

$$\tan(90-A_c) = (1-\mu^2)/2\mu$$

Where A_c represents the critical angle for cutting and μ is coefficient of friction

The erosion rate is significantly varies with effect of angle for brittle and ductile materials, specially the angle related with maximum rate of erosion. These differences can easily be

identified by different modes of damage linked with different types of materials. Brittle materials are more easily fractured under normal impact condition rather than ductile materials and it tends to increase abraded volume of wear that caused due to ploughing or cutting. For brittle materials rate of erosion is increase with increase with the angle where as in ductile material ploughing and cutting are predominant modes with negligible fracture.

From Archads Equation of wear,

$$V=K (L/P) X$$

Where Vis the volume of wear; X is the sliding distance; L is the load; P is the penetration hardness and K is the chances of wear that the rupture of any given junction will results in wear. Figure 1.16 shows the systematic diagram of erosion wear

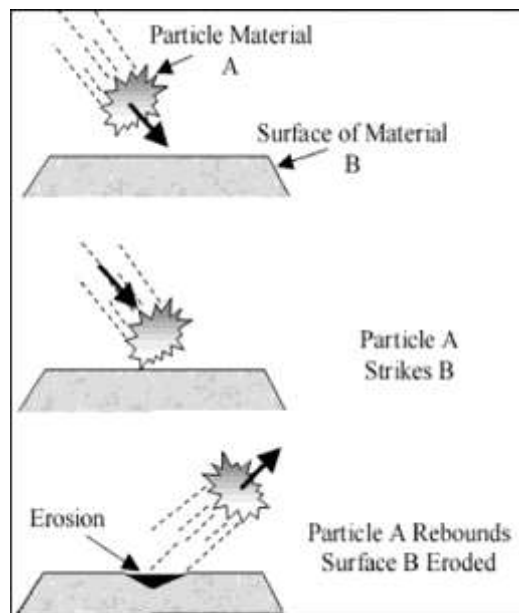


Figure 1.12 systematic diagram of erosion wear [36]

1.5.Motivation for this research work

Presently researchers have been focusing on materials diamond-like carbon (DLC) [37-53], carbon nanotubes (CNTs) [54-56], graphite-like carbon [44, 57-60] in order to fabricate coatings with excellent wear resistance, corrosion resistant, high thermal conductivity, and damping capacity. DLC and CNTs are carbon allotropes of sp^2 and sp^2 & sp^3 hybridizations respectively. Amorphous carbon coating have shown excellent adhesion and friction resistance with potential application towards forming lubricant free sheet metal process [61]. In recent years, numerous research have been done to enhance wear performance of carbon-based coating materials. Even though lots of techniques are available for investigating physical and mechanical performance of DLC/CNTs coatings but still no standard procedures is available

for calculating tribological properties of coated materials. To test tribological behaviors of DLC/CNTs, tribometers are used under ambient pressure with appropriate temperature and relative humidity. It has been examined that sliding speed, applied load, sliding distance and temperature are the most critical parameters which affect both friction and wear resistance. So in order to optimize and enhance frictional and wear behaviour, optimum test conditions must be used. Fig.1.13 shows variation in Coefficient of friction for DLC (H-DLC/W-DLC) coating with N-based coating (TiCN/TiAl/TiN) material. A comparative study shows value of coefficient of friction (COF) of DLC (H-DLC/W-DLC) is lowest for W-DLC (0.10) due to carbon-rich layer on the substrate while N-based coating shows COF value greater than 0.45 due to the adhesion of titanium to the N-based coating surface [62].

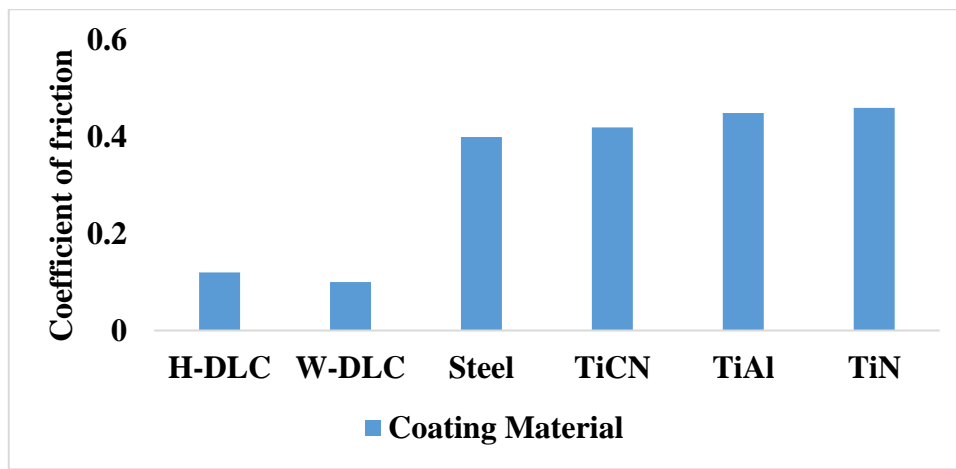


Fig. 1.13 Variation in Coefficient of friction of different coating material [62]

Li et al. [63] examined DLC/GLC/CrN coatings on stainless steel under different environmental condition. In a comparative study, CrN (2h) coating shows excellent load bearing capacity, high hardness, roughness, low friction coefficient and good adhesion strength under atmospheric and oil lubricating condition due to better lubrication of oil, high stability and viscosity. Another study based on Cr/GLC coating on seawater [64] and DLC coating on steel [65] reveals that due to dimple induce graphitization, COF and wear rate value decreases significantly as the dimple density increases. Praveen et al. [66] observed uniform deposition of CNTs particles on CNTs-Zn composite along with excellent corrosion resistance as CNTs layer deposition provides a physical barrier to the erosion. Zr-GLC nanocomposite coating found coefficient of friction (0.06) and wear rate ($9 \times 10^{-17} \text{ m}^3/\text{Nm}$) values at an applied load of 1N while coefficient of friction (0.10) and wear resistance ($1.3 \times 10^{-16} \text{ m}^3/\text{Nm}$) values increase as the applied load increases to 3N [67]. A study based on Cr/GLC coating examined on stainless steel substrate and sliding against SiC, Si₃N₄, Al₂O₃, ZrO₂ and WC shows the friction coefficient value increases in ascending order as $\mu_{\text{Si}_3\text{N}_4} < \mu_{\text{SiC}} < \mu_{\text{WC}} < \mu_{\text{Al}_2\text{O}_3} < \mu_{\text{ZrO}_2}$ [68].

Nowadays a number of automotive components have been coated with carbon nanotubes (CNTs) or diamond-like Carbon (DLC) coatings, to enhance tribological properties. Various such applications of nanotechnology opens up prospects for the deposition of novel smart carbon-based material.

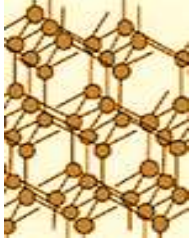
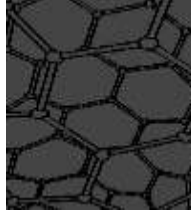
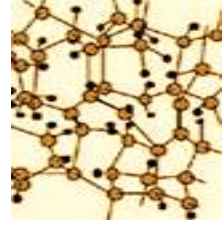
Due to rapid development in technology, highly accurate and precise components are highly demanded by industry. A small scratch can also be responsible for the failure of the component because tribology and stress concentration acts on the scratches, which corresponds to the development of fractures on the surface. To improve tribology in piston rings, researchers have advocated surface modification using nano HVOF, thermal and plasma spray, ceramic or metallic alloying, nitriding, and hard chrome plating. Thermal spray and HVOF deposition are two well-known coating processes for adjusting chemical, mechanical, and tribological properties while preserving the geometry of the piston ring. Coating technology is a novel strategy for reducing the environmental impact of IC engines. Using typical Chromium coatings as a baseline, tungsten doped carbon coatings improved friction, while bilayer and multilayer coatings improved wear resistance. Even though an enriched and comprehensive understanding of tribological systems has been accomplished, but still there are several points need to be researched for procurement of more accurate system. Efforts have been made for the usage of carbon coating in the functional application. It has to be emphasized that for better result a realistic mechanism between the substrate material and deposition parameters i.e. variation in temperature, additives used, the rate of deposition etc. are to be established. Till date, we have developed an efficient tribological system, but then still there is numerous points' need consideration for improving the system.

This chapter includes different of carbon coating, Protective coating, High temperature coating, Role of coating, HVOF process and deposition and tribological condition of HVOF based composite coating.

2.1.MAJOR TYPES, PROPERTIES AND TRIBOLOGICAL BEHAVIOR OF CARBON BASED COATING

Carbon-based materials have been used on coatings in a variety of disciplines of engineering and technology during the previous few decades. Table 2.1 compares the structure of various carbon materials often used for coating deposition.

Table 2.1. Comparison of Carbon-based material structure [59]

	DIAMOND	CNTs (Carbon Nanotube)	DLC (Diamond Like Carbon)
STRUCTURE			
HYBRIDIZATION	Crystalline (sp^3 bonding)	Amorphous (sp^2 bonding)	Amorphous (sp^2 & sp^3 bonding)
CONSTITUENT ELEMENT	C	C	C:H
PROPERTY	Insulator	Semiconductor/ Metal	Conductor
PROCESS	PACVD	Arc discharge, CVD	PACVD
PROCESSING TEMPERATURE	700-900 °C	800-1000 °C	300-500 °C

2.1.1. DIAMOND LIKE CARBON (DLC)

DLC is sp^3 hybridized, metastable, amorphous carbon with good mechanical, optical, chemical and tribological properties. DLC film has carbon bonded atom of sp^2 and sp^3 hybridization with sufficient quantity of hydrogen. DLC film possesses good chemical inertness, impermeability, biocompatibility, high hardness, scratch resistance and also have

good anti wear resistance and anti-sticking property [69-74]. Figure 2.1 shows SEM image of DLC coating surface and cross sectional images obtained by PIID and PEMS + PIID techniques [69]. Although DLC has been used widely as coating material but still doping of elements like fluorine, silicone, nitrogen, are widely used for enhancing frictional and wear properties. DLC coating is typically used in tools, engine components, automobile parts, internal coating of pipes, molds for soft metal. Wang et al. [37] examined that deposition of a fluorine-DLC coated film on Ti6Al4V alloy, reduces both friction coefficient and wear rate with increasing content of fluorine in DLC film, due to the establishment of anti-wear film with sufficient adhesion strength of F-DLC film and low friction coefficient is obtained on comparing with H-DLC coating [47]. The hardness and young modulus value decreases with increase in F-content. The H/E ratio (hardness/ young modulus) reaches upto 0.107. Dalibon *et al.*[75] concluded that thick DLC coating shows good wear resistance with low coefficient of friction and also exhibits low H/E ratio (0.1).

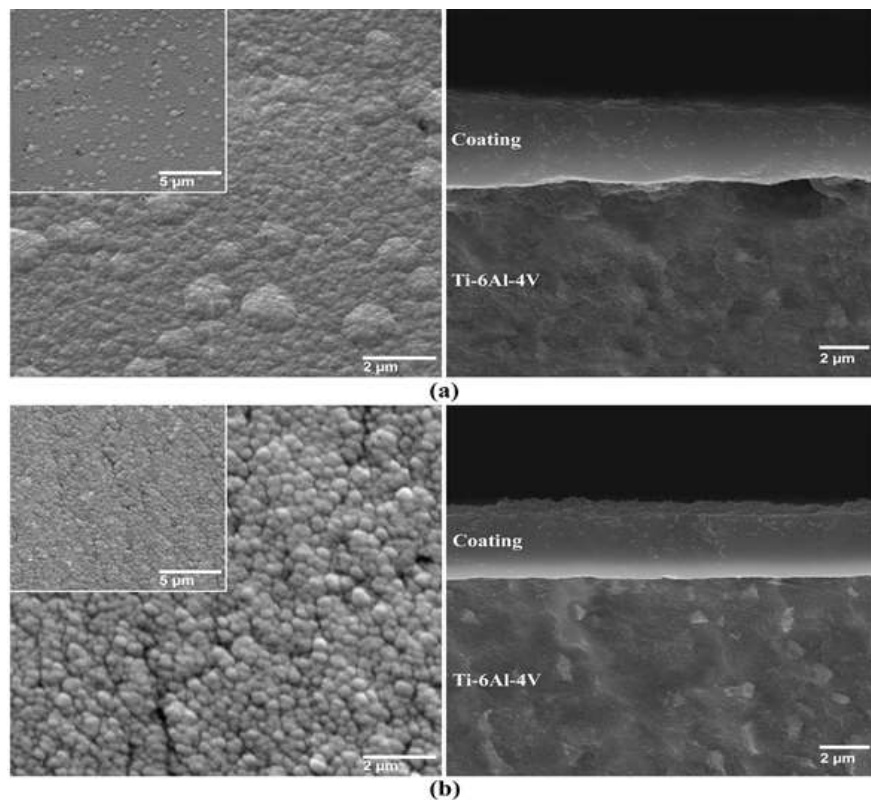


Figure 2.1 SEM image for DLC coating surface morphology obtained by (a) PIID and (b) PEMS + PIID techniques [69]

Figure 2.2 shows variation in friction coefficient value for multilayer DLC film, hard DLC film and soft DLC film at different lubricating (oil) conditions. Rubig et al. [40] studied tribological behavior on thick DLC deposition using plasma assisted chemical vapor deposition (PACVD). Under the lubricating conditions, it exhibited fatigue wear for polished

surface while no fatigue wear for the rough surface was observed. It was also observed that the use of excessive lubrication also helps in the elimination of fatigue wear. Arsalan et al. [41] who examined DLC film deposition on steel surface using hybrid magnetron sputtering technique revealed that with an increase in diameter and dimple density %, wear rate also increased. Increase in wear rate may be attributed to the decrease in load carrying capacity of line contact. It is also observed that optimum dimple density % and diameter significantly reduces friction coefficient and wear rate.

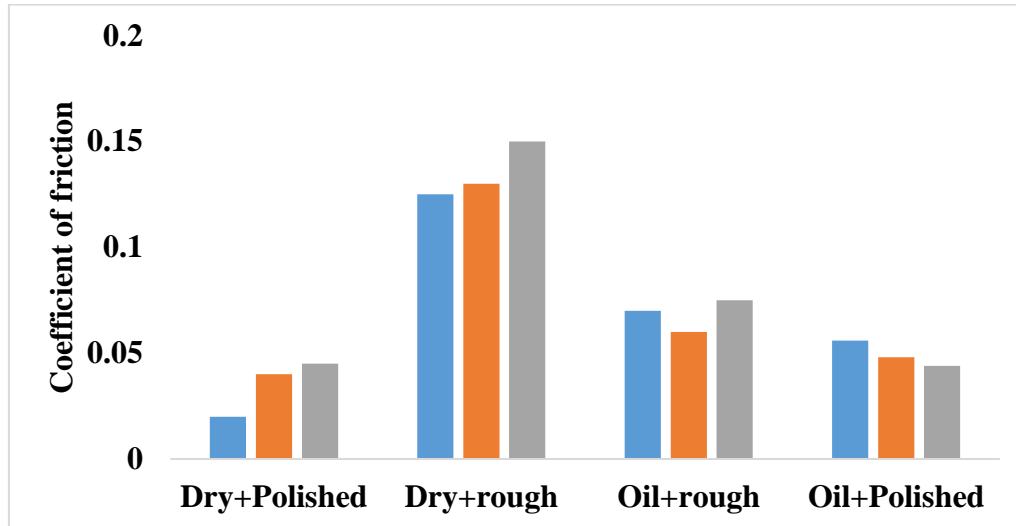
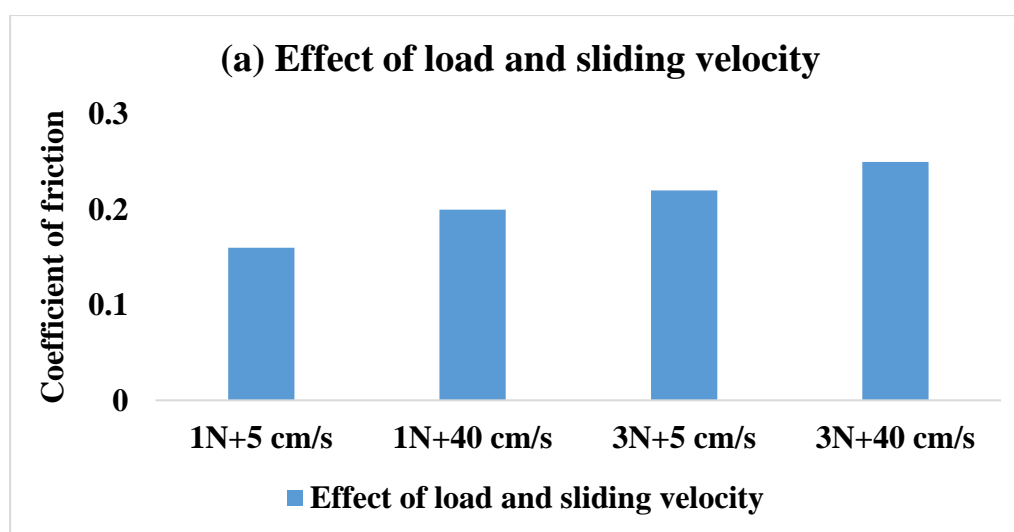


Figure 2.2 Variation in Friction coefficient value at different lubricating condition for (a) Multilayer DLC film (b) Hard DLC film (c) Soft DLC film [78]

Salvaro et al. [42] examined GCI surface coated with DLC layer using PECVD under a lubricating condition and further observed that DLC surface exhibited spalling wear (brittle) while GCI surface exhibited abrasion wear. DLC and GLC were seen to exhibit surface roughness value approx. 5.65 and 10.04nm, respectively and relatively dense and smooth surface morphology, when deposited using closed field unbalanced magnetron sputtering (CFUBMS) technique [43]. A study shows that DLC coating on counter surface reduces the friction coefficient values to about 0.1 and also protect the counter surface from scuffing wear upto the normal applied load of 600N [76]. Pillari *et al.* [77] examined magnesium alloy composite coated with DLC film using SEM technique and observed that DLC film is uniformly distributed in composite with excellent corrosive and wear resistance. DLC film can be categorized on the basis of hydrogen contents present in the film as hydrogenated (Dymon) and hydrogen free (Graphit) with a hydrogen quantity of about 40% and approx. 1%, respectively [78]. It is evident from the study that Graphit-iC shows good load bearing capacity, low friction and better wear rate under environmental condition and distilled water [79]. Hydrogenated DLC coating shows low friction coefficient, better wear resistance and

good stretch resistance [80] in comparison with hydrogen free DLC coating on CrCoMo alloy [81] while Zr-DLC coating on steel/silicon wafers [82] and Cr-DLC coating on Si/WC-Co cemented carbide [83] using magnetron sputtering show homogeneous surface morphology with low friction, good wear resistance and no oxidation on counter surface [82]. Mo-W doped DLC coating shows amorphous structure with dense, continuous columnar structure and low friction coefficient value of non-hydrogenated DLC coating on steel substrate at room temperature [84]. Akaike *et al.* [85] examined DLC, Si-DLC or F-DLC using DC pulsed PECVD technique and observed that F-DLC exhibit low static friction in comparison to other coating material. A comparative study of hydrogen free DLC coating on Ti6Al4V alloy shows good adhesion strength with better wear resistance on comparison with non-hydrogenated DLC film on CoCrMo and stainless steel substrate using FVCA technique [86]. It has been observed that plasma nitriding and DLC coating on steel show good wear resistance with improved friction coefficient, good fatigue strength, improved adhesion strength while no influence on mechanical properties like tensile strength was seen [87]. Si-DLC coated rubber shows almost 1.4 times increase in meyer hardness value than uncoated surface and COF value of coated surface 0.20-0.25, drastically reduces from 1.4-1.9 of uncoated surface [88]. Aboua *et al.* [89] results show COF value decreases from 0.0521 to 0.0314 as the temperature increased from 80°C to 100 °C, respectively. The effect of carbon diffusion on DLC surface coating leads to polishing wear and abrasive wear as the main wear mechanism. DLC coating on ACM rubber increases substrate adhesion strength higher than 40MPa and COF, due to good interface strength and viscoelastic property of substrate and film [90]. The effect of DLC coating material under different test conditions is illustrated in figure 2.3.



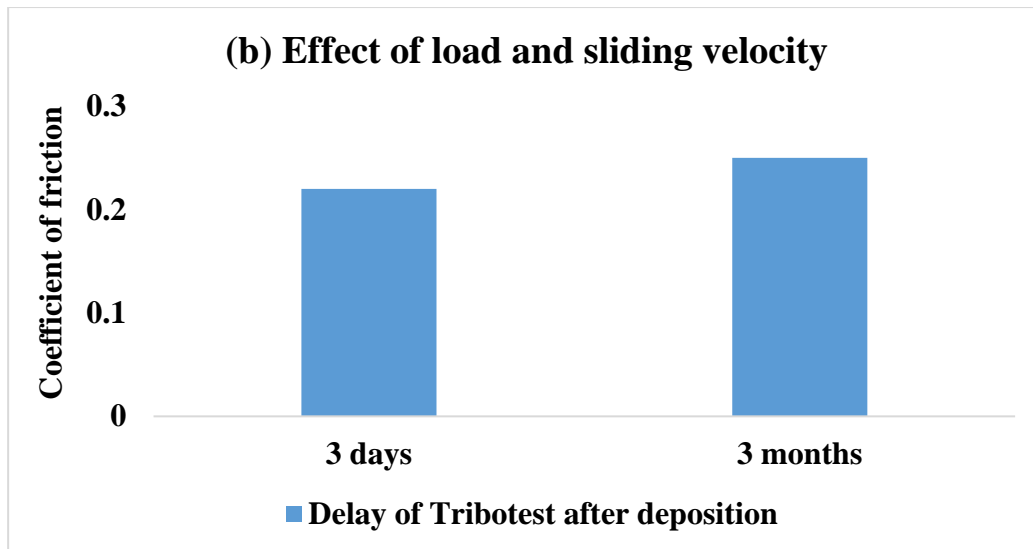


Figure 2.3 Variation in COF at different test condition of DLC coating (a) Effect of load and sliding velocity (b) Effect of sample aging [90]

Deposition of DLC film enhances wear resistance, shows excellent abrasive wear resistance with low mass loss, good corrosive resistance, improved adhesion strength, low coefficient of friction under dry sliding conditions and have anti wear properties which reduces the use of lubricant additives, and are dangerous to the surroundings.

2.1.2. CARBON NANOTUBES (CNT)

Carbon nanotubes possess self-lubricating nature with inherent physical as well as mechanical properties. Owing to unique characteristics, CNT enhances the distinct attributes of materials like tribological properties, thermal as well as electrical conductivity, and stability at high temperature, high durability and hardness. Application of nanotubes in Nano transistors, Nano cars, Nanodiodes, atomic instruments have made CNTs attractive/ a promising candidate for coating deposition. CNTs can be categorized on the basis of diameter formed by bending over a sheet of carbon nanotube into single-walled carbon nanotubes (SWCNTs) or multi-walled carbon nanotubes (MWCNTs). SWCNTs have a diameter range of 1-2nm while MWCNTs are less than 100nm in diameter formed by turning over a sheet of carbon nanotubes [56]. Even though SWCNTs are having excellent mechanical properties, they are not used widely as a coating material. SWCNT possess higher cost of fabrication and purification compared with MWCNTs. MWCNTs are prone to have “telescopic effect” i.e. an Inner layer of nanotube needs to be pulled-out by an outer layer of nanotubes under tensile strength. The MWCNTs surface can be modified using acid treatment via atom transfer radical polymerization (ATRP). The presence of a functional group like an

oxygenated group on MWCNT surface improves adhesive strength, COF and wear resistance as it plays a role of anchorage at the interface with adjacent layers [56].

A study based on inclusion of polyethylene oxide (PEO) in CNTs coating, reveals increase in interfacial force and adhesion strength between PEO-CNTs, which eventually results in reduction of friction coefficient value up to 0.3 as the wt. % of polyethylene oxide increased in the composite coating [54]. Another study observed a homogeneous dispersion of MWCNTs in nanocomposite coating with decrease in friction coefficient value to 0.419 at 300 mm/s and wear resistance when the sliding speed is increased. The decrease in values may be endorsed due to the graphitization effect of MWCNTs (formation of NiO and graphene layers) on the sliding surface [91]. Umeda et al. [92] examined low friction coefficient value of 0.19 on comparing with 0.95 values of uncoated surface, low wear rate and increased micro hardness value. This may be attributed to the formation of interfacial bonding and carbon solid-state diffusion between CNTs coating and Ti plate under dry sliding condition. The addition of CNT powder also enhances high temperature wear resistance, more static and lower friction coefficient value than the Ti substrate [93]. Sinha et al. [94] observed excellent wear resistance and low friction coefficient when ultra-high molecular weight polyethylene (UHMWPE) nanocomposite coating with 0.1 wt. % SWCNTs was used. It was also observed that under 240,000 cycle nanocomposite coating does not fail, when another experimental condition is 4N applied load, 0.41 m/s sliding speed, 2000 RPM rotational speed and sliding against steel, brass and Si₃N₄. Lee et al. [95] examined that as the applied load on a dual layer of Ag/CNT coating increases wear rate also increases but friction coefficient decreased. The nanocomposite coating shows excellent tribological properties, especially no wear on coating films, substrate or counter surface and low friction coefficient as observed in comparison to DLC coating. It was seen that with an increase in temperature, coefficient of friction value decreases up to 0.07. This decrease in COF may be due to fading of nanocomposite coating with a rise in temperature. Figure 2.4 shows variation in SEM micrograph, 2-D profile and EDX analysis of nanocomposite coating with an overcoat of PFPE at 80°C and 120°C [96].

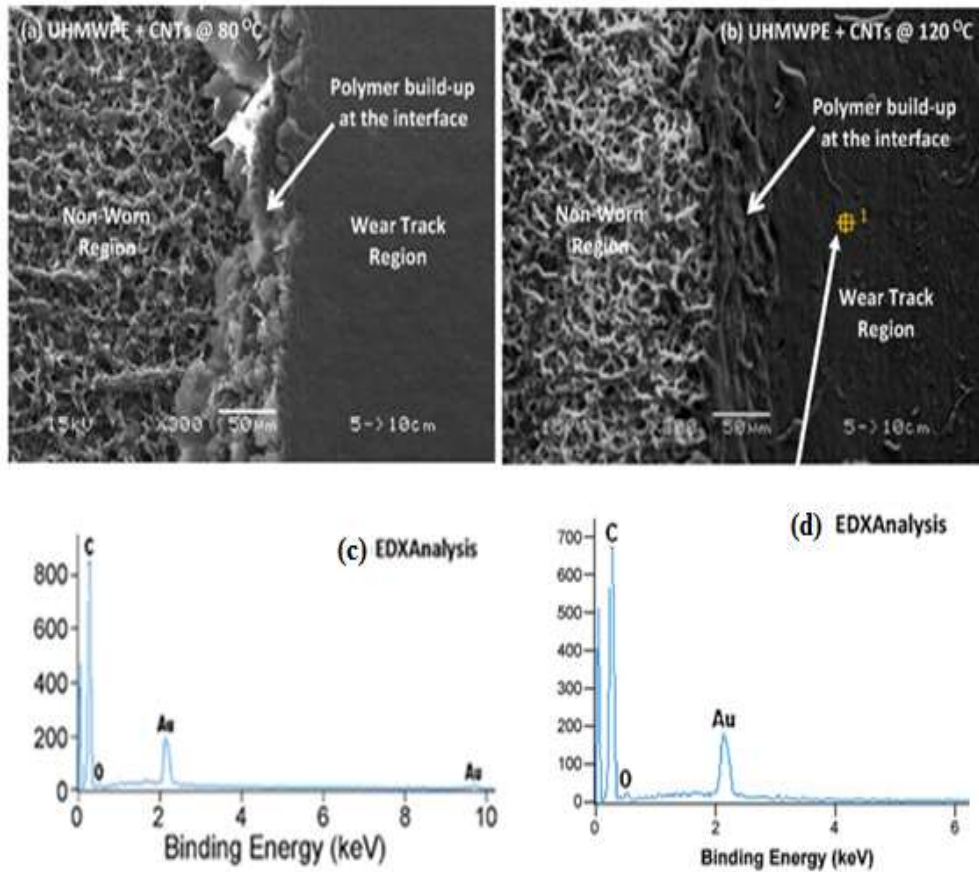


Figure 2.4 (a) SEM micrograph at 80°C (b) SEM micrograph at 120°C (c) EDX spectrum at 80°C (d) EDX spectrum at 120°C nanocomposite coating with overcoat of PFPE [96]

In the present work, deposition techniques, tribological conditions and properties of carbonous materials based coating on different substrate materials especially on steel based alloy are reviewed for piston ring application. Nevertheless, friction and wear behaviour are most interesting points not only for the researchers but also for the industrial purpose. Wear and frictional behaviour have a wide range of application in industries such as piston ring, ball bearing, and wind sheet wipers. Different Strategies have been discussed for successful deposition of CNTs/DLC film with a comparative study based on variable deposition condition. It is quite evident from literature survey that diamond-like carbon (DLC) has shown good anti-wear property, good anisotropic property with high thermal conductivity, good adhesion strength; when deposited on steel based substrate material and also chemical vapor deposition techniques (CVD), and magnetron sputtering deposition are most commonly used deposition techniques, to attain systematized coating with controlled and tailored properties. The coefficient of friction and wear value is much lower for DLC coated substrate than the corresponding uncoated substrate materials, since it separates and avoids the interaction between counter surface and substrate material, owing to carbon diffusion and viscoelastic

behaviour. Thus DLC coating along with good control system and optimum experimental conditions may contribute to improved life of piston ring and may reduce friction and wear between piston-cylinder arrangements.

2.2.DEPOSITION PARAMETERS OF CARBON COATING

There are several parameters which affect DLC/CNTs coating deposition process such as deposition rate, arc current, film thickness, patch size and deposition time. Table 2.2 shows deposition techniques along with deposition parameters used with CNTs/DLC as coating material. Salah et al. [97] examined deposition of DLC coating using pulsed laser deposition system with different substrate temperatures ranging from 100-500°C. The increase in substrate temperature induces a substantial change in the surface morphology of DLC film and also improved graphitization. Deposition temperature significantly affects the morphology, tribology and mechanical properties of a coating. When the deposition temperature of coating exceeds 400°C, deterioration in tribological characteristics of the coating is observed, due to formation of graphite phase [98]. Akbulut et al. [99] observed that Ni-Co/MWCNTs Nano composite coatings show excellent wear resistance, high load bearing capacity, higher surface roughness, and higher hardness value when deposited with DC (direct current), PRC (pulse reverse current) and PC (pulse current) electro-deposition methods. DC produced deposition result shows large grain size with irregular polyhedral crystals, while PC method result shows crystallite size grain and PRC method shows spherical cluster surface piled with equal sized grains. Deposition of C: H films on NBR with variable arc current and deposition rate using ETP-CVD technique was done and it was noted that at low arc current debris are formed which hold out the surface and results in higher friction coefficient. On the other end at high arc current hard and brittle C: H film is formed that contributes to rise in friction coefficient [100]. Deposition of CrN/GLC coating on a steel plate with 7.9 mm coating thickness, using arc ion plating and magnetron sputtering show good adhesive strength and 3% reduction in friction with almost 60% decrease in wear [58]. Ren et al. [60] observed homogeneous and uniformly dense surface morphology with low coefficient of fiction, low wear value and no grooves, depositing GLC coating on polyaryl-ether-ether-ketone (PEEK) using unbalanced magnetron sputtering with PVD system. The texture density for GLC film has no or little effect on tribological performance. A study based on the surface topography of coating material reveals that C:H:W film shows high surface roughness value while CrN/TiN coating helps in improvement of surface smoothness [101]. Ti-DLC film deposition on AISI 52100 steel using magnetron sputtering technique shows very fine and smooth worn surface morphology with small crystal dispersed in the amorphous phase and exhibits lower friction coefficient value

than PFPE [102]. Ti-DLC coating on Ti6Al4V alloy using PVD technique and variable deposition parameter shows good corrosion resistance, low friction coefficient and excellent wear rate using PBS solution [103]. Deposition of DLC film on rubber using magnetron sputtering technique [104-115] and using PACVD [104, 116-120] technique shows good surface morphology, excellent wear resistance, good solid lubricant and lower friction coefficient value. Another study based on DLC coating on HNBR using CVD technique in C_2H_2/Ag plasma shows crack and wrinkle surface morphology. It is also noted that COF value decreases from 0.182 to 0.167 as the wrinkle/ cracks increase on coated rubber [121]. The advancement in the coating process, now allows the researchers to exactly optimize the surface properties of the material which are required in the test condition. Table 2.2 (Appendix 1) illustrates film thickness, coating type and material used in the enhancement of different properties.

2.3. Tribological conditions of carbon based coating materials

Because of the impacts of carbon diffusion on the wear process, researchers assume that polishing wear and abrasive wear are the key processes involved in CNTs/DLC surface layer wear. Figure 2.5 depicts the four steps of the wear mechanism, which are further explained below:

1st stage: Asperities of DLC/CNTs film try to penetrate into the softer counter surface due to applied load, ultimately result in plastic flow of material around coated surface.

2nd stage: Plugging of counter surface by coated asperities results in abrasive wear, due to increase in frictional forces and temperature. An increase in carbon diffusion weakens the coated surface asperities, resulting in micro-cleavage.

3rd stage: Increase in carbon diffusion reduces atomic bond strength than frictional forces, which results in micro-cleavage in polishing wear. Hence, friction coefficient and roughness on coated surface decreases.

4th stage: Further increase in carbon diffusion implies weakening of coated film, increase in smoothness and decrease in friction coefficient. Strengthening of counter surface and smoothness of coated surface results in stabilization of friction coefficient.

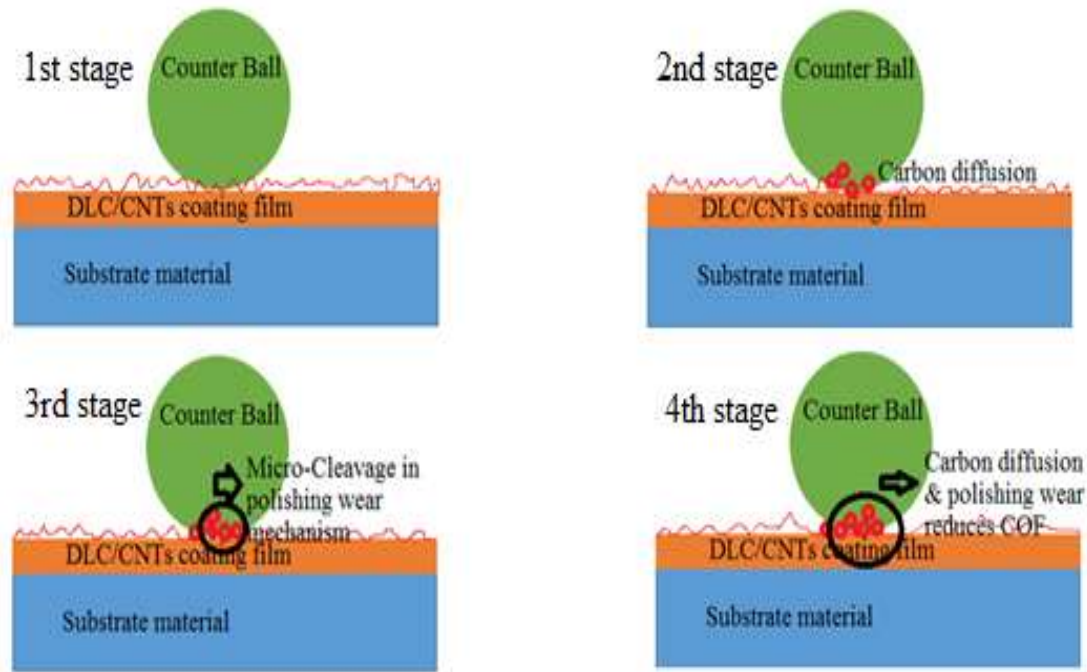


Figure 2.5 Process of wear mechanism [24]

In addition, there are several other conditions which may affect tribology of system. Table 2.3 (Appendix 2) illustrates experimental details of researchers, in order to enrich system performance. Details comprises of substrate material, coating material, deposition technique, tribometer, experimental condition like load, sliding speed, sliding distance, testing time, temperature used by researchers in their article with some concluding remarks. It is quite evident from the literature analysis that pin-on-disk [41, 43, 60, 61, 89] and ball-on-disk [37-39, 91-94] mainly used tribometers for tribological analysis. It is also seen that load and sliding velocity are the critical experiment conditions which govern increase or decrease in micro hardness, friction coefficient and wear resistance.

2.4.HIGH TEMPERATURE COATINGS

High temperature resistant coatings are intended to withstand temperature from 150°C to 760°C and protect materials from erosion and corrosion. Natural or inorganic materials such as epoxy novolac, epoxy or silicone can be used for high temperature resistance. In general, high temperature coatings can be distinguish into two different parts as;

- Diffusion coating, which is used when mass is diffused or shaped up with certain degree of synthesis.
- Overlay coating, which is used to deposit materials on the surface

High temperature processes is one of the most important and vital for critical parts incorporate in drive units, automotive, energy generation, chemical, waste burning, and coal

conversion industry, metal, ceramic and glass processing. Subsequently, erosion and oxidation are the materials degradation processes which have turned out to be vital life restricting processes that regularly restrain the service temperature and ultimately effects the unwavering quality and productivity. Since mid-1970s, thermal spray coatings have fundamental applications in automotive and gas turbine industries. Amid to this period, thermal spray coating have enormous upgradation in the properties, compositions and structures in tailor planned coatings with repeatable and controlled spray forms of parameters. The effective utilization of these coatings requires understanding of process parameters of spraying procedure, predictions of deteriorating mechanisms and prerequisites application.

Industrial use of high temperature coatings are:

- Power industry
- Aerospace industries
- Military grade coating
- Petrochemical industries
- Manufacturing industries

Industrial application of high temperature coatings are:

- Industrial coatings manufacturing
- Automotive coatings
- Original equipment manufacturers coating
- Aerospace coatings
- Custom coatings applications
- BBQ pit coating
- Construction protective coatings
- Industrial maintenance coating

Protective surface treatments are generally utilized both at low and high temperature. Currently, high temperature applications are mainly restricted to aerospace and automotive applications. Table 2.4 shows different coating functions and coating materials used at high temperature coating while table 2.5 shows general property criteria of coating systems for elevated temperature services.

Table 2.4 Shows the different coating functions and coating materials properties used for high temperature coating

S. No.	Coating Material Property	Coating Property
1	Hard particle inclusion	Improvement in abrasiveness
2	Radiative heat transfer and thermal conductivity should be lower	Surface temperature reduction
3	Hard, dense material	Particulate erosion resistance
4	Chemically stable and impervious oxide scale	Hot corrosion reduction
5	Rub tolerance via plastic deformation	Increased abrasability wear
6	Required thermodynamically stable oxide former	Oxidation rate drop

Table 2.5 General property criteria of coating systems for elevated temperature services

S. No	Coating property	criteria
1	Coating composition must reactant constituents to meet scale reformation and have protection ability;	Resistance to erosion and corrosion
2	Stress resistant	Microstructural stability and Mechanical strength
3	Smooth surface texture with precision cast component	Aerodynamic properties
4	Compatible with gross thermal or structural mismatch; and development of embrittling phases must be avoided	System adhesion, bonding and interface stability

2.5.ROLE OF THE COATINGS

Recent engine design patterns requires increased service life, reduced emission, higher efficiency and low fuel consumption. This encourages the researchers and industrialist to utilized lightweight materials like magnesium, aluminum and its alloys rather than using cast iron and steel for engine parts. As the wear, corrosion and friction behavior of aluminum and its alloys are not good for piston ring, cylinder liner, hence surface modification is essential for protection of surface.

A tribology study reveals that even 15-20% reduction in wear/friction can significantly reduce economic costs in relation to environmental benefits [1]. Regardless of their influence on environment change, almost an account 85% consumed energy were from economical fossil fuels. A study reveals that environment change may effectually alleviated or even reversed if

60% reduction is achieved by 2050 in harmful emission [2]. This is ample defy as 75% of the automobile industry is still proposed to rely upon the use of IC engines up to 2040 [3]. For the time being, the abrupt concern as regards of emissions and fuel economy have to be meritoriously addressed. The IC engines proficiency can be boosted through pertinent properties of fuel, operating conditions and mechanical design [4-6].

Modern engines endure higher mechanical and thermal loads because of their components high power to light weight ratio [7], nearly 4-15% fuel energy of IC engines was consumed to overcome friction [8] and almost about 40-55% of these losses were in accounts of piston rings [9]. There are fair number of analytical and experimental studies based upon inefficiency of piston rings. Today, significant gains in IC engine tribological performance are directly linked to surface geometry optimization, improved lubrication, and the use of unusual coating materials. Piston rings are of particular significance among engine components, as friction loses 40-45 percent of total energy. Piston assembly tribological performance has a significant impact on power loss, hazardous exhaust emissions, and fuel consumption. IC engine piston rings must maintain a dynamic seal under chemical, thermal, and tribological environments.

Piston ring failure is common phenomenon even after constant research of piston cylinder assembly and failure may arise due to wear, fluctuation in temperature, operating environment, fatigue, corrosion and oxidation. Surface modification or lubrication can improve piston ring wear resistance. The optimization of lubrication regime [10], surface topography [11-12], and surface modification [13] are all mentioned in the literature as ways to improve piston component performance.

To overcome wear, friction and for protection of surface, lubricant additives can be used for severe conditions. Boundary lubrication and elasto-hydrodynamic lubrication regime can be used between piston ring and cylinder liner contact. The use of additive in boundary lubrication can be used to reduce wear and friction, due to formation of tribo-film on the surface materials. The use of additives in engine oil, results in emission of various hazardous elements likes Zn, S, Mo, P etc., which affect the environments. To overcome this problems, different materials can be used for cylinder liner and piston rings, which are having ultra-low friction, high durability and wear resistant properties.

Surface modification or coating deposition is one of the most important approach in reduction of friction and wear. In coating deposition, thermal spray coating, HVOF, APS and Plasma Spray coating [128, 129] are one of the few deposition process which can be used to deposit material on light metal alloys. High hardness is responsible for high wear resistant and reduced friction. It is noted that metallic, composite and ceramic coatings shows good friction

and wear resistant properties on comparing with conventional materials used for piston rings and cylinder liner.

2.6.HIGH VELOCITY OXY-FUEL (HVOF) THERMAL SPRAY COATING

HVOF spray is one of the most popular thermal spray coating techniques which can approximately deposit 12 mm of thick layer and is having highest deposition rate on comparing with other techniques. HVOF spray works on supersonic gas speed with MACH no. greater than 5 [26]. In this process, large amount of fuel gas and air is supplied to combustion chamber. In combustion chamber, oxygen and spraying fuel are ignited. Gases flow through convergent-divergent nozzle with a speed greater than 1500m/s [26]. The commonly used fuel gases are propylene, acetylene, LPG, hydrogen and kerosene.



Figure 2.6 systematic diagram of HVOF thermal spray system

The systematic diagram of HVOF thermal spray system is shown the figure 2.6. In the present research, HIPOJET- 2700M metallizing system is for HVOF coating deposition. It is a low cost affordable system which can be used to provide good quality of coating. This process can be used to provide good characteristic properties with most economical cost in regards to environmental benefits [26]. There are various advantages of HIPOJET- 2700M coating system:

- High hardness
- Lower porosity

- Good wear resistance
- Thick coating
- High bond strength
- Fine finishing
- Good surface finish- as sprayed

The HVOF metallizing system consists of following main parts:

- Pressure Blaster
- Spray Booth
- HIPOJET-2700M Gun
- The control panel
- Powder Feeder
- Gas Vaporizer
- Hose Kit
- Gas and air control unit
- Air compressor

2.6.1. PRESSURE BLASTER

The MEC make PR-9182 model pressure blaster is used to deposit additive layer on the substrate materials with the help of dry compressed air. Abrasive particles comes out from the blast nozzle with high velocity and used for removal/ preparation of substrate materials. The dust produced during blasting process is collected using pressure blasting cabinet, which is used to reduce noise levels produce during blasting process and also used to ventilate dust and fumes from the chamber [26]. In this, a high efficiency fabric dust is used to collect dust. The systematic diagram of pressure blaster of HVOF thermal spray system is shown in the figure 2.7.



Figure 2.7 systematic diagram of pressure blaster of HVOF thermal spray system

2.6.2. SPRAY BOOTH (CYCLONE DUST COLLECTOR)

It is a type of mechanical separators which works on the principle of centrifugal force, and used to remove metallic or dust particles from air stream of spraying zone. It is also used to provide high separation velocity [26]. The systematic diagram of spray booth of HVOF thermal spray system is shown in the figure 2.8.



Figure 2.8 systematic diagram of spray booth

2.6.3. HIPOJET-2700M GUN

The spray gun is used to spray powder with supersonic velocity. The standard gun is set to spray HVOF grade powders using a fuel gases like LPG (Liquefied petroleum gas), propylene, propane or natural gas. In our present research MEC make HIPOJET-2700M Gun is used as spraying gun for powder [26]. The systematic diagram of HIPOJET-2700M Gun of HVOF thermal spray system is shown in the figure 2.9. The internal axial-feed powder injection is a feature of the gun design. High thermal efficiency, maximal particle heating, and unrestricted gas and powder movement are all possible thanks to specially built water-cooled gas mixing and combustion chambers. High particle velocities create dense, low oxide coatings as a result, which lowers operating costs. Since every hose connection enters the cannon axially, the overall design is streamlined and small. The adaptable gun body design enables simple maintenance procedures.



Figure 2.9 HVOF spray gun HIPOJET® 2700 [26]

2.6.4. Control Panel

The MEC make control panel model one of the most important part of HIPOJET-2700M HVOF powder spray system which is connected between gun and gas supply and also acts as a heart of HVOF system. It is a precious equipment used for measuring and regulating oxygen flow, air and fuel gas to HVOF powder flame spray gun [26]. It is one of the most reliable gas flow indicator which aids to highest quality of coating. It is a durable device made for securely regulating and monitoring the oxygen, fuel gas, and air flow to the HIPOJET-2700 Spray Gun. It is a dependable gas flow indicator and aid to the greatest coating quality because it is connected to the gas supply and the gun.

This console has three pressure gauges: one for oxygen (0–21 kg/cm²), one for fuel gas (LPG or propane) (0–10 kg/cm²), and one for air (0–10 kg/cm²). Gas regulators and air regulators

installed on gas cylinders and air control units, respectively, allow the pressure to be adjusted. In order to measure the flow of these gases in SLPM, the control panel also includes three flow metres (one for oxygen, one for fuel gas, and one for air). The systematic diagram of control panel of HVOF thermal spray system is shown in the figure 2.10.

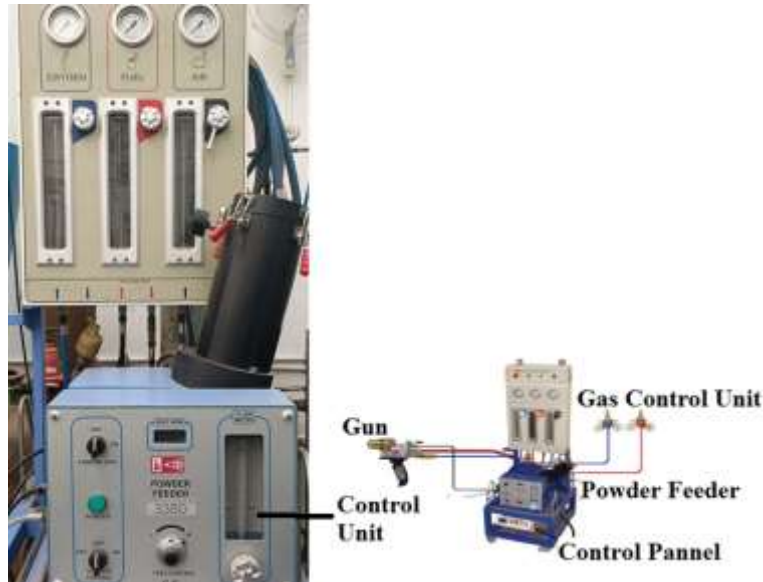


Figure 2.10 HVOF powder spray system used in the current study [26]

2.6.5. Powder Feeder

The MEC make PF-700/PF-3350 powder feeder is used as accurate powder feeder system in thermal spray applications. The powder feeder system consists of powder container pressurized by carrier gas, in which powder is filled in the slot of powder wheel. The powder wheel delivers the powder to powder feed hose, where carrier gas carries the powder to spray gun [26]. Powder is inserted into slots in the powder wheel at the canister's base. The powder is forced into the exit ports by the rotating powder wheel. The powder is moved from the exit ports through the powder hose and onto the thermal spray gun by an inert carrier gas. To endure the spray environment, the system is constructed. Optional temperature control for the blanket heater with configurable increment. The systematic diagram of powder feeder of HVOF thermal spray system is shown in the figure 2.11.



Figure 2.11 systematic diagram of powder feeder of HVOF thermal spray system

2.7.HVOF BASED COMPOSITE COATING FOR WEAR RESISTANCE APPLICATIONS

Using the HVOF thermal spraying process, Tyagi *et al.* created a carbon coating on a cast iron substrate with a blend of NiCr, CrC, Mo, and carbon powder for piston applications. Wear testing the coated substrates on a high temperature tribometer was used to improve the abrasion resistance qualities of the carbon-based composite coating, which is critical for piston coating applications. The authors used the Signal to Noise ratio and Taguchi approach methodology to validate the test results. The scientists made several noteworthy observations, including a decrease in wear as the coating temperature increased, which could be related to the development of carbides at the specific temperature of 300°C as evident from the lowest wear at that particular temperature. [128]

Agüero *et al.*, coated AISI 4340 low alloy steel substrates with WCCoCr composite powder by using High Velocity Oxy-Fuel thermal spray. The authors used powder particles with different sizes and flame energies to obtain different results, and observed that the use of HVOF resulted in the generation of WCCoCr coating with extremely low porosity and high density and hardness, when compared to simple electrolytically plated Cr hard coating. While the WC particle sizes didn't really affect the quality of the coating significantly, the smaller particle size powder led to a greater spraying efficiency, and thus led to cost cutting. It was thus confirmed, that the WCCoCr coatings can be successfully used in landing gear actuators, and show better performance than electroplated Cr hard coatings. [131]

Bhosale *et al.*, developed sprayed composite coatings of WC-Cr₃C₂-Ni by using High Velocity Oxy-Fuel technique. The composite coating was wear tested using a ball-on-disk tribometer at ambient temperatures using alumina ball as a counter body. The authors noted that HVOF led to the formation of dense coatings due to the high kinetic energy of the particles being sprayed on to the substrate, as well as formation of splats that stack over each other, which resulted in a lower porosity of the coating. The authors concluded that wear resistance of WC-Cr₃C₂-Ni coated specimens is much lower than uncoated specimens, thus coatings can be employed in automotive and aeronautical applications [136].

Picas *et al.*, argued the viability of HVOF sprayed chrome over traditional hard chrome platings due to the toxic features of the latter towards the environment and the human health. The authors, thus, obtained three CrC-NiCr powders and deposited them using HVOF to generate coatings, and upon wear testing realised that the tribological and mechanical properties of the coatings depended upon the carbide and agglomerate size generated by the powders due to the coating process. The authors also noted that the finer sized powders resulted in coatings with lower hardness, and being more prone to wear [137].

Pandey *et al.*, investigated the Mo blended composite coating that was successfully deposited on steel substrates via HVOF thermal spray. The authors intended to enhance the residual stresses by using Taguchi method. ANOVA method was used by the authors to analyze the process parameters of Taguchi method (temperature, load and frequency) for the Mo based composite coating. It was experimentally found that for percentage change in residual stresses, the biggest contribution is shown by temperature (64.19%), followed by frequency (21.82%) and then followed by load (6.31%) [138].

Bolelli *et al.*, deposited WC-10Co4Cr hardmetal coatings using both HVOF and HVAF thermal spray methods and subjected these generated coatings to tribological testing. The authors observed that both HVOF and HVAF were capable of generating WC-10Co4Cr coatings with high density. HVOF was found to cause higher carbon loss and thus had lower WC content than HVAF in the coatings. It was also noted that the finer the feedstock powder used for coating, denser and harder is the coating that is produced. It was also observed that the coatings formed by both HVOF as well as HVAF at room temperatures have better performance than hard electroplated chromium coatings [139].

Lee *et al.*, investigated the effect of mixing of feedstock powder with different particle sizes on the wear and fracture resistance of WC-10Co-4Cr coatings, that are deposited using HVOF thermal spray. The dry sliding wear properties of these coatings prepared with different powder

sizes and powder mixing ratios were assessed using a pin-on-disk tribometer at room temperature. The authors observed that the tribological properties of coatings sprayed with mixed powders are much better than the coatings generated using single powders as the feedstock. This observation was attributed to the decrease of porosity and hence the increase of hardness of the coating due to using powders with different particle sizes [140].

Keshavamurthy *et al.*, compared the wear resistance characteristics of tungsten carbide HVOF coating on a steel substrate along with a hard chrome electro plated steel substrate. The authors developed the said coatings, and then subjected the coatings to a characterization using SEM (scanning electron microscopy) and XRD (x-ray diffraction) and then subjected the coated substrate to a wear test on a tribometer. The experimental results showed that at all loads and sliding velocities of the pin on the coated substrate, the wear resistance of WC (tungsten carbide) was much better than hard chrome coated substrate. It was hence concluded that HVOF sprayed tungsten carbide coatings are good alternatives to hard chrome plating for wear resistance applications [141].

Ramesh *et al.*, deposited Mo and Mo-10%SiC coatings on mild steel substrate using high velocity oxy-fuel thermal spray. The coated specimens were subjected to characterisation using SEM and EDAX. Molybdenum was selected as the coating material since it's a transitional metal having low thermal coefficient of expansion and can also act as a lubricant. Microstructural studies of the coated substances highlighted grain refinement due to unique dispersion effects due to the addition of SiC. The microhardness studies highlighted an increase of 7% micro-hardness in Mo components and 23% increase of micro-hardness in case of Mo-10%SiC in case of comparison with an uncoated Mild Steel substrate [142].

Walia *et al.* produced a powdered blend of iron-molybdenum composite, NiCr, CrC, and Mo for a piston ring coating that was coated utilising plasma thermal spray. The authors planned to gradually raise the weight by weight proportion of NiCr from 10% in the first coating blend to 50% in the final coat blend, with 10% increments in between. The scientists used a pin-on-disk tribometer to evaluate the coated substrates and found that as the weight by weight percentage of NiCr increased, the specific wear rate of the coated substrates decreased. It was discovered that the coated substrate with a 50 percent NiCr weight by weight composition wore and abraded the least [143].

Picas *et al.*, investigated the impact of HVOF spray parameters on the coating generated by thermal spraying WC-CoCr powders on a substrate. It was observed by the authors that the particle temperature in-flight as well as the kinetic energy and velocity of the coating particles

affect the hardness, density and wear resistance of the generated coating. The greatest hardness and wear resistance was observed in those coatings which provided the agglomerates sufficient duration to completely melt and hence generate splats with less porosity. The authors also observed that almost all HVOF sprayed WC-CoCr coatings showed better mechanical and tribological properties than substrates with electroplated hard chrome [144].

Zhao *et al.*, studied the impact of spray parameters and other particle in-flight properties on the on the mechanical and tribological properties of the generated coatings using on-line particle monitoring. The authors studied substrates coated using WC-CoCr powder, thermal sprayed using high velocity oxy-fuel (HVOF). The wear behaviour of the coated substrates was then evaluated by rubber wheel testing and pin-on-disk tribometer wear testing. The authors found that the powder feed rate and the total gas flow rate influenced the particle in-flight properties. It was concluded that a higher gas flow rate leads to a shorter spray distance and lower powder feed rate, whereas higher particle temperature and velocity leads to harder and denser coatings [145].

Bolelli *et al.*, produced a TiC – 25vol.% (Fe-20wt.%Cr-5wt.%Al) powder by high energy ball milling for wear and corrosion which was free from hazardous than WC-CoCr and Cr₃C₂-NiCr, and was processed by High Velocity Oxygen-Fuel spraying. hard and dense layers was obtained with plausible good deposition efficiency of 54%. TiC-FeCrAl on tribological testing unveiled that coatings are favourable for sliding contacts. Ball on disc wear rates were significantly lower than HVOF-sprayed Cr₃C₂-NiCr reference against an Al₂O₃ counterpart, both at 400°C and at room temperature but still WC-CoCr. Performed better. For high stressed abrasion TiC-FeCrAl coatings appeared resulted by extensive brittle fracture less befitting since higher wear rates than HVOF-sprayed Cr₃C₂-NiCr. Limited corrosion resistance of FeCrAl matrix was observed when electrochemical polarization test in 0.1 M HCl was conducted [146].

Dave *et al.*, deposited chromium based coatings like CrN and Cr₂O₃ using RF reactive magnetron sputtering. Standard tooling materials like brass, aluminium and mild steel acted as substrates with identical dimensions for the coatings to be deposited on. These coated substrates were then wear tested using pin on disk tribometer at variable loads and sliding speeds. The authors observed that the chromium coated substrates had a greater wear and abrasion resistance as well as longer service life, thus concluding that coatings can improve the longevity of materials [147].

Wang *et al.*, deposited WC-Co coatings onto grit blasted mild steel substrate using High Velocity Oxy-Air Fuel thermal spray, in order to study the effects of high temperature on the

wear properties of the coating. The temperature for sliding wear tests was varied from 25°C to 550°C, and it was found that the minimum coefficient of friction and wear rate was observed at 450°C. This reduced friction was attributed to the formation of oxides like WO₃ and CoWO₄, which had a lubricating effect on the coating. The substrate heat treated at 450°C was also found to show the maximum value of Vickers microhardness at 1378 HV [148].

Venkatesh *et al.*, studied the wear behaviour of Chromium carbide-Nickel rich alloy MMC coatings with different varieties of carbide contents at ambient temperature and 600°C, generated using laser cladding technology. The wear rate of the coatings was observed to be a function of the percentage of carbide content in the coating which was significantly higher at 600°C when compared to 25°C. The authors also observed that laser clad coatings were much more abrasion resistant than detonation gun sprayed and plasma sprayed coatings at the elevated temperature of 600°C. This was attributed to weak bonding of the splats to the substrate and to each other in cases of detonation and plasma sprayed coatings [149].

Gong *et al.*, suggested the immense potential of WC-Co-Cr coatings to replace traditional hard chrome platings on aircraft landing gear, owing to their great wear resistance and environmentally favourable properties over hard chrome platings. The authors mixed WC particles into the coating during deposition via two types of single particle size distribution as well as two different types of bimodal particle size distributions. After checking the microstructure and the wear behaviour, it was observed that the coating containing single particle size distribution of 1.2 µm-sized WC particles showed the best wear resistance [150].

Venkateswarlu *et al.*, used high velocity oxy-fuel (HVOF) and oxy-acetylene (OA) thermal sprays to deposit diamond reinforced composite (DRC) coatings with different amounts of diamond content and then subjected these coated substrates to two body wear tests. The results of the wear tests showed that the HVOF sprayed coatings showed a less specific wear rate than the oxy-acetylene sprayed coated substrates. This difference in wear rate was attributed to the increase in abrasive grit size from finer to coarser. The authors concluded that HVOF sprayed specimens showed better resistance to abrasion due to the lower porosity of the coating, and the higher bond strength between reinforced particulates and the matrix [151].

Federici *et al.*, investigated the dry sliding tribological properties of cast iron disk samples coated with WC-10Co-4Cr and Cr₃C₂-25NiCr using HVOF, against uncoated samples of the cast iron disk at room temperature and at an elevated temperature of 300°C. These coated and uncoated samples were subjected to wear testing using a pin on disk tribometer. It was observed that the uncoated sample faced extremely high wear rate at elevated temperature due to the

thermal softening of the substrate, whereas in case of the coated samples, the wear rate was close to negligible, due to a lack of sufficiently high temperature to induce softening of the coating. The study affirms and indicates the viability of using HVOF thermal spray to coat materials for braking system applications and other automotive contact applications to ensure the longevity of the parts and reduce the release of particulate matter in to the environment [152].

Zhang *et al.*, deposited WC-10Co-4Cr and Cr₃C₂-25NiCr coatings on H13 steel substrate using high velocity oxy-fuel thermal spray in order to investigate the microstructure, wear resistance and thermal shock of the said coatings. The author also sprayed NiCr powder between the substrate and the coating to improve the thermal stability of WC-10Co-4Cr. Upon conducting the said experiments, the authors realised that the adhesive strength of Cr₃C₂-25NiCr (64.40MPa) is far superior to that of WC-10Co-4Cr (61.69 MPa). The friction and wear tests of both the coatings led to the confirmation of Cr₃C₂-25NiCr having a much better abrasion resistance to WC-10Co-4Cr, despite having a greater coefficient of friction at 500°C and 600°C [153].

Thiruvikraman *et al.*, used statistical techniques like response surface methodology (RSM), analysis of variance (ANOVA) and regression analysis to establish empirical relationship between the parametrs of HVOF thermal spray coating with coating characteristics like adhesion bond strength and lap shear bond strength of HVOF sprayed WC-CrC-Ni coatings [154].

Zórawski *et al.*, deposited two different coatings containing a blend of the NiCrBSi and Fe₂O₃ powders using High Velocity Oxy-Fuel and Plasma spray respectively. The phase composition of both the sprayed coatings was then determined and analysed by the authors using X-ray diffraction. The authors observed that the use of plasma spray stream caused the transformation of haematite in to magnetite, whereas such transformation in case of the HVOF spray was minimal. The intensity of the generated Fe₂O₃ and Fe₃O₄ peaks was also found to be significantly different in case of the plasma and the HVOF sprayed coatings. It was ultimately concluded that in case of plasma sprayed coatings, the coefficient of friction depended upon the pressure of the plasma gas used, whereas in case of HVOF sprayed coatings, the presence of the amount of Fe₂O₃ dictated the value of the coefficient of friction of the coating [155].

Pulsford *et al.*, argued the functionality and the excellence of High Velocity Oxy-Fuel thermal spray method for generating coatings in situations where complex shaped parts of a substrate can't be coated with line of sight based coating methods, and thus developed WC-Co-

Cr coatings inside cylindrical pipes having internal diameters of 70mm, 90mm and 110mm. The generated coatings and microstructures were analyzed using XRD, SEM and EDS. These coated pipes were subjected to wear testing at loads of 96 N and 240 N using ball on disk tribometer by the author, and it was found by them that the coating sprayed on the 90mm pipe had the greatest microhardness and fracture toughness which led to lower specific wear rate at all loads, and the pipe with 110mm internal diameter had the greatest specific wear rate at all loads due to poor inferior toughness [156].

Das et al., developed a HVOF feedstock containing a mixture of bronze and 10 wt% diamond powder by ball milling on a bearing steel substrate. Mechanical and microstructural properties were analyzed of these reinforced coatings and compared to pure bronze coating. Ball on disc sliding configuration was used to assess tribological performances of these coatings using a Cr steel counter body. A notable improvement in the wear resistance was perceived in bronze coatings reinforced with diamond. Plastic deformation of the uppermost layer was observed in case of pure bronze coatings. With the addition of diamond phase, a reduced degree of plastic deformation was observed [157].

For the last many years, HVOF has proved its significant importance after undergone considerable changes in its technology which is completely industrial-based to thermal spraying technology. It has been already proved from many studies that coating developed by HVOF is far superior to other thermal spray coatings and these coatings are more compatible with cemented carbide. The coating developed with the use of HVOF technology has good tribological properties such as low porosity, high density, which provides a uniform coating on the surface of substrates. Nevertheless, excess amount of heat release during the coating on to the substrate in HVOF spray process, so special care is required for cooling process or break off spraying process can be used for preventing from the surface defects. HVOF techniques are restricted to the coating of ceramics material because it works at high temperature and not support the ceramics material and causes defects. There are several deposition parameters of the HVOF process that affect carbon-based composite coatings such as fuel rate, carrier gases, deposition time, powder feed rate, spraying distance, and coating thickness.

There are several parameters as shown in table 2.6 (Appendix 3), which affect HVOF coating deposition process such as deposition rate, additive layer, arc current, deposition time, film thickness, and flow rate.

2.8.RESEARCH GAP

Even though a deeper and more thorough understanding of tribological systems has been achieved, there are still a few aspects that need to be investigated in order to procure a more precise system. Carbon coating has been attempted to be used in a functional application. It must be stressed that a realistic mechanism between the substrate material and deposition parameters, such as deposition rate, additives used, temperature change, and so on, must be developed for better results. We have constructed an effective tribological system to far, but there are still a number of aspects that need to be considered in order to improve the system:

1. Few research has been carried the deposition of agricultural waste based carbon Coatings using HVOF technique.
2. Enough effort must be made to create environmentally friendly piston ring coatings.
3. Enough effort has not been put into improving deposition efficiency and productivity in terms of particle size. Determination of the best deposition technique, as well as process factors such as deposition rate, arc current, temperature variation, additives employed, and surface treatment, among others.
4. Various scholars have differing viewpoints on the effect of some of the variables on the response parameters, such as the sliding velocity, applied load, temperature, distance, and time, as well as relative humidity.

After reviewing the literature critically, brainstorming with the supervisors and field expert, the research gap and the objectives of the present study have been formulated. The present investigation is mainly focused on the development and characterization of carbon coating for piston ring applications.

3.1.SCOPE

The heart of the engine is its piston and piston rings. The longevity of the piston and piston rings directly affects the engine's lifespan. The life and efficiency of the engine may be impacted by micron-sized wear. Therefore, in order to improve engine efficiency, researchers must lengthen the lifespan of the piston and ring assembly. As needed, a layer of a different material can be put to the piston ring at a precise thickness to extend the life of the ring and liner subsystem and decrease wear. The piston rings can be coated using a variety of deposition techniques, including physical vapour deposition, hard chrome plating, chemical vapour deposition, high velocity oxy-fuel coating, etc. Because of its high deposition efficiency, flexibility to deposit a variety of materials, and low deposition cost, the HVOF technology is the most adaptable.

The automobile industry faces a tremendous problem in trying to improve the effectiveness of piston-cylinder assembly and extend the life of piston rings without raising production costs. Previous initiatives mostly aimed to lessen friction between rings and cylinder liners. It has taken a while to develop coating that is resistant to wear. The wear-resistant coating for piston rings application was developed previously, but little effort was made to optimise the coating formula utilised for the application. Furthermore, the substrate material needed for the coatings deposition and piston rings tribo test was not prepared internally.

3.2.RESEARCH OBJECTIVES

In light of the gaps mentioned above, the present investigation aims to develop the coatings for the pistons ring applications with the following objectives:

- Development of environment friendly carbon coating on substrate material used for piston ring applications.
- Characterization of developed coatings with the help of SEM-EDS, Raman spectral test, and XRD.

- Analyze the various response parameters on developed coating i.e. residual stress, surface roughness and micro hardness used for piston ring application.
- Study of high temperature wear behaviour of developed coating on substrate material.
- Comparative analysis of developed coatings for piston ring application.

3.3.RESEARCH METHODOLOGY

The proposed research work is aimed at studying the mechanical and physical properties of some coating on substrate material used for piston rings application. Figure 3.1. shows the research methodology used in the present study. The work will comprise of following phases:

- HVOF technique available in DTU, will be chosen to provide good physical & mechanical properties to the piston rings.
- Candidate materials for the study will be selected in consultation with automobile industries of Delhi-NCR.
- The bonding of the particle on the substrate depends on the formation of adiabatic shear bonds at the interface.
- The analysis was made to determine the nature of bonding viz. Mechanical, metallurgical and chemical.
- The influence of surface quality and surface properties were analysed to explain the nature of bonding based on analysis of the interface.
- The wear behaviour of the coated sample, as well as uncoated samples in an actual working environment of power generation system by the help of tribometer, was done.
- To characterise the products formed on the surface during testing and the analysis was done using X-ray diffractometer (XRD), Scanning Electron Microscope (SEM).
- The study of the frictional behaviour of the coating was done using high temperature Pin on Disc tribometer and the wear behaviour of the coating under different operating parameters.

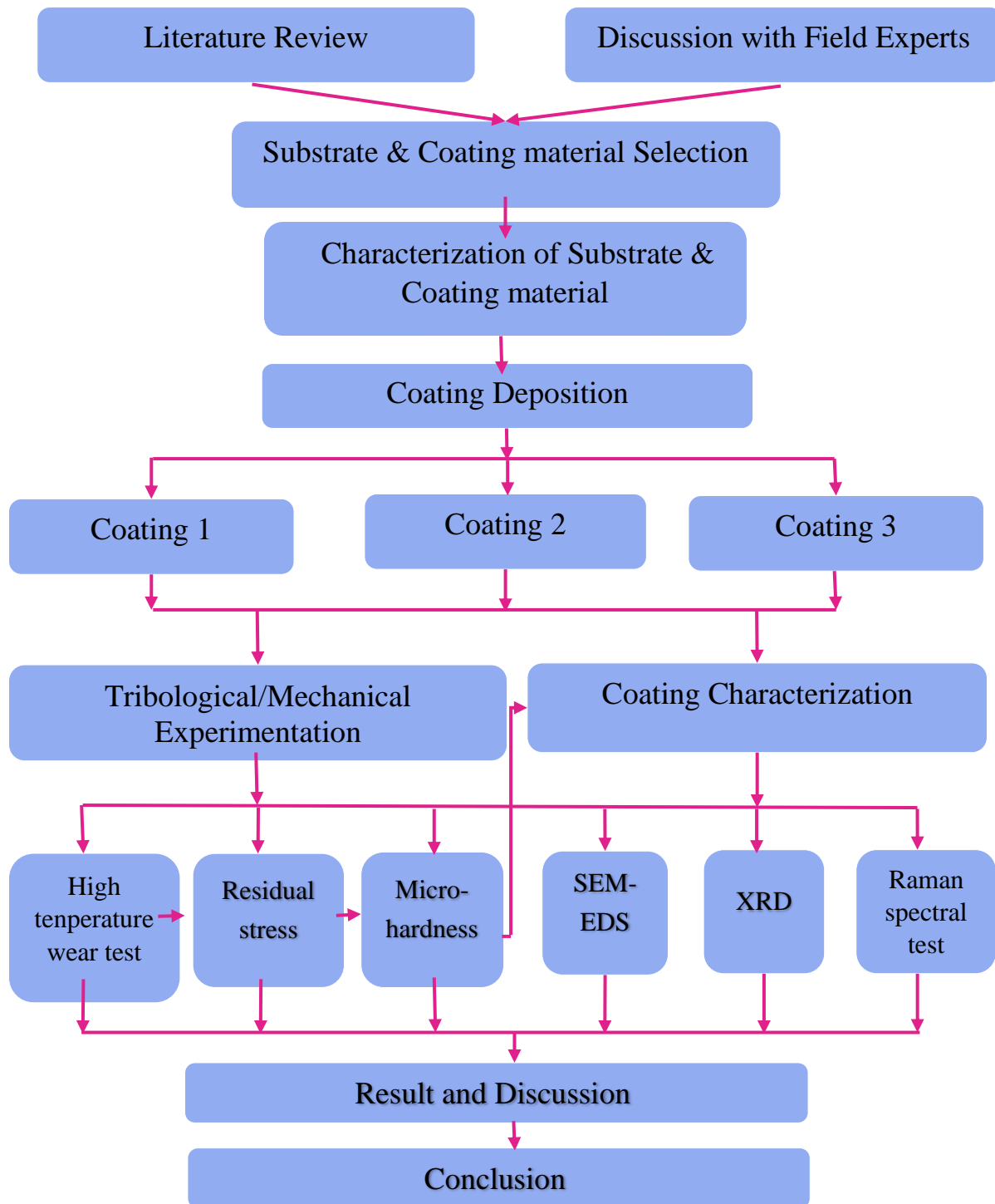


Figure 3.1. Flow diagram of research methodology

This chapter contains a description of the experimental equipment used and the procedures adopted for deposition, characterizations and tribological investigation of the deposited coatings

4.1. SAMPLES CHARACTERIZATION

4.1.1. FIELD EMISSION SCANNING ELECTRON MICROSCOPY

JOEL manufactured FESEM attached with EDS, accessible at IUAC, Delhi, was used to evaluate the surface morphology, elemental, and microstructural composition of produced coatings, as shown in fig.4.1 [184, 193]. It's a type of electron magnifying lens that captures images of the item by inspecting it with high-vitality light. The electrons work with the iotas in the specimen to deliver signals. "Coating prevents the specimen from accumulating static electric charge during electron irradiation." Because the specimen chamber is under high vacuum, a sample for SEM must be entirely dry. To examine the microstructure of the coating material used to protect the wear track. Subsequently it was placed on a job holder, which was then transferred inside the scanning electron microscope's chamber. The surface morphology of the wear track was determined using scanning electron microscopy, which revealed the wear mechanism under varied loading circumstances and speeds. To examine surface morphology through FESEM, Working Distance=12600 um, Accelerating Voltage=15000 Volt, Magnification=1000, Emission Current=80000 nA Deceleration Voltage = 0 Volt, etc. parameters were chosen.



Figure 4.1 Systematic diagram of FESEM attached with EDS

4.1.2. HIGH RESOLUTION X-RAY DIFFRACTION

HRXRD (PANalytical systems) was used to characterise and confirm the crystal structure and phase identification of coatings utilising Cu anode material, 45KV generator voltage, and 40mA tube current in conventional Bragg mode at IUAC, Delhi, as shown in fig. 4.2. (a) [184, 193]. The scattering pattern formed when a beam of radiation or particles (such as X-rays or neutrons) interacts with a substance is used to analyse the structure of the material using an X-ray diffractometer. A typical diffractometer has a base of emission, a monochromator for wavelength selection, slits for beam shape control, a sample, and a detector. The use of a semitransparent beam stop allows the odds to calculate the amount of radiation absorbed by the sample based on the intensity measured during the beam stop. The worn surface specimen was placed in an X-ray room. The specimen was scanned from 10 to 120 degrees, using a scanning speed of 2 degrees per minute, as shown in fig. 4.2. (b).

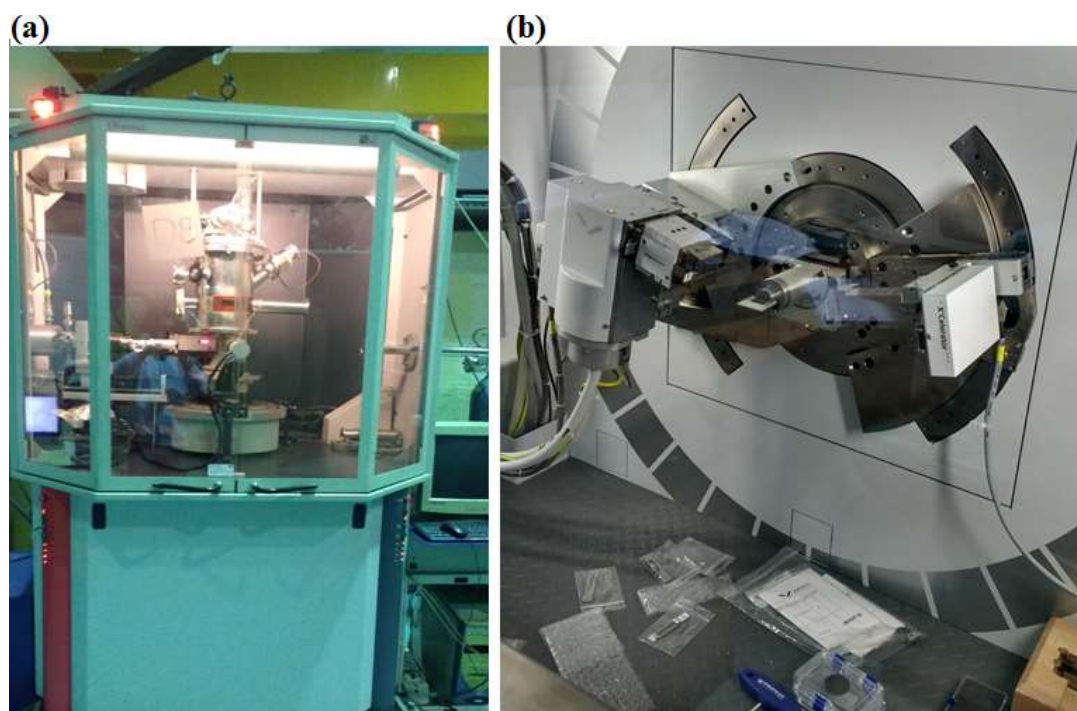


Figure 4.2 (a) systematic diagram of HRXRD (b) angle of diffraction angle from 10° to 120°

4.1.3. RAMAN SPECTRUM

The micro-Raman spectrometer (Renishaw) with a spectral range of 3500 cm^{-1} and a resolution of 1 cm^{-1} , available at IUAC, Delhi, was utilised to characterise and confirm the peaks of elements contained in the produced coatings, as shown in fig. 4.3. The technique of Raman spectroscopy has been widely employed to investigate the structural features of carbon coatings.

Along with hydrogen, the carbon coating (C:H) contains sp², sp³, and even sp¹ bound carbon sites.



Figure 4.3 systematic diagram of Raman Spectrum

4.2.MECHANICAL TESTING

4.2.1. SURFACE ROUGHNESS MEASUREMENT

Surface roughness was measured by Taylor Hobson precision machine having resolution of 0.01 micrometer. The surface roughness was measured after polishing at different points on the coated samples. The average surface roughness are reported in the chapter 5 of present study. The specimens are ground with 80-2000 grit emery paper and polished with 1/0, 2/0 and 3/0 grit alumina paste powder. Fig. 4.4 shows the systematic diagram of Taylor Hobson precision machine used to measured surface roughness in present study.

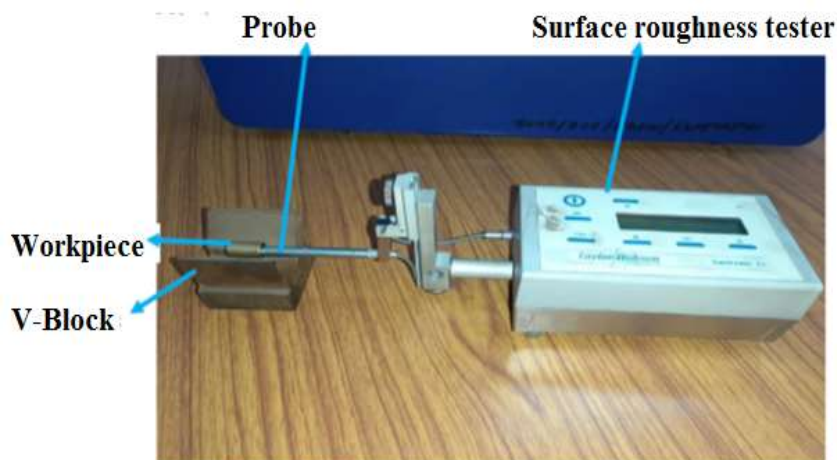


Figure 4.4 systematic diagram of Taylor Hobson precision machine used to measured surface roughness

4.2.2. MICRO-HARDNESS

The produced carbon coating's micro hardness was measured using a FIE model MV1-PC micro Vickers' hardness tester. The square pyramidal diamond stylus indenter on the micro hardness tester was used to perform tests with an indentation time of 20s, a dwell time of 5s, and a maximum applied load of 1000mN on the stylus. The average values of the hardness values were plotted in chapter 5 of the current study, which were measured at three separate places of each sample. The systematic diagram of Vickers' hardness tester is shown in Figure 4.5.



Figure 4.5 systematic diagram of Vickers's hardness tester.

4.2.3. RESIDUAL STRESS

The internal stresses created on the carbon coatings were evaluated using a Pulstec residual stress analyzer (-X360, XRD). The residual stress was investigated using the $\cos(\alpha)$ approach based on Bragg's law, as given in the equation and depicted in figure 4.6, with a 45° X-ray indentation and sensor unit support. The varied orientations of grain crystals that satisfy Bragg's law cause X-ray diffraction. Because of the variation in crystal orientation, diffracted X-rays form a cone around the incident x-ray axis.

$$n\lambda = 2d \sin\theta$$

Where n (an integer) is the "order" of reflection, λ is the incident X-rays' wavelength, d is the crystal's interplanar spacing, and θ is the angle of incidence equal to the angle of scattering.

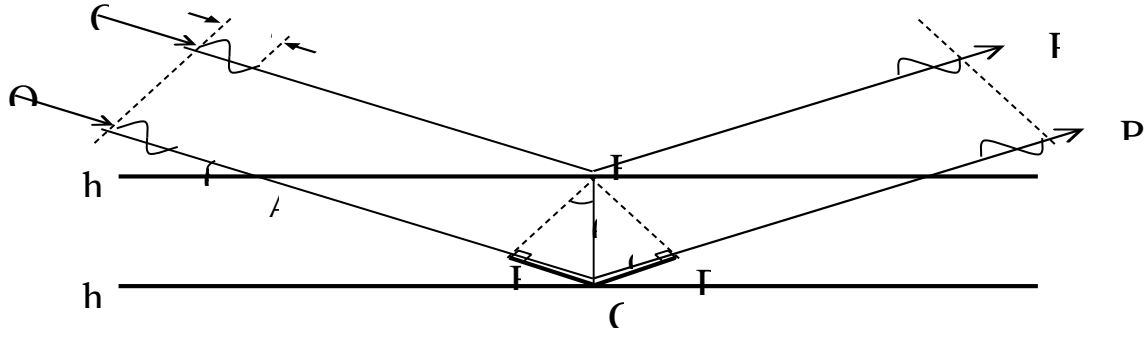


Figure 4.6 systematic representation of Bragg's law

Residual stresses on coated samples emerge as a result of biaxial applied load and thermal stresses on the body, as seen in figure 4.7, and can be calculated using the following equations [193]:

$$\sigma = \sigma_{\text{thermal}} + \sigma_n \quad (1)$$

Where,

$$\sigma_n = \frac{1}{2} \{ (\sigma_x + \sigma_y) + (\sigma_x - \sigma_y) \cos 2\theta \} + \tau_{xy} \sin 2\theta \quad (2)$$

$$\sigma_{\text{thermal}} = \left\{ \frac{\alpha TL - \lambda}{L} \right\} E \quad (3)$$

Therefore the total residual stress developed on the material will be:

$$\sigma_x = - \frac{E}{1 + \nu} \cdot \frac{1}{\sin 2\eta} \cdot \frac{1}{\sin 2\psi_o} \cdot \left(\frac{\partial \varepsilon \alpha_1}{\partial \cos \alpha} \right) \quad (4)$$

where σ_x is residual stress developed on the surface, ν is poisson ratio, η is diffraction lattice angle, ψ_o is X-rays incident angle and α is the azimuth angle of Debye ring, E is young's modulus.

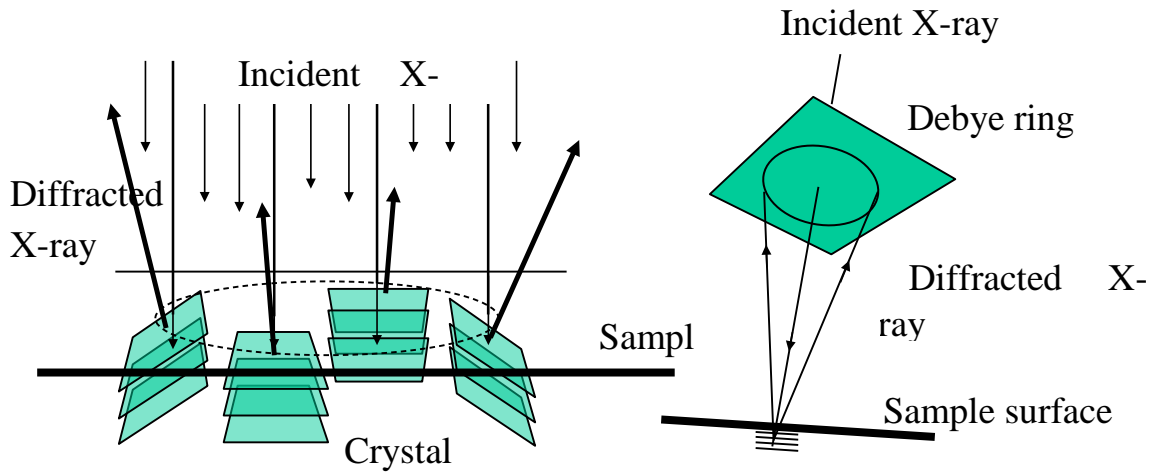


Figure 4.7 systematic diagram of residual stress of coating

Biaxial applied load and thermal stresses formed on the body, resulting in residual stresses on the coated samples. The residual stress concentration in the substrate material is represented by the Debye ring created by a single brief duration X-ray exposure of incident ray. The position of Debye rings was precisely measured to determine residual stress. Their locations are a direct reflection of the amount of tension they are under. The concentrations of residual stress are represented by several colour combinations, such as red for the highest concentration and blue for the lowest. The systematic diagram of the residual stress analyser is shown in Figure 4.8.



Figure 4.8 systematic diagram of residual stress analyzer

4.3. TRIBOLOGICAL TEST

The tribological test is a method of characterizing the friction coefficient, wear and frictional force between two materials in relative motion. The pin-on-disc wear testing is used to calculate wear behavior of developed coating and it comprises of three parts and is shown in the fig. 4.9 (a).

- High temperature tribometer
- Chiller
- Controlling panel and Computer attached with software

The wear behaviour of carbon and composite coatings was evaluated using the TR-20L-PHM800-DHM850 high temperature tribometer. Advanced motion control module, high-temperature stage (ambient to 850°C for disc heating and 800°C for pin heating), applied load (20-200N), sliding velocity, and environment chamber to test non-toxic, non-corrosive atmosphere were all operational attachments on the rotary tribometer. The disc speed can be measured using a proximity sensor with a range of 300 to 3000rpm, a minimum count of 1rpm, and an accuracy of

11% of the measured speed in rpm. The frictional force can be measured using a load cell with a range of 0 to 200N, a minimum count of 0.1N, and an accuracy of 0.11% in N. A LVDT sensor can monitor wear with a range of 0-2000m and a minimum count of 1 micron. The experimental tests were done without lubrication over a 1500m travel distance, using a G99 grade pin with an 8mm diameter and a surface roughness of 10nm, temperatures ranging from 150 to 350°C, loads ranging from 50 to 70N, and sliding velocity ranging from 1 to 3m/s. One steel cylindrical pin (8*25 mm) and one cuboidal plate (70*70*5 mm) with carbon and composite coating were employed in the tribological test. Table 4.1 shows the details of the wear test, where CC stands for carbon coating as well as composite coating, and suffix 1, 2, and 3 were utilised to distinguish test circumstances during tribological testing of carbon and composite coatings. COF is a function of temperature, load, velocity, and material property in the current investigation, as shown in the equation [184]:

$$\mu_{\text{cof}} = f\{T, V, L, Y\} \quad (5)$$

Theoretically wear volume can be calculated using equation (6) and volume loss of material can be calculated using equation (7) [184]:

$$\text{Wear volume} = \frac{\pi(r - \sqrt{r^2 - d^2/4})}{6(3d^2/(4+h) + h^2)} \quad (6)$$

$$\text{Volume loss (mm}^3\text{)} = \frac{\text{Mass loss (gm)} * 10000}{\text{Density } (\frac{\text{gm}}{\text{cm}^3})} \quad (7)$$

The coated surfaces of piston rings and cylinder bore follows Gaussian asperities after termination of running wear without alter surface topography significantly [33]. The total load carrying capacity between cylinder bore and piston rings can be calculated using equation [34] and as shown in the fig. 4.10 (c).

$$W_t = \int_0^R (dW_a + p dA) \quad (8)$$

During tribological test, rolling, sticking and sliding friction occurs on the symmetrical surface. Considering the equilibrium of forces during tribological testing:

$$(\sigma_r + d\sigma_r)(r + dr)d\theta - \sigma_r r d\theta - 2\sigma_\theta \sin\frac{d\theta}{2} dr - 2\tau_r (r d\theta dr) = 0 \quad (9)$$

$$\frac{d\sigma_r}{dr} + \left[\frac{\sigma_r - \sigma_\theta}{r} \right] - 2\frac{\tau_r}{h} = 0 \quad (10)$$

Considering sliding friction all over the surface and sliding force will be acting on the surface during radius R. The pressure distribution on the entire surface without sticking will be given the equation:

$$\int \frac{-dp}{p} = -\frac{2\mu}{h} r \int dr \quad (11)$$

$$\ln P = -\frac{2\mu}{h} r + \frac{2\mu}{h} R + \ln \sigma_0 \quad (12)$$

$$P_s = \sigma_0 e^{\frac{2\mu}{h}(R-r)} \quad (13)$$

Therefore the total sliding forces without sticking on the surfaces will be:

$$dF = P_s * 2\pi r dr \quad (14)$$

$$F_s = \int_0^R \left\{ \sigma_0 + \frac{2K}{h} (R-r) \right\} 2\pi r dr \quad (15)$$

Considering sticking friction all over the surface and sticking force will be acting on the surface during radius R_s . The pressure distribution on the entire surface without sliding will be given the equation

$$\int -dp = -\frac{2\mu}{h} \int dr \quad (16)$$

$$P = -\frac{2\mu}{h} r + \frac{2\mu}{h} R + \sigma_0 \quad (17)$$

$$P_{st} = P_s + \frac{2K}{h} R_{st} - \frac{2K}{h} r \quad (18)$$

$$P_{st} = P_s + \frac{2K}{h} (R_{st} - r) \quad (20)$$

Therefore the total sticking forces without sliding on the surfaces will be:

$$dF = P_{st} * 2\pi r dr \quad (21)$$

$$F_{st} = \int_0^{R_s} \left\{ P_s + \frac{2K}{h} (R_s - r) \right\} 2\pi r dr \quad (22)$$

During tribological testing, both rolling and forging forces (sticking + sliding) will occur on the symmetrical surface. Initially sticking friction will occur on the surface from radius 0 to R_s and sliding force will be acting on the surface during radius R_s to R , while rolling force will be acting on the entire surface. Therefore the total forces on the surface:

$$\text{Total Force} = \int_0^{R_s} \left\{ P_s + \frac{2K}{h} (R_s - r) \right\} 2\pi r dr + \int_{R_s}^R \left\{ \sigma_0 e^{\frac{2\mu}{h}(R-r)} \right\} 2\pi r dr + \sigma_0 b \sqrt{RV} h \quad (23)$$

Where μ is coefficient of friction, P is pressure exerted, σ is stress generated during the process.

In this study, dry lubrication was utilised to investigate the behaviour of carbon and composite coatings in extreme conditions where the tribological system is operating without lubrication, as well as the influence of high temperatures on carbon and composite coatings for piston ring applications. Figure 4.9 depicts a pin on disc tribometer, a wear track, and a model tribometer, while figure 4.10 (a) wear disc and pin before and after developed coating test (b) wear disc and pin after developed coating test (c) wear behaviour of produced coating.

Table 4.1 Details of wear test experiments

Designation	Process Parameter	CC	CC1	CC 2	CC 3
A	Temperature(°C)	Room Temp.	150	250	350
B	Sliding velocity (m/s)	1	1	1	1
C	Load (N)	50	50	50	50
<p>Constant parameters:</p> <p>Pin material: carbon coating on mild steel substrate</p> <p>Counterpart material: cylinder liner of Mild steel</p> <p>Lubrication condition: Dry condition</p> <p>Sliding distance: 1500m</p> <p>Environment: Non-corrosive and Non-toxic</p> <p>Relative Humidity: 40%</p> <p>Disc heating: Room temperature</p> <p>Pin Diameter: 8mm</p> <p>Operational attachments: Same for all test</p>					



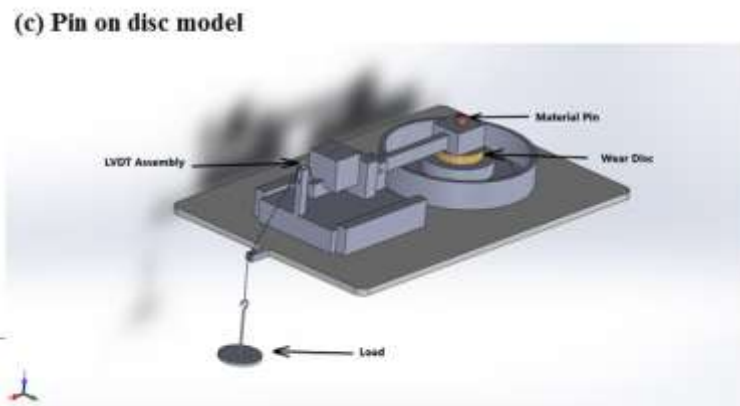
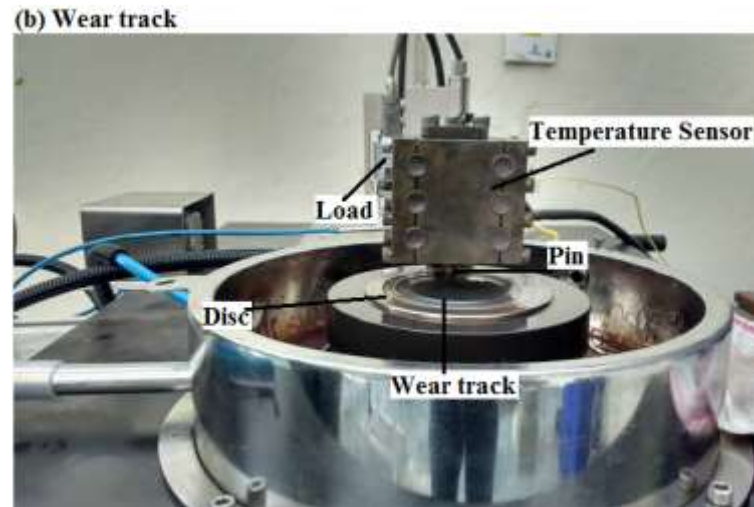


Figure 4.9 (a) Pin on disk tribometer (b) wear track (c) Tribometer, model of developed coating



(b) Wear Disc & Pin after wear test

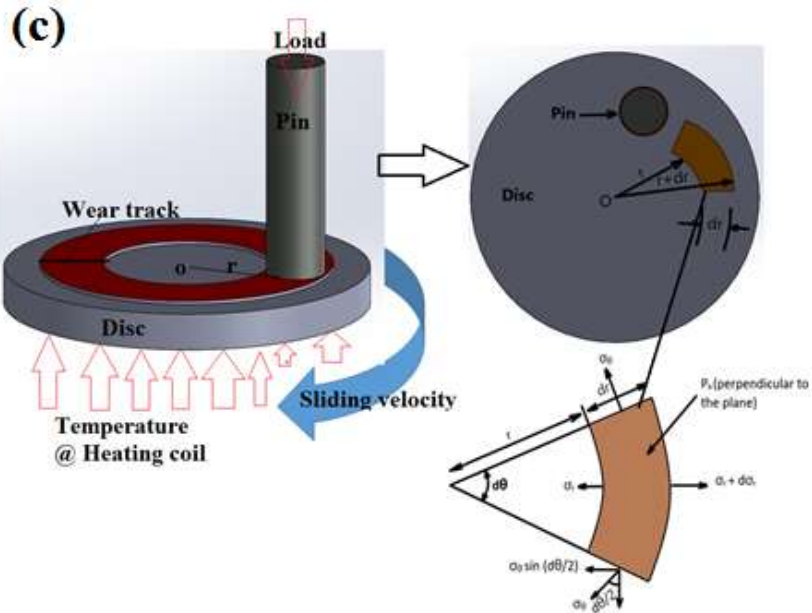


Figure 4.10 (a) wear disc & pin before test (b) wear disc & pin after test (c) wear behavior of developed coating.

4.4.DESIGN OF EXPERIMENT

It was concluded from the literature review that temperature, sliding velocity, and load are the processing parameters that influence tribological behavior of environment friendly HVOF based carbon coating. Table 4.2, shows trial condition parameters trial condition chosen for the experiment at all process condition in the procedure of COF, and wear of HVOF based carbon and carbon based composite coating.

The practice of S/N ratio is recommended by Taguchi in order to measure better quality characteristics deviating. Therefore higher S/N ratio will be the best level for the optimum trial for process parameters. The S/N ratio for lower-the-better type trial process may be figured as follows:

$$(S/N)_{LB} = -10 \log \left[\frac{1}{R} \sum_{j=1}^R (X_j^2) \right] \quad (1)$$

where X_j , $j = 1, 2, 3 \dots n$ are values of response lower as compared to test conditions

ANOVA (Analysis of variance), implemented to recognize statistically significant parameters in the test experimental results. Through ANOVA and S/N ratio analyses, optimum arrangement of parameters was predicted.

Table 4.2 Design parameters and trial conditions chosen for the Taguchi's experiment

Designation	Process Parameter	Level-1	Level-2	Level-3
A	Temperature(°C)	150	250	350
B	Sliding velocity (m/s)	1	2	3
C	Load (N)	50	60	70

4.5.SAMPLE PREPARATION

The substrate materials selected in the present research study is mild steel procured from Badli, Delhi. Table 4.3 shows the chemical composition of selected substrate materials. The substrate material is prepared in the form of plates of size 70*70 mm and having a thickness of 5 mm. The counter face pin was of mild steel having length of 20mm and diameter of 8 mm. It is a medium strength alloy steel.

Table 4.3 Chemical composition of steel substrate

Element	C	Mn	Si	S	P	Cr	Ni	Mo	Cu	Fe
% Composition	0.16	1.07	0.24	0.01	0.01	0.10	0.02	0.02	0.17	Bal

4.6.CARBON POWDER PREPARATION

The carbon coating powder was developed from agricultural waste. Initially the agricultural waste was heated into the thermal furnace at 1 MPa and 550°C temperature, to produced carbon powder as shown the fig.4.11. The produced carbon powder was then blend in the ball mill for 8 hours, to get carbon powder with reduced size of 40-50±5 µm as shown in the fig. 4.12. The

physiochemical properties of produced powder is heat of fusion, grain size, density and melting point powder was 110KJ/mol, 60 μ m, 2.10g/cm³ and 3500 \pm 100⁰C respectively.



Figure 4.11 systematic diagram of carbon powder preparation



Figure 4.12 systematic diagram of ball mill

4.7.CARBON BASED COMPOSITE POWDER PREPARATION

The carbon based composite coating was developed using agricultural waste produced carbon powder, tungsten carbide powder, molybdenum powder, titanium oxide and aluminum oxide powder. Initially, all the powders (C+WC+Mo+TiO₂+Al₂O₃ powders) were blend together in the ball mill for about 8 hours, to get carbon based composite powder with reduced size of 40-50 \pm 5

µm. The ball milling operation was performed for homogeneous and uniform distribution composite powder.

4.8.COATING PREPARATION

The coatings were formulated using MEC make HIPOJET HVOF thermal spray system, available at DTU. The HVOF thermal spray coating system equipment were HIPOJET-2700 spray gun, control panel, X-Y manipulator, powder feeder operating with argon, oxygen and LPG cylinder. Initially, to achieve a smooth surface, a 70*70*5 mm mild steel plate was first ground with 80-2000 grit emery paper and then polished using alumina paste. After that, a MEC PR-9182 model pressure blaster was used to prepare and deposit a SiC additive layer on the substrate material, with the dust generated in the blast cabinet being collected in a dust collector. The SiC additive layer was employed to increase the adhesive strength between the substrate and the coating. In the HVOF thermal spray process, the HIPOJET-2700M MEC HVOF system was utilised to spray carbon and carbon-based composite powder at supersonic speed jet. For the growth of carbon and carbon-based composite coatings, the steel plate and powder spray system were supplied with a constant supply of N₂ gases. The deposition parameters used to grow the environmental friendly HVOF coating are shown in Table 4.4.

Table 4.4 Details of coating deposition.

No.	Parameters used	Standards
1.	Coating Composition	Carbon powder and carbon based composite powder
2.	Substrate material	Mild Steel plate
3.	Deposition technique	HVOF
4.	Powder feed rate	4 Kg/h
5.	Surface pre-treatment	Acetone
6.	Treatment time	10 min.
7.	Carrier gases	N ₂
8.	Fuel flow rate	10 ±1 (/h
9.	Deposit efficiency (%)	55

This chapter includes the characterization, residual stress, micro-hardness, surface roughness and high temperature tribological test of:

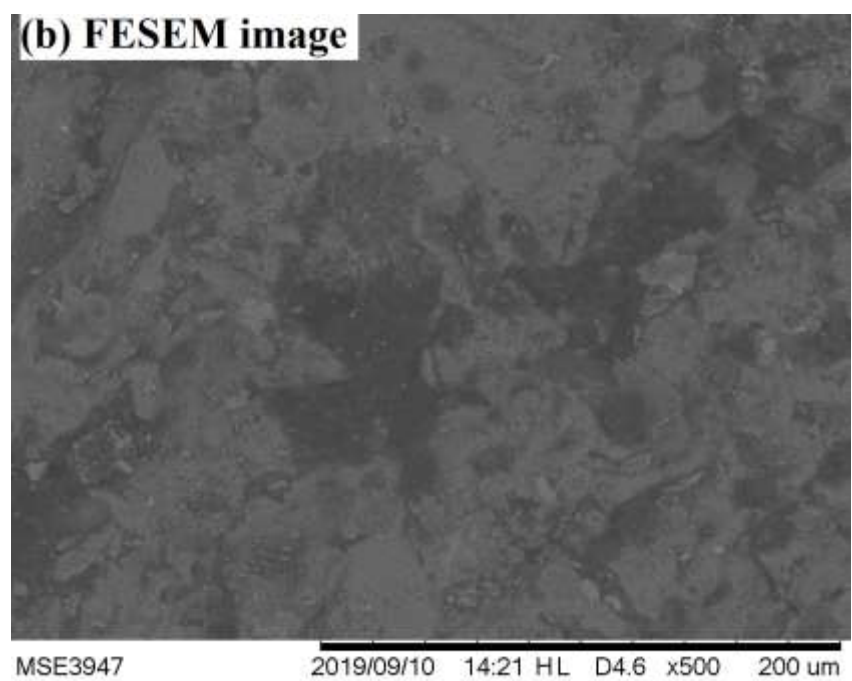
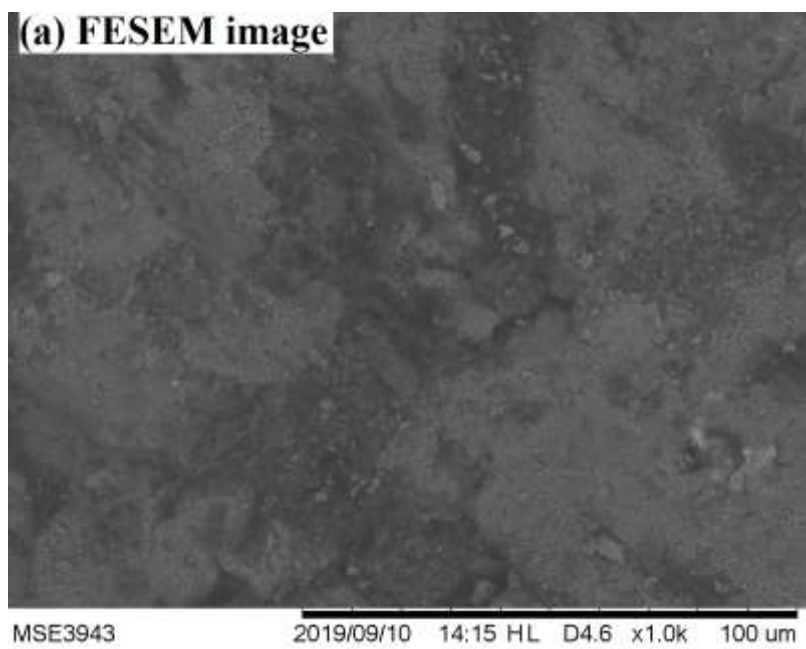
Part 1: Carbon coating for the piston rings application prepared by HVOF spray technique.

Part 2: Carbon based composite coating for the piston rings application prepared by HVOF spray technique.

5.1.SAMPLES CHARACTERIZATION

The microstructure and surface morphology of substrate materials is shown the fig. 4.1 (a-b), while figure 5.1 (c) shows the EDS result of uncoated sample. FESEM image shows uniformity with less porosity and void defects. The HRXRD results of substrate material is shown in the figure 5.2. The 2 theta peaks was observed to be at 44.5-45° and at 65°, which confirms the presence of ferrite particles in the substrate material. The technique of Raman spectroscopy has been widely employed to investigate the structural properties of developed coatings. The Raman spectral peak for substrate material is approximately 1400-1600 cm⁻¹, as shown in the figure 5.3.

The mechanical and tribological property of polished surface was examined and found that the surface roughness (0.26µm), Micro-hardness (313.3 HV), residual stress (80MPa), COF (0.65), Wear (200 microns), of substrate material. Figure 5.4, 5.5, 5.6 shows the surface roughness, residual stress and micro-hardness results of uncoated samples respectively.



(c) EDS result of uncoated sample

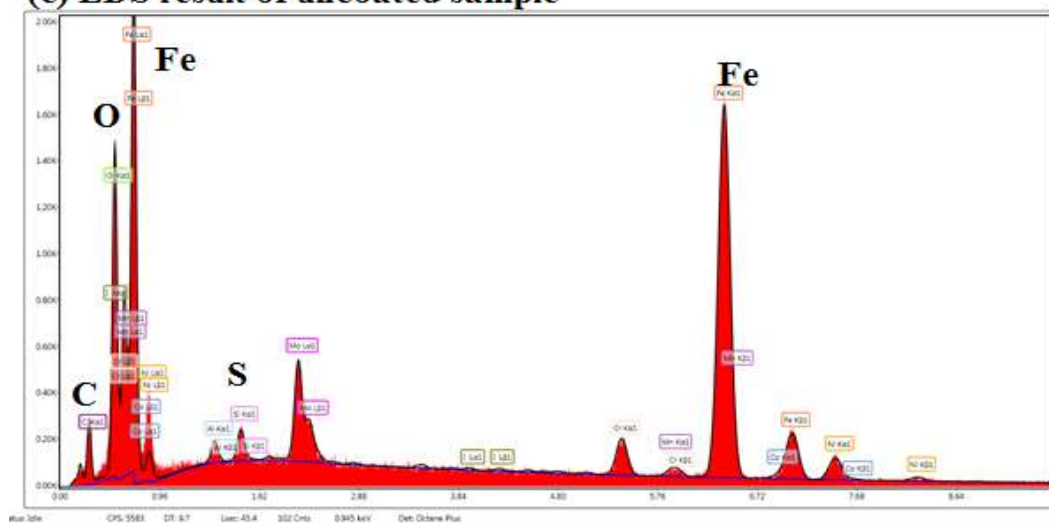


Figure 5.1 (a-b) FESEM image (c) EDS result of uncoated samples

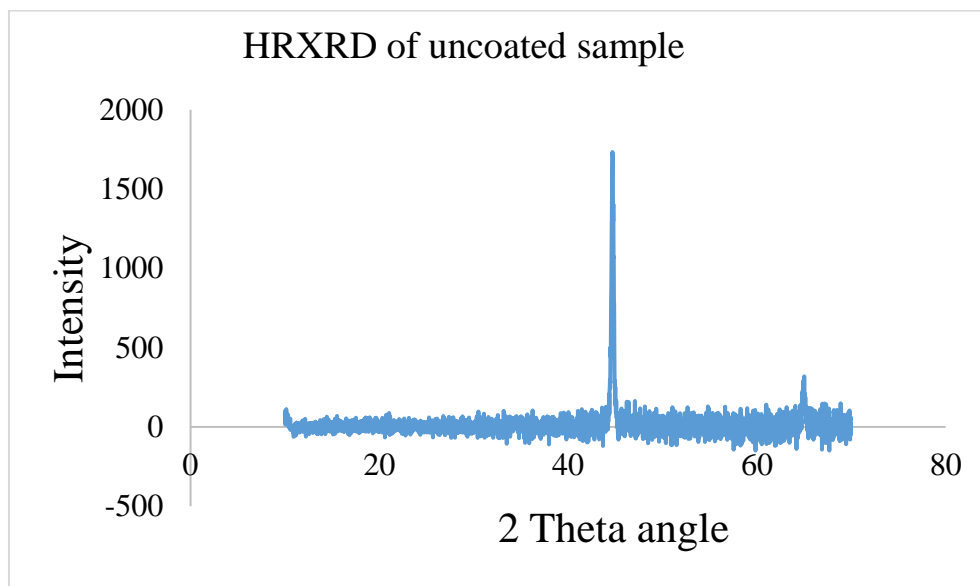


Figure 5.2 HRXRD result of uncoated samples

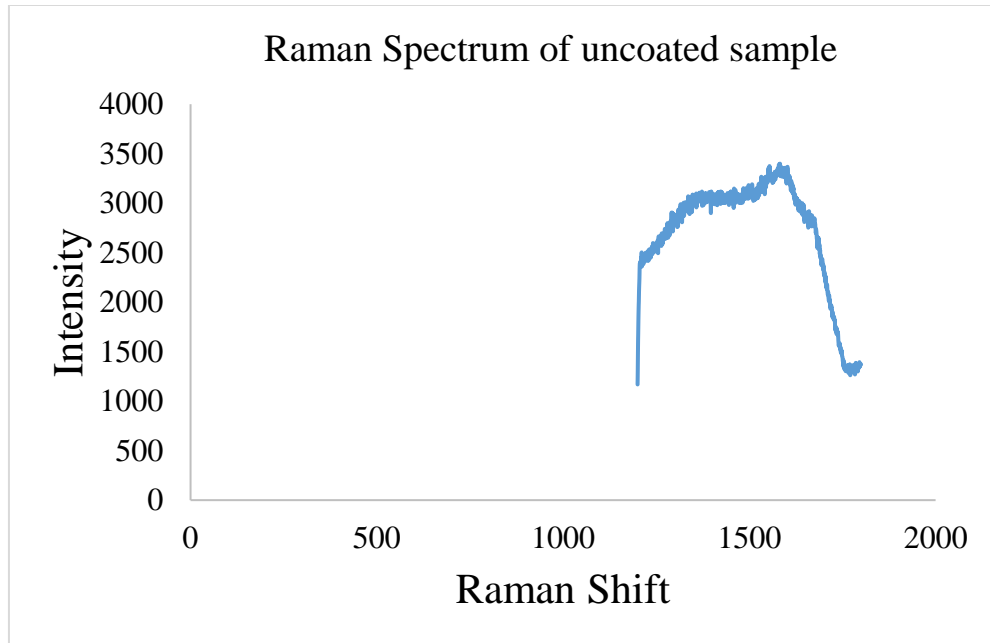


Figure 5.3 Raman spectrum result of uncoated samples

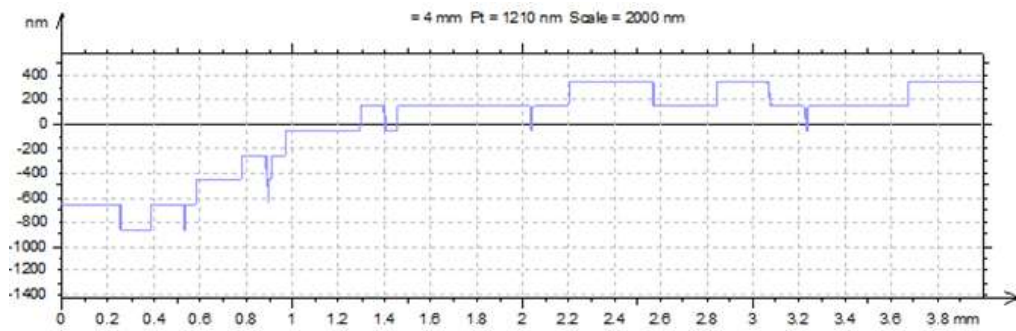
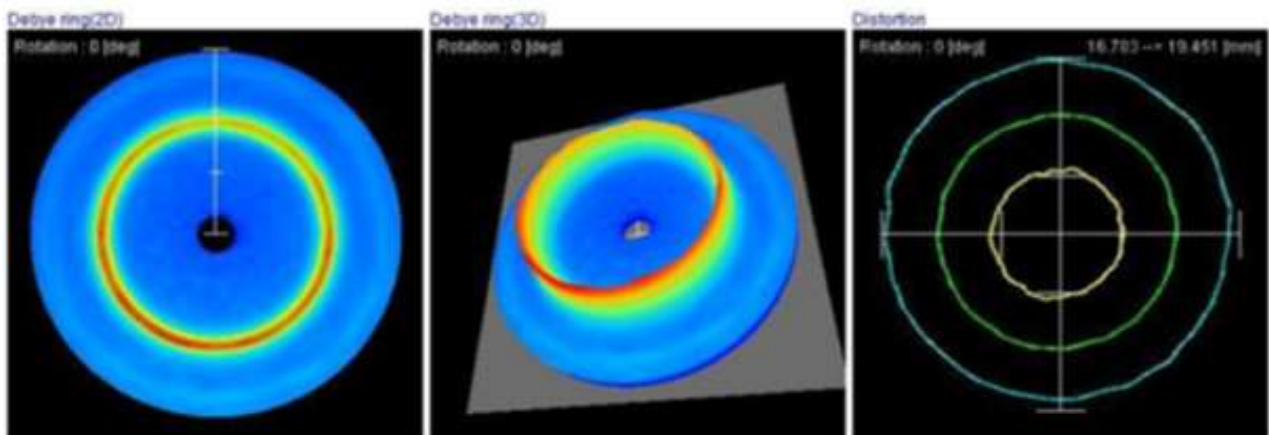
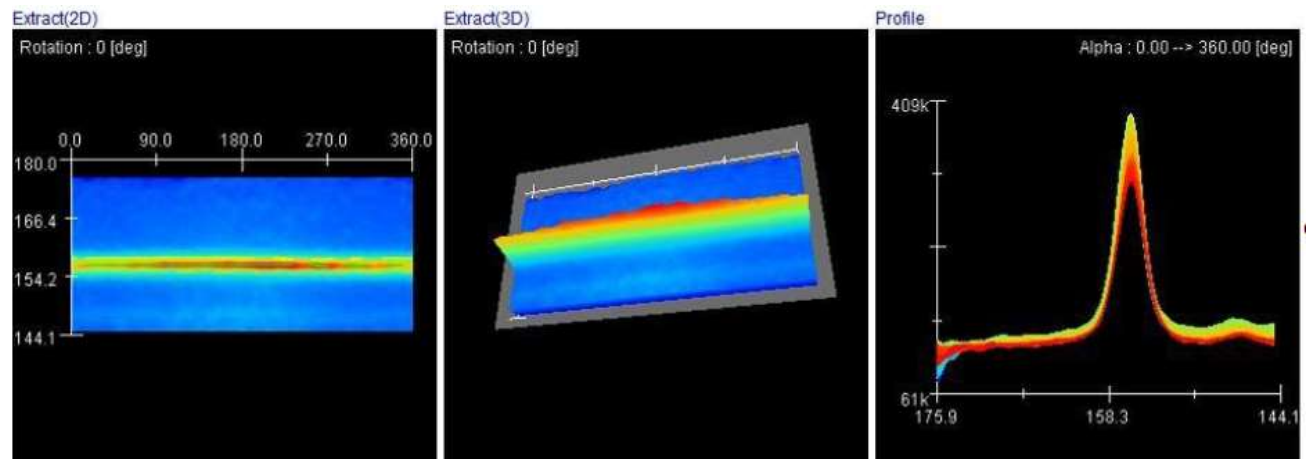
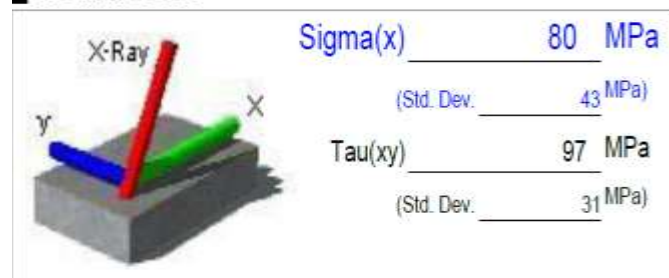


Figure 5.4 Surface roughness results of uncoated sample

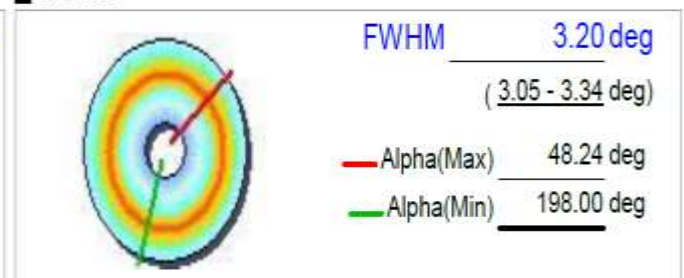




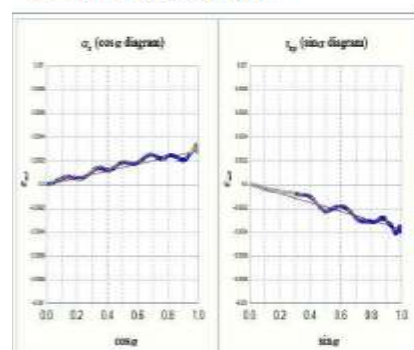
Residual stress



FWHM



Residual stress graph



FWHM graph

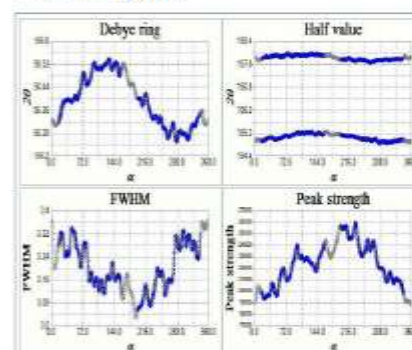


Figure 5.5 Residual stress results of uncoated sample

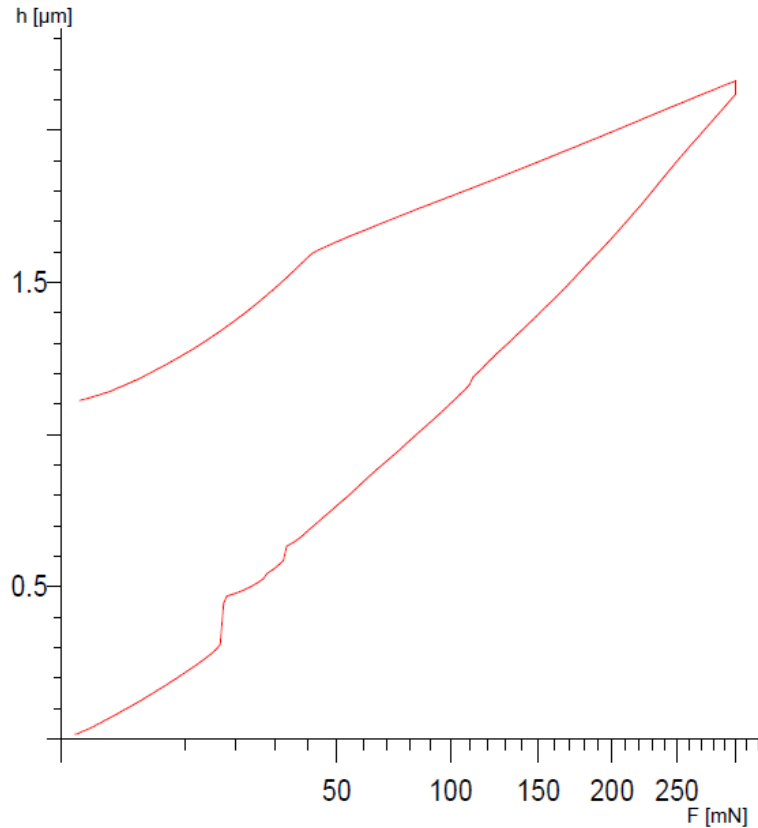


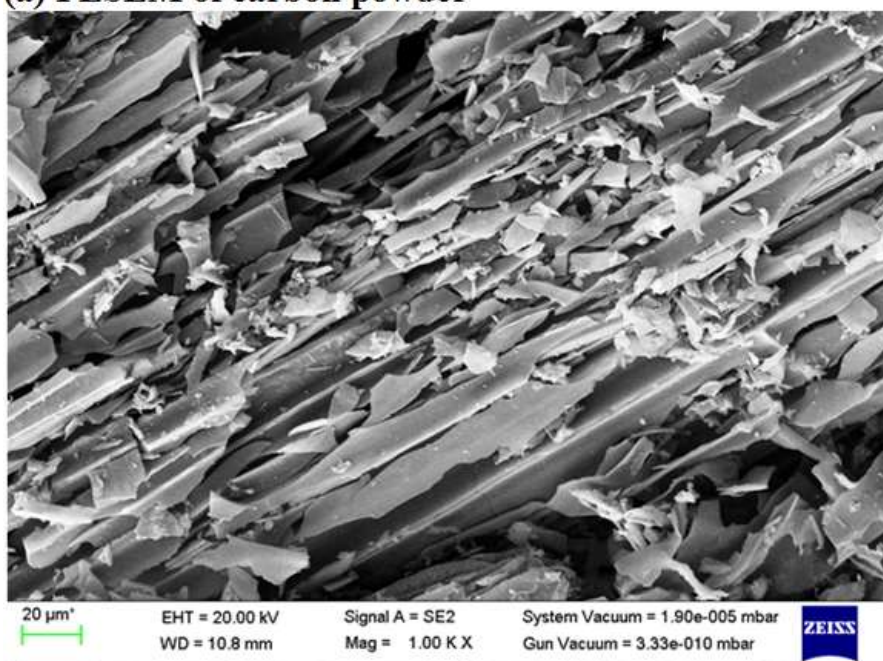
Figure 5.6 Micro-hardness results of uncoated sample

5.2. POWDER CHARACTERIZATION

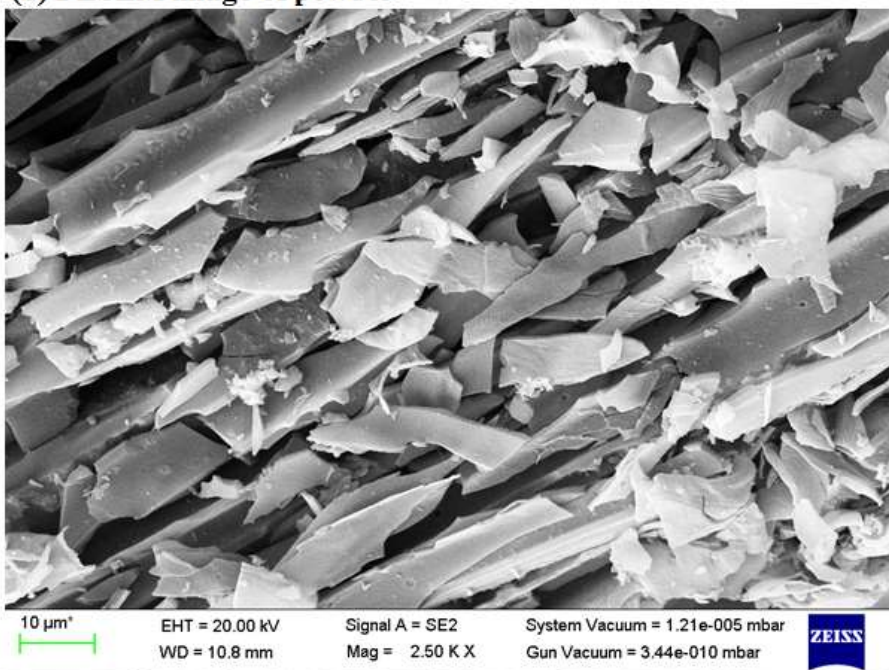
Fig. 5.7 (a-c) shows the FESEM images of agricultural waste produced powder. while fig.5.8 shows the HRXRD image of agricultural waste produced powder. The carbon produced by agricultural waste can be used for chromium absorption and waste water treatment, as well as helping to reduce dangerous gas emissions and chlorine removal. The carbon produced has great commercial value, and the powders produced also have high density, carbon content, and mechanical properties. Fig. 5.9 (a-c) shows the FESEM images of powder at 550⁰C, while fig. 5.10 shows the HRXRD image of powder at 550⁰C. Carbon powder exhibits needle-like structure, as well as flakes, pith, flatter, and fibre structures, as seen in a FESEM image at X 250 resolution. The presence of a pebble-like structure with a varied size of 10-100 μm was also observed. At higher resolution, flake-like structures may be observed, as well as flakes breaking apart during milling process. At increased resolution, the powder reveals a polycrystalline structure. It was also observed that fiber surface contains residual material with parallel stripes and also contains fragile and fragmented structure. Fig. 5.8 shows the prominent peak of powder was observed at 2θ angle of 22° -23° and smaller peaks were observed at 2θ angle of 44.5° -45° and 72° – 73°. Fig. 5.10 The

HRXRD of carbon powder at 550°C shows that the prominent peak were observed at 2θ angle of $22^\circ - 23^\circ$, $43.5^\circ - 44^\circ$, $44.5^\circ - 45^\circ$, 73° and smaller peaks were also observed at 2θ angle of $88^\circ - 89^\circ$, $111.5^\circ - 112^\circ$ and $112^\circ - 112.5^\circ$.

(a) FESEM of carbon powder



(b) FESEM image of powder



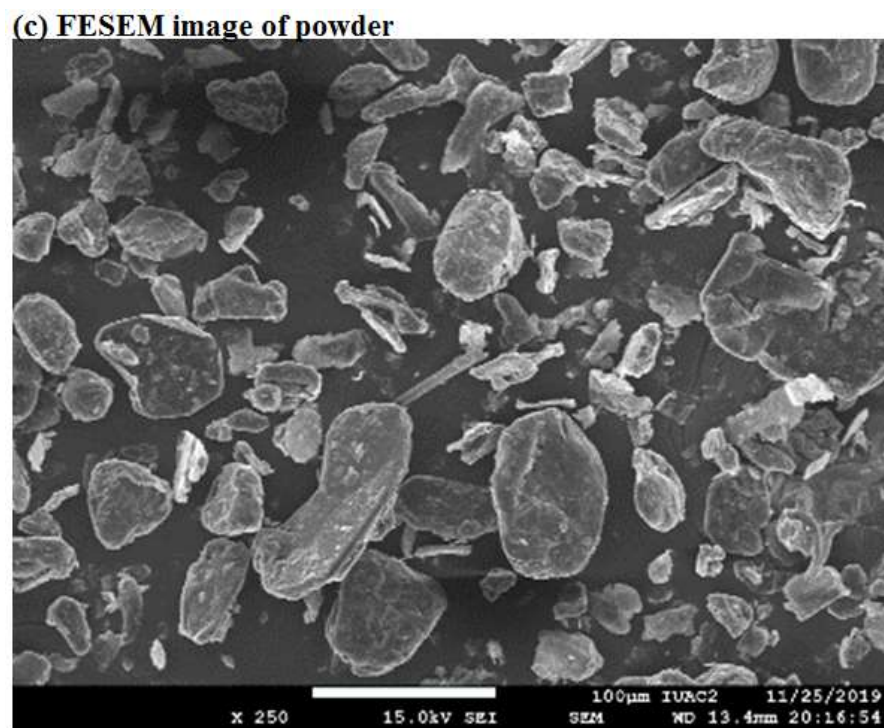


Fig 5.7 (a-c) FESEM image of agricultural waste produced powder

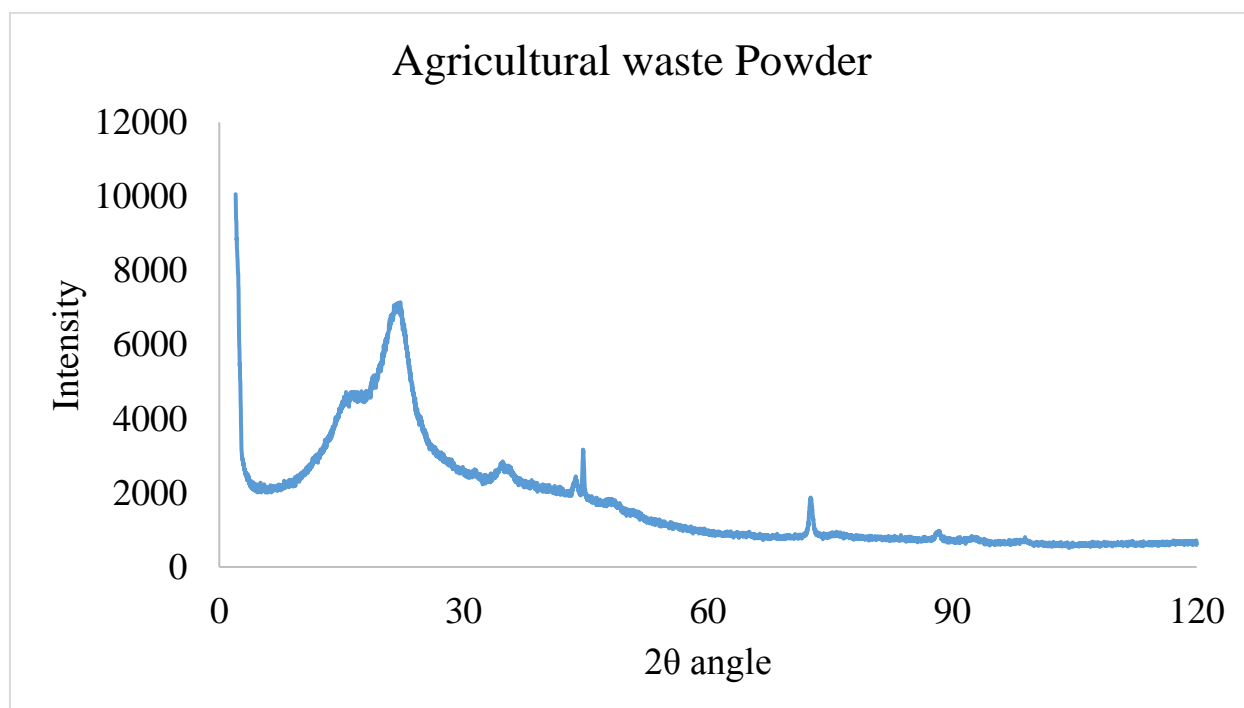
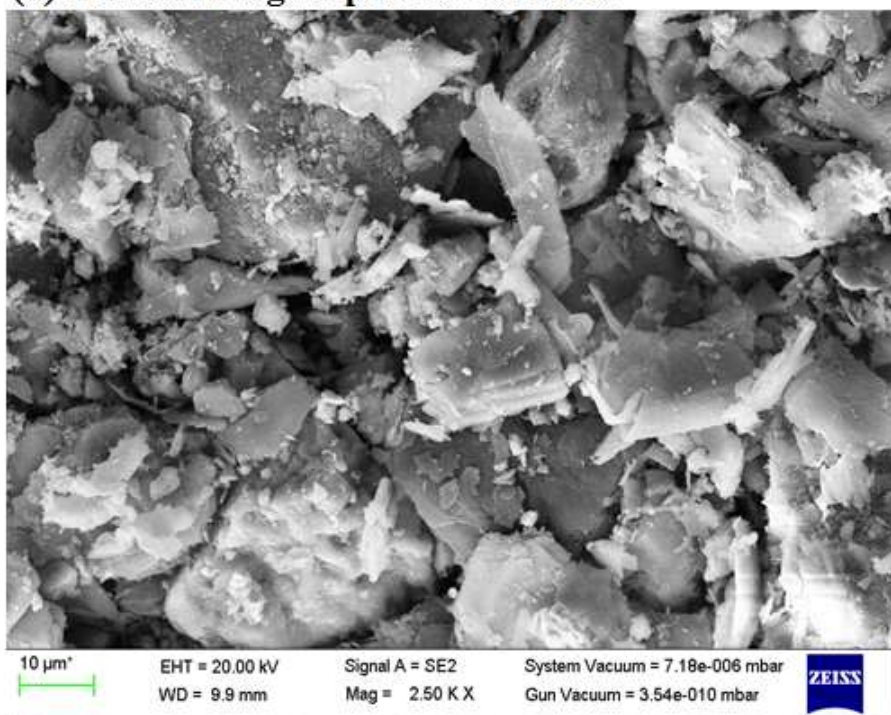
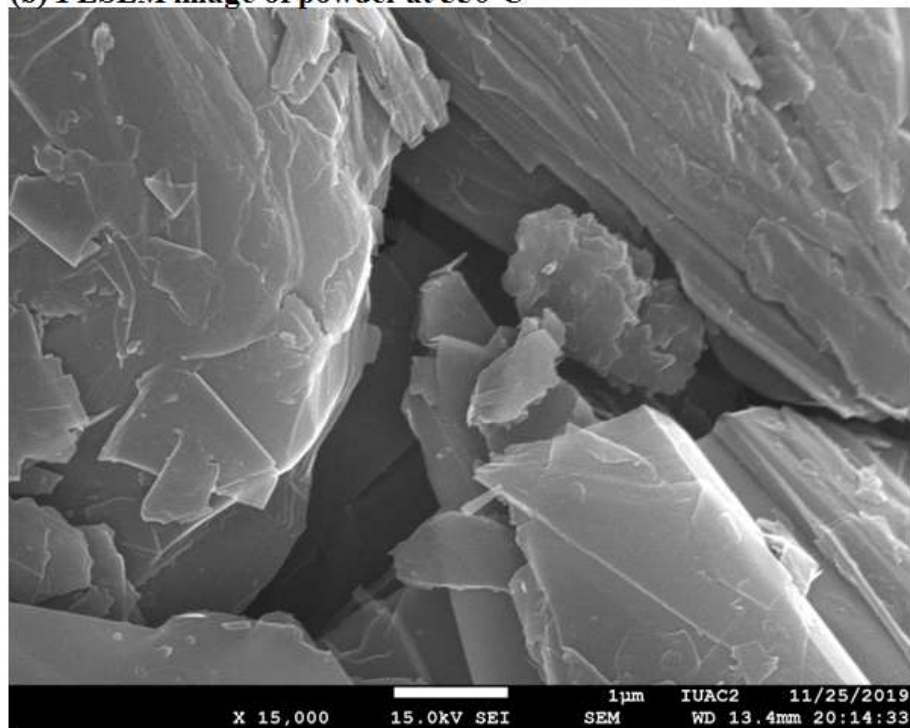


Fig. 5.8 HRXRD image of agricultural waste produced powder

(a) FESEM image of powder at 550°C



(b) FESEM image of powder at 550°C



(c) FESEM image of powder at 550°C

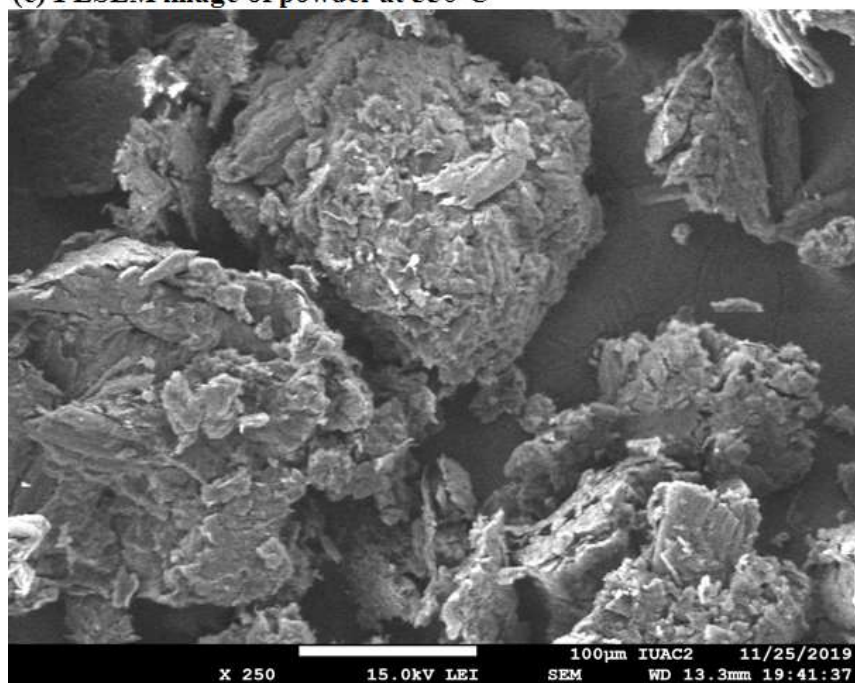


Fig 5.9 (a-c) FESEM image of powder at 550°C

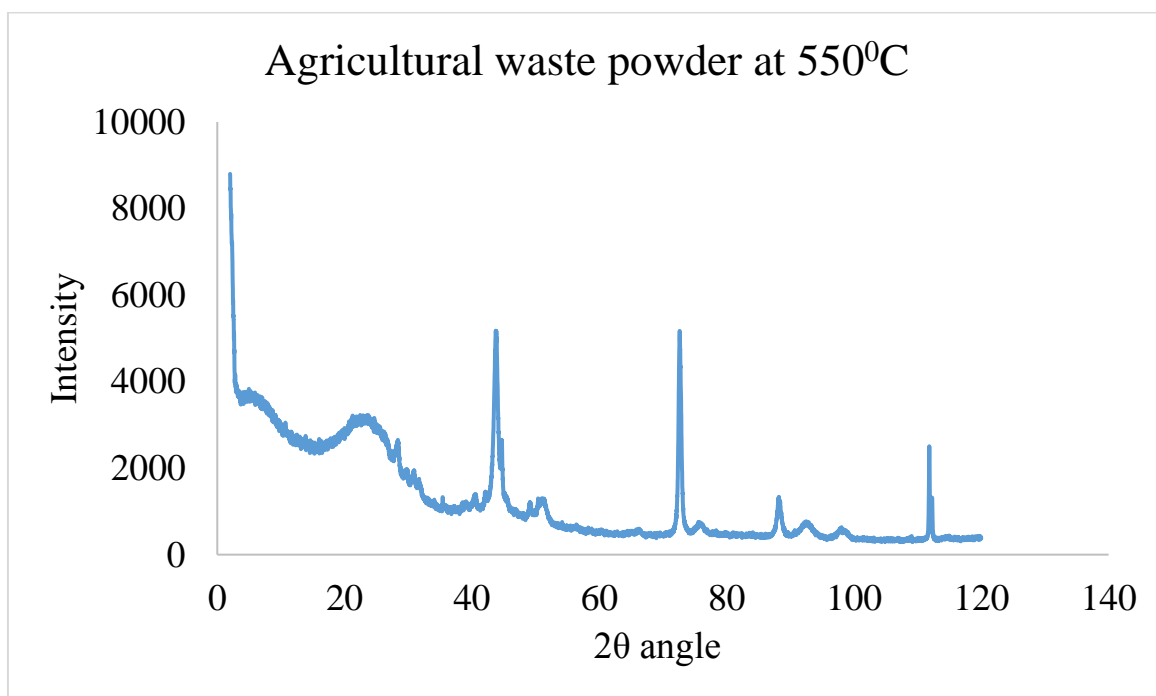


Figure 5.10 HRXRD image of powder at 550°C

Fig. 5.11 and fig. 5.12 shows the FESEM and HRXRD results of composite powders respectively. The FESEM images of composite powders shows that powder was uniformly

distributed. It was also observed that spherical shape with pebbles like structure along with pith, flatter. The Fig. 5.12 shows the prominent peak of composite powder was observed at 2θ angle of 26° - 27° and smaller peaks were observed at 2θ angle of 9 - 10° , 28 - 30° , 30 - 32° , 35 - 36° , 44 - 45° , 48 - 49° , 52° , and 64 - 64.5° .

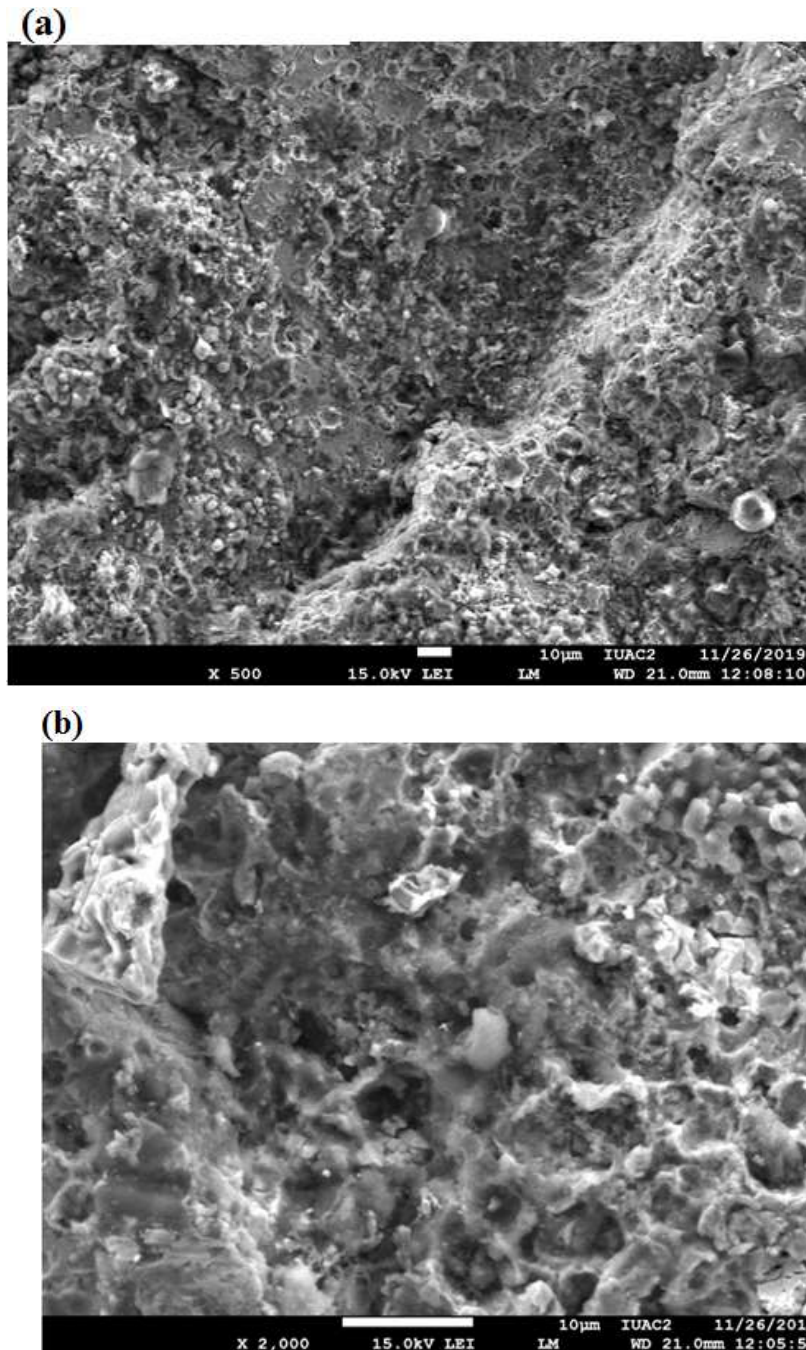


Figure5.11 (a-b) FESEM image of composite powder

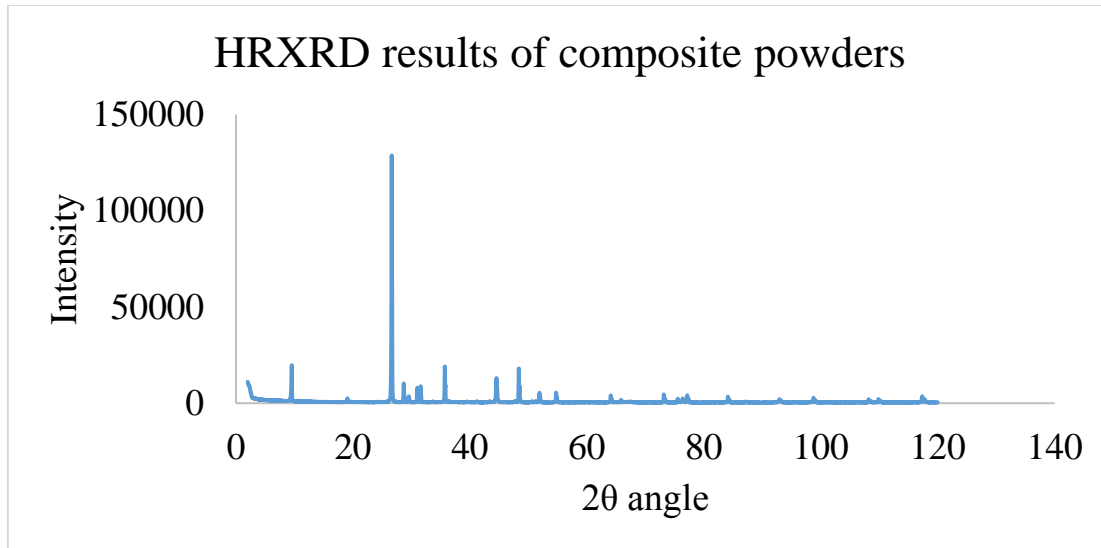


Fig.5.12 HRXRD image of composite powder

PART 1:

5.3. CARBON COATING CHARACTERIZATION

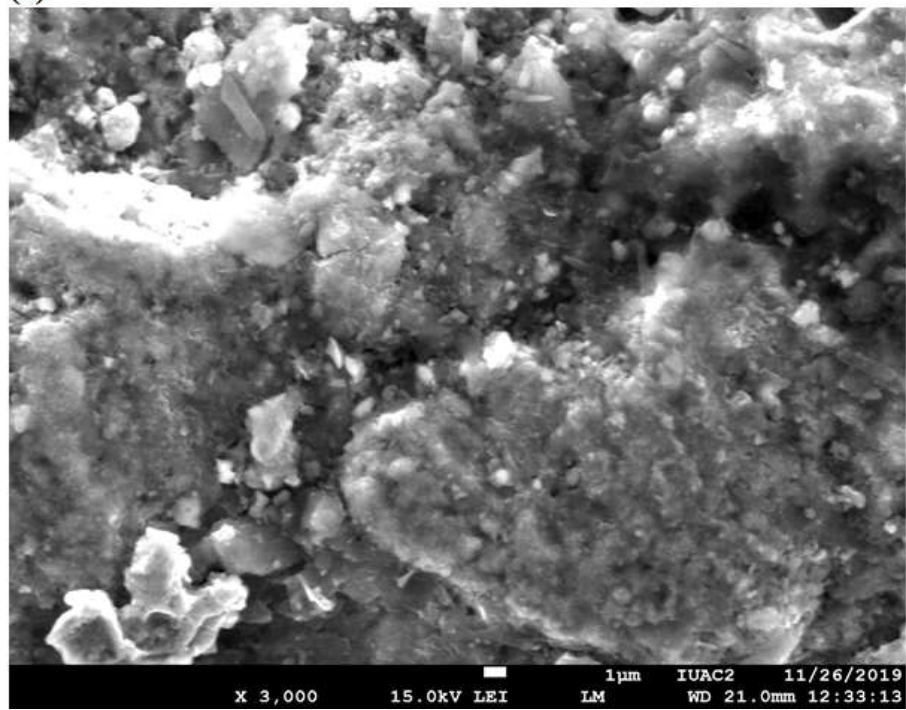
5.3.1. FESEM+EDS RESULTS OF CARBON COATING

Fig. 5.13 (a-c) illustrates the FESEM image of surface and cross-sectional morphology along with bonding conformity of carbon coatings. It is quite clear from FESEM image that carbon coating was deposited uniformly and homogeneously ranging from 350-450μm. The deposited carbon show presence of semi-molten, molten and un-melted grains of agricultural waste along with formation of lamellae [184]. It was also observed that some void and porosity were also observed on carbon coating. Fig. 5.13 (d) and table 5.13 shows the EDS result of carbon coating and confirms the deposition of weight% in developed coating as 80% carbon, 15% oxygen and rest weight % of aluminium (1.65%), iron (0.65%) and tungsten (1.60%).

Table 5.1 EDS result of carbon coating

Element	Weight%	Atomic%
C K	80.83	86.62
O K	15.35	12.35
Al K	1.65	0.79
Fe K	0.56	0.13
W M	1.60	0.11
Totals	100.00	

(a)



(b)



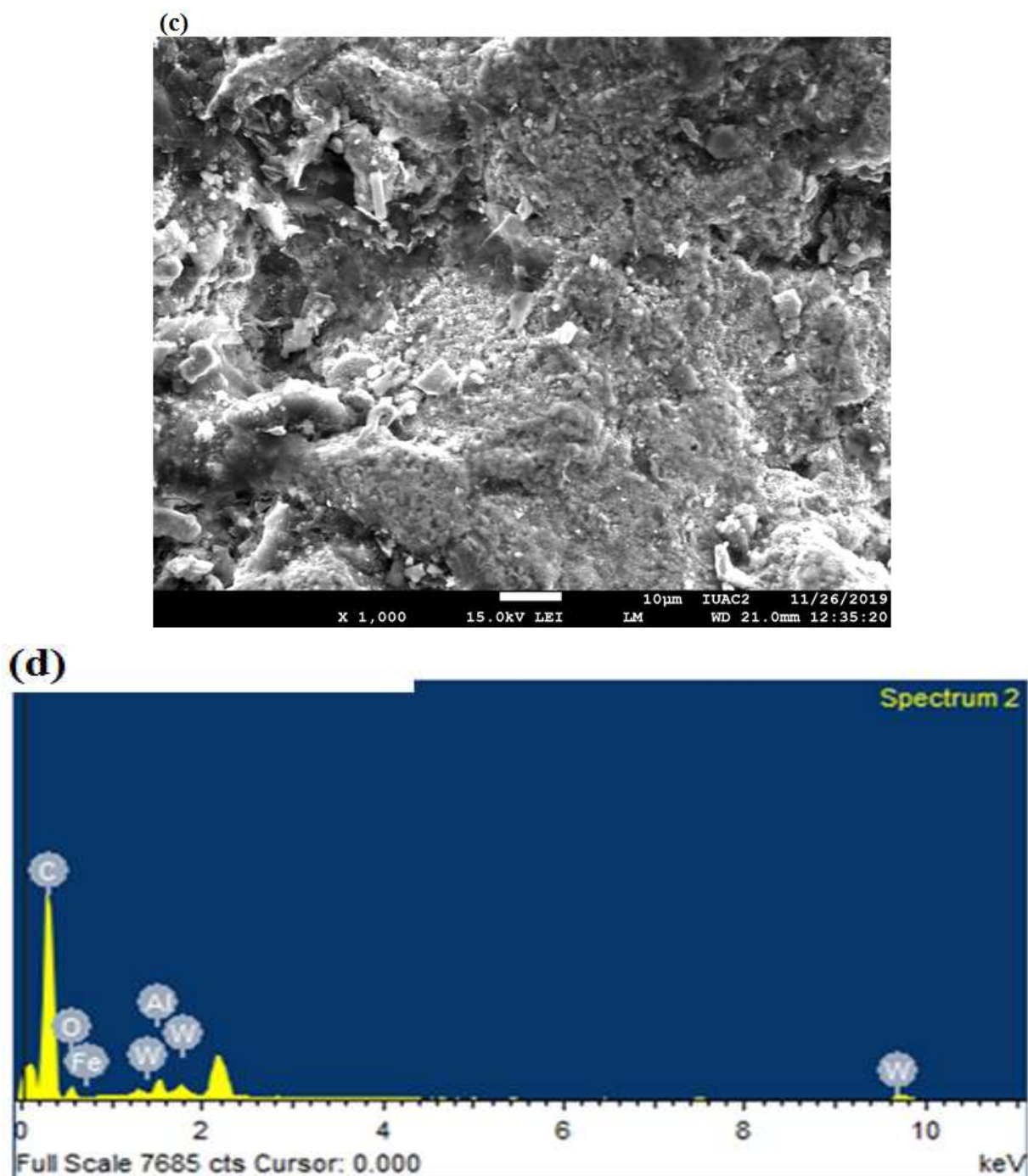


Figure 5.13 (a-d) FESEM+ EDS image of carbon coating

5.3.2. HRXRD RESULT OF CARBON COATING

Fig. 5.14 shows the HRXRD spectra on the carbon coating. In the present case carbon peaks at $2\theta = 13.9^\circ$, $2\theta = 16.8^\circ$, $2\theta = 25.2^\circ$ and at $2\theta = 44.6^\circ$ respectively were observed on developed coating. The XRD peaks shows the formation of ferrite and graphite structures [184].

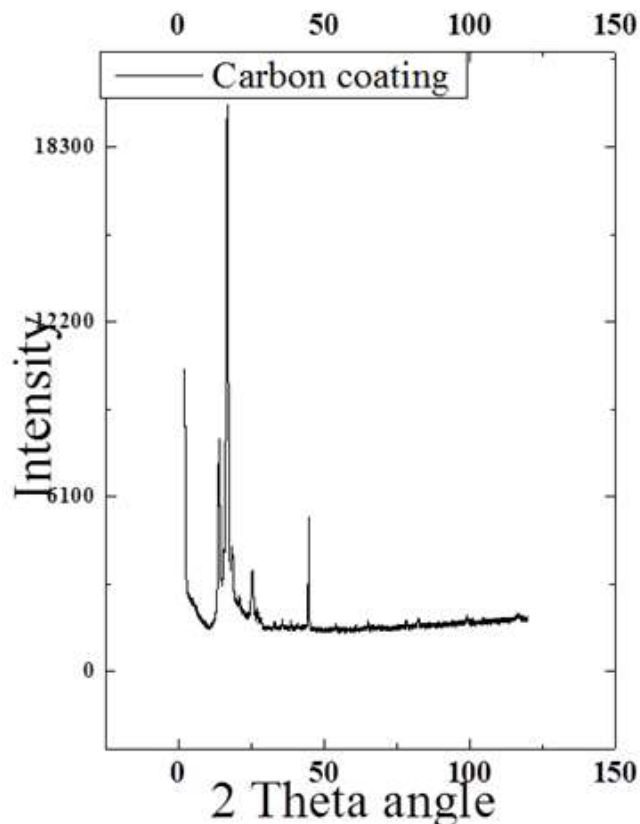


Figure 5.14 HRXRD result of carbon coating

5.3.3. RAMAN SPECTRUM OF CARBON COATING

Fig. 5.15 shows the captured Raman spectra peak on the developed coating with presence of hybridized carbon peak. To examine structural properties of coating materials Raman spectroscopy has been used by the researchers. In the present research, prominent peaks were observed at 1140, 1340-1350 and 1550-1600 cm^{-1} on the carbon coating. It is noted that peaks around 1340-1350 cm^{-1} and at 1140 cm^{-1} shows sp^1 or sp^2 hybridized carbon deposition on the developed coating, while peaks around 1550-1600 cm^{-1} shows presence of sp^3 hybridization with presence of DLC coating as testified in formerly research [184-187].

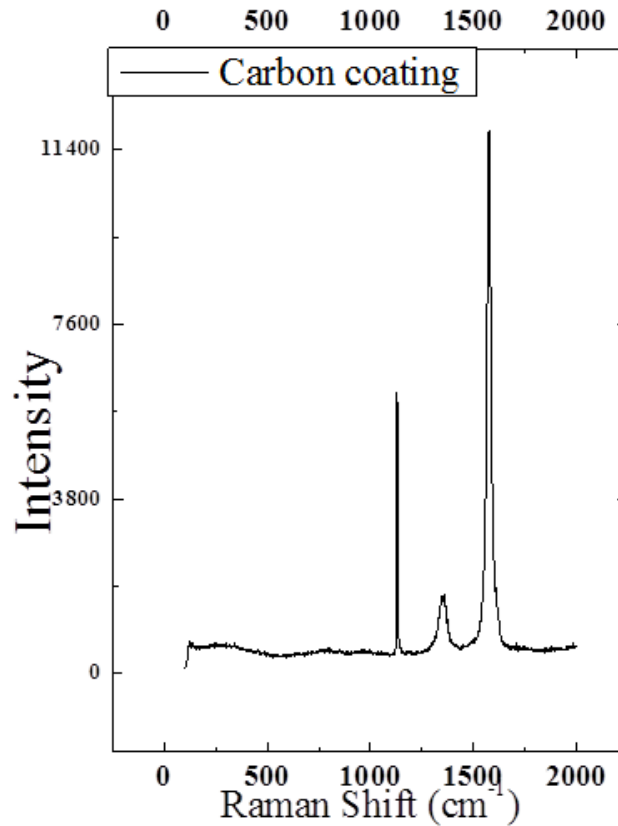
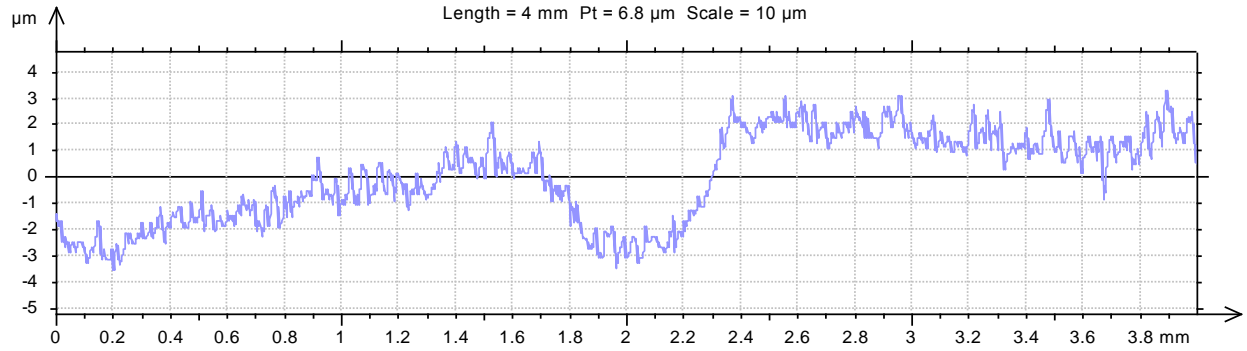


Figure 5.15 Raman Spectra result of carbon coating

5.4.MECHANICAL CHARACTERIZATION OF CARBON COATING

5.4.1. SURFACE ROUGHNESS

Fig. 5.16 shows the surface roughness of coatings deposited by agriculture waste powder in presence nitrogen, oxygen and LPG using high velocity oxy-flame (HVOF). The developed coating obtained after HVOF spray technique was rough, so in order to get surface smooth, initially, the developed coating was ground with emery paper of grit size 80-3000. After that, the cut samples was polished 1/0, 2/0 alumina paste. The smoothing of surface was done due to constraint of Taylor Hobson precision machine used in present investigation. The experimental result shows that surface roughness value of carbon coating (CC) was 0.445 μm .



Parameters calculated on the profile Profile

* Parameters calculated by mean of all the sampling lengthes.
 * A microroughness filtering is used, with a ratio of 2.5 μm .

Roughness Parameters, Gaussian filter, 0.8 mm

Ra	=	0.445 μm	
Rz	=	2.97 μm	
Rq	=	0.557 μm	
Rp	=	1.79 μm	
Rv	=	1.18 μm	
Rt	=	3.57 μm	
Rsk	=	0.555	
Rku	=	3.56	
Rmr	=	2 %	(1 μm under the highest peak)
Rdc	=	0.904 μm	(20%-80%)
RSm	=	0.0518 mm	
RDq	=	5.63 °	
RLq	=	0.0356 mm	
RLo	=	0.503 %	
RzJIS	=	2.15 μm	
R3z	=	2.27 μm	
RPc	=	4.38 pks/mm	(+/- 0.5 μm)
Rc	=	1.15 μm	

Figure 5.16 Surface roughness of carbon coating

5.4.2. MICRO-HARDNESS

Fig. 5.17 shows the micro-hardness of coatings deposited by agriculture waste powder in presence nitrogen, oxygen and LPG using high velocity oxy-flame (HVOF). The experimental result shows that micro-hardness value of carbon coating (CC) before wear test exhibits 520 HV. The micro-hardness value of samples CC 1, CC 2 and CC 3 after wear test was 540, 565 and 580 HV. The experimental results shows that as the test conditions of temperature ranging from 150 to 350°C, 1 load 50 N and sliding velocity 1 m/s respectively increases the micro-hardness rapidly

increased from 520 to 580 HV and hardness stabilized ~580HV. The micro-hardness test showed 11.5% increase in micro-hardness at test condition of 1 m/s sliding velocity, 350°C temperature, and 50N load. The experimental result shows as the temperature, load and velocity increases, the micro-hardness of carbon coating increases significantly as studied by Tyagi et al. [184], and similar trends was also attain the present hardness test. The rapidly increase in micro-hardness is due to strong adhesion between coating particles, formation of oxides, carbides layer and agglomerate size of powders for piston rings [184]. Matikainen et al. [188] investigated HVOF developed coating and experimental result shows that higher velocity particles enhances hardness of developed coating. It is also noted that presence of hard phased structured micron size carbon particles works as an impediment contrary to deformation, finally results increase in hardness [189].

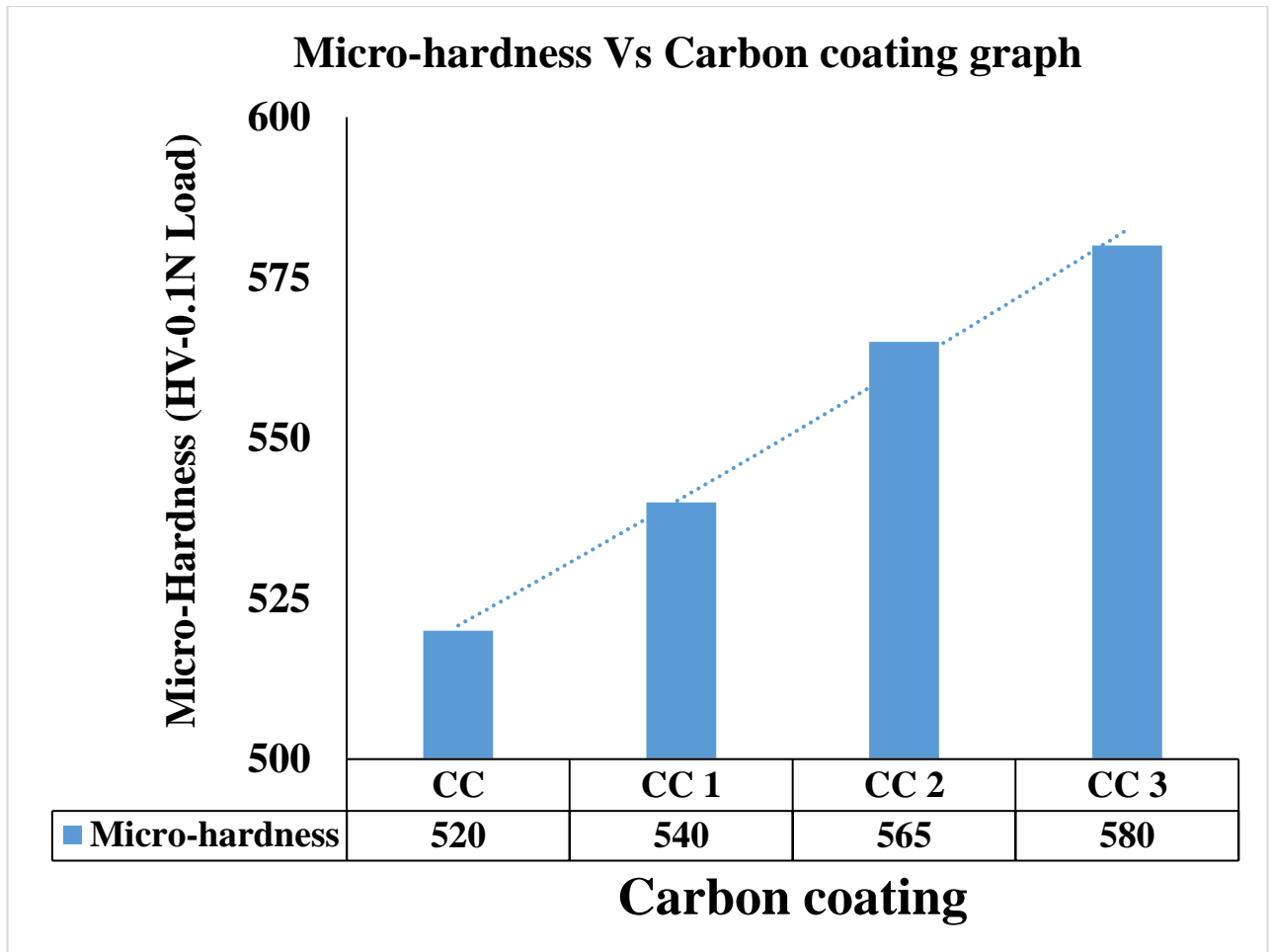


Figure 5.17 Micro-hardness Vs carbon coating graph

5.4.3. RESIDUAL STRESS

Fig. 5.18 shows the residual stress of coatings deposited by agriculture waste powder in presence nitrogen, oxygen and LPG using high velocity oxy-flame (HVOF). The experimental result shows that the residual stress developed on the carbon coating (CC) before wear test exhibits -193 MPa. The residual stress value of samples CC 1, CC 2 and CC 3 after wear test was -107, -50 and -5 MPa. The experimental results shows that as the test conditions of temperature ranging from 150 to 350°C, load 50 N and sliding velocity 1 m/s respectively increases the residual stress rapidly decreased in the range of -107 to -5 MPa. The residual stress test showed ~97% decrease in residual stress, at test condition of sliding velocity of 1 m/s, 350°C temperature, and 50N load. Compressive residual stresses are established due to bombing of high velocity particles on the substrate material. Further increase in temperature, load and sliding velocity during tribo test, tensile internal stresses are developed which balances the compressive stresses [184, 190]. The increase in temperature during testing condition results increase in thermal stresses and negligible structural stress. The increase in thermal stress results decrease in residual stress. Skordaris et al. [191], in there research reported that as the temperature increases, thermal stresses on the coating also increases but the structural stress developed on the samples remains stable upto 400°C.

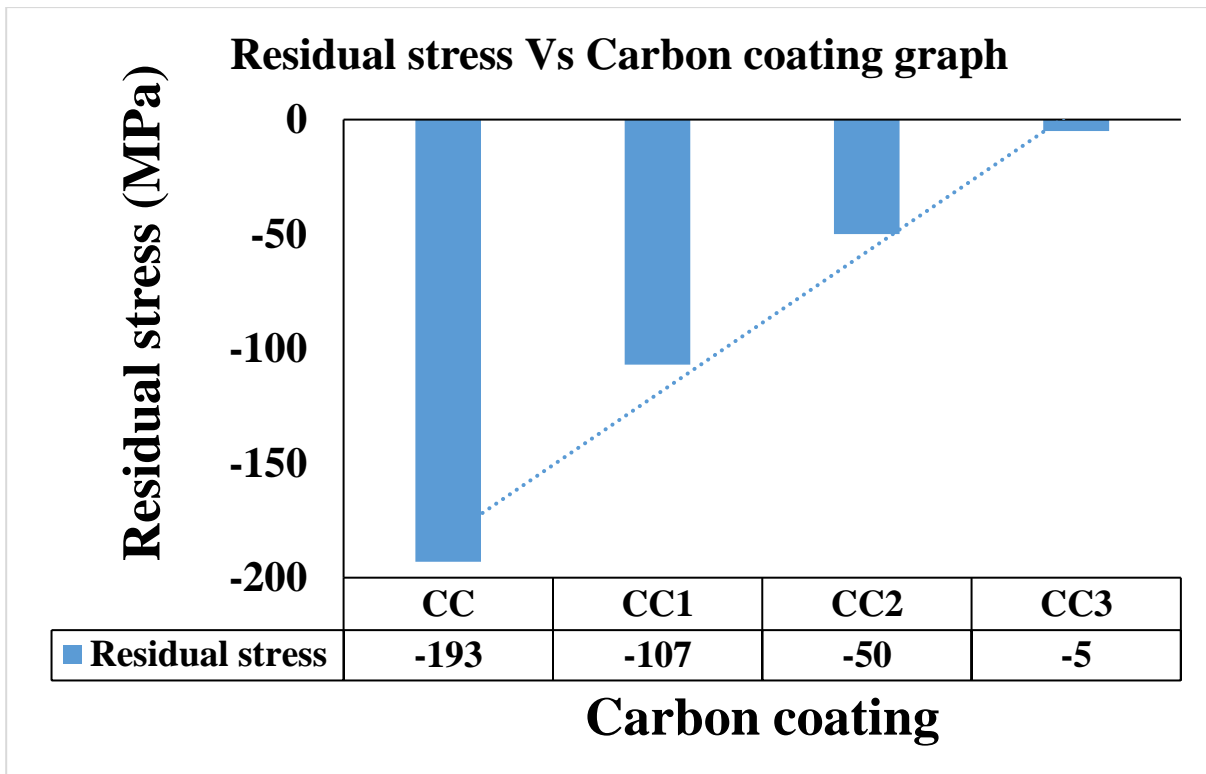
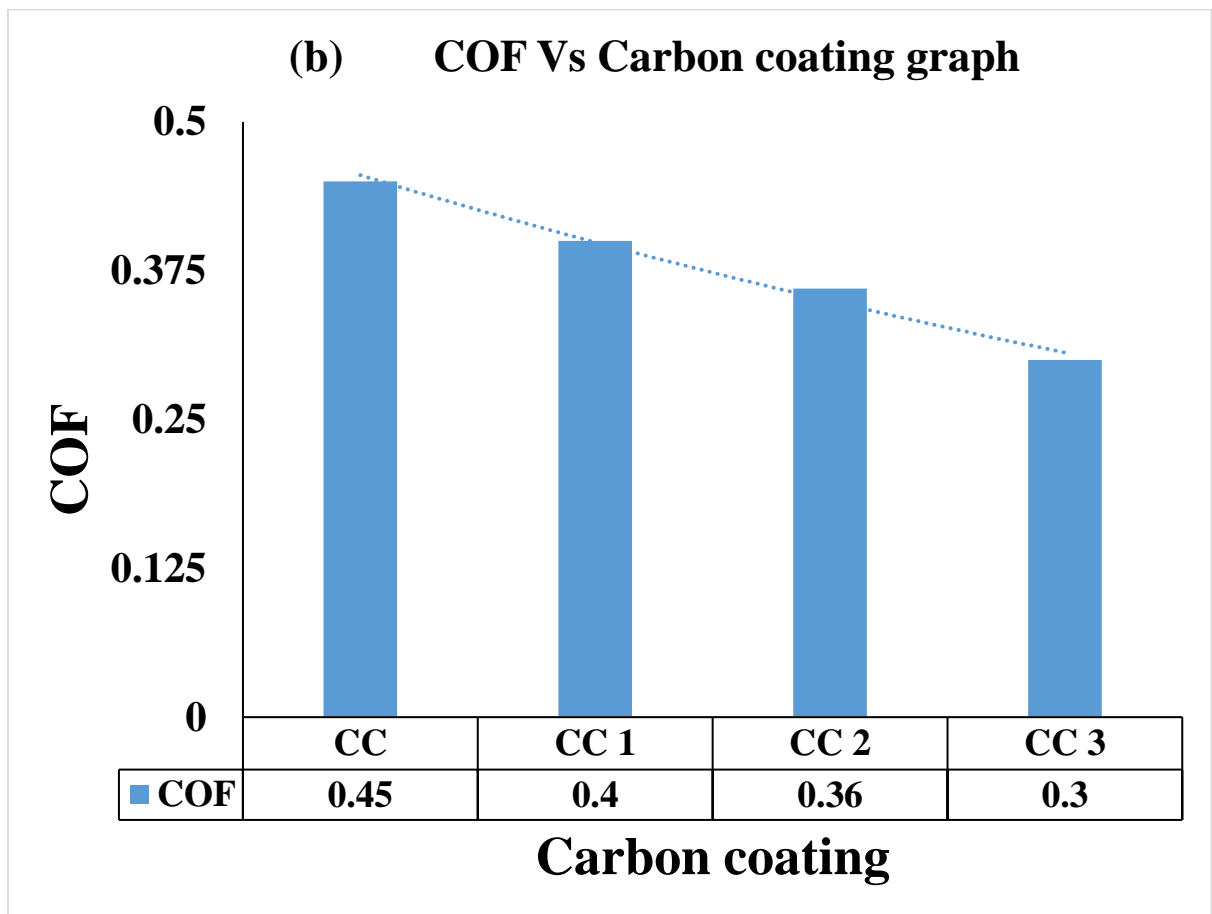
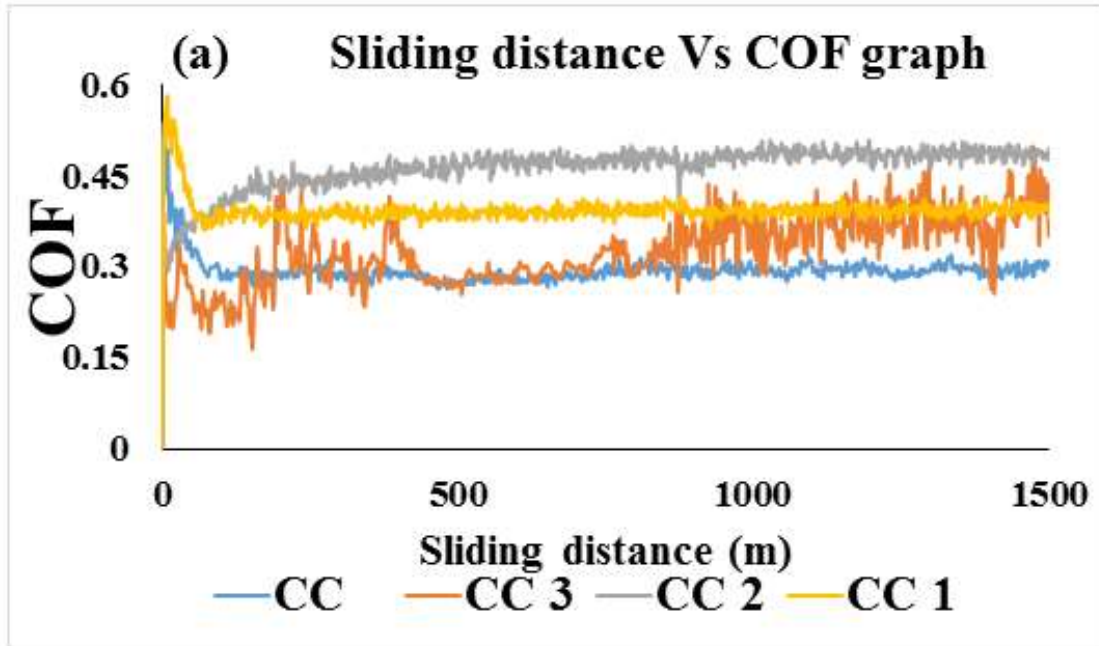


Figure 5.18 Residual stress Vs carbon coating graph

5.5. TRIBOLOGICAL CHARACTERIZATION OF CARBON COATING

5.5.1. COF & WEAR BEHAVIOR OF CARBON COATING

The experimental result shows that the COF and wear values developed on the carbon coating (CC) at idle conditions was 0.45 and 150 μm respectively. The COF value of samples CC 1, CC 2 and CC 3 was 0.40, 0.36 and 0.3 respectively, while wear values of samples CC 1, CC 2 and CC 3 was 100, 66 and 45 μm respectively. The tribological performance was evaluated using pin-on-disk tribometer which showed COF in the range of 0.3 to 0.40 as shown in fig. 5.19 (a-b), while fig. 5.19 (c) shows that wear was in the range of 45-100 μm , at test condition of temperature ranging from 150 to 350°C, load 50 N and sliding velocity 1 m/s respectively. The tribological analysis of carbon coating was done to evaluate the wear behavior for wear resistance applications. The tribological test showed 50% decrease in COF and 70% reduction in the wear at test condition of 1 m/s sliding velocity, 350°C temperature, and 50N load. During wear testing COF, and wear values first increases and after that become stable during running-in process between carbon coating and counterpart, due to good interfacial strength and excellent adhesive strength. Presence of carbon and hydrogen content, leads to graphitization effect and forms a thin solid lubricated layer [129, 184, 185]. Tyagi et al. [190] and Matikainen et al. [188] investigated HVOF developed coating and experimental result shows that higher velocity particles enhances wear resistance properties of developed coating [185, 188, 190], and similar trends was also attain the present tribological study. The experimental results that as the load, velocity and temperature increases, COF & wear behavior of carbon coating decreases significantly according to stribeck theory [192], and similar trends was also attain the present tribological study. The deviation of friction & wear by sliding distance shows approximately 500m run-in-stage, after that a stable stage [128, 136]. During running stage, carbon coating shows severe fluctuation in COF and wear, but later on became stable after introduction of graphitization effect in the coating. It was quite clear from experimental analysis that as the carbon contents increases friction and wear of carbon based coating decreases, since generally carbon phases acts as a good lubricants (solid lubricated layer) [185]. The changes phase structure and stoichiometry composition, formation of additive layer and oleo phobic behavior of developed carbon coatings played an important role that results decrease in friction and wear.



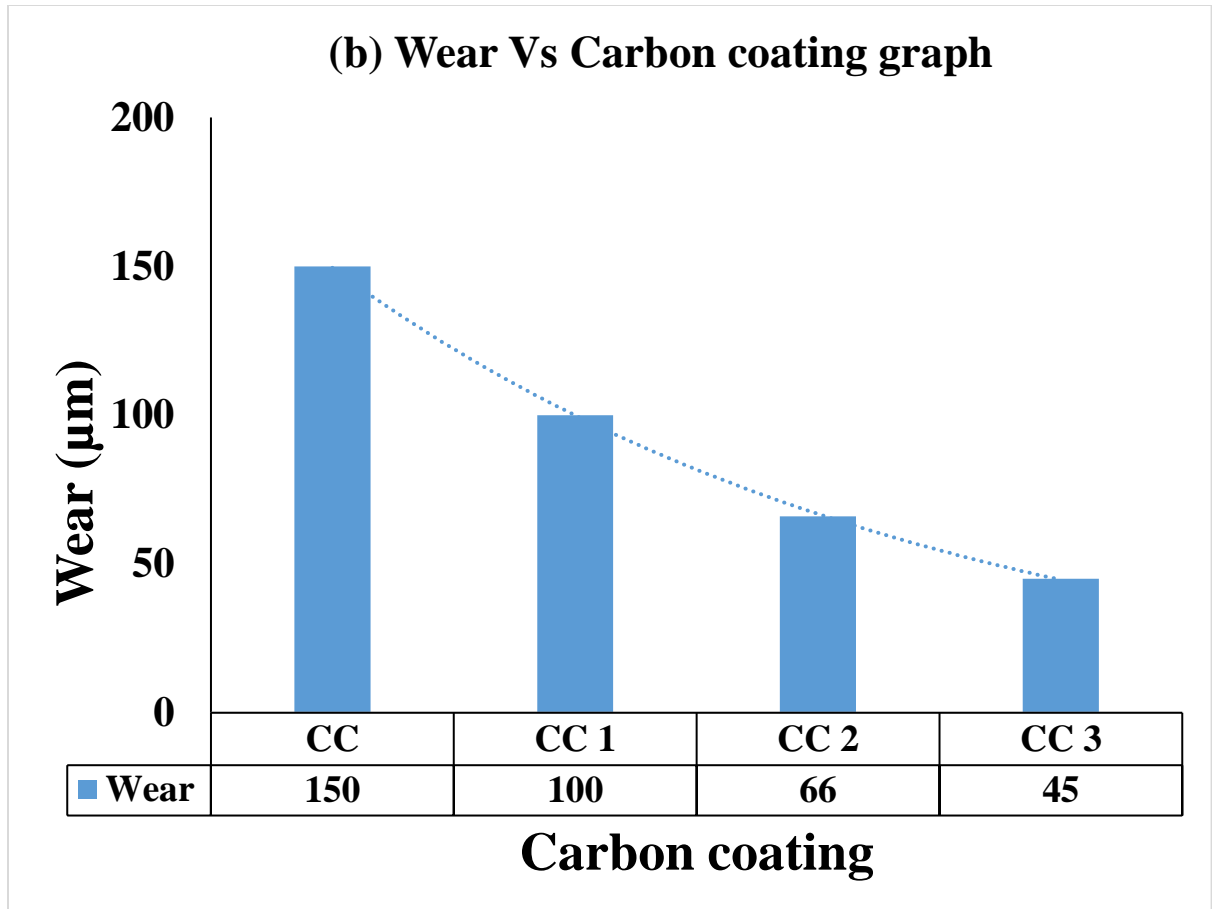


Figure 5.19 (a-b) COF (c) Wear Vs sliding distance graph carbon coating

5.5.2. WEAR MECHANISM OF CARBON COATING

The FESEM images shows wear characteristics of worn out surfaces of developed carbon coatings and is revealed in fig. 5.20. (a-b). FESEM obtained after wear test shows brittle structure with grains look along with conversion of amorphous to polycrystalline structure of carbon coating. It was quite clear that metallic abrasive particles are entrenched in the developed carbon coating or adhesive wear. The carbon coating shows ploughing action with presence of chip off particles, rubbing action along with worn out particles were seen during wear test [129]. It is also noted that formation of tribofilm and diffusion of carbon particles increases as the test conditions increases [184]. Wear mechanism of worn surfaces, oxide formation, cracks, micron size carbon particles, formation and delamination layer formation confirms erosion, indicates abrasive wear as dominant wear mechanism on developed coating. EDS results of worn surfaces and confirms the formation of tribo films and oxides, due to the increase in Carbon (C) and oxygen

(O) contents. Fig. 5.20. (b-d) shows micron size carbon particles, delamination layer formation, tribo-oxidative layer, transfer layer” formation and graphitization effect at variable test condition. At variable test conditions, wear occur mainly by plowing (plastic deformation). Deep grooves and scratches (possibly formed during plowing action caused due to micron size carbon crystallites) were present on the carbon coating. The micron size of carbon particles of developed coating work as a barrier against plastic deformation and results in abrasive wear resistance [129]. However, the surface morphology of carbon coating revealed less plastic deformation, between developed coating and counterbody occur during friction and wear test.

Different stages of wear behavior of carbon coating is illustrated as:

1st stage:

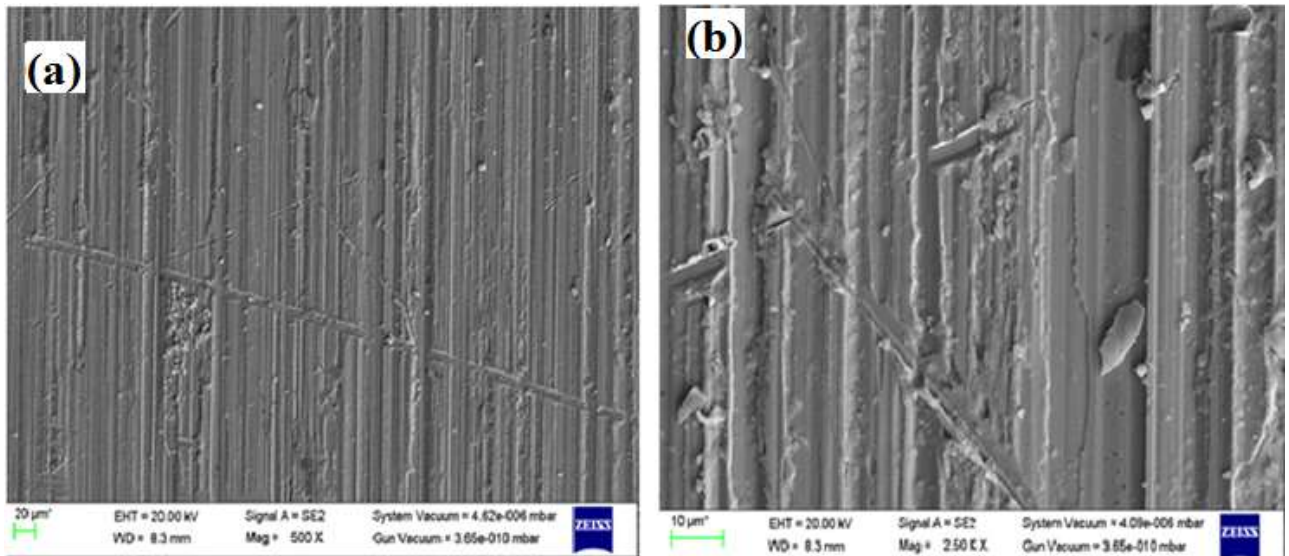
Initially, asperities of developed coating shot to penetrate into disc during running condition, when variable load, sliding velocity and temperature is applied, results in plastic deformation.

2nd stage:

Ploughing of disc by carbon coating asperities results in formation of tribofilm formation (due to carbon diffusion and oxide layer formation), which results in weakening of asperities.

3rd stage:

Increase in oxides, carbides layer formation and carbon diffusion shows smoothening of coating surface and lastly consequences in COF and wear reduction.



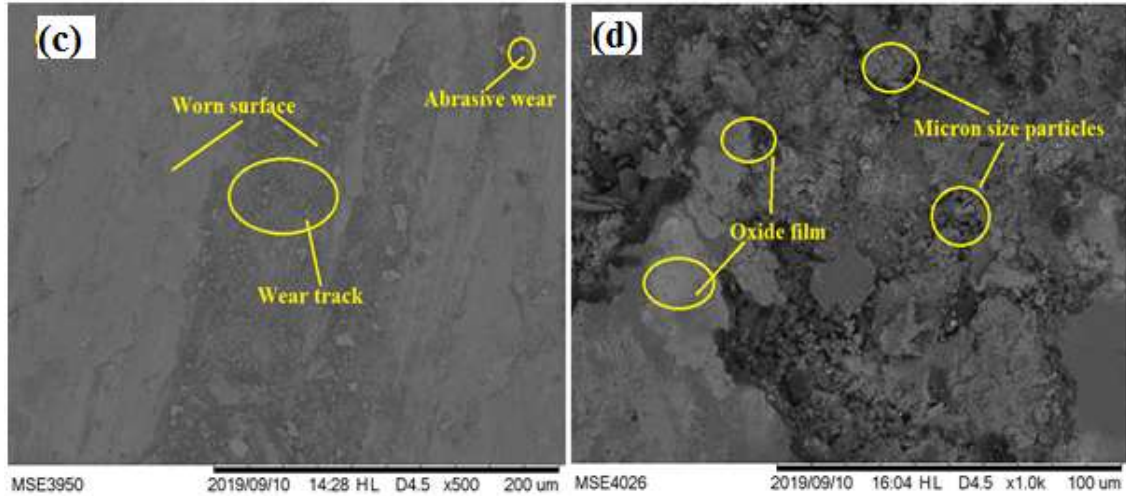


Figure 5.20 FESEM images of worn surfaces of carbon coating

5.5.3. Effects of parameters on Coefficient of friction (COF) for Carbon coating

All experimental results for process conditions were recorded in the table 5.2 and were examined to find out the effects of all parameters. Lower-the-better type, eminence characteristic was chosen for analysis of S/N ratio data for COF, and wear and test results at all condition were converted into S/N ratio

Table 5.2 Experimental results of Taguchi L₉ OA of COF, and Wear for Carbon Coating

Trial no.	COF			S/N ratio (db)	Wear			S/N ratio (db)
	R ₁	R ₂	R ₃		R ₁	R ₂	R ₃	
1	0.23	0.23	0.22	12.89	200	200	200	-46.0206
2	0.18	0.18	0.18	14.89	150	150	150	-43.5218
3	0.09	0.09	0.09	20.91	70	70	70	-36.9020
4	0.19	0.18	0.18	14.73	160	160	155	-43.9924
5	0.16	0.16	0.17	15.73	110	110	110	-40.8279
6	0.1	0.11	0.11	19.43	70	70	70	-36.9020
7	0.14	0.14	0.14	17.07	90	90	90	-39.0849
8	0.15	0.16	0.16	16.09	100	100	100	-40.0000
9	0.08	0.08	0.08	21.93	55	40	40	-33.1702
Mean(Overall)= 0.14					Mean(Overall)= 110.37			

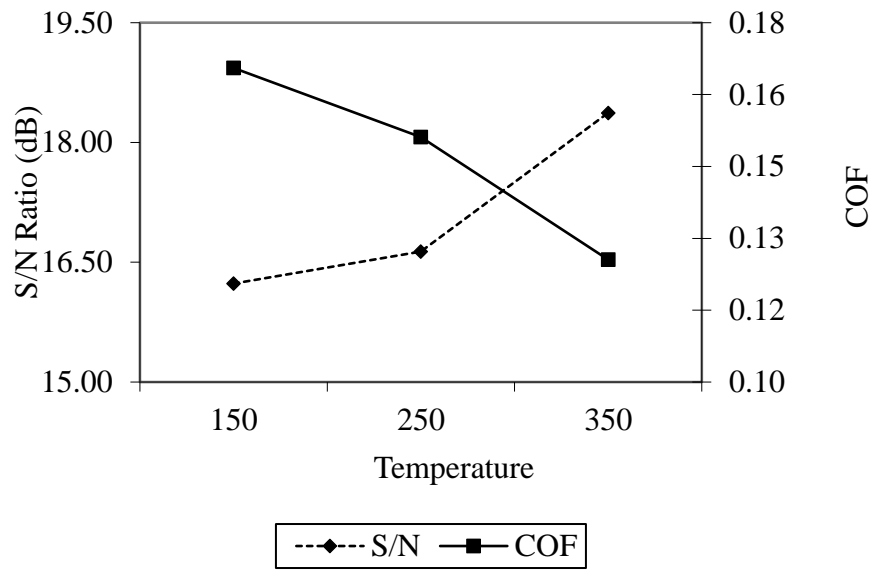
The main effects and average values of COF and S/N ratio for all parameters at trial T1, T2 and T3 were calculated and were illustrated in table 5.3 and also plotted in fig. 5.21.

Table 5.3 Main Effects and average values of COF (S/N ratio and raw data) for carbon coating

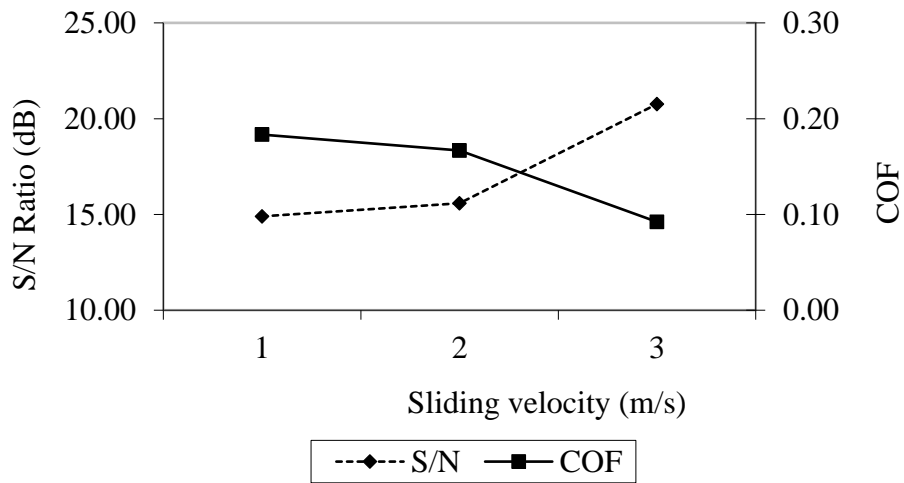
Parameter	Trial	Temperature (°C)		Sliding velocity (m/s)		Load (N)	
Data		Raw Data	S/N Ratio	Raw Data	S/N Ratio	Raw Data	S/N Ratio
	T1	0.16	16.23	0.18	14.90	0.16	16.13
	T2	0.15	16.63	0.16	15.57	0.14	17.18
	T3	0.12	18.37	0.09	20.76	0.13	17.90
	T2-T1	-0.01	0.39	-0.01	0.67	-0.01	1.04
	T3-T2	-0.02	1.73	-0.07	5.18	-0.01	0.721
Difference (T3-T2)-(T2-T1)		-0.01	1.33	-0.05	4.51	-0.001	-0.32

Fig. 5.21 (a) shows deviation of COF with respect to the temperature on the carbon coating. The result shows that COF obtained at 350°C temperature was lowest on comparing with 150°C and 250°C temperature for the carbon coating. However, the S/N ratio was highest at 350°C temperature on comparing with 150°C and 250°C temperature for the carbon coating. The above result shows that as the COF value was lower, when the carbon coating temperature was 350°C and a greater value of S/N ratio suggest a stronger signal and lesser noise, hence offers an optimum test results at the same trial condition. The reduction in COF at high temperature may be attributed due to formation of coherent tribo-oxidative lubricious layer or due to graphitization effect at C: H surface, which finally results decrease in COF. In the present work, COF decreases as temperature increases and at constant relative humidity, due to micron size carbon particles and formation of graphitized like lubricious.

(a) Effect of Temperature on S/N and COF



(b) Effect of Sliding velocity on S/N and COF



(c) Effect of Load on S/N and COF

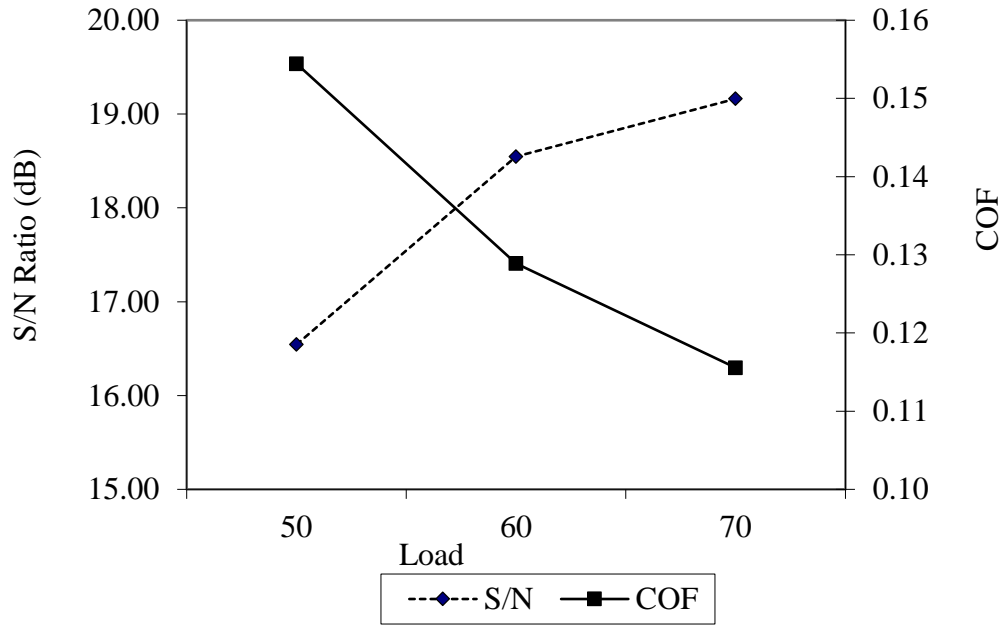


Figure 5.21. shows deviation of COF with parameters (a) Temperature ($^{\circ}\text{C}$) (b) Sliding velocity (m/s) (c) Load (N) of carbon coating

From the fig. 5.21 (b) it can be observed that there is a decrease in the value of COF as the sliding velocity increases from 1 to 3 m/s. The lowest value of COF was obtained for the highest sliding velocity of 3 m/s, while COF obtained was highest at 1m/s sliding velocity for the chosen range. The S/N ratio corresponds 3m/s was highest and decreases as the sliding velocity decreases. The decrease in COF at increasing speed may be attributed due to increase in formation of degree of transfer layer (solid lubricious graphitized layer) [138, 185]. In present work, COF decreases from 0.18 to 0.09 as the sliding velocity increases from 0.1 to 0.3 m/s. The decrease in COF may be due to formation of solid lubricious graphitized layer during steady state conditions. In assessment with other experimental results under similar test conditions, [138] COF obtained in the research work shows better test results for carbon coating.

Fig. 5.21(c) shows deviation of COF with respect to the load. The results show that the COF obtained was maximum at load of 50 N and decreases with increase in load from 50 to 70 N. However, S/N ratio value for COF was maximum at a load 70 N followed by 60 N and 50 N, while S/N ratio value was minimum at 70 N and maximum at 50N. In the present work, COF decreases as the load was increased during running condition and on comparing with other experimental

results [185], COF obtained in present research shows better results for the developed carbon coating under similar test conditions.

As lower-the-better type of quality characteristic was chosen for better results, a lower value of COF was sought. It is quite evident from fig. 5.21 that COF was optimum i.e. minimum at trial 3 of parameter A (350°C), trial 3 of the parameter B (3 m/s) and trial 3 of the parameter C (70 N). On the other hand, the trial parameters A, B and C, the lowest values of mean response correspond to the highest values of S/N ratio. From the above discussion it was clear that COF decreases as the temperature, sliding velocity and load increases, due to micron size particle of carbon which work as a barrier against plastic deformation or due to formation of graphitized like lubricious layer.

To examine the significance of parameters of COF, ANOVA was performed. Table 5.4. shows the pooled ANOVA S/N data and raw data of COF. It was quite evident that process parameters A, B, and C considerably affect mean and variation in COF. The percentage contribution of sliding velocity (75.49 %) was highest followed by temperature (12.93 %) and load (8.09 %) for COF.

Table 5.4. Pooled ANOVA for COF (S/N ratio and raw data) for carbon coating

Source type	SS		DOF		V		F-Ratio		SS'		P (%)	
	Raw data	S/N data	Raw data	S/N data	Raw data	S/N data	Raw data	S/N data	Raw data	S/N data	Raw data	S/N data
Temperature (°C)	0.007	7.74	2	2	0.003	3.87	49.35	31.48	0.007	7.50	12.93	10.07
Sliding velocity (m/s)	0.04	61.70	2	2	0.02	30.85	283.11	250.76	0.04	61.46	75.49	82.54
Load (N)	0.004	4.75	2	2	0.002	2.37	31.23	19.31	0.004	4.506	8.09	6.05
E (Pooled)	0.001	0.24	20	2	0.00007	0.12	-	-	0.001	0.98	3.47	1.32
Total	0.05	74.45	26	8	-	-	-	-	0.05	74.45	100	100

SS= Sum of squares; DOF= Degree of freedom; V= Variance; SS'= pure sum of squares

5.5.3.1. Estimation of optimal performance characteristics

5.5.3.1.1. Optimal values of response characteristics for COF (predicted mean)

Table 5.5 shows the average values of COF at optimum level of significant parameters. The optimum value of the estimated mean (μ) COF can be obtained as follow [185]:

$$\mu_{\text{COF}} = A_3 + B_3 + C_3 - 2T \quad (2)$$

$$\mu_{\text{COF}} = 0.06$$

Table 5.5 Average values of COF at optimal levels for carbon coating

Trail	COF
A ₃	0.12
B ₃	0.09
C ₃	0.13
T	0.14
A ₃ = trail 3 of temperature; B ₃ = trail 3 of sliding velocity; C ₃ = trail 3 of load; T= average value of response	

The Confirmation experiments (CI_{CE}) for 95 % confidence interval and confidence interval population (CI_{POP}) was calculated by using equations:

$$CI_{\text{CE}} = \sqrt{F_a(1, f_e) V_e \left[\frac{1}{n_{\text{eff}}} + \frac{1}{R} \right]} \quad (3)$$

$$CI_{\text{POP}} = \sqrt{\frac{F_a(1, f_e) V_e}{n_{\text{eff}}}} \quad (4)$$

where $F_a(1, f_e)$ = F ratio at the confidence level of (1-a) against DOF 1 and degree of freedom error f_e ; R= sample size for confirmation experiments; V_e = variance error; $n_{\text{eff.}} = \left(\frac{N}{1+\text{DOF}} \right)$; N= total no. of trials; and DOF = total degree freedom associated in the estimate of mean response.

The values obtained by the ANOVA are:

$$N = 27; f_e = 20; V_e = 0.000075; n_{\text{eff.}} = 3.86; R = 3; F_{0.05}(1, 20) = 3.49$$

$$\text{From eq. 3 } CI_{\text{CE}} = \pm 0.012$$

$$\text{From eq. 4 } CI_{\text{POP}} = \pm 0.0082$$

The predicted optimum values for COF is given by:

$$CI_{CE} : 0.048 < \mu < 0.072$$

$$CI_{POP} : 0.051 < \mu < 0.068$$

The optimum values of COF were predicted at the designated trials of significant parameters.

Temperature (A, trial 3) = 350°C

Sliding velocity (B, trial 3) = 3 m/s

Load (C, trial 3) = 70 N

5.5.3.1.2. Confirmation experiments

Three confirmation tests were performed at the optimal situation of the process parameters. For COF process parameters were set temperature at trail 3 (350°C), sliding velocity at trail 3 (3 m/s), and load at trail 3 (70N). The average value for COF of carbon coating was measured as 0.06 which was in the predicted optimum range of 95 % confidence interval for COF for the carbon coating.

5.5.4. Effects of parameters on Wear for Carbon coating

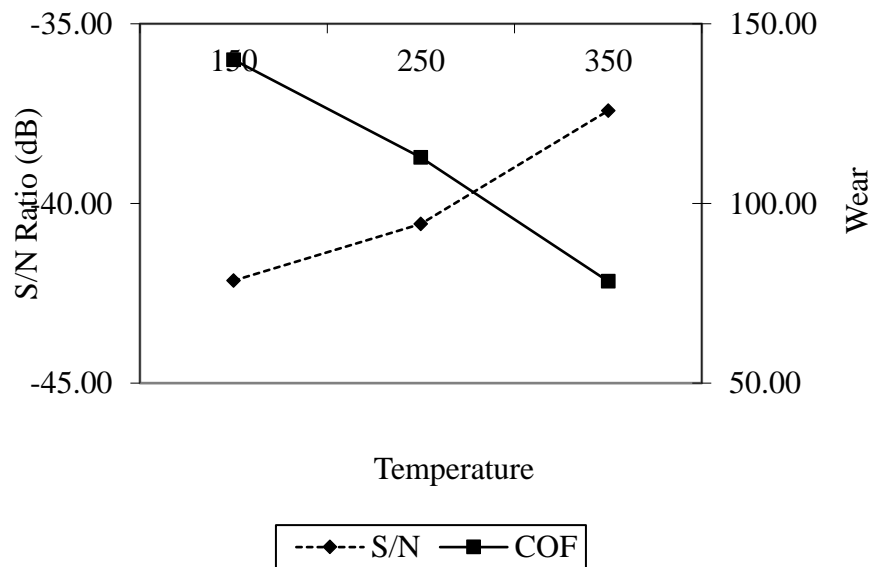
The main effects and average values of wear and S/N ratio for all parameters at trail T1, T2 and T3 were calculated and were illustrated in table 5.6 and also plotted in fig. 5.22.

Table 5.6 Main Effects and average values of wear (S/N ratio and raw data) for carbon coating

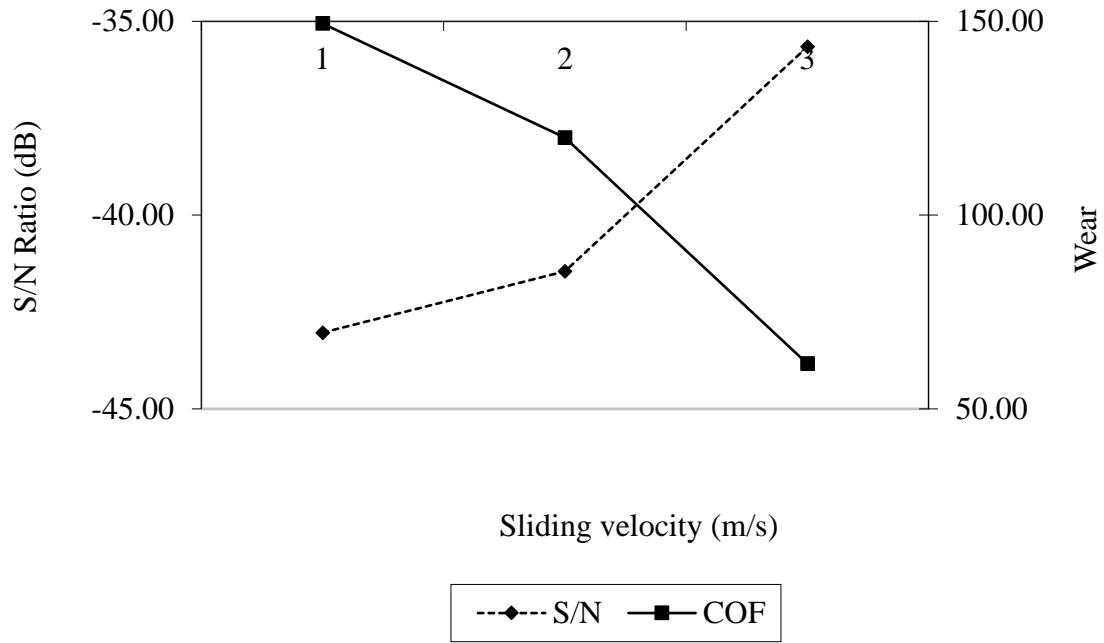
Parameter	Trial	Temperature (°C)		Sliding velocity (m/s)		Load (N)	
Data		Raw Data	S/N Ratio	Raw Data	S/N Ratio	Raw Data	S/N Ratio
	T1	140	-42.14	149.44	-43.033	123.33	-40.97
	T2	112.77	-40.57	120.0	-41.45	117.77	-40.22
	T3	78.33	-37.41	61.66	-35.65	90.0	-38.93
	T2-T1	-27.22	1.57	-29.44	1.58	-5.55	0.74
	T3-T2	-34.44	3.15	-58.33	5.79	-27.77	1.29
Difference (T3-T2)-(T2-T1)		-7.22	1.58	-28.88	4.20	-22.22	0.544

Fig. 5.22 (a) shows deviation of wear with respect to the temperature on the carbon coating. The result shows that wear obtained at 350°C temperature was lowest on comparing with 150°C and 250°C temperature for the carbon coating. However, the S/N ratio was highest at 350°C temperature on comparing with 150°C and 250°C temperature for the carbon coating. The above result shows that as the wear value was lower, when the carbon coating temperature was 350°C and a greater value of S/N ratio suggest a stronger signal and lesser noise, hence offers an optimum test results at the same trial condition. The reduction in wear at high temperature may be attributed due to formation of coherent tribo-oxidative lubricious layer or due to graphitization effect at C: H surface, which finally results decrease in wear. In the present work, wear decreases as temperature increases and at constant relative humidity, due to micron size carbon particles and formation of graphitized like lubricious.

(a) Effect of Temperature on S/N and Wear



(b) Effect of Sliding velocity on S/N and Wear



(c) Effect of Load on S/N and Wear

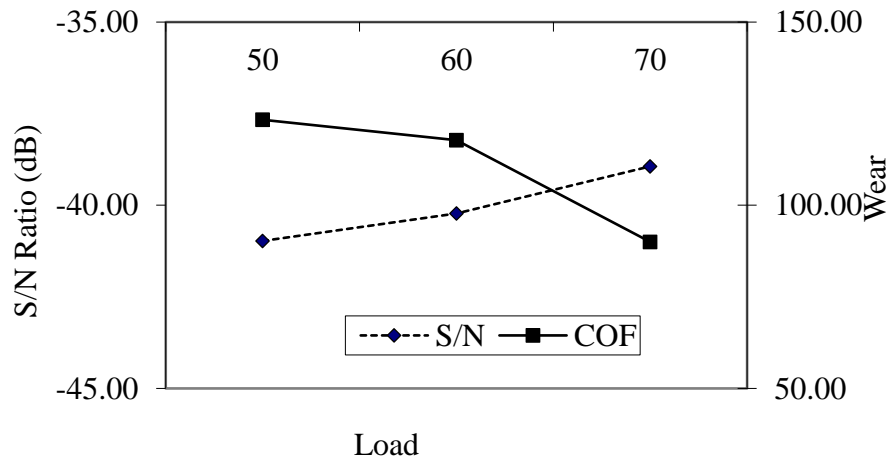


Figure 5.22 shows deviation of wear with parameters (a) Temperature ($^{\circ}\text{C}$) (b) Sliding velocity (m/s) (c) Load (N) of carbon coating

From the fig. 5.22 (b) it can be observed that there is a decrease in the value of wear as the sliding velocity increases from 1 to 3 m/s. The lowest value of COF was obtained for the highest sliding velocity of 3 m/s, while wear obtained was highest at 1m/s sliding velocity for the chosen

range. The S/N ratio corresponds 3m/s was highest and decreases as the sliding velocity decreases. The decrease in wear may be due to formation of solid lubricious graphitized layer during steady state conditions. In assessment with other experimental results under similar test conditions, [185] wear obtained in the research work shows better test results for carbon coating.

Fig. 5.22(c) shows deviation of wear with respect to the load. The results show that the wear obtained was maximum at load of 50 N and decreases with increase in load from 50 to 70 N. However, S/N ratio value for wear was maximum at a load 70 N followed by 60 N and 50 N, while S/N ratio value was minimum at 70 N and maximum at 50N. It was noted that due to increase in load, there was a formation of graphitized layer which helps in reduction of wear during running condition [185]. In the present work, wear decreases as the load was increased during running condition and on comparing with other experimental results [138, 185], COF obtained in present research shows better results for the developed carbon coating under similar test conditions.

As lower-the-better type of quality characteristic was chosen for better results, a lower value of wear was sought. It is quite evident from fig. 5.22 that wear was optimum i.e. minimum at trial 3 of parameter A (350°C), trial 3 of the parameter B (3 m/s) and trial 3 of the parameter C (70 N). On the other hand, the trial parameters A, B and C, the lowest values of mean response correspond to the highest values of S/N ratio. From the above discussion it was clear that wear decreases as the temperature, sliding velocity and load increases, due to micron size particle of carbon which work as a barrier against plastic deformation or due to formation of graphitized like lubricious layer.

To examine the significance of parameters of Wear, ANOVA was performed. Table 5.7 shows the pooled ANOVA S/N data and raw data of wear. It was quite evident that process parameters A, B, and C considerably affect mean and variation in wear. The percentage contribution of sliding velocity (59.62 %) was highest followed by temperature (28.43 %) and load (9.36 %) for Wear.

Table 5.7 Pooled ANOVA for Wear (S/N ratio and raw data) for carbon coating

Source type	SS		DOF		V		F-Ratio		SS'		P (%)	
	Raw data	S/N data	Ra w data	S/ N data	Raw data	S/N data	Raw data	S/N data	Raw data	S/N data	Ra w data	S/N data
Temperature (°C)	17190.74	34.80	2	2	8595.37	17.40	144.37	106.29	1707.166	34.48	28.43	26.13
Sliding velocity (m/s)	35924.07	90.43	2	2	17962.03	45.21	301.69	276.15	3580.50	90.10	59.62	68.29
Load (N)	5740.74	6.366	2	2	2870.37	3.18	48.21	19.43	56.21	6.03	9.36	4.57
E (Pooled)	1190.74	0.32	20	2	59.53	0.16	-	-	1547.96	1.31	2.57	0.99
Total	60046.29	131.93	26	8	-	-	-	-	60046.29	131.93	100	100
SS= Sum of squares; DOF= Degree of freedom; V= Variance; SS'= pure sum of squares												

5.5.4.1. Estimation of optimal performance characteristics

5.5.4.1.1. Optimal values of response characteristics for Wear (predicted mean)

Table 5.8 shows the average values of wear at optimum level of significant parameters. The optimum value of the estimated mean (μ) wear can be obtained as follow [138]:

$$\mu_{\text{wear}} = A_3 + B_3 + C_3 - 2T \quad (2)$$

$$\mu_{\text{wear}} = 9.25$$

Table 5.8 Average values of Wear at optimal levels for carbon coating

Trail	Wear
A ₃	78.33
B ₃	61.66
C ₃	90
T	110.37
A ₃ = trail 3 of temperature; B ₃ = trail 3 of sliding velocity; C ₃ = trail 3 of load; T= average value of response	

The Confirmation experiments (CI_{CE}) for 95 % confidence interval and confidence interval population (CI_{POP}) was calculated by using equations:

$$CI_{CE} = \sqrt{F_a(1, f_e) V_e \left[\frac{1}{n_{eff}} + \frac{1}{R} \right]} \quad (3)$$

$$CI_{POP} = \sqrt{\frac{F_a(1, f_e) V_e}{n_{eff}}} \quad (4)$$

where $F_a(1, f_e)$ = F ratio at the confidence level of (1-a) against DOF 1 and degree of freedom error f_e ; R = sample size for confirmation experiments; V_e = variance error; $n_{eff.} = \left(\frac{N}{1+DOF} \right)$; N = total no. of trials; and DOF = total degree freedom associated in the estimate of mean response.

The values obtained by the ANOVA are:

$$N = 27; f_e = 20; V_e = 59.53; n_{eff.} = 3.86; R = 3; F_{0.05}(1, 20) = 3.49$$

$$\text{From eq. 3 } CI_{CE} = \pm 11.09$$

$$\text{From eq. 4 } CI_{POP} = \pm 7.33$$

The predicted optimum values for wear is given by:

$$CI_{CE} : -1.84 < \mu < 20.34$$

$$CI_{POP} : 1.92 < \mu < 16.58$$

The optimum values of wear were predicted at the designated trials of significant parameters.

$$\text{Temperature (A, trial 3)} = 350^\circ\text{C}$$

$$\text{Sliding velocity (B, trial 3)} = 3 \text{ m/s}$$

$$\text{Load (C, trial 3)} = 70 \text{ N}$$

5.5.4.1.2. Confirmation experiments

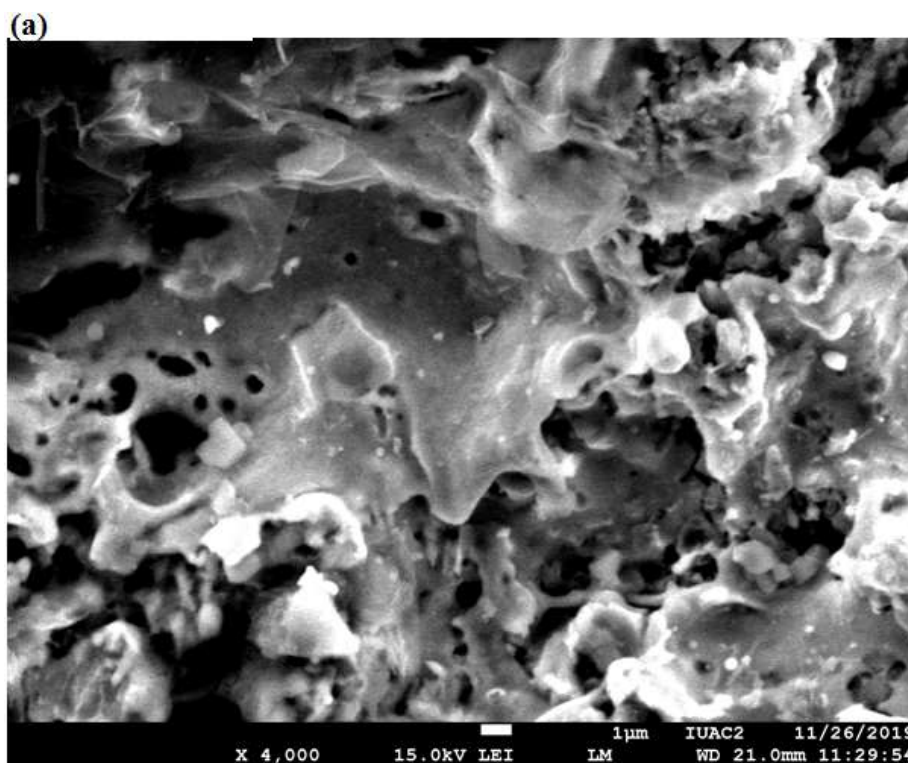
Three confirmation tests were performed at the optimal situation of the process parameters. For wear process parameters were set temperature at trail 3 (350°C), sliding velocity at trail 3 (3 m/s), and load at trail 3 (70N). The average value for wear of carbon coating was measured as 9.25 μm which was in the predicted optimum range of 95 % confidence interval for wear for the carbon coating.

PART 2:

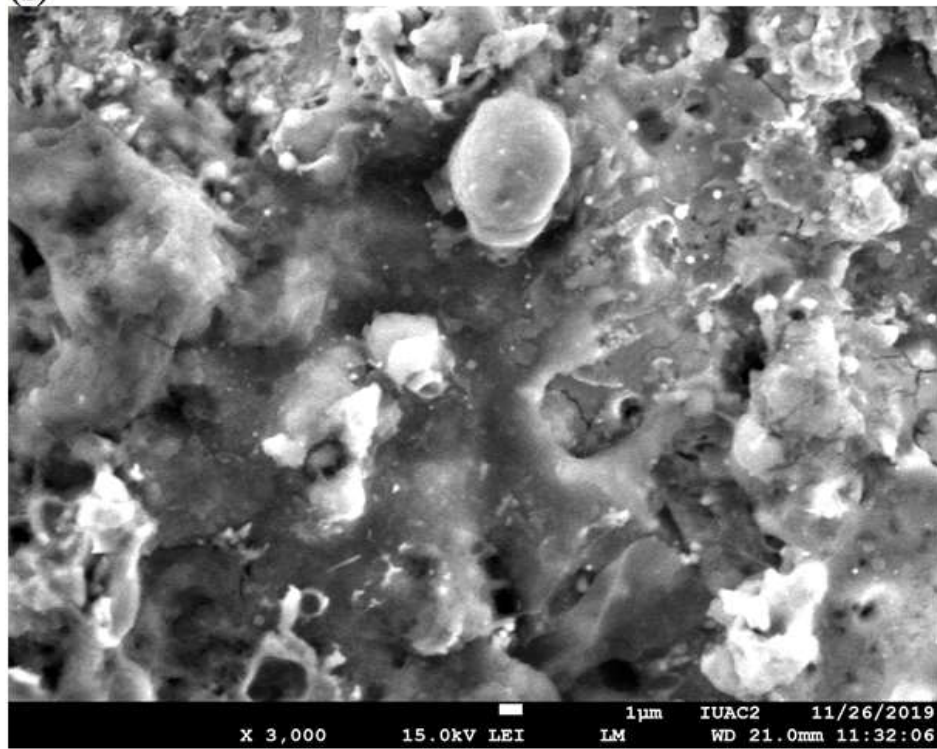
5.6.CARBON BASED COMPOSITE COATING CHARACTERIZATION

5.6.1. FESEM+EDS RESULTS OF CARBON BASED COMPOSITE COATING

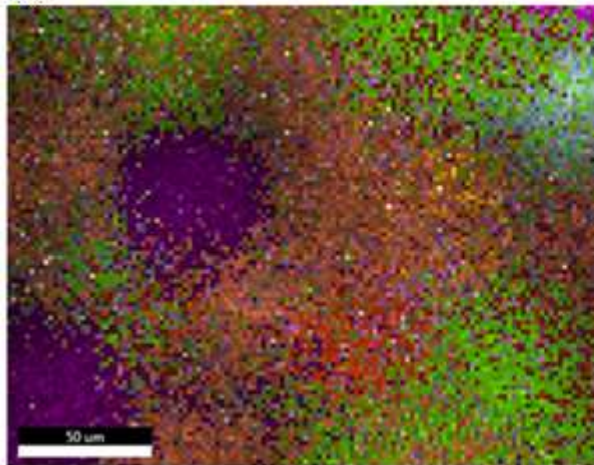
Fig. 5.23 (a-b) illustrates the FESEM image of surface and cross-sectional morphology along with bonding conformity of C+WC+Mo+TiO₂+Al₂O₃ blend composite coatings. It is quite clear from FESEM image at x2000 and x4000 flake like structures with formation of lamellae are seen along with presence of semi-molten, molten and un-melted grains of composite particles along with formation of lamellae [193]. It was observed from the FESEM shows splat formation which confirms uniform and homogeneous coating. In addition, solidified droplet with flattened and cracked structured were formed due to increase in temperature. Carbon composite coating was deposited uniformly and homogeneously ranging from 380-430µm. Fig. 5.23 (c-d) shows the EDS mapping results of composite coating and confirms the deposition of weight% in developed coating as 14% carbon, 18% oxygen, 7% W, 2% Mo, 2% Ti, 15% Al and rest weight % of iron (26%), 6% Mg, 6% Si, 2% Cr, 2% Mn and 2% Ni.



(b)



(c)



14% C K	14% C	2% CrK	2% Cr
18% O K	18% O	2% MnK	2% Mn
6% MgK	6% Mg	26% FeK	26% Fe
15% AlK	15% Al	2% NiK	2% Ni
6% SiK	6% Si		
7% W M	7% W		
2% MoL	2% Mo		
2% TiK	2% Ti		

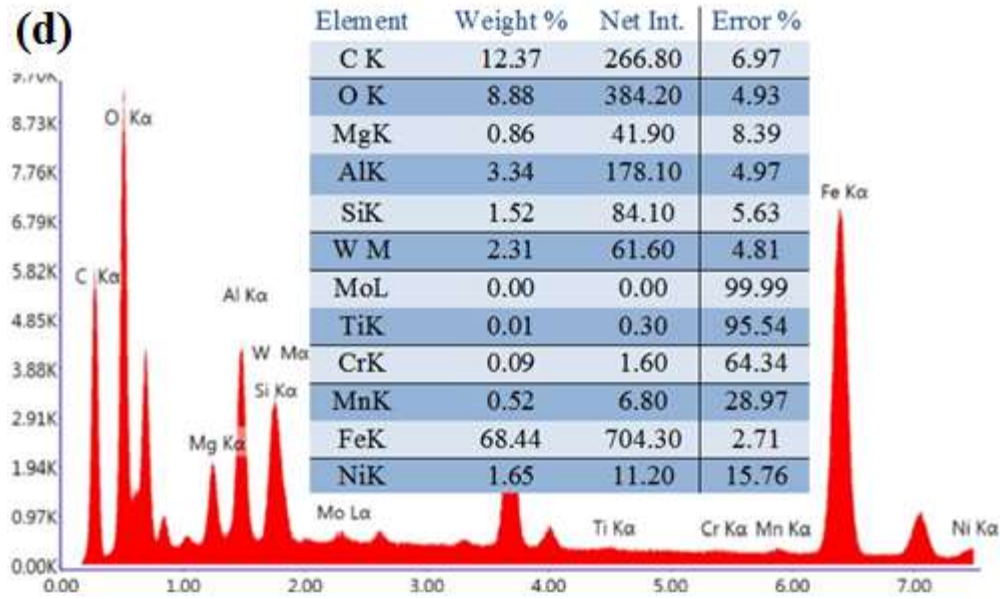


Figure 5.23 (a-b) FESEM images (c-d) EDS mapping result of composite coating

5.6.2. HRXRD OF CARBON BASED COMPOSITE COATING

Fig. 5.24 shows the HRXRD spectra on the 10%C+WC+Mo+TiO₂+Al₂O₃ blend composite coating. In the present case peaks at $2\theta = 13-15^\circ$, $2\theta = 16-18^\circ$, $2\theta = 25.5^\circ$ and at $2\theta = 44.5^\circ$, $2\theta = 65, 78$ respectively were observed on developed coating.

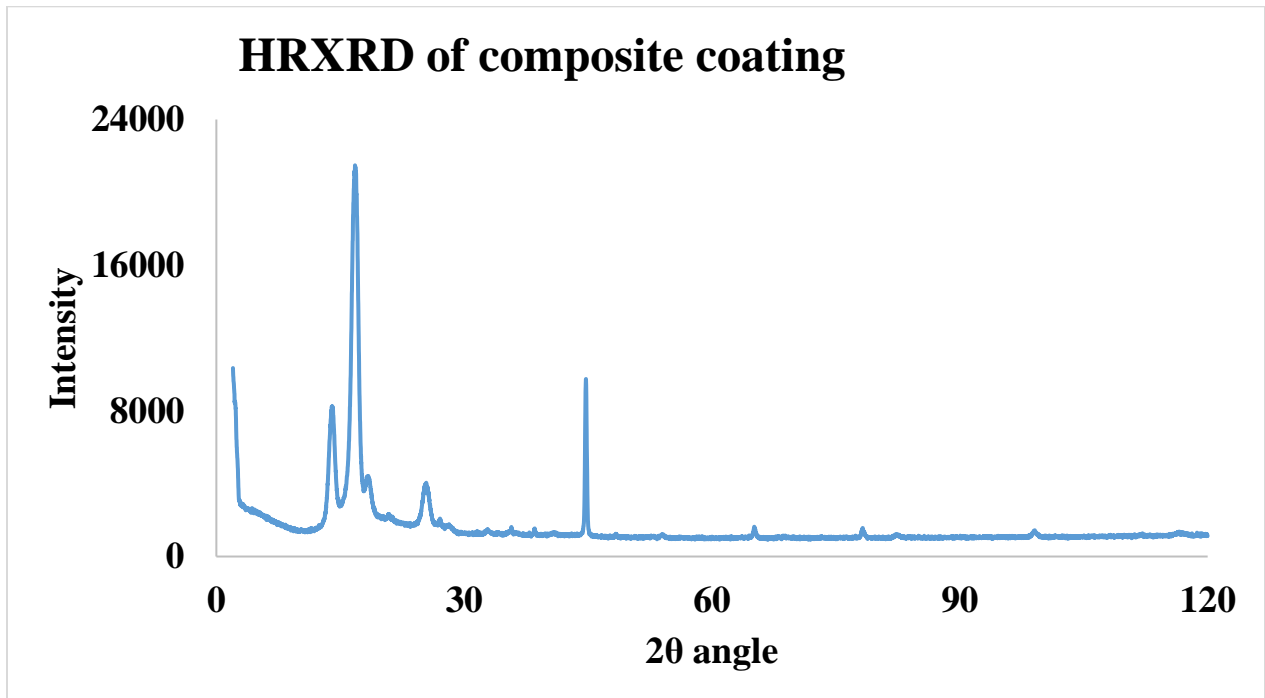


Figure 5.24 HRXRD result of composite coating

5.6.3. RAMAN SPECTRUM OF CARBON BASED COMPOSITE COATING

Fig. 5.25 shows the captured Raman spectra peak on the developed coating with presence of hybridized carbon peak. To examine structural properties of coating materials Raman spectroscopy has been used by the researchers. In the present research, prominent peaks were observed at 1125-1135, 1340-1360 and 1570-1590 cm^{-1} on the C+WC+Mo+TiO₂+Al₂O₃ blend composite coating. It is noted that peaks around 1340-1350 cm^{-1} and at 1130 cm^{-1} shows sp^1 or sp^2 hybridized carbon deposition on the developed coating, while peaks around 1560-1580 cm^{-1} shows presence of sp^3 hybridization with presence of DLC coating as testified in formerly research [185-187].

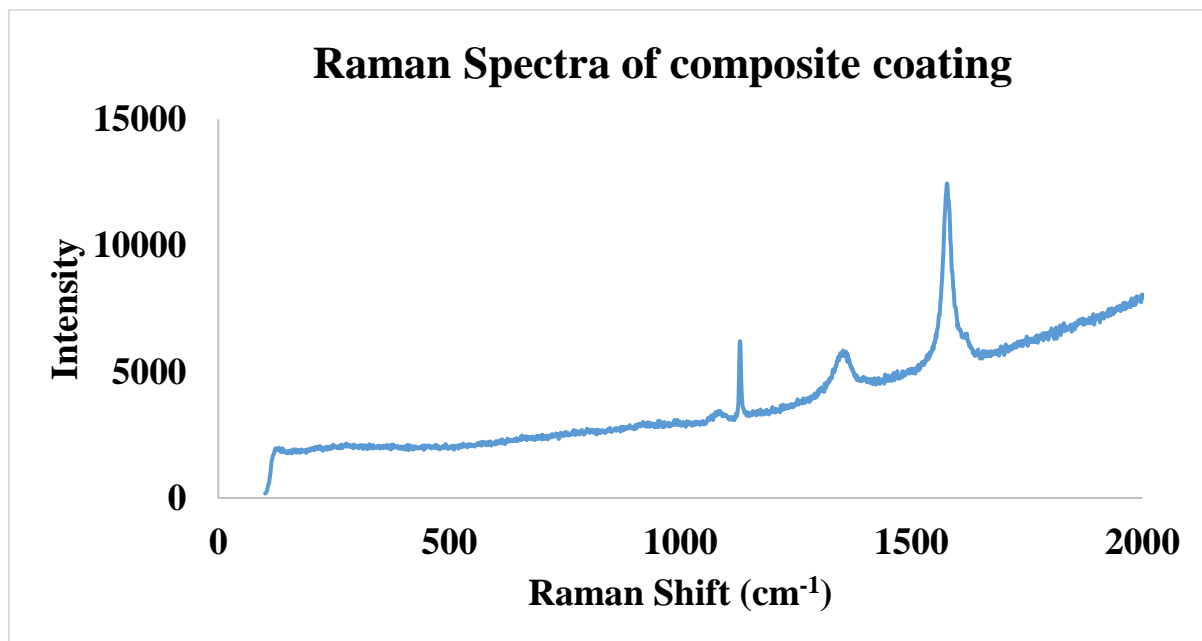


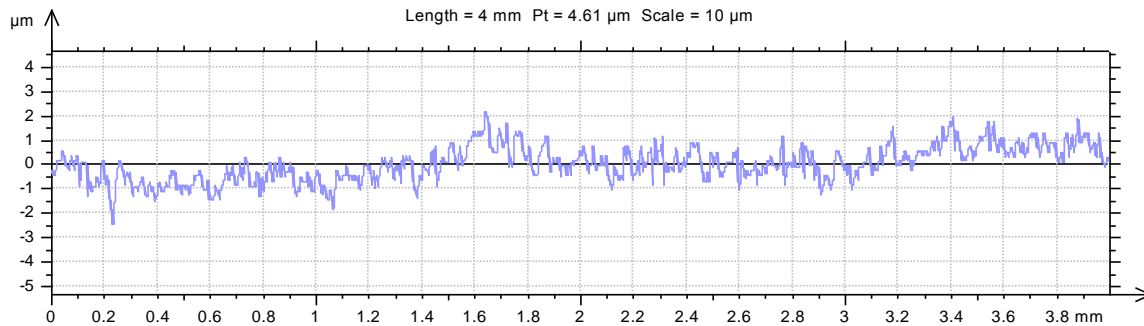
Figure 5.25 Raman spectra result of composite coating

5.7. MECHANICAL CHARACTERIZATION OF CARBON BASED COMPOSITE COATING

5.7.1. SURFACE ROUGHNESS

Fig. 5.26 shows the surface roughness of C+WC+Mo+TiO₂+Al₂O₃ blend composite coatings deposited in presence of N₂, O and LPG using HVOF process. The developed coating obtained after HVOF spray technique was rough, so in order to get surface smooth, initially, the developed coating was ground with emery paper of grit size 80-3000. After that, the cut samples were polished with 1/0, 2/0 alumina paste. The smoothing of surface was done due to constraint of

Taylor Hobson precision machine used in present investigation. The experimental result shows that surface roughness value of carbon composite coating (CC) was $0.345\text{ }\mu\text{m}$.



Parameters calculated on the profile Profile

- * Parameters calculated by mean of all the sampling lengths.
- * A microroughness filtering is used, with a ratio of $2.5\text{ }\mu\text{m}$.

Roughness Parameters, Gaussian filter, 0.8 mm

Ra	=	$0.345\text{ }\mu\text{m}$	
Rz	=	$2.43\text{ }\mu\text{m}$	
Rq	=	$0.43\text{ }\mu\text{m}$	
Rp	=	$1.22\text{ }\mu\text{m}$	
Rv	=	$1.21\text{ }\mu\text{m}$	
Rt	=	$2.82\text{ }\mu\text{m}$	
Rsk	=	0.115	
Rku	=	3.13	
Rmr	=	15%	($1\text{ }\mu\text{m}$ under the highest peak)
Rdc	=	$0.738\text{ }\mu\text{m}$	(20%-80%)
RSm	=	0.0443 mm	
RDq	=	5.74°	
RLq	=	0.027 mm	
RLo	=	0.506%	
RzJIS	=	$1.67\text{ }\mu\text{m}$	
R3z	=	$1.83\text{ }\mu\text{m}$	
RPc	=	7.19 pks/mm	($\pm 0.5\text{ }\mu\text{m}$)
Rc	=	$0.979\text{ }\mu\text{m}$	

Figure 5.26 Surface roughness result of composite coating

5.7.2. MICRO_HARDNESS

The micro-hardness of C+WC+Mo+TiO₂+Al₂O₃ blend composite coatings deposited in presence of N₂, O and LPG using HVOF process are listed in figure 5.27. The experimental result shows that micro-hardness value of carbon based composite coating (CC) before wear test exhibits 550 HV. The micro-hardness value of samples CC 1, CC 2 and CC 3 after wear test was 590, 620 and 650 HV. The experimental results of hardness for composite coating shows that as the test condition of temperature ranging from 150 to 350°C, load 50 N and sliding velocity 1 m/s respectively, increases hardness rapidly increases from 590 to 650 HV. The hardness was found to increase ~15% at test condition of 50N load, 1 m/s sliding velocity and 350°C temperature. The increase in hardness is due to the formation of oxides and sulphides layers, agglomerate size of powders and strong adhesive force between coating particles [129]. The experimental result shows as the temperature, load and velocity increases, the micro-hardness of C+WC+Mo+TiO₂+Al₂O₃ blend composite coating increases significantly as studied by Tyagi et al. [184], and similar trends was also attain the present hardness test. Matikainen et al. [188] investigated HVOF developed coating and experimental result shows that higher velocity particles enhances hardness of developed coating. It is also noted that presence of hard phased structured micron size carbon particles works as an impediment contrary to deformation, finally results increase in hardness [189].

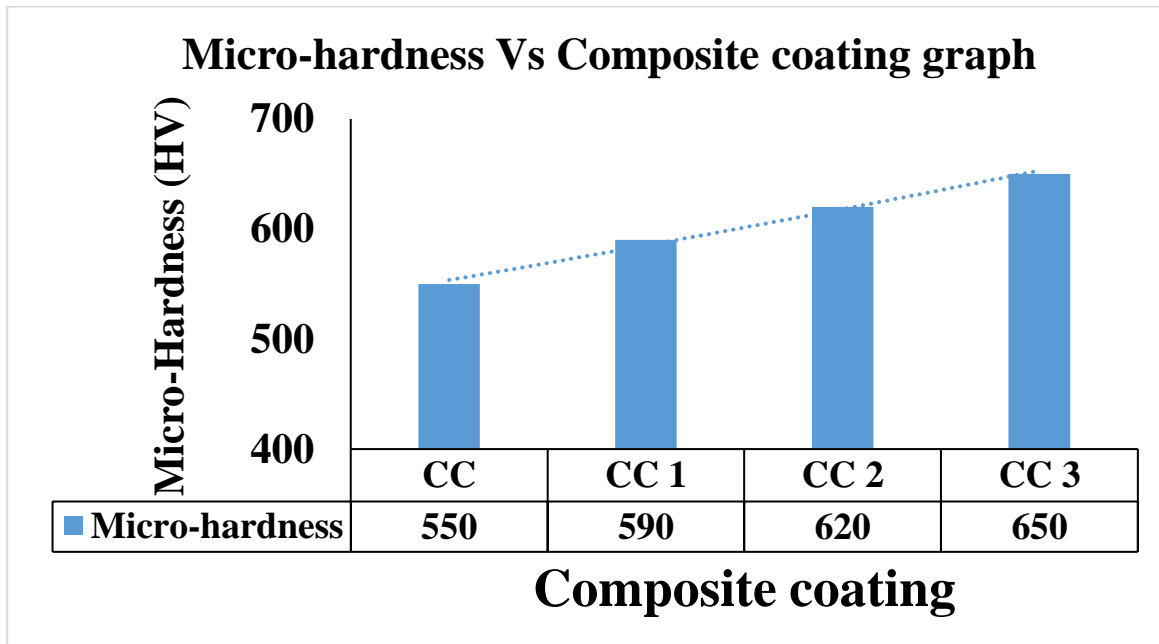


Figure 5.27 Micro-hardness Vs composite coating graph

5.7.3. RESIDUAL STRESS

The residual stress of C+WC+Mo+TiO₂+Al₂O₃ blend composite coatings deposited in presence of N₂, O and LPG using HVOF process are listed in figure 5.28. The experimental result shows that the residual stress developed on the carbon based composite coating (CC) before wear test exhibits -132 MPa. The residual stress value of samples CC 1, CC 2 and CC 3 after wear test was -91, -45 and -3 MPa. The experimental results of residual stress for composite coating shows that as the test condition of temperature ranging from 150 to 350°C, load 50 N and sliding velocity 1 m/s respectively, increases residual stress rapidly decreases from -91 to -3 HV. The residual stress was found to decreases ~97.7% at test condition of 50N load, 1 m/s sliding velocity and 350°C temperature. Compressive residual stresses are established due to bombing of high velocity particles on the substrate material. Further increase in temperature, load and sliding velocity during tribo test, tensile internal stresses are developed which balances the compressive stresses [184, 185]. Skordaris et al. [191], in there research reported that as the temperature increases, thermal stresses on the coating also increases but the structural stress developed on the samples remains stable upto 400°C [190].

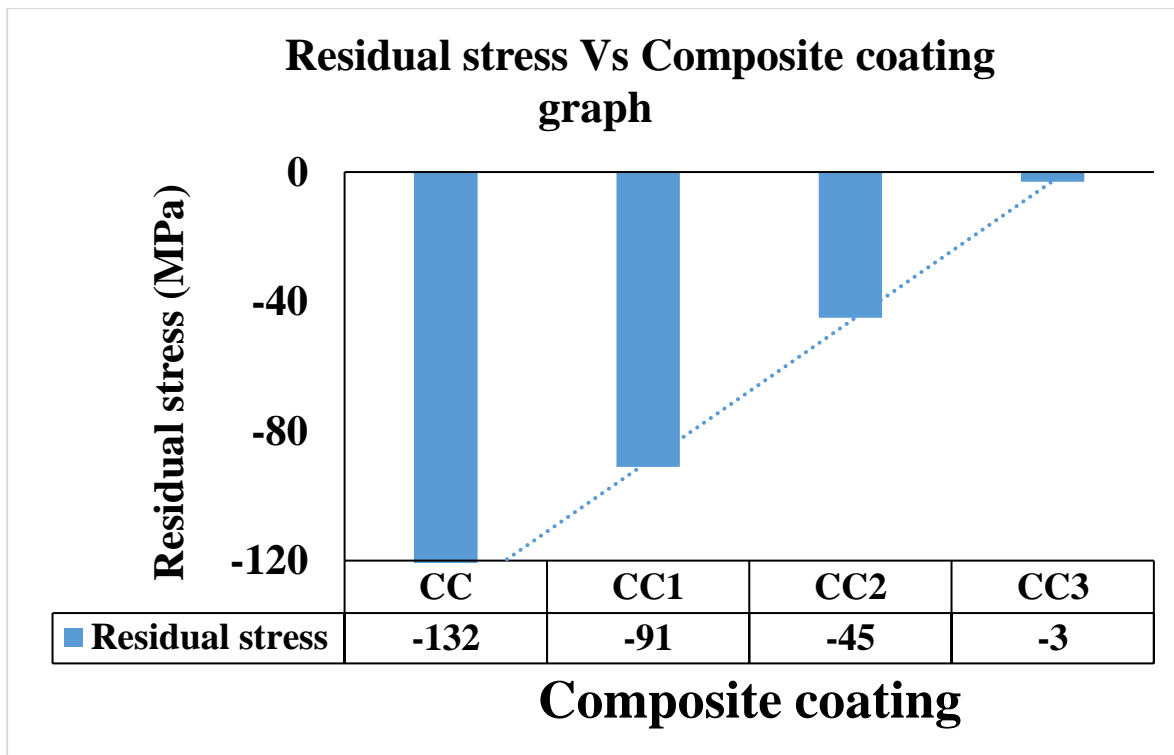
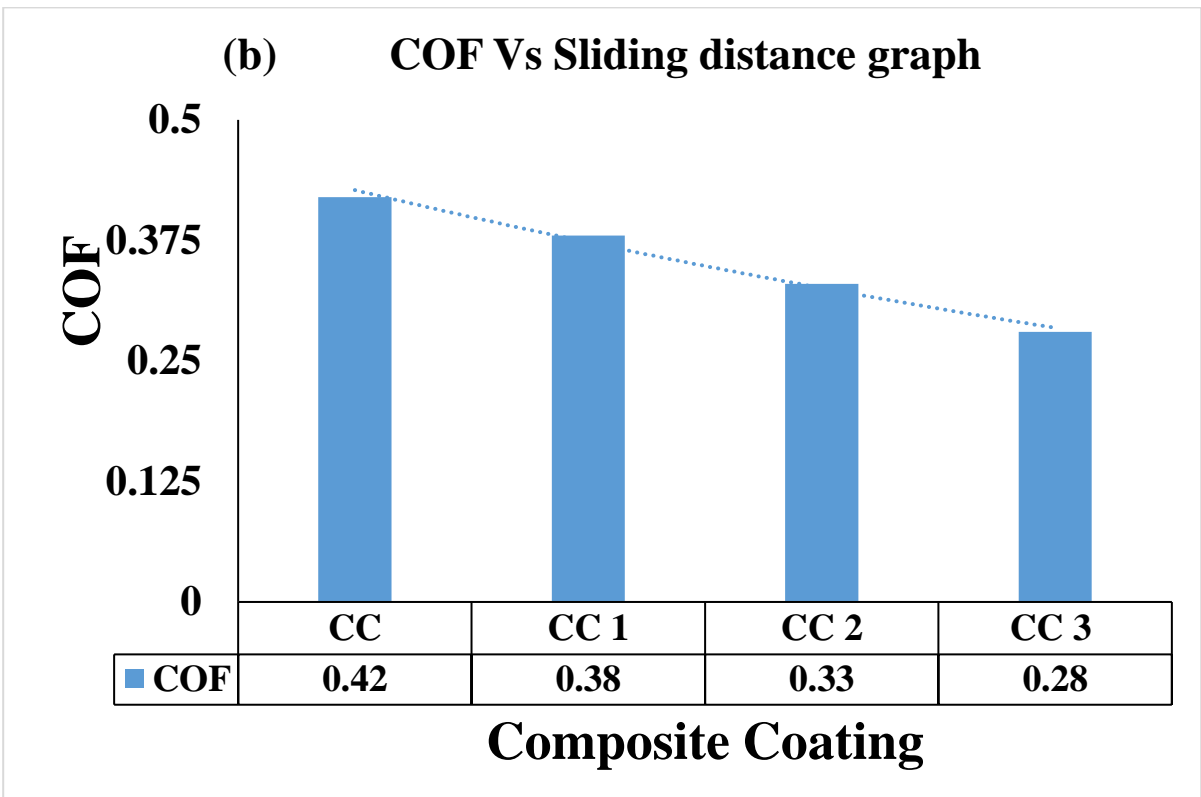
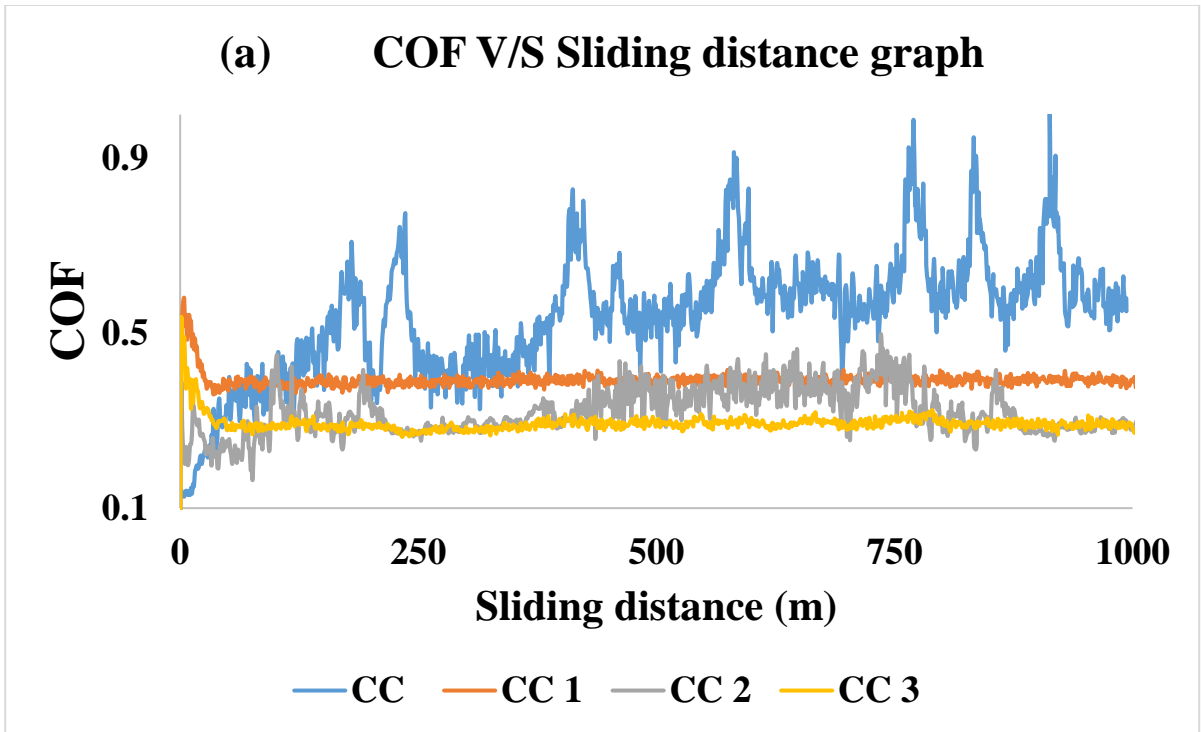


Figure 5.28 Residual stress Vs composite coating graph

5.8. TRIBOLOGICAL CHARACTERIZATION OF CARBON BASED COMPOSITE COATING

5.8.1. COF & WEAR BEHAVIOR OF CARBON BASED COMPOSITE COATING

The experimental result shows that the COF and wear values developed on the carbon based composite coating (CC) at idle conditions was 0.42 and 130 μm respectively. The COF value of samples CC 1, CC 2 and CC 3 was 0.38, 0.33 and 0.28 respectively, while wear values of samples CC 1, CC 2 and CC 3 was 90, 55 and 30 μm respectively. The tribological performance was evaluated using pin-on-disk tribometer which showed COF in the range of 0.28 to 0.38 as shown in fig. 5.29 (a-b), while fig. 5.29 (c) shows that wear was in the range of 30-90 μm , at test condition of temperature ranging from 150 to 350°C, load 50 N and sliding velocity 1 m/s respectively. The tribological analysis of carbon based composite coating was done to evaluate the wear behavior for wear resistance applications. The tribological test showed 33.3% decrease in COF and 76.9% reduction in the wear at test condition of 1 m/s sliding velocity, 350°C temperature, and 50N load. During wear testing COF, and wear values first increases and after that become stable during running-in process between composite coating and counterpart, due to good interfacial strength and excellent adhesive strength. Presence of carbon and hydrogen content, leads to graphitization effect, and formation of sulphide forms a thin solid lubricated layer [185, 190]. Tyagi et al. [184] and Matikainen et al. [188] investigated HVOF developed coating and experimental result shows that higher velocity particles enhances wear resistance properties of developed coating and similar trends was also attain the present tribological study. The experimental results that as the load, velocity and temperature increases, COF & wear behavior of carbon coating decreases significantly according to stribeck theory [192], and similar trends was also attain the present tribological study. The deviation of friction & wear by sliding distance shows approximately 500m run-in-stage, after that a stable stage [128]. During running stage, carbon coating shows severe fluctuation in COF and wear, but later on became stable after introduction of graphitization effect in the coating. It was quite clear from experimental analysis that as the carbon contents increases friction and wear of carbon based coating decreases, since generally carbon phases acts as a good lubricants (solid lubricated layer) [190]. The changes phase structure and stoichiometry composition, formation of additive layer and oleo phobic behavior of developed carbon coatings played an important role that results decrease in friction and wear.



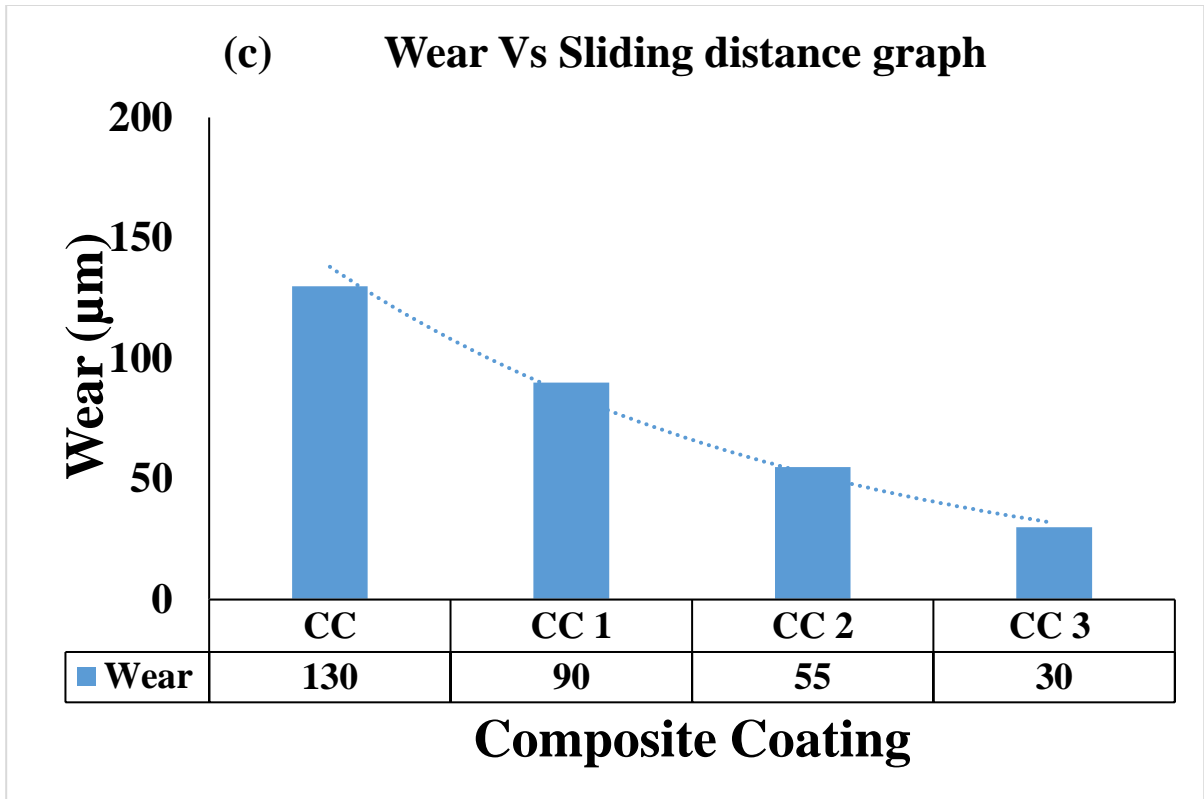


Figure 5.29 (a) COF (b) Wear Vs Sliding distance graph carbon composite coating

5.8.2. WEAR MECHANISM OF CARBON BASED COMPOSITE COATING

The FESEM images shows wear characteristics of worn out surfaces of developed C+WC+Mo+TiO₂+Al₂O₃ blend composite coatings and is revealed in fig. 5.30 (a-d). FESEM obtained after wear test shows brittle structure with grains look along with conversion of amorphous to polycrystalline structure of composite coating. It was quite clear that metallic abrasive particles are entrenched in the developed composite coating or adhesive wear. The carbon coating shows ploughing action with presence of chip off particles, rubbing action along with worn out particles were seen during wear test [184]. It is also noted that formation of tribofilm and diffusion of carbon particles increases as the test conditions increases [184, 190]. It was also noted that the composite coating shows micron size carbon particles, delamination layer formation, tribo-oxidative layer, transfer layer” formation and graphitization effect at variable test condition. At variable test conditions, wear occur mainly by plowing (plastic deformation). Deep grooves and scratches (possibly formed during plowing action caused due to micron size carbon crystallites) were present on the carbon coating. The micron size of carbon particles of developed coating work as a barrier against plastic deformation and results in abrasive wear resistance [189]. However, the

surface morphology of carbon coating revealed less plastic deformation, between developed coating and counterbody occur during friction and wear test.

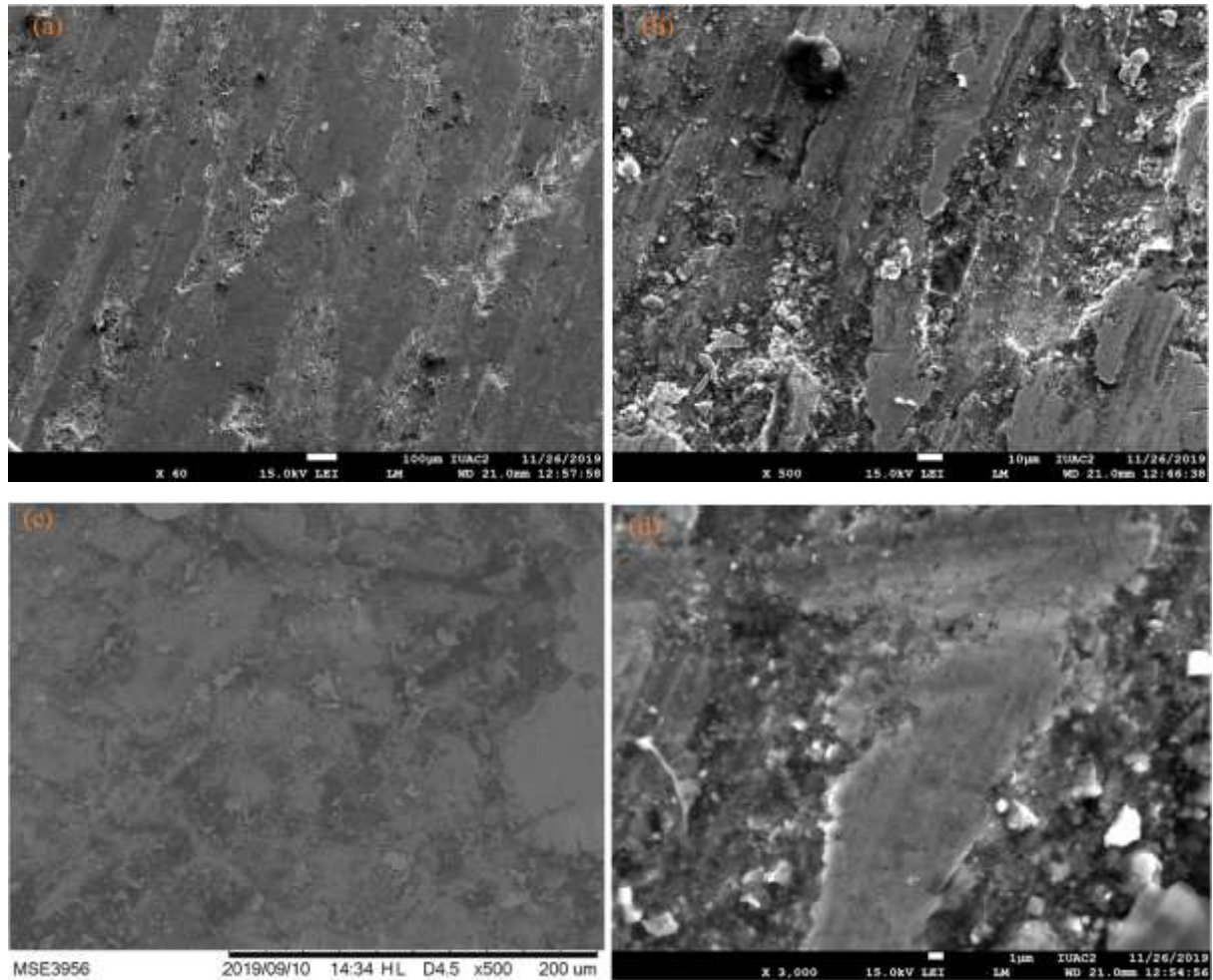


Figure 5.30 FESEM images of wear characteristics of composite coating

Different stages of wear behavior of carbon based composite coating is illustrated and as shown in fig. 5.31:

1st stage:

Initially, asperities of developed coating shot to penetrate into disc during running condition, when variable load, sliding velocity and temperature is applied, results in plastic deformation.

2nd stage:

Ploughing of disc by composite coating asperities results in formation of tribofilm formation (due to carbon diffusion, carbides and oxide layer formation), which results in weakening of asperities.

3rd stage:

Increase in oxides, carbides layer formation and carbon diffusion shows smoothening of coating surface and lastly consequences in COF and wear reduction.

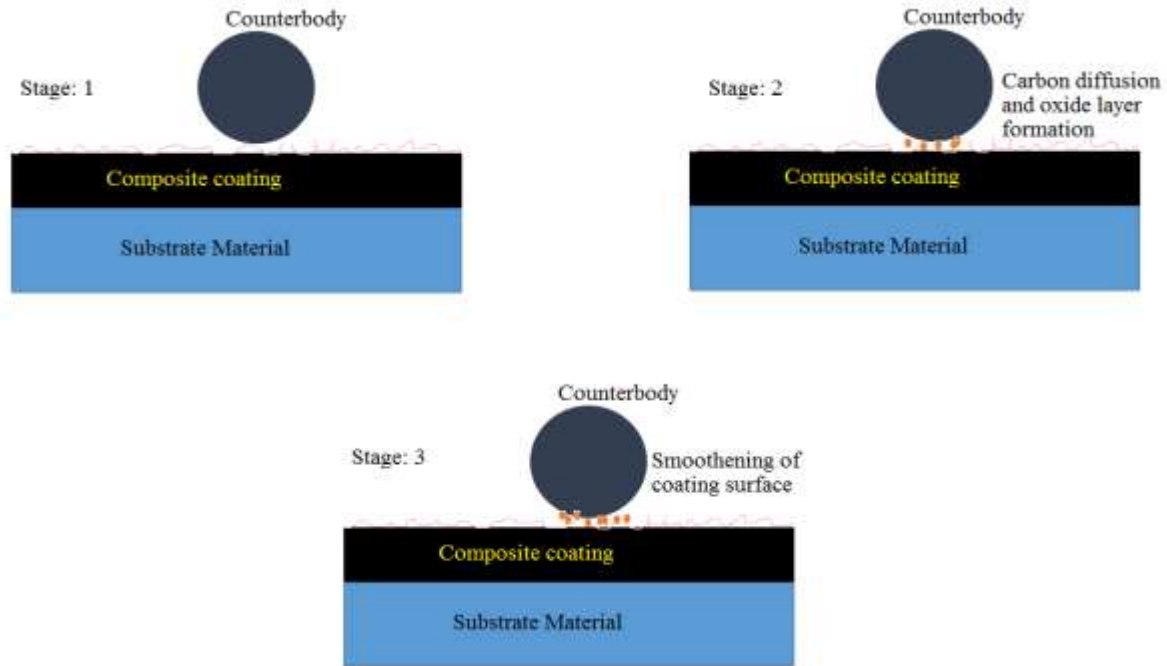


Figure 5.31 Stages of wear mechanism of carbon-based composite coating

5.8.3. Effects of parameters on Coefficient of friction (COF) for Carbon based composite coating

All experimental results for process conditions were recorded in the table 5.9 and were examined to find out the effects of all parameters. Lower-the-better type, eminence characteristic was chosen for analysis of S/N ratio data for COF, and wear and test results at all condition were converted into S/N ratio

Table 5.9 Experimental results of Taguchi L₉ OA of COF, and Wear for Carbon based Composite coating

Trial no.	COF			S/N ratio (db)	Wear			S/N ratio (db)
	R ₁	R ₂	R ₃		R ₁	R ₂	R ₃	
1	0.21	0.21	0.21	13.5556	160	160	160	-44.0824
2	0.15	0.15	0.15	16.4782	140	140	140	-42.9226

3	0.07	0.07	0.07	23.0980	50	50	50	-33.9794
4	0.18	0.17	0.17	15.2191	135	135	135	-42.6067
5	0.15	0.15	0.14	16.6689	100	100	100	-40.0000
6	0.12	0.10	0.10	19.4056	65	65	65	-36.2583
7	0.13	0.13	0.13	17.7211	80	80	80	-38.0618
8	0.14	0.15	0.15	16.6689	90	90	90	-39.0849
9	0.06	0.06	0.07	23.9434	45	35	35	-31.7367
Mean(Overall)= 0.13					Mean(Overall)= 95.37			

The main effects and average values of COF and S/N ratio for all parameters at trail T1, T2 and T3 were calculated and were illustrated in table 5.10 and also plotted in fig. 5.32.

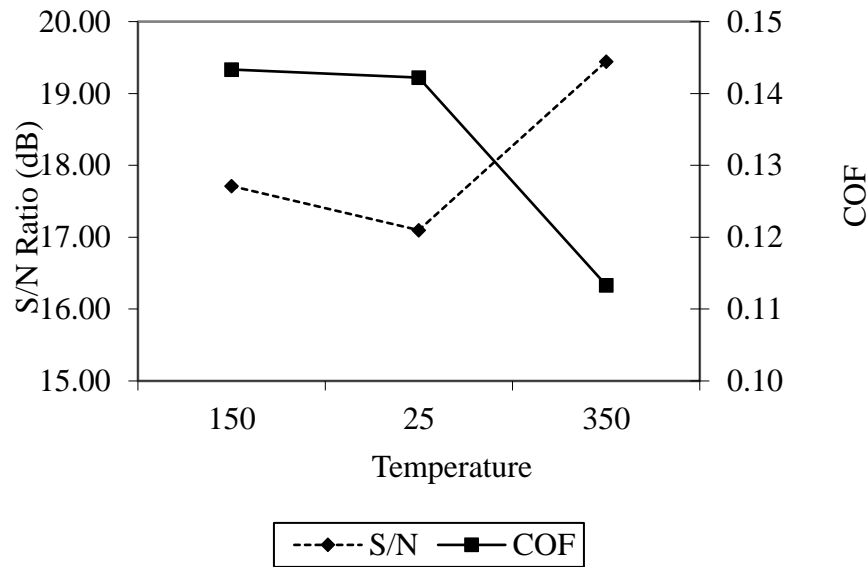
Table 5.10 Main Effects and average values of COF (S/N ratio and raw data) for composite coating

Parameter	Trial	Temperature (°C)		Sliding velocity (m/s)		Load (N)	
Data		Raw Data	S/N Ratio	Raw Data	S/N Ratio	Raw Data	S/N Ratio
	T1	0.14	17.71	0.17	15.49	0.15	16.54
	T2	0.14	17.09	0.14	16.60	0.12	18.54
	T3	0.11	19.44	0.08	22.14	0.116	19.16
	T2-T1	-0.001	-0.613	-0.02	1.10	-0.026	20.0
	T3-T2	-0.02	2.34	-0.06	5.54	-0.013	0.616
Difference (T3-T2)-(T2-T1)		-0.02	2.95	-0.04	4.43	0.012	-1.38

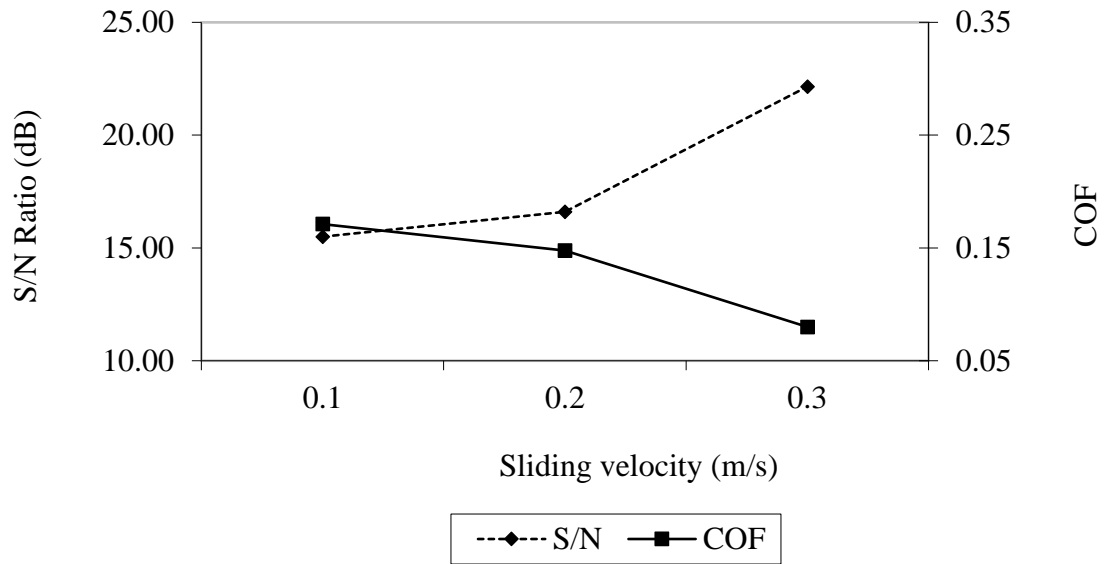
Fig. 5.32 (a) shows deviation of COF with respect to the temperature on the carbon based composite coating. The result shows that COF obtained at 350°C temperature was lowest on comparing with 150°C and 250°C temperature for the carbon based composite coating. However,

the S/N ratio was highest at 350°C temperature on comparing with 150°C and 250°C temperature for the carbon based composite coating. The above result shows that as the COF value was lower, when the carbon based composite coating temperature was 350°C and a greater value of S/N ratio suggest a stronger signal and lesser noise, hence offers an optimum test results at the same trial condition. The decrease in COF may be attributed due to formation of carboxylic functional group. The reduction in COF at high temperature may be attributed due to formation of coherent tribo-oxidative lubricious layer or due to graphitization effect at C: H surface, which finally results decrease in COF. In the present work, COF decreases as temperature increases and at constant relative humidity, due to micron size carbon particles, ceramics and formation of graphitized like lubricious.

(a) Effect of Temperature on S/N and COF



(b) Effect of Sliding velocity on S/N and COF



(c) Effect of Load on S/N and COF

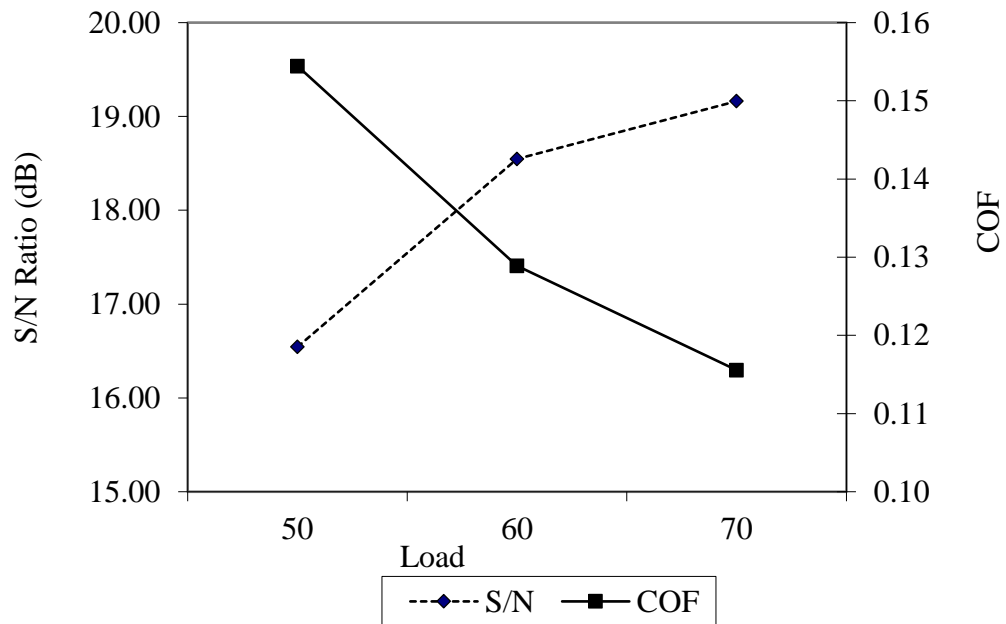


Figure 5.32 shows deviation of COF with parameters (a) Temperature ($^{\circ}\text{C}$) (b) Sliding velocity (m/s) (c) Load (N) of composite coating

From the fig. 5.32 (b) it can be observed that there is a decrease in the value of COF as the sliding velocity increases from 1 to 3 m/s. The lowest value of COF was obtained for the highest sliding velocity of 3 m/s, while COF obtained was highest at 1m/s sliding velocity for the chosen range. The S/N ratio corresponds 3m/s was highest and decreases as the sliding velocity decreases. The decrease in COF at increasing speed may be attributed due to increase in formation of degree of transfer layer (solid lubricious graphitized layer) [138]. The decrease in COF may be due to formation of solid lubricious graphitized layer during steady state conditions.

Fig. 5.32(c) shows deviation of COF with respect to the load. The results show that the COF obtained was maximum at load of 50 N and decreases with increase in load from 50 to 70 N. However, S/N ratio value for COF was maximum at a load 70 N followed by 60 N and 50 N, while S/N ratio value was minimum at 70 N and maximum at 50N. It was noted that due to increase in load, there was a formation of graphitized layer which helps in reduction of COF during running condition [138]. In the present work, COF decreases as the load was increased during running condition and on comparing with other experimental results [138, 185], COF obtained in present research shows better results for the developed carbon coating under similar test conditions.

As lower-the-better type of quality characteristic was chosen for better results, a lower value of COF was sought. It is quite evident from fig. 5.32 that COF was optimum i.e. minimum at trial 3 of parameter A (350°C), trial 3 of the parameter B (3 m/s) and trial 3 of the parameter C (70 N). On the other hand, the trial parameters A, B and C, the lowest values of mean response correspond to the highest values of S/N ratio. From the above discussion it was clear that COF decreases as the temperature, sliding velocity and load increases, due to micron size particle of carbon which work as a barrier against plastic deformation or due to formation of graphitized like lubricious layer.

To examine the significance of parameters of COF, ANOVA was performed. Table 5.11 shows the pooled ANOVA S/N data and raw data of COF. It was quite evident that process parameters A, B, and C considerably affect mean and variation in COF. The percentage contribution of sliding velocity (74.76 %) was highest followed by load (12.85 %) and temperature (9.46 %) for COF.

Table 5.11 Pooled ANOVA for COF (S/N ratio and raw data) for composite coating

Source type	SS		DOF		V		F-Ratio		SS'		P (%)	
	Raw data	S/N data	Ra w data	S/ N data	Raw data	S/N data	Raw data	S/N data	Raw data	S/N data	Ra w data	S/N data
Temperature (°C)	0.005	8.88	2	2	0.002	4.44	43.12	27.64	0.005	8.56	9.46	8.86
Sliding velocity (m/s)	0.04	76.18	2	2	0.020	38.09	333.92	236.93	0.04	75.86	74.76	78.49
Load (N)	0.007	11.25	2	2	0.003	5.62	58.22	35	0.006	10.93	12.76	11.31
E (Pooled)	0.001	0.32	20	2	0.00006	0.16	-	-	0.001	1.28	2.92	1.33
Total	0.053	96.64	26	8	-	-	-	-	0.05	96.64	100	100
SS= Sum of squares; DOF= Degree of freedom; V= Variance; SS'= pure sum of squares												

5.8.3.1. Estimation of optimal performance characteristics

5.8.3.1.1. Optimal values of response characteristics for COF (predicted mean)

Table 5.12 shows the average values of COF at optimum level of significant parameters. The optimum value of the estimated mean (μ) COF can be obtained as follow [138]:

$$\mu_{\text{COF}} = A_3 + B_3 + C_3 - 2T \quad (2)$$

$$\mu_{\text{COF}} = 0.04$$

Table 5.12 Average values of COF at optimal levels for composite coating

Trail	COF
A ₃	0.11
B ₃	0.08
C ₃	0.11
T	0.13
A ₃ = trail 3 of temperature; B ₃ = trail 3 of sliding velocity; C ₃ = trail 3 of load; T= average value of response	

The Confirmation experiments (CI_{CE}) for 95 % confidence interval and confidence interval population (CI_{POP}) was calculated by using equations:

$$CI_{CE} = \sqrt{F_a(1, f_e) V_e \left[\frac{1}{n_{eff}} + \frac{1}{R} \right]} \quad (3)$$

$$CI_{POP} = \sqrt{\frac{F_a(1, f_e) V_e}{n_{eff}}} \quad (4)$$

where $F_a(1, f_e)$ = F ratio at the confidence level of (1-a) against DOF 1 and degree of freedom error f_e ; R = sample size for confirmation experiments; V_e = variance error; $n_{eff.} = \left(\frac{N}{1+DOF} \right)$; N = total no. of trials; and DOF = total degree freedom associated in the estimate of mean response.

The values obtained by the ANOVA are:

$$N = 27; f_e = 20; V_e = 0.00006; n_{eff.} = 3.86; R = 3; F_{0.05}(1, 20) = 3.49$$

$$\text{From eq. 3 } CI_{CE} = \pm 0.011$$

$$\text{From eq. 4 } CI_{POP} = \pm 0.0072$$

The predicted optimum values for COF is given by:

$$CI_{CE} : 0.029 < \mu < 0.051$$

$$CI_{POP} : 0.032 < \mu < 0.047$$

The optimum values of COF were predicted at the designated trials of significant parameters.

$$\text{Temperature (A, trial 3)} = 350^\circ\text{C}$$

$$\text{Sliding velocity (B, trial 3)} = 3 \text{ m/s}$$

$$\text{Load (C, trial 3)} = 70 \text{ N}$$

5.8.3.1.2. Confirmation experiments

Three confirmation tests were performed at the optimal situation of the process parameters. For COF process parameters were set temperature at trail 3 (350°C), sliding velocity at trail 3 (3 m/s), and load at trail 3 (70N). The average value for COF of wear coating was measured as 0.04 which was in the predicted optimum range of 95 % confidence interval for COF for the carbon coating.

5.8.4. Effects of parameters on Wear for Carbon based composite coating

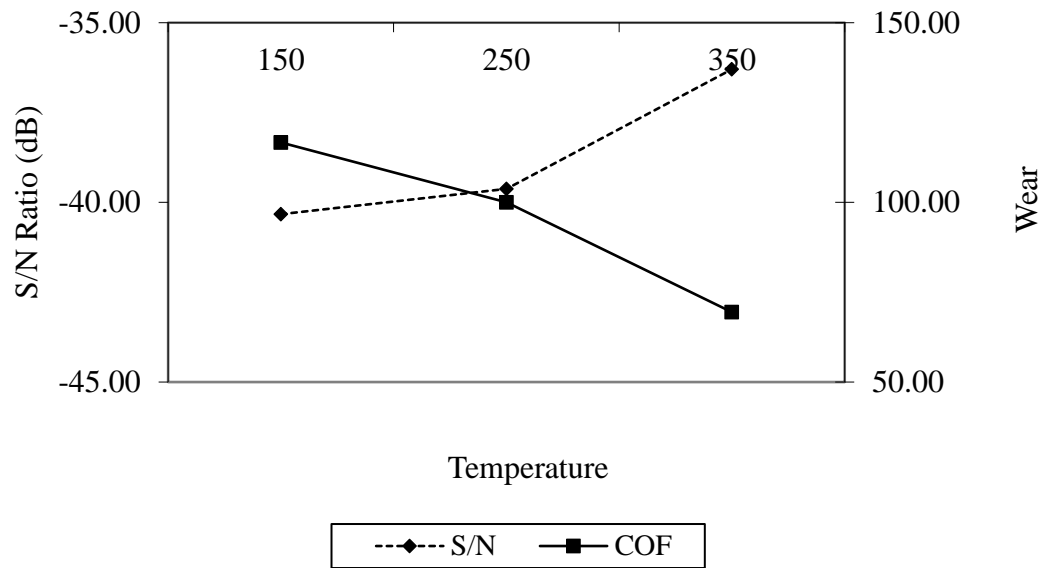
The main effects and average values of wear and S/N ratio for all parameters at trial T1, T2 and T3 were calculated and were illustrated in table 5.13 and also plotted in fig. 5.33.

Table 5.13 Main Effects and average values of wear (S/N ratio and raw data) for composite coating

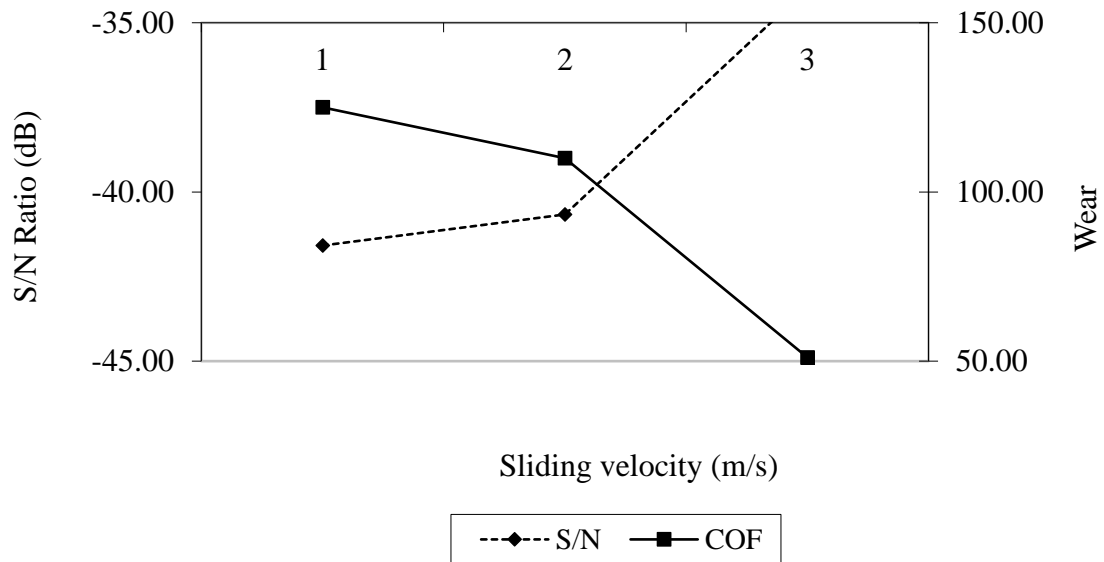
Parameter	Trial	Temperature (°C)		Sliding velocity (m/s)		Load (N)	
Data		Raw Data	S/N Ratio	Raw Data	S/N Ratio	Raw Data	S/N Ratio
	T1	116.66	-40.32	125.0	-41.58	105.0	-39.80
	T2	100.0	-39.62	110.0	-40.66	104.44	-39.08
	T3	69.44	-36.29	51.1	-33.99	76.66	-37.34
	T2-T1	-16.66	0.70	-15.0	0.91	-0.55	0.72
	T3-T2	-30.55	3.32	-58.88	6.67	-27.77	1.74
Difference (T3-T2)-(T2-T1)		-13.88	2.62	-43.88	5.76	-27.22	10.2

Fig. 5.33 (a) shows deviation of wear with respect to the temperature on the carbon based composite coating. The result shows that wear obtained at 350°C temperature was lowest on comparing with 150°C and 250°C temperature for the carbon coating. However, the S/N ratio was highest at 350°C temperature on comparing with 150°C and 250°C temperature for the carbon coating. The above result shows that as the wear value was lower, when the carbon coating temperature was 350°C and a greater value of S/N ratio suggest a stronger signal and lesser noise, hence offers an optimum test results at the same trial condition. The reduction in wear at high temperature may be attributed due to formation of coherent tribo-oxidative lubricious layer or due to graphitization effect at C: H surface, which finally results decrease in wear. In the present work, wear decreases as temperature increases and at constant relative humidity, due to micron size carbon particles and formation of graphitized like lubricious.

(a) Effect of Temperature on S/N and Wear



(b) Effect of Sliding velocity on S/N and Wear



(c) Effect of Load on S/N and Wear

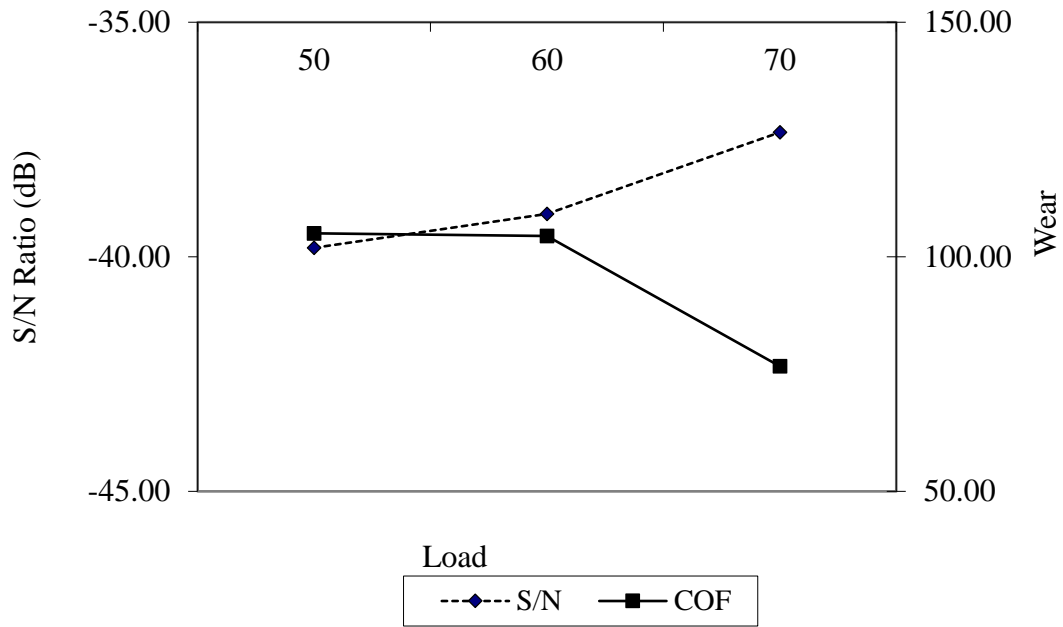


Figure 5.33 shows deviation of wear with parameters (a) Temperature ($^{\circ}\text{C}$) (b) Sliding velocity (m/s) (c) Load (N) of composite coating

From the fig. 5.33 (b) it can be observed that there is a decrease in the value of wear as the sliding velocity increases from 1 to 3 m/s. The lowest value of COF was obtained for the highest sliding velocity of 3 m/s, while wear obtained was highest at 1m/s sliding velocity for the chosen range. The S/N ratio corresponds 3m/s was highest and decreases as the sliding velocity decreases. The decrease in wear may be due to formation of solid lubricious graphitized layer during steady state conditions. In assessment with other experimental results under similar test conditions, [138] wear obtained in the research work shows better test results for carbon based composite coating.

Fig. 5.33 (c) shows deviation of wear with respect to the load. The results show that the wear obtained was maximum at load of 50 N and decreases with increase in load from 50 to 70 N. However, S/N ratio value for wear was maximum at a load 70 N followed by 60 N and 50 N, while S/N ratio value was minimum at 70 N and maximum at 50N. It was noted that due to increase in load, there was a formation of graphitized layer which helps in reduction of wear during running condition [138]. In the present work, wear decreases as the load was increased during running condition and on comparing with other experimental results [138], COF obtained in present

research shows better results for the developed carbon based composite coating under similar test conditions.

As lower-the-better type of quality characteristic was chosen for better results, a lower value of wear was sought. It is quite evident from fig. 5.33 that wear was optimum i.e. minimum at trial 3 of parameter A (350°C), trial 3 of the parameter B (3 m/s) and trial 3 of the parameter C (70 N). On the other hand, the trial parameters A, B and C, the lowest values of mean response correspond to the highest values of S/N ratio. From the above discussion it was clear that wear decreases as the temperature, sliding velocity and load increases, due to micron size particle of carbon which work as a barrier against plastic deformation or due to formation of graphitized like lubricious layer.

To examine the significance of parameters of Wear, ANOVA was performed. Table 5.14 shows the pooled ANOVA S/N data and raw data of wear. It was quite evident that process parameters A, B, and C considerably affect mean and variation in wear. The percentage contribution of sliding velocity (64.004 %) was highest followed by temperature (24.01 %) and load (10.94 %) for Wear.

Table 5.14 Pooled ANOVA for Wear (S/N ratio and raw data) for composite coating

Source type	SS		DOF		V		F-Ratio		SS'		P (%)	
	Raw data	S/N data	Raw data	S/N data	Raw data	S/N data	Raw data	S/N data	Raw data	S/N data	Raw data	S/N data
Temperature (°C)	10324.07	27.84	2	2	5162.03	13.92	302.98	55.45	10290.0	27.33	24.01	19.38
Sliding velocity (m/s)	27457.40	103.06	2	2	13728.70	51.53	805.81	205.28	27423.33	102.56	64.00	72.73
Load (N)	4724.07	9.61	2	2	2362.03	4.80	138.64	19.14	4690.00	9.10	10.94	6.45
E (Pooled)	340.74	0.50	20	2	17.03	0.25	-	-	442.96	2.008	1.03	1.42
Total	42846.29	141.02	26	8	-	-	-	-	42846.29	141.02	100	100

SS= Sum of squares; DOF= Degree of freedom; V= Variance; SS'= pure sum of squares

5.8.4.1. Estimation of optimal performance characteristics

5.8.4.1.1. Optimal values of response characteristics for Wear (predicted mean)

Table 5.15 shows the average values of wear at optimum level of significant parameters. The optimum value of the estimated mean (μ) wear can be obtained as follow [138]:

$$\mu_{\text{wear}} = A_3 + B_3 + C_3 - 2T \quad (2)$$

$$\mu_{\text{wear}} = 6.47$$

Table 5.15 Average values of Wear at optimal levels for composite coating

Trail	Wear
A ₃	69.44
B ₃	51.11
C ₃	76.66
T	95.37
A ₃ = trail 3 of temperature; B ₃ = trail 3 of sliding velocity; C ₃ = trail 3 of load; T= average value of response	

The Confirmation experiments (CI_{CE}) for 95 % confidence interval and confidence interval population (CI_{POP}) was calculated by using equations:

$$CI_{CE} = \sqrt{F_a(1, f_e) V_e \left[\frac{1}{n_{eff}} + \frac{1}{R} \right]} \quad (3)$$

$$CI_{POP} = \sqrt{\frac{F_a(1, f_e) V_e}{n_{eff}}} \quad (4)$$

where $F_a(1, f_e)$ = F ratio at the confidence level of (1-a) against DOF 1 and degree of freedom error f_e ; R= sample size for confirmation experiments; V_e = variance error; $n_{eff.} = \left(\frac{N}{1+DOF} \right)$; N= total no. of trials; and DOF = total degree freedom associated in the estimate of mean response.

The values obtained by the ANOVA are:

$$N = 27; f_e = 20; V_e = 17.037; n_{eff.} = 3.86; R = 3; F_{0.05}(1, 20) = 3.49$$

$$\text{From eq. 3 } CI_{CE} = \pm 5.93$$

$$\text{From eq. 4 } CI_{POP} = \pm 3.92$$

The predicted optimum values for wear is given by:

$$CI_{CE} : 0.54 < \mu < 12.4$$

$$CI_{POP} : 2.55 < \mu < 10.39$$

The optimum values of wear were predicted at the designated trials of significant parameters.

Temperature (A, trial 3) = 350°C

Sliding velocity (B, trial 3) = 3 m/s

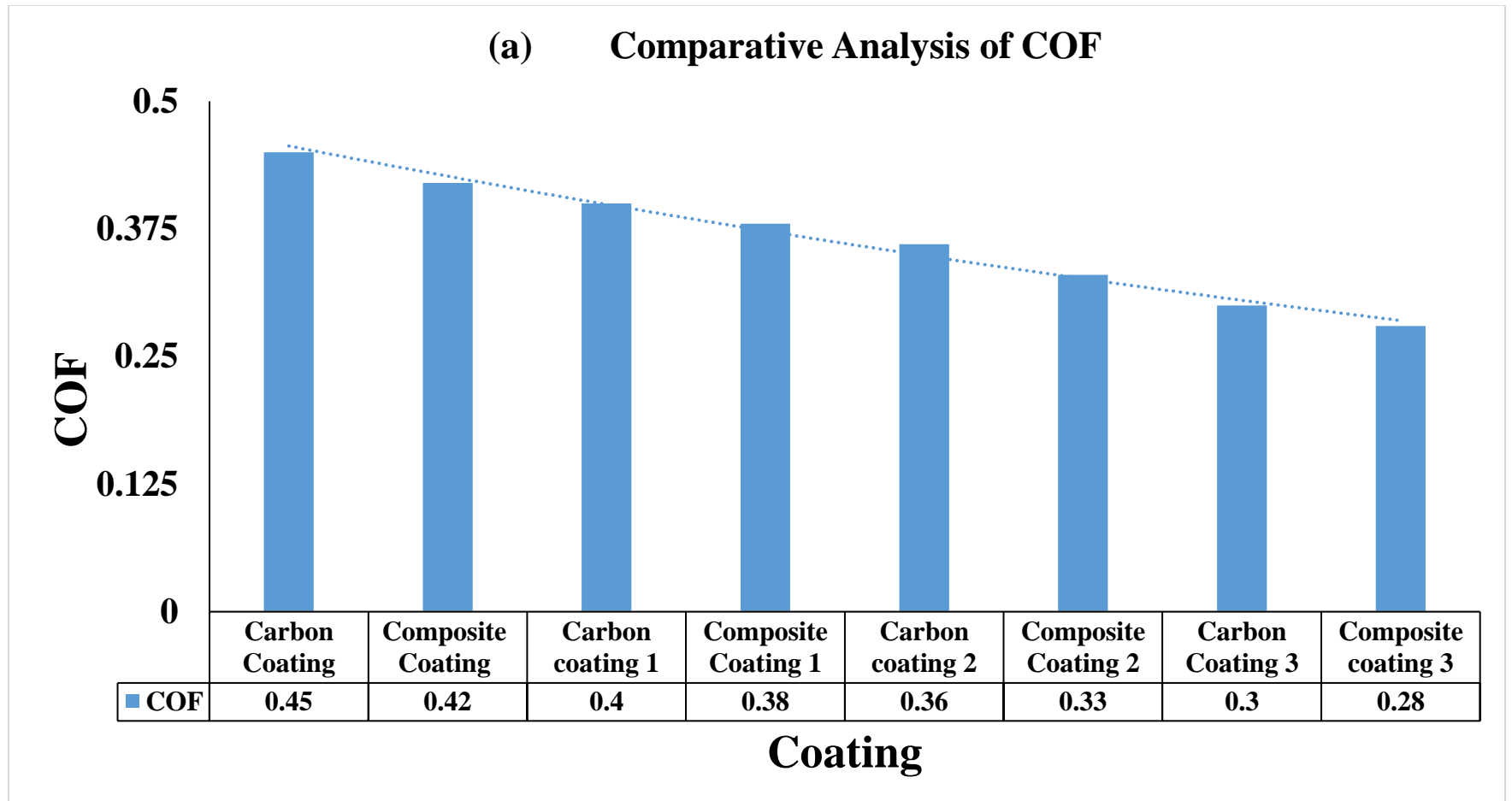
Load (C, trial 3) = 70 N

5.8.4.1.2. Confirmation experiments

Three confirmation tests were performed at the optimal situation of the process parameters. For wear process parameters were set temperature at trail 3 (350°C), sliding velocity at trail 3 (3 m/s), and load at trail 3 (70N). The average value for wear of carbon based composite coating was measured as 6.47 μm which was in the predicted optimum range of 95 % confidence interval for wear for the carbon based composite coating.

This chapter includes the comparative analysis of tribological and mechanical properties of carbon coating and carbon based composite coating for piston rings.

The in depth experimental test results of tribological and mechanical properties of developed coatings were discussed in chapter 5. However, it is pertinent to mention here the interested test result observation of tribological and mechanical properties of developed coatings. The experimental result shows that the COF and wear values developed on the carbon coating (CC) at idle conditions was 0.45 and 150 μm respectively while the COF and wear values on carbon based composite coating was found 0.42 and 130 μm respectively. The tribological performance was evaluated using pin-on-disk tribometer which showed COF of carbon coatings varies from 0.3 to 0.40 wear varies between 45-100 μm , while on the other end COF of composite coatings varies from 0.28 to 0.38 wear varies between 30-90 μm , at test condition of temperature ranging from 150 to 350°C, load 50 N and sliding velocity 1 m/s respectively as shown in fig. 6.1. The experimental results of COF for composite coating is almost 6.7% less than carbon coating at test condition of temperature ranging from 150 to 350°C, load 50 N and sliding velocity 1 m/s respectively. The experimental results of wear also reveals that for composite coating is almost 16-20% less than carbon coating at test condition of temperature ranging from 150 to 350°C, load 50 N and sliding velocity 1 m/s respectively. It was quite clear from experimental analysis that the composite coating shows better test results on comparing with carbon coating under same test conditions, due to good interfacial strength and excellent adhesive strength. Presence of carbon and hydrogen content, leads to graphitization effect, and formation of sulphide forms a thin solid lubricated layer [184, 193].



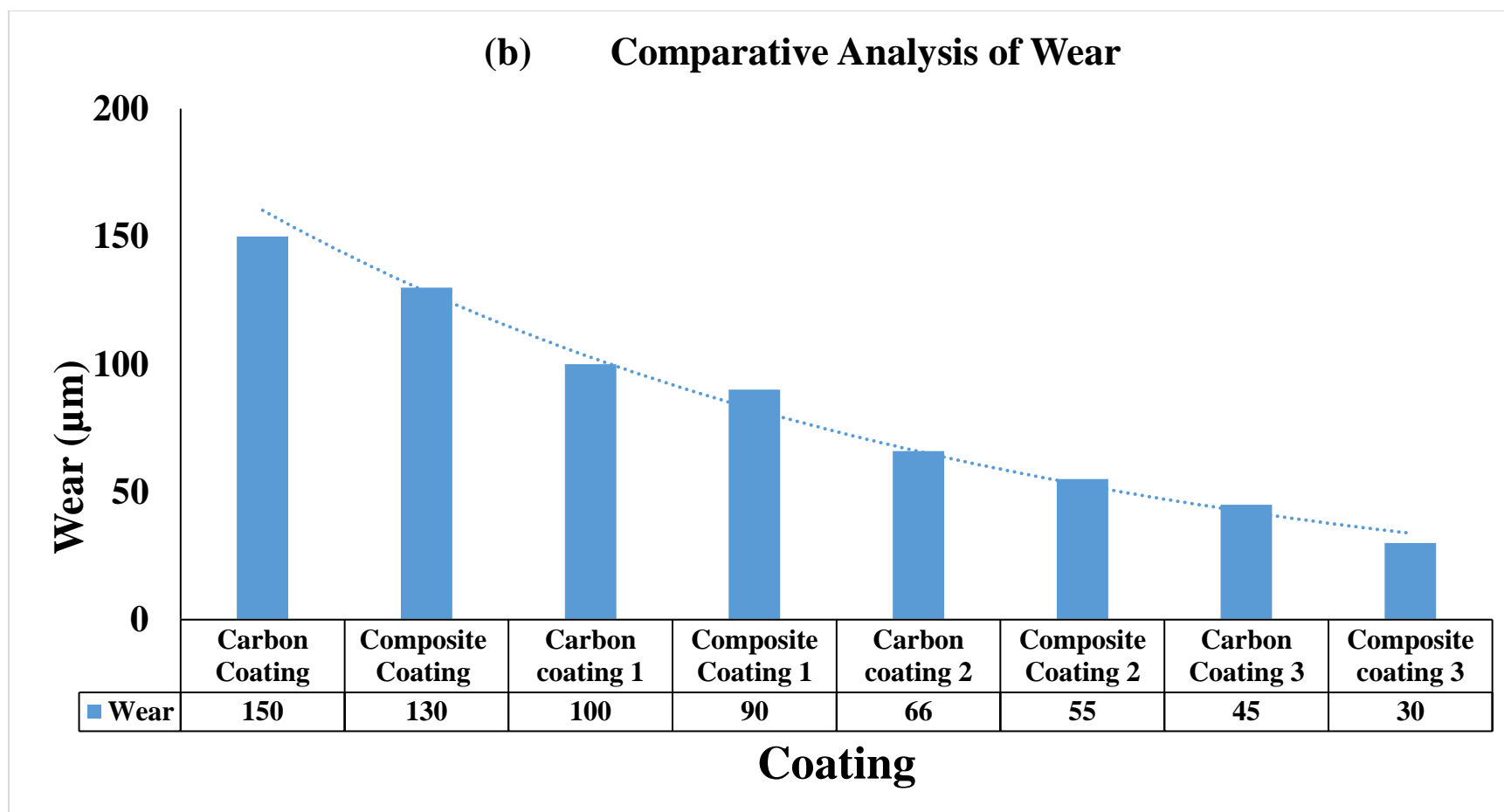


Figure 6.1 Comparative analysis of (a) COF (b) Wear of developed Coatings

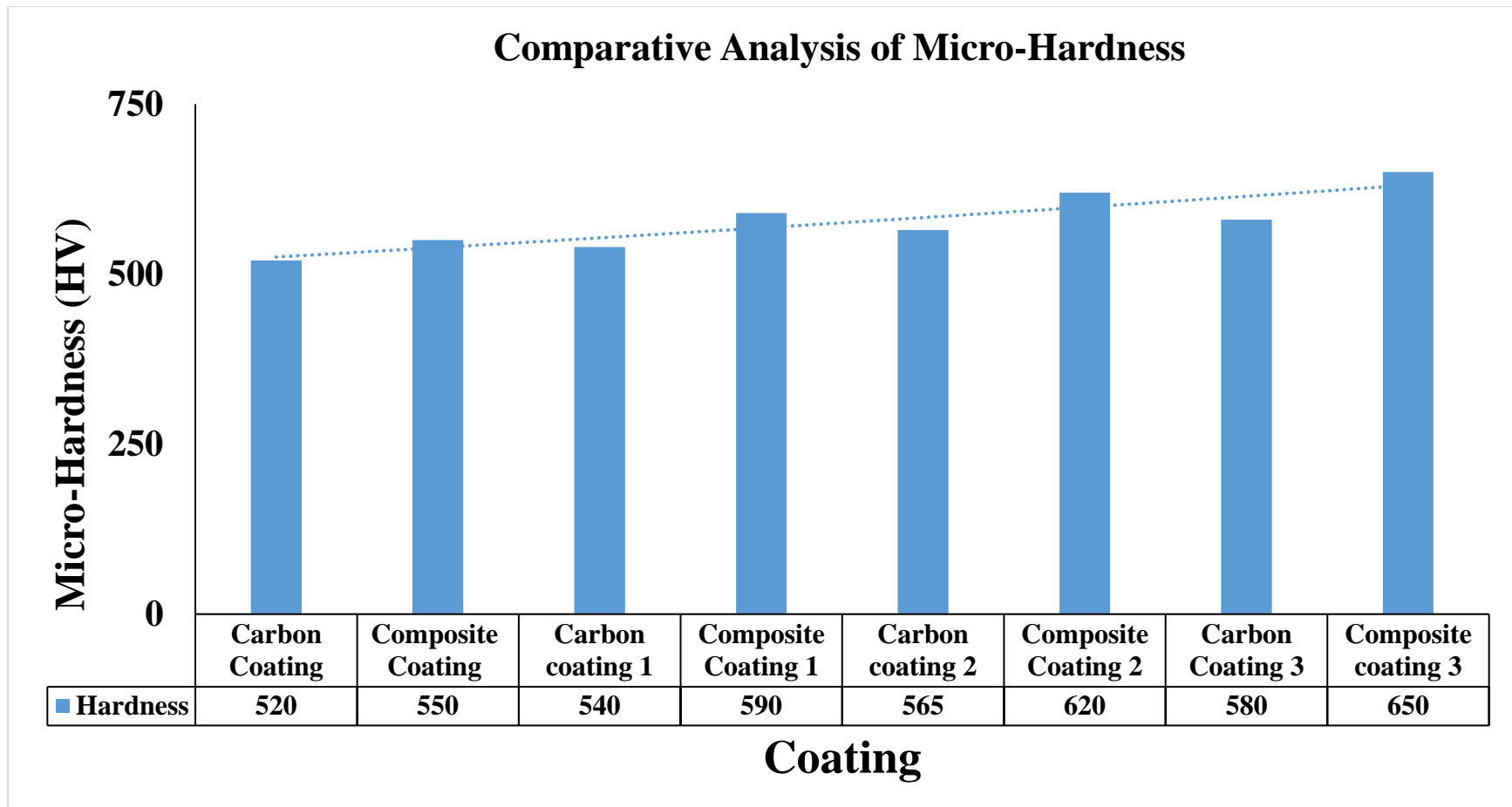


Figure 6.2 Comparative analysis of micro-hardness developed of Coatings

The experimental result shows that micro-hardness value of carbon coating exhibits 520 HV while composite coating shows 550HV micro-hardness value at room temperature. The micro-hardness value of carbon coating varies 540 to 580 HV respectively, on the other end hardness values of composite coating varies from 590 to 650 HV respectively, as the test conditions of temperature ranging from 150 to 350°C, load 50 N and sliding velocity 1 m/s respectively as shown in figure 6.2. The experimental results of micro-hardness for composite coating is almost 8-12% greater than carbon coating at test condition of temperature ranging from 150 to 350°C, load 50 N and sliding velocity 1 m/s respectively. It was quite clear from experimental analysis that the composite coating shows better test results on comparing with carbon coating under same test conditions, due to the formation of oxides and sulphides layers, agglomerate size of powders and strong adhesive force between coating particles [184]. It is also noted that presence of hard phased structured micron size carbon particles works as an impediment contrary to deformation, finally results increase in hardness [188].

The experimental result shows that residual stress value of carbon coating exhibits -193 MPa while composite coating shows -140 MPa residual stress value at room temperature. The residual stress value of carbon coating varies from -107 to -5 MPa respectively, on the other end residual stress values of composite coating varies from -91 to -3 MPa respectively, as the test conditions of temperature ranging from 150 to 350°C, load 50 N and sliding velocity 1 m/s respectively as shown in figure 6.3. The experimental results of residual stress for composite coating is almost 14-25% less than carbon coating at test condition of temperature ranging from 150 to 350°C, load 50 N and sliding velocity 1 m/s respectively. It was quite clear from experimental analysis that the composite coating shows better test results on comparing with carbon coating under same test conditions, due to the formation of oxides and sulphides layers, agglomerate size of powders and strong adhesive force between coating particles [185]. Skordaris et al. [191], in there research reported that as the temperature increases, thermal stresses on the coating also increases but the structural stress developed on the samples remains stable upto 400°C.

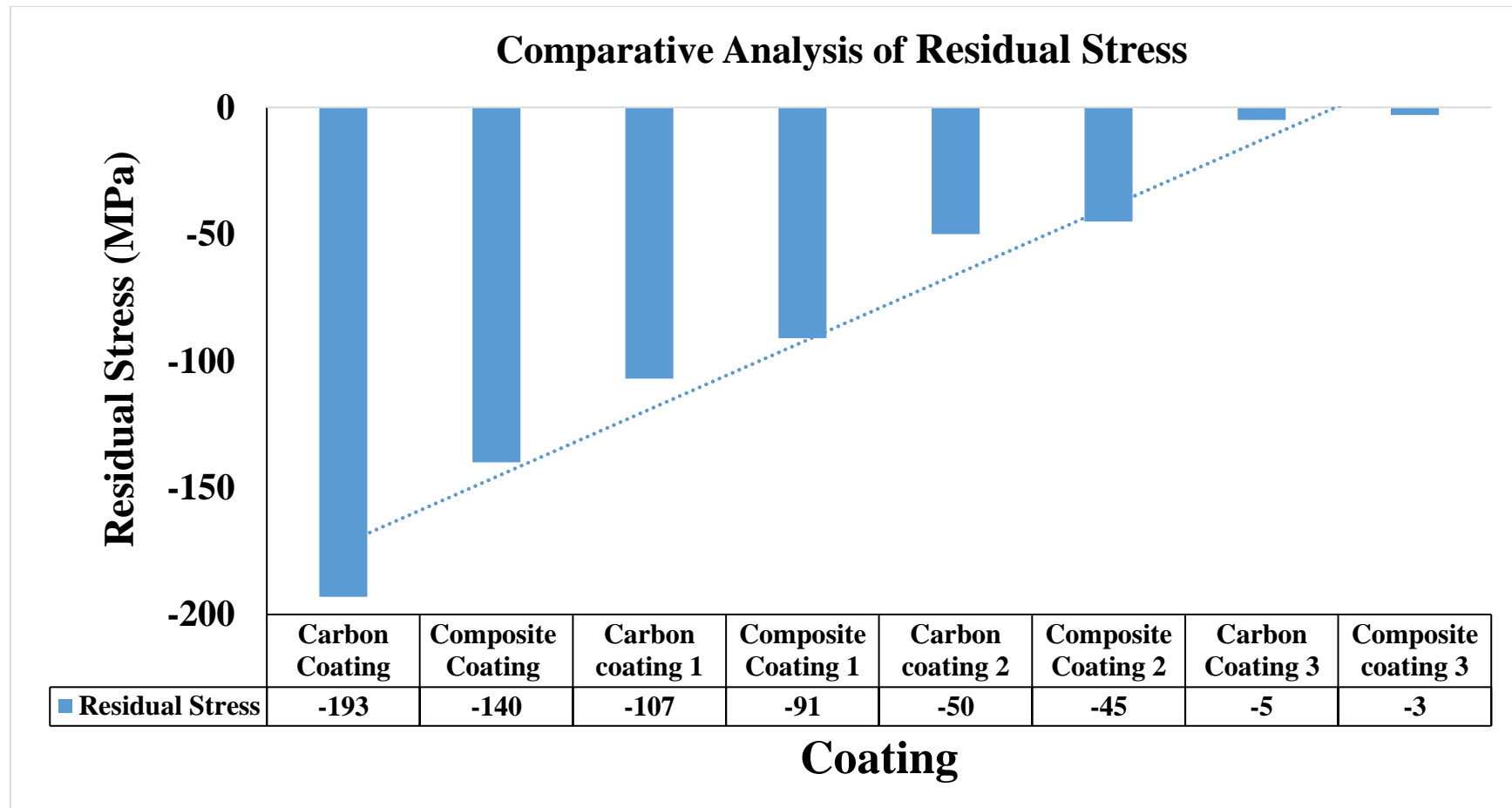


Figure 6.3 Comparative analysis of residual stress of developed Coatings

This chapter contains salient conclusions. Important conclusions of the investigation regarding carbon and carbon based composite coating have been presented with significant findings have been drawn from performed experimentation.

To abate frictional loss, emission and optimization of advance coatings is vital for piston rings, thick low friction environment friendly carbon coatings have been successfully deposited by agriculture waste powder in presence nitrogen, oxygen and LPG using high velocity oxy-flame (HVOF). The present work evaluates the microstructure, surface morphology, tribological and mechanical properties of carbon coating and carbon based composite coating for piston rings.

The major results of carbon coatings are:

1. FESEM+EDS, HRXED & Raman spectra confirms deposition of coating which exhibits typical laminar and molten structure.
2. The experimental result shows that surface roughness value of carbon coating (CC) was 0.445 μm .
3. The experimental result shows that micro-hardness value of carbon coating (CC) before wear test exhibits 520 HV. The micro-hardness value of samples CC 1, CC 2 and CC 3 after wear test was 540, 565 and 580 HV. The experimental results shows that as the test conditions of temperature ranging from 150 to 350°C, load 50 N and sliding velocity 1 m/s respectively increases the micro-hardness rapidly increased from 520 to 580 HV and hardness stabilized ~580HV. The micro-hardness test showed 11.5% increase in micro-hardness at test condition of 1 m/s sliding velocity, 350°C temperature, and 50N load.
4. The experimental result shows that the residual stress developed on the carbon coating (CC) before wear test exhibits -193 MPa. The residual stress value of samples CC 1, CC 2 and CC 3 after wear test was -107, -50 and -5 MPa. The experimental results shows that as the test conditions of temperature ranging from 150 to 350°C, load 50 N and sliding velocity 1 m/s respectively increases the residual stress rapidly decreased in the range of -107 to -5 MPa. The residual stress test showed ~97% decrease in residual stress, at test condition of sliding velocity of 1 m/s, 350°C temperature, and 50N load.

5. The experimental result shows that the COF and wear values developed on the carbon coating (CC) at idle conditions was 0.45 and 150 μm respectively. The COF value of samples CC 1, CC 2 and CC 3 was 0.40, 0.36 and 0.3 respectively, while wear values of samples CC 1, CC 2 and CC 3 was 100, 66 and 45 μm respectively. The tribological performance was evaluated using pin-on-disk tribometer which showed COF in the range of 0.3 to 0.40 and wear was in the range of 45-100 μm , at test condition of temperature ranging from 150 to 350°C, load 50 N and sliding velocity 1 m/s respectively.
6. The tribological analysis of carbon coating was done to evaluate the wear behavior for wear resistance applications. The tribological test showed 50% decrease in COF and 70% reduction in the wear at test condition of 1 m/s sliding velocity, 350°C temperature, and 50N load.
7. The percentage contribution of sliding velocity (75.49 %) was highest followed by temperature (12.93 %) and load (8.09 %) for COF.
8. The percentage contribution of sliding velocity (59.62 %) was highest followed by temperature (28.43 %) and load (9.36 %) for Wear.

The major results of carbon based composite coatings are:

1. FESEM+EDS, HRXED & Raman spectra confirms deposition of coating which exhibits typical semi-molten, molten and un-melted grains of composite particles along with formation of lamellae.
2. The experimental result shows that surface roughness value of carbon based composite coating (CC) was 0.345 μm .
3. The experimental result shows that micro-hardness value of carbon based composite coating (CC) before wear test exhibits 550 HV. The micro-hardness value of samples CC 1, CC 2 and CC 3 after wear test was 590, 620 and 650 HV. The experimental results of hardness for composite coating shows that as the test condition of temperature ranging from 150 to 350°C, load 50 N and sliding velocity 1 m/s respectively, increases hardness rapidly increases from 590 to 650 HV. The hardness was found to increase ~15% at test condition of 50N load, 1 m/s sliding velocity and 350°C temperature.
4. The experimental result shows that the residual stress developed on the carbon based composite coating (CC) before wear test exhibits -132 MPa. The residual stress value of samples CC 1, CC 2 and CC 3 after wear test was -91, -45 and -3 MPa. The experimental results of residual stress for composite coating shows that as the test condition of temperature ranging from 150 to 350°C, load 50 N and sliding velocity 1

m/s respectively, increases residual stress rapidly decreases from -91 to -3 HV. The residual stress was found to decreases ~97.7% at test condition of 50N load, 1 m/s sliding velocity and 350°C temperature.

5. The experimental result shows that the COF and wear values developed on the carbon based composite coating (CC) at idle conditions was 0.42 and 130 μm respectively. The COF value of samples CC 1, CC 2 and CC 3 was 0.38, 0.33 and 0.28 respectively, while wear values of samples CC 1, CC 2 and CC 3 was 90, 55 and 30 μm respectively. The tribological performance was evaluated using pin-on-disk tribometer which showed COF in the range of 0.28 to 0.38 as shown in fig. 5.15 (a-b), while fig. 5.15 (c) shows that wear was in the range of 30-90 μm , at test condition of temperature ranging from 150 to 350°C, load 50 N and sliding velocity 1 m/s respectively.
6. The tribological analysis of carbon based composite coating was done to evaluate the wear behavior for wear resistance applications. The tribological test showed 33.3% decrease in COF and 76.9% reduction in the wear at test condition of 1 m/s sliding velocity, 350°C temperature, and 50N load.
7. The percentage contribution of sliding velocity (74.76 %) was highest followed by load (12.85 %) and temperature (9.46 %) for COF.
8. The percentage contribution of sliding velocity (64.004 %) was highest followed by temperature (24.01 %) and load (10.94 %) for Wear.

Major Comparative analysis results:

1. The experimental results of COF for composite coating is almost 6.7% less than carbon coating at test condition of temperature ranging from 150 to 350°C, load 50 N and sliding velocity 1 m/s respectively.
2. The experimental results of wear for composite coating is almost 16-20% less than carbon coating at test condition of temperature ranging from 150 to 350°C, load 50 N and sliding velocity 1 m/s respectively.
3. The experimental results of micro-hardness for composite coating is almost 8-12% greater than carbon coating at test condition of temperature ranging from 150 to 350°C, load 50 N and sliding velocity 1 m/s respectively.
4. The experimental results of residual stress for composite coating is almost 14-25% less than carbon coating at test condition of temperature ranging from 150 to 350°C, load 50 N and sliding velocity 1 m/s respectively.

This chapter introduces scope for further research in carbon and carbon based composite coating.

As it is clear till now that surface modification using HVOF thermal spray technique is a vital to develop coating. There is a need to increase the scope of this process. There is a need to do lot of work in this field.

- Wear behavior of coatings on different work-piece pairs could be studied.
- Tribological studies of coating powder with different processing techniques can be studied.
- Tribological studies can be done at some other values of testing parameters like load, temperature and sliding speed.
- Cost-effectiveness analysis can be done for different types of coatings.
- Attempts can be made to estimate the useful life of these coated steels by extrapolation of the laboratory data by mathematical modeling.
- Attempts can be made to replace Piston ring materials with present research work material.

Appendix 1

Table 2.2 Deposition Parameters for CNT/DLC coating

Source	Coating Material**	Substrate*	Deposition Technique***	Deposition Parameters					
				Arc current (A)	Time (min.)	Additive layer	Clean/Treatment	Pressure (Pa)	Gas supply
Hentour <i>et al.</i> [39]	Carbon/Al ₂ O ₃ Coating	Stainless steel	Dip coating	-	25	-	N ₂	-	-
Ryu <i>et al.</i> [54]	CNTs (20nm)	Poly ethylene oxide	Spin coater	-	-	-	Si	-	-
Han <i>et al.</i> [38]	C-H film/carbon Nano hoops	Si/ stainless steel	MS	2-4	0.5-200	Ti/TiN/TiCN	N ₂ , methane	0.4-3.3	Ar
Arsaln <i>et al.</i> [41]	DLC	Steel	CFUBMS	20, 60	30, 90	Cr	Ar	-	Ar, C ₂ H ₄
Du <i>et al.</i> [44]	DLC/GLC	Ti6Al4V	CFUBMS	-	-	-	Ar	-	-
Dalibon <i>et al.</i> [75]	DLC	Stainless steel	PACVD	-	14h	-	N ₂ , H ₂	2mbar	HMDSO, C ₂ H ₂
Salah <i>et al.</i> [97]	DLC	Glass slide	PLD	-	-	Cu	-	-	-
Costa <i>et al.</i> [43]	DLC/TiN/CrN/WC	Ti6Al4V/ Al-bronze	PVD	-	7-10 h	Cr, Al ₂ O ₃	H ₂ O:HF:HNO ₃	21-41 kPa	-
Akbulut <i>et al.</i> [99]	Co-Ni/MWCNTs	Cu plate	ED	5A/dm ²	30	-	H ₂ O,HCl,HNO ₃	-	-

Ren <i>et al.</i> [60]	GLC	PEEK	M.S.	1.2	100	Si	Acetone, alcohol	2×10^{-3}	Ar ⁺
Bai <i>et al.</i> [67]	GLC	Ti6Al4V	M.S.	3	-	-	-	-	Ar, N ₂
Zheng <i>et al.</i> [45]	DLC	Ti6Al7Nb	Arc ion plating/M.S	0.2-1	15-30	-	Alcohol	4×10^{-3}	Ar
Hatem <i>et al.</i> [69]	DLC	Ti-6Al-4V	M.S.	100	120	SiC	Ar	1.3	-
Zou <i>et al.</i> [101]	Cr-DLC	Si and WC-Co	M.S./ Ion plating	20-40	80	-	Acetone methanol	4×10^{-4}	Ar, C ₂ H ₂
Praveen <i>et al.</i> [66]	CNTs	CNTs-Zn	ED	4A/ dm ²	-	-	H ₂ O, HCl	-	-
Muller <i>et al.</i> [84]	DLC	HSS	M.S.	-	-	Mo, W	HIPIMS ion	-	Ar, N ₂
Pillari <i>et al.</i> [77]	DLC	Mg alloy	RF sputtering	-	30	-	-	6.94* 10 ⁻² mbar	Ar
Stallard <i>et al.</i> [79]	DLC	Tool steel	M.S./ PECVD	-	-	Cr	Ar ⁺	-	Ar
Bayon <i>et al.</i> [103]	DLC	Ti6Al4V	Cathodic arc coating	60-140	-	Ti	Alkaline	10 ⁻⁶ mbar	Ar ⁺ , H
Niu <i>et al.</i> [57]	GLCH/ nitride	Ti6Al4V	MS	-	8h	Cr/WC/W	Acetone	0.2	C ₂ H ₂
Vitu <i>et al.</i> [82]	Zr- DLC	Ti alloy	M.S.	-	-	Ti/TiCN/Ti N	-	0.4	Ar, CH ₄
Wang <i>et al.</i> [337]	F-DLC	Ti6Al4V Alloy	HCPIII	0.5-0.9	20	Si ion	Ethanol, acetone, N ₂	1.5	Ar, CF ₄ , C ₂ H ₄
Rubig <i>et al.</i> [40]	DLC (45-55 μm)	Steel	PACVD	-	-	Si	-	-	Ar, C ₂ H ₄
Salvaro <i>et al.</i> [42]	Nitride+ DLC	Grey cast iron (GCI)	PECVD	-	25	Si	methane	-	-

Hatipoglu <i>et al.</i> [91]	MWCNTs	Ni	ED	0.30 mA/ cm ²	120	Ni	HCl, nitric acid	-	-
Aboua <i>et al.</i> [89]	DLC	High carbon steel	-	-	-	Metal	-	-	Methane
Penkov <i>et al.</i> [98]	DLC	Si	HEFID	0.02 mA/ cm ²	-	Ag	H ₂ O:H: HNO ₃	1*10 ⁻⁴	Cu
Li <i>et al.</i> [63]	Ti/ MWCNTs	Ti alloy	Laser Deposition	-	-	Ti	H ₂ O:HF: HNO ₃	-	Ar
Zhao <i>et al.</i> [94]	C:H film	Steel	PECVD	-	-	Cr	-	-	C ₂ H ₂
Banerji <i>et al.</i> [62]	DLC	Ti-6Al-4V	M.S.	-	-	Cr	Ar	2-5	N ₂
Wang <i>et al.</i> [68]	Cr/GLC	Si wafer/ stainless steel	M.S.	3	30	-	Acetone	0.4	Ar
Solis <i>et al.</i> [80]	WC/C:H	Steel	PECVD	-	-	Cr	Ar ⁺	-	Ar
Benedetti <i>et al.</i> [72]	DLC	42CrMo4V	PECVD	-	60	-	-	-	N+ Ar
Voevodin <i>et al.</i> [73]	DLC/ H- DLC	Ti/ TiC	M.S.	-	30	-	Ar	-	-
Shum <i>et al.</i> [65]	DLC	Steel	CFUBMS	-	-	Cr	-	2*10 ⁻⁶ Torr	-
Thirumala <i>et al.</i> [104]	DLC	Elastomer	PACVD	-	10-15	-	Soap solution, H ₂ O	2*10 ⁻³	Ar, C ₂ H ₂
Zhang <i>et al.</i> [86]	DLC	Stainless steel/ CoCrMo/ Ti6Al4V	FCVA	22	30	-	Acetone, alcohol	3*10 ⁻³	Ar
Li <i>et al.</i> [63]	DLC/ GLC/ CrN	Si wafer/ stainless steel	PVD	3	120	Cr	Acetone, alcohol	4*10 ⁻³	Ar, C ₂ H ₂

Feng <i>et al.</i> [102]	Ti/DLC	Steel	MS	2	30	Ti	Acetone, ethanol	$2 \cdot 10^{-3}$	Ar, CH ₄
Martinez <i>et al.</i> [106]	DLC	ACM rubber	PECVD	-	-	-	Ar, C ₂ H ₂ , H ₂	-	-
Pal <i>et al.</i> [105]	DLC	HNBR	P-CVD / CFUBMS	-	60-120	-	Detergent, boiling water, Ar, C ₂ H ₂ , H ₂	-	Ar, C ₂ H ₂
Aoki <i>et al.</i> [108]	DLC	Butyl rubber	RF-M.S.	-	-	-	Acetone	10	Ar, CH ₄
Martinez <i>et al.</i> [112]	H-DLC	NBR	VD with RF	-	3h	-	Ar ion	$3 \cdot 10^{-6}$ mbar	-
Schenkel <i>et al.</i> [90]	DLC	ACM rubber	PACVD	-	500ns		Detergent, Ar, C ₂ H ₂ , H ₂	-	Ar, C ₂ H ₂
Suresh Kannan, A. Ghosh [49]	DLC/MCD/N CD	Carbide	PVD/PACVD	-	-	Cr/CrN	Acetylene	-	CH ₄ , H ₂
K.-H. Dittrich, D. Oelsner [51]	DLC	Substrate	ARC-process	100	45	TiCN-C	-	0.1-0.3	He/N ₂ /C ₂ H ₂
Martinez <i>et al.</i> [120]	DLC	ACM rubber	PACVD	-	60-120	-	Detergent, boiling water, Ar, C ₂ H ₂ , H ₂	-	Ar, C ₂ H ₂
Masami <i>et al.</i> [88]	Si-DLC	Fluoro rubber	PBII	-	5	Si	Ethanol	1.2-3	TMS
Hirata <i>et al.</i> [46]	DLC	Trench-shaped pattern	PBII	-	-	-	-	0.4	Argon ion
Kang <i>et al.</i> [48]	DLC	Ti-6Al-4V ELI	FVA	-	80	TiCN	Ethanol, acetone	$1 \cdot 10^{-5}$	N ₄ , C ₂ H ₂

Wang <i>et al.</i> [122]	Ni-P-D	Mild steel	Electroless plating	-	90	-	alkaline solution	-	-
Xu <i>et al.</i> [123]	CVD diamond	Molybdenum	DC-Arc Plasma Jet method	-	180	-	Alcohol	-	CH ₄ , H ₂
Xiang <i>et al.</i> [124]	Diamond	Carbide	CVD	1.5	0.5 h	-	Acetone/ Hydrogen	1.79 kPa	-
Piazza [125]	ta-C:H films	PC	DECR plasma reactor	-	5	-	Ar	13.3- 146.6 mPa	C ₂ H ₂
Yehia <i>et al.</i> [126]	WC- TiC- Co/diamond	WC- TiC- Co	Electroless process	-	120	-	Acetone, NaOH	-	Formaldehyde
Chen <i>et al.</i> [127]	Diamond	Steel	-	-	210 s	Ni-Cr-P alloy	Acetone	6*10 ⁻⁴	-

Appendix 2

Table 2.3 Tribological conditions of carbon based coating materials

Source	Deposition Technique	Coating Material	Substrate	Tribo-meter	Experimental condition				
					Sliding speed (m/s)	Testing time (min.)	Load (N)	Temp. ($^{\circ}\text{C}$)	Sliding distance (m)
Wang <i>et al.</i> [37]	HCPIII	F-DLC	Ti6Al4V	Ball-on-disk	0.0016	60	5	37 \pm 2	-
Han <i>et al.</i> [38]	M. S.	C-H film /carbon Nano hoops	Si / stainless steel	Ball-on-disk	0.1414	-	3N/ 5mm	20	360
Hentour <i>et al.</i> [39]	Dip coating	Carbon/ Al ₂ O ₃ Coating	Stainless steel	Ball-on-disk	0.1	-	2	21-25	250
Ryu <i>et al.</i> [54]	Spin coater	CNTs	Poly ethylene oxide	Reciprocating	0.004	-	10 mN	-	-
Rubing <i>et al.</i> [41]	PACVD	DLC	Steel	Pin-on-disk	200	-	8	22	2000
Arsaln <i>et al.</i> [42]	M. S.	DLC	Steel	-	-	-	10	24 \pm 1	-
Salvaro <i>et al.</i> [43]	PECVD	Nitride+ DLC	Grey cast iron (GCI)	Reciprocating	-	-	80	60	0.01
Du <i>et al.</i> [44]	CFUBMS	DLC/ GLC	Ti6Al4V	Cyl./ Plane	-	-	200	24 \pm 1	-

Dalibon <i>et al.</i> [75]	PACVD	DLC	Stainless steel	Pin-on-disk	-	12	5 & 45	-	500
Hatipo-glu <i>et al.</i> [91]	ED	MWCNTs	Ni	Ball-on-disk	0.1-0.3	-	1	-	-
Lee <i>et al.</i> [95]	Spin/ Electro less coating	CNTs/ Ag	Silicon wafer	reciprocating	0.002	600 cycle	0-30 mN	24	-
Umeda <i>et al.</i> [92]	-	MWCNTs	Ti plate	Ball-on-disk	9.8	50	0.031	-	113
Aboua <i>et al.</i> [89]	-	DLC	High carbon steel	Pin-on-disk	0.1	60	5	-	405
Sinha <i>et al.</i> [94]	Dip coating	UHMWPE/ SWCNT	Steel	Ball-on-disk	0.41	-	4	25±2	-
Sinha <i>et al.</i> [96]	FCVA	UHMWPE/ SWCNT	Steel	Plate-on-cyl.	0.11	-	60	28	25000
Tas <i>et al.</i> [76]	-	DLC	Grey cast iron	Reciprocating sliding	0.15	-	0-600	-	-
Salah <i>et al.</i> [97]	PLD	DLC	Glass slide	Ball-on-disk	0.16	-	3	25±2	4
Penkov <i>et al.</i> [98]	HEFIBD	DLC	Si	reciprocating	0.001	-	400 mN	24	2
Costa <i>et al.</i> [43]	PVD	DLC/ TiN/ CrN/WC	Ti6Al4V/Al- bronze	Pin-on-disk	0.5	-	5	-	3000

Li <i>et al.</i> [93]	Laser Deposition	Ti/ MW CNTs	Ti alloy	Ball-on-disk	764 rpm	60	10	500	2.5
Akbulut <i>et al.</i> [99]	ED	Co-Ni/ MWCNTs	Cu plate	Ball-on-disk	0.005-0.015	-	1	-	1000
Zhao <i>et al.</i> [61]	PECVD	C:H film	Steel	Pin-on-disk	120 rpm	-	500	-	10
Wan <i>et al.</i> [58]	Arc ion plating	CrN/ GLC	Steel	Ball-on-disk	5 mm/ min	-	0-100	25	0.005
Ren <i>et al.</i> [60]	M.S.	GLC	PEEK	Pin-on-plate	0.1	120	3	23±2	-
Zheng <i>et al.</i> [45]	Arc ion plating/M.S.	DLC	Ti6Al7Nb	Flat-on-ball	-	-	10 & 50	23	-
Bai <i>et al.</i> [67]	M.S.	GLC	Ti6Al4V	Ball-on-disk	0.1	-	1 & 3	-	-
Banerji <i>et al.</i> [62]	M.S.	DLC	Ti6Al4V	Pin-on-disk	0.12	-	5	25	-
Hatem <i>et al.</i> [69]	PIID/ PEMS	DLC	Ti6Al4V	Universal	0.1	30	10	-	10
Praveen <i>et al.</i> [66]	ED	CNTs	CNTs-Zn	-	-	-	-	-	-
Zou <i>et al.</i> [83]	M.S./Ion plating	Cr-DLC	Si and WC-Co	Ball-on-disk	0.2	-	10	-	-
Wang <i>et al.</i> [68]	M.S.	Cr/GLC	Si wafer/ stainless steel	Ball-on-disk	-	30	5	20±2	-

Pagnoux <i>et al.</i> [70]	PSA	DLC	Steel	-	0.024	-	70	25	-
Mobarak <i>et al.</i> [71]	Ion beam	DLC	Stainless steel	Four ball	1200 rpm	3600	392.4	100	-
Muller <i>et al.</i> [84]	M.S.	DLC	HSS	Pin-on-disk	0.1	-	1 and 2	26	1000
Solis <i>et al.</i> [80]	PECVD	WC/C:H	Steel	Pin-on-plate	0.1	6 hr.	10-50	20±2	-
Pillari <i>et al.</i> [77]	RF sputtering	DLC	Mg alloy	-	-	-	-	-	-
Benedetti <i>et al.</i> [72]	PECVD	DLC	42CrMo4V	-	-	140 hr.	-	-	2000 km
Madej <i>et al.</i> [101]	PVD	C:H/ DLC	Steel	Ball-on-disk	0.1	-	10	22±2	1000
Stallard <i>et al.</i> [79]	M.S./ PECVD	DLC	Tool steel	Pin-on-disk	0.05	-	10, 40, 80	20±5	720
Sharma <i>et al.</i> [78]	PECVD	DLC	Steel	Ball-on-disk	0.02	-	1, 4, 8	-	-
Voevodin <i>et al.</i> [73]	M.S.	DLC/ H- DLC	Ti/ TiC	Ball-on-disk	0.2	-	0.1, 0.2, 0.5	-	0.06
Bayon <i>et al.</i> [103]	Cathodic arc coating	DLC	Ti6Al4V	Ball-on-disk	0.063	20	5	-	-
Shum <i>et al.</i> [65]	M.S.	DLC	Steel	Reciprocated slider	0.005	200	70	-	-

Niu <i>et al.</i> [57]	DCMS	GLCH/ nitride	Ti6Al4V	Reciprocated slider	0.02	-	60	25	-
Thirumala <i>et al.</i> [104]	PACVD	DLC	Elastomer	Ball-on-disk	0.01	-	1	25	-
Akaike <i>et al.</i> [85]	PECVD	F-DLC/ Si-DLC	Stainless steel	-	-	-	-	-	-
Vitu <i>et al.</i> [82]	M.S.	Zr- DLC	Ti alloy	Pin-on-disk	0.15	1000/ 5000/ 30000 Cycle	5	25	-
Zhang <i>et al.</i> [81]	FCVA/ PIID/ PEVCD	H-DLC	CoCrMo	Ball-on-disk	0.025	50000 cycle	2	-	6
Zhang <i>et al.</i> [86]	FCVA	DLC	Stainless steel/ CoCrMo Ti6Al4V	Ball-on-disk	0.021	150, 000 cycle	2	-	5
Morita <i>et al.</i> [87]	M.S.	DLC	Steel	Ball-on-disk	0.04	-	29.4	-	450
Li <i>et al.</i> [63]	PVD	DLC/ GLC/ CrN	Si wafer/ stainless steel	Reciprocating	0.02	60	5-50	22±2	5
Ye <i>et al.</i> [64]	M.S.	Cr/ GLC	Si wafer	Ball-on-disk	-	30	10	20±2	5
Feng <i>et al.</i> [102]	MFMS	Ti/DLC	Steel	Ball-on-disk	0.055	30	20	25	5
Pal <i>et al.</i> [105]	P-CVD / M.S.	DLC	HNBR	Ball-on-disk	-	-	1	23±2	10000 laps

Martinez <i>et al.</i> [106]	PECVD	DLC	ACM rubber	Ball-on-disk	0.1	-	-	-	10000 laps
Bui <i>et al.</i> [109]	M.S.	Ti-DLC	HNBR	Ball-on-disk	0.1	-	1 & 3	20	-
Aoki <i>et al.</i> [108]	RF-M.S.	DLC	Butyl rubber	Ball-on-disk	0.1	-	0.5-5	-	-
Bui <i>et al.</i> [109]	M.S.	H-DLC	HNBR	Ball-on-disk	0.1	-	1 & 3	23	10000 laps
Lubwama <i>et al.</i> [110]	M.S.	DLC/ Si-DLC	Acrylo NBR rubber	Pin-on-disk	0.1	-	5	23±2	-
Pei <i>et al.</i> [111]	M.S.	W-DLC	FKM, ACM, HNBR	Ball-on-disk	0.1	-	1, 3 and 5	20	10000 laps
Martinez <i>et al.</i> [112]	VD with RF	H-DLC	NBR	reciprocating	0.010, 0.101, 0.0058	60, 120, 300	10 & 40	23±2	225, 387, 3870, 9675
Lubwama <i>et al.</i> [113]	M.S./ PECVD	DLC/ Si-DLC	Nitrile rubber	Pin-on-disk	0.1	-	1 & 5	23±2	-
Lubwama <i>et al.</i> [114]	M.S./ PECVD	DLC/ Si-DLC	Nitrile rubber	Pin-on-disk	0.1	-	1 & 5	-	5000 revolution
Pei <i>et al.</i> [116]	M.S./ p-CVD	DLC	HNBR	Ball-on-disk	0.1	-	1	20	10000 laps
Pei <i>et al.</i> [115]	PACVD	DLC	HNBR	Ball-on-disk	0.1	-	1, 3, 5	20-23	10000 laps

Pei <i>et al.</i> [117]	M.S.	W-DLC	Fluoro carbon/ HNBR	Ball-on-disk	0.1	-	1	20	10000 laps
Pei <i>et al.</i> [118]	p-CVD	DLC	HNBR	Ball-on-disk	0.1	-	1	20	10000 laps
Martinez <i>et al.</i> [119]	PACVD	DLC	ACM rubber	Ball-on-disk	0.2	-	1	20	10000 laps
Martinez <i>et al.</i> [120]	PACVD	DLC	ACM rubber	Ball-on-disk	0.2	-	1	-	10000 laps
Ikeyema <i>et al.</i> [88]	PBIII	Si-DLC	Fluoro rubber	Reciprocating	0.01	10	0.49	25	300 laps
Pei <i>et al.</i> [121]	M.S.	DLC	HNBR	Ball-on-disk	0.1	-	1, 3	20-22	10000 laps
Schenkel <i>et al.</i> [90]	PACVD	DLC	ACM Rubber	Ball-on-disk	0.1, 0.2, 0.4	-	1, 3	20	10000 laps
Pei <i>et al.</i> [100]	ETP-CVD	C:H film	NBR rubber	Ball-on-disk	0.1	-	1, 3	20-23	10000 laps
Nakahigashi <i>et al.</i> [59]	RF p-CVD	H-DLC	Rubber	-	0.1	-	0.5	-	1000 laps
Kang <i>et al.</i> [48]	FVA	DLC	Ti-6Al-4V ELI	Pin-on-disk	150 rpm	-	20	-	-
Suresh Kannan, A. Ghosh [49]	PVD/ PACVD	DLC/MCD/NC D	Carbide	Pin-on-disk	5	-	10	-	-

Meerkamm <i>et al.</i> [53]	PVD/ PACVD	DLC	Metal/Plastic	Pin-on-disk	10	-	10	23±1	1000
Wang <i>et al.</i> [122]	Electro-less plating	Ni-P-D	Mild steel	-	300 rpm	15	4.9		-

Appendix 3

Table 2.6 Deposition parameters of HVOF based coating

Source	Coating Material	Substrate	Deposition Technique	Deposition Parameters									
				Pressure (Pa)	Clean/Treatment	Additive layer	Carrier gas	Gas supply	Flow rate fuel	Powder feed rate	Spraying distance	Coating thickness	Powder size
158	WC-25WB-10Co-5NiCr, MoB-25NiCr	stainless steel, uncoated AISI 410 steel substrate	HVOF		Acetone	16Cr 5Ni	Oxygen		23(l/h)	95	350		45 ± 15 µm
159	10wt %diamond-bronze(ball and disc setup)	AISI 52100 bearing steel	HVOF	80psi	ultrasonically vibrated isopropyl alcohol solution	25 wt% alumina		O ₂ ,N ₂	50	40g/min	100 mm		30 ± 5 µm

160	WC-10%Ni and WC- 20%Cr3C2– 7% Ni	Stainless steel 1Cr18Ni9Ti	HVOF		alumina grits			O2	0.3 , L·min ⁻¹	70	380	350 ± 20 μm	15–40 μm
161	CrC- NiCrFeSiBCo C(35-65%) ,CrC- NiCrFeSiBCo C(80-20%)	SS316 steel	HVOF	6 kg/cm ² (fu el),9(o)		Cr, C		LPG oxygen		38 gm/min			20± 4 μm
162	Nickel (95%)- Aluminum (5%)	304 stainless	HVOF		Alumin a and ethanol. .			Nitro gen, oxygen					
163	Ni	mild and 316 AISI 1008 mild steel	HVOF			16Cr 5Ni		Oxyg en		23 g/min		(< 25 μm)	
164	WC- 10Co4Cr	304 stainless steel	HVOF and HVOGF(sigle model)		ultrason ic bath with acetone and Al2O3		oxyg en		56 m3 /h oxygen flux, 22.7 L/h	75 g/min	370 mm	450± 20 μm.	1.4–1.6 μm

									kerosene flux				
165	WC- 10Co4Cr	304 stainless steel	HVOF and HVOGF(Multi model)		ultrason ic bath with acetone and Al2O3		oxyg en		100 L/min oxygen flux, 33 L/min propane flux,	45 g/min	240 mm	450± 20 µm.	2.2–2.5
166	(WC-10Ni)	Carbon steel AISI 1040	HVOF				C2H2 Ar N2		30, 45 and 60 L.p.m (liquid per minute			45 ± 11 mm	
167	WC- 10Co4Cr	304 stainless steel substrates	HVOF(2 different fuel),		60 mesh Al2O3,act one				56.6 m3 /h oxygen, 22.7 L/h kerosene	75 g/min	370 mm	450 µm.	0.08– 0.18 µm nano
168	Ni20Cr	ASTM - SA213 -T24 boiler steel.	HVOF		1 mm Al 2 O 3		H2/O 2		35L/m in		250mm	260 ± 20 µm	

169	WC-10Co-4Cr	AISI 304 stainless steel	HVOF		alumina				f 22 lph, oxygen, kerosene flow rate of 22 lph	90 g/min	13 in		20–70 μm
170	WC-CoCr	martensitic stainless steel	HVOF	0.5-1 Mpa	acetone	Cu-Sn, SiC-graphite			Oxygen(950 L/min, Kerosene 24 L/h		380mm		70 μm
171	CoNiCrAlY	Inconel 718	HVOF	2.5 bar	ultrasonic cleaning		N2 (6,5 slpm)	N2	15- 20 slpm	20 g/min	200 mm	98 \pm 8 μm	-37+ 5 μm
172	WC-CoCr	low carbon steel (S355)	HVOF	13-11 bar	grit-blasted			Hydrogen and oxygen	Nitrogen-32 slpm,oxygen-770 to 960 Kerosene-14,16,18 $\cdot\text{h}^{-1}$	1 m/s	200 mm		5–25 μm

173	Stellite 6	low carbon steel	GTAW hot-wire cladding And HVOF		Alumina, Acetone			Nitrogen, oxygen, carbon dioxide		250 mm/s	380 mm		38–45 μm
174	Silicon (Si), Chromium Carbide (Cr_3C_2), Boron (B), Nickel (Ni) and Chromium (Cr)	Inconel 718 (Ni based)	HVOF	, Hydrogen pressure = 8 kgf/cm ² , Oxygen pressure = 12 kgf/cm ² ,	Alumina powder (grit 45)	Silicon (Si), Chromium Carbide (Cr_3C_2), Boron (B), Nickel (Ni), and Chromium (Cr)		Nitrogen, oxygen	Hydrogen flow rate = 55 l/min, Oxygen flow rate = 30 l/min	80 g/min,	20 cm	150–200 μm	
175	WC - 10Co4Cr	316L stainless steel	HVOF		Al ₂ O ₃ , 60 mesh (250 μm)		Kerosene and nitrogen		Oxygen = 845 ml·min ⁻¹ , Kerosene = 480 ml·min ⁻¹	11.9 g·min ⁻¹	300 mm		

176	Ni-20%Cr and Cr ₃ C ₂ - 25%NiCr	iron- based superalloy A-286	HVOF	Oxygen: 11 kg/cm ² Hydrogen pressure: 8 kg/cm ²	alumina				14 lpm	30 g/min	20 cm		64 μm(Ni- 20%Cr) 43 μm(Cr ₃ C ₂ - 25%NiCr)
177	Ni-20Cr ₂ O ₃	Mild steel, SS 202 steel, and SS 304 steel	HVOF	Oxygen: 6900 LMP Fuel (LPG): 70	alumina					25 g/min	120 mm		-30 μm
178	ZrB ₂ -SiC- MoSi ₂ /Mo	C/Si substrate	HVOF	O=200 L min ⁻¹ H =600 L min ⁻¹	alumina	Mo			600 L min ⁻¹		300mm		70 μm
179	WC-25WB- 10Co-5NiCr and MoB- 25NiCr	16Cr5Ni low carbon martensitic stainless steels	HVOF	O=55 L min ⁻¹	Al ₂ O ₃				23(l/h)	95 g/min	350 mm		-45 to +15 μm
180	WC- Co/NiCrAlYSi (80-20%),WC-	SS316		O=250 LPM					LPG 60 LPM	38 gm/min	200MM		-45 to +15 μm

	Co/NiCrAlYSi (35–65%),												
181	Ni-20Cr	n SA 516 boiler steels	HVOF	O =260 slpm	Al ₂ O ₃ and toulene			oxyge n	LPG 60 slpm	35-40 g/min	150mm		74 μm
182	Cr ₃ C ₂ – 50NiCrMoNb	carbon steel substrates (S235)	HVOF	383 slpm		Cr ₃ C 2		oxyge n	Propan e=70 slpm	60 g/min	230 mm	5 mm	-45 + 15
183	y Ni ₂₁ Cr, Ni ₅ Al, and Ni ₂₁ Cr ₇ AlY	low carbon steel	HAVF	Air=0.8 MPa	Al ₂ O ₃ and toulene			Air	Propan e=0.70 MPa	150g/mi n	300mm	250	

1. Szeri, A.Z. and Rohde, S.M., 1981. Tribology: friction, lubrication, and wear.
2. Bayindir, K.Ç., Gözükcük, M.A. and Teke, A., 2011. A comprehensive overview of hybrid electric vehicle: Powertrain configurations, powertrain control techniques and electronic control units. *Energy conversion and Management*, 52(2), pp.1305-1313.
3. Colton, W.M., 2011. The Outlook for Energy: A View to 2040. Exxon Mobil Corporation.
4. Abdel-Rahman, A.A., 1998. On the emissions from internal-combustion engines: a review. *International Journal of Energy Research*, 22(6), pp.483-513.
5. Roberts, A., Brooks, R. and Shipway, P., 2014. Internal combustion engine cold-start efficiency: A review of the problem, causes and potential solutions. *Energy Conversion and Management*, 82, pp.327-350.
6. Demirbas, A., 2009. Political, economic and environmental impacts of biofuels: A review. *Applied energy*, 86, pp.S108-S117.
7. Enomoto, Y., Furuhashi, S. and Minakami, K., 1985. Heat loss to combustion chamber wall of 4-Stroke gasoline engine: 1st report, heat loss to piston and cylinder. *Bulletin of JSME*, 28(238), pp.647-655.
8. Rahnejat, H., 2010. Tribology and dynamics of engine and powertrain: Fundamentals. applications and future trends.
9. Richardson, D.E., 2000. Review of power cylinder friction for diesel engines. *J. Eng. Gas Turbines Power*, 122(4), pp.506-519.
10. Nevshupa, R., Conte, M., Del Campo, A. and Roman, E., 2016. Analysis of tribochemical decomposition of two imidazolium ionic liquids on Ti-6Al-4V through mechanically stimulated gas emission spectrometry. *Tribology International*, 102, pp.19-27.
11. Profito, F.J., Tomanik, E. and Zachariadis, D.C., 2016. Effect of cylinder liner wear on the mixed lubrication regime of TLOCs. *Tribology International*, 93, pp.723-732.
12. Zavos, A.B. and Nikolakopoulos, P.G., 2015. Simulation of piston ring tribology with surface texturing for internal combustion engines. *Lubrication Science*, 27(3), pp.151-176.
13. Igartua, A., Nevshupa, R., Fernandez, X., Conte, M., Zabala, R., Bernaola, J., Zabala, P., Luther, R. and Rausch, J., 2011. Alternative eco-friendly lubes for clean two-stroke engines. *Tribology International*, 44(6), pp.727-736.

14. Bell, J.C., 1998. Gasoline engine valve train design evolution and the antiwear requirements of motor oils. *Proceedings of the Institution of Mechanical Engineers, Part J: Journal of Engineering Tribology*, 212(4), pp.243-257.
15. Tung, S.C. and Gao, H., 2003. Tribological characteristics and surface interaction between piston ring coatings and a blend of energy-conserving oils and ethanol fuels. *Wear*, 255(7-12), pp.1276-1285.
16. Coy, R.C., 1997. Practical applications of lubrication models in engines. *Mechanical Engineering Publications Ltd.(UK)*, pp.197-209.
17. Tomanik, E., Profito, F.J. and Zachariadis, D.C., 2013. Modelling the hydrodynamic support of cylinder bore and piston rings with laser textured surfaces. *Tribology international*, 59, pp.90-96.
18. Liu, Z., Meng, X., Wen, C., Yu, S. and Zhou, Z., 2019. On the oil-gas-solid mixed bearing between compression ring and cylinder liner under starved lubrication and high boundary pressures. *Tribology International*, 140, p.105869.
19. Saidur, R., Rezaei, M., Muzammil, W.K., Hassan, M.H., Paria, S. and Hasanuzzaman, M., 2012. Technologies to recover exhaust heat from internal combustion engines. *Renewable and sustainable energy reviews*, 16(8), pp.5649-5659.
20. He, M., Zhang, X., Zeng, K. and Gao, K., 2011. A combined thermodynamic cycle used for waste heat recovery of internal combustion engine. *Energy*, 36(12), pp.6821-6829.
21. Morris, N., Mohammadpour, M., Rahmani, R., Johns-Rahnejat, P.M., Rahnejat, H. and Dowson, D., 2018. Effect of cylinder deactivation on tribological performance of piston compression ring and connecting rod bearing. *Tribology International*, 120, pp.243-254.
22. Roensch, M.M., 1940. Piston-ring coatings and their effect on ring and bore wear. *SAE Transactions*, pp.221-228.
23. Jackson, J.E., 1941. Wear-resistant coatings of diesel cylinder liners (No. 410085). *SAE Technical Paper*.
24. Tyagi, A., Walia, R.S., Murtaza, Q., Pandey, S.M., Tyagi, P.K. and Bajaj, B., 2019. A critical review of diamond like carbon coating for wear resistance applications. *International journal of refractory metals and hard materials*, 78, pp.107-122.
25. Davis, J.R. ed., 2004. *Handbook of thermal spray technology*. ASM international.
26. WWW.mecpl.com, ©2007-2019, Metallizing Equipment Co. Pvt. Ltd. All Right Reserved

27. https://www.google.com/url?sa=i&url=http%3A%2F%2Ffab.cba.mit.edu%2Fclasses%2F961.04%2Fprojects%2FRegXuProj%2FMasProjII.htm&psig=AOvVaw2_yjW-ytG9qnqgus8uYkez&ust=1651387930944000&source=images&cd=vfe&ved=0CAwQjRxqFwoTCMj59cuZu_cCFQAAAAAdAAAAABAr
28. <https://www.gordonengland.co.uk/coldspray.htm>
29. SM Pandey, RS Walia and Qasim Murtaza, “Synthesis and Characterization of Some Coating Used for Piston Ring Application”, Delhi Technological University, PhD Thesis.
30. A. (Alfons) Fischer, K. Bobzin, Friction, wear and wear protection : International Symposium on Friction, Wear and Wear Protection 2008, Aachen, Germany, Wiley-VCH, 2009.
31. https://www.google.com/url?sa=i&url=https%3A%2F%2Fwww.researchgate.net%2Ffigure%2FAdhesive-wear-mechanism-a-before-contact-b-during-contact-c-after-contact-2_fig1_339090448&psig=AOvVaw1ZZWi paVLCdr4lg2T59WK&ust=1651388829784000&source=images&cd=vfe&ved=0CAwQjRxqFwoTCLC-_v6cu_cCFQAAAAAdAAAAABAD
32. R.C.D.Richardson, The maximum hardness of strained surfaces and the abrasive wear of metals and alloys, *Wear*. 10 (1967) 353–382.
33. https://www.google.com/url?sa=i&url=https%3A%2F%2Fwww.substech.com%2Fdo kuwiki%2Fdoku.php%3Fid%3Dmechanisms_of_wear&psig=AOvVaw0hMceSZ6ae6 LsV2yh3qWRT&ust=1651389161068000&source=images&cd=vfe&ved=0CAwQjRxqFwoTCPjg7Zaeu_cCFQAAAAAdAAAAABAD
34. W.A. Glaeser, *Characterization of Tribological Materials*, Second Edition, Momentum Press, 2012.
35. Du, L., Huang, C., Zhang, W., Li, T. and Liu, W., 2011. Preparation and wear performance of NiCr/Cr₃C₂–NiCr/hBN plasma sprayed composite coating. *Surface and Coatings Technology*, 205(12), pp.3722-3728.
36. Joseph Stokes, “Theory and application of the Sulzer Metco HVOF (High Velocity Oxy-Fuel) Thermal spray process”, ISBN 1-87232-753-2, ISSN 1649-8232.
37. Wang, J., Ma, J., Huang, W., Wang, L., He, H. and Liu, C., 2017. The investigation of the structures and tribological properties of F-DLC coatings deposited on Ti-6Al-4V alloys. *Surface and Coatings Technology*, 316, pp.22-29.

38. Han, X., Zheng, J., Hao, J. and Zhang, S., 2017. The microstructure, mechanical and tribological properties of aC: H films with self-assembled carbon nanohoops. *Surface and Coatings Technology*, 311, pp.27-34.
39. Hentour, K., Marsal, A., Turq, V., Weibel, A., Ansart, F., Sobrino, J.M., Chen, Y.M., Garcia, J., Cardey, P.F. and Laurent, C., 2016. Carbon nanotube/alumina and graphite/alumina composite coatings on stainless steel for tribological applications. *Materials Today Communications*, 8, pp.118-126.
40. Rübzig, B., Heim, D., Forsich, C., Dipolt, C., Mueller, T., Gebeshuber, A., Kullmer, R., Holecek, R., Lugmair, C., Krawinkler, M. and Strobl, V., 2017. Tribological behavior of thick DLC coatings under lubricated conditions. *Surface and coatings technology*, 314, pp.13-17.
41. Arslan, A., Masjuki, H.H., Kalam, M.A., Varman, M., Mosarof, M.H., Mufti, R.A., Quazi, M.M., Khuong, L.S., Liaqat, M., Jamshaid, M. and Alabdulkarem, A., 2017. Investigation of laser texture density and diameter on the tribological behavior of hydrogenated DLC coating with line contact configuration. *Surface and Coatings Technology*, 322, pp.31-37.
42. Salvaro, D.B., Giacomelli, R.O., Binder, R., Binder, C., Klein, A.N. and de Mello, J.D.B., 2017. Assessment of a multifunctional tribological coating (nitride+ DLC) deposited on grey cast iron in a mixed lubrication regime. *Wear*, 376, pp.803-812.
43. Costa, M.Y.P., Cioffi, M.O.H., Voorwald, H.J.C. and Guimaraes, V.A., 2010. An investigation on sliding wear behavior of PVD coatings. *Tribology International*, 43(11), pp.2196-2202.
44. Du, D., Liu, D., Ye, Z., Zhang, X., Li, F., Zhou, Z. and Yu, L., 2014. Fretting wear and fretting fatigue behaviors of diamond-like carbon and graphite-like carbon films deposited on Ti-6Al-4V alloy. *Applied surface science*, 313, pp.462-469.
45. Zheng, X.Y., Zhang, Y.R. and Zhang, B.R., 2017. Effect of N-ion implantation and diamond-like carbon coating on fretting wear behaviors of Ti6Al7Nb in artificial saliva. *Transactions of Nonferrous Metals Society of China*, 27(5), pp.1071-1080.
46. Hirata, Y., Kato, T. and Choi, J., 2015. DLC coating on a trench-shaped target by bipolar PBII. *International Journal of Refractory Metals and Hard Materials*, 49, pp.392-399.
47. Sung, J.C., Kan, M.C. and Sung, M., 2007. Fluorinated DLC for tribological applications. *International Journal of Surface Science and Engineering*, 1(4), pp.429-440.

48. Kang, S., Lim, H.P. and Lee, K., 2015. Effects of TiCN interlayer on bonding characteristics and mechanical properties of DLC-coated Ti-6Al-4V ELI alloy. *International Journal of Refractory Metals and Hard Materials*, 53, pp.13-16.
49. Kannan, I.S. and Ghosh, A., 2017. Impact of intra-bond orbital hybridization and morphology of diamond coatings on machining performance of coated end mill cutters. *International Journal of Refractory Metals and Hard Materials*, 68, pp.130-141.
50. Charitidis, C.A., 2010. Nanomechanical and nanotribological properties of carbon-based thin films: a review. *International Journal of Refractory Metals and Hard Materials*, 28(1), pp.51-70.
51. Dittrich, K.H. and Oelsner, D., 2002. Production and characterization of dry lubricant coatings for tools on the base of carbon. *International Journal of Refractory Metals and Hard Materials*, 20(2), pp.121-127.
52. Editorial, Superhard materials, 2002. *Journal of Refractory Metals and Hard Materials*, 20:91-92.
53. Meerkamm, H., Fruth, W., Krumpiegl, T. and Schaufler, C., 1999. Mechanical and tribological properties of PVD and PACVD wear resistant coatings. *International Journal of Refractory Metals and Hard Materials*, 17(1-3), pp.201-208.
54. Ryu, B.H., Barthel, A.J., Kim, H.J., Lee, H.D., Penkov, O.V., Kim, S.H. and Kim, D.E., 2014. Tribological properties of carbon nanotube–polyethylene oxide composite coatings. *Composites science and technology*, 101, pp.102-109.
55. Moghadam, A.D., Omrani, E., Menezes, P.L. and Rohatgi, P.K., 2015. Mechanical and tribological properties of self-lubricating metal matrix nanocomposites reinforced by carbon nanotubes (CNTs) and graphene—a review. *Composites Part B: Engineering*, 77, pp.402-420.
56. Al-Kawaz, A., Rubin, A., Badi, N., Blanck, C., Jacomine, L., Janowska, I., Pham-Huu, C. and Gauthier, C., 2016. Tribological and mechanical investigation of acrylic-based nanocomposite coatings reinforced with PMMA-grafted-MWCNT. *Materials Chemistry and Physics*, 175, pp.206-214.
57. Niu, R., Li, J., Wang, Y., Chen, J. and Xue, Q., 2016. Structure and tribological behavior of GLCH/nitride coupled coatings on Ti6Al4V by nitriding and magnetron sputtering. *Diamond and Related Materials*, 64, pp.70-79.
58. Wan, S., Pu, J., Li, D., Zhang, B. and Tieu, A.K., 2017. Tribological performance of CrN and CrN/GLC coated components for automotive engine applications. *Journal of Alloys and Compounds*, 695, pp.433-442.

59. Nakahigashi, T., Tanaka, Y., Miyake, K. and Oohara, H., 2004. Properties of flexible DLC film deposited by amplitude-modulated RF P-CVD. *Tribology International*, 37(11-12), pp.907-912.
60. Ren, S., Huang, J., Cui, M., Pu, J. and Wang, L., 2017. Improved adaptability of polyaryl-ether-ether-ketone with texture pattern and graphite-like carbon film for bio-tribological applications. *Applied Surface Science*, 400, pp.24-37.
61. Zhao, R., Steiner, J., Andreas, K., Merklein, M. and Tremmel, S., 2018. Investigation of tribological behaviour of aC: H coatings for dry deep drawing of aluminium alloys. *Tribology International*, 118, pp.484-490.
62. Banerji, A., Bhowmick, S. and Alpas, A.T., 2014. High temperature tribological behavior of W containing diamond-like carbon (DLC) coating against titanium alloys. *Surface and Coatings Technology*, 241, pp.93-104.
63. Li, Z., Guan, X., Wang, Y., Li, J., Cheng, X., Lu, X., Wang, L. and Xue, Q., 2017. Comparative study on the load carrying capacities of DLC, GLC and CrN coatings under sliding-friction condition in different environments. *Surface and Coatings Technology*, 321, pp.350-357.
64. Ye, Y., Wang, C., Wang, Y., Zhao, W., Li, J. and Yao, Y., 2015. A novel strategy to enhance the tribological properties of Cr/GLC films in seawater by surface texturing. *Surface and Coatings Technology*, 280, pp.338-346.
65. Shum, P.W., Zhou, Z.F. and Li, K.Y., 2013. Investigation of the tribological properties of the different textured DLC coatings under reciprocating lubricated conditions. *Tribology International*, 65, pp.259-264.
66. Praveen, B.M., Venkatesha, T.V., Naik, Y.A. and Prashantha, K., 2007. Corrosion studies of carbon nanotubes–Zn composite coating. *Surface and Coatings Technology*, 201(12), pp.5836-5842.
67. Bai, W.Q., Xie, Y.J., Li, L.L., Wang, X.L., Gu, C.D. and Tu, J.P., 2017. Tribological and corrosion behaviors of Zr-doped graphite-like carbon nanostructured coatings on Ti6Al4V alloy. *Surface and Coatings Technology*, 320, pp.235-239.
68. Wang, C., Ye, Y., Guan, X., Hu, J., Wang, Y. and Li, J., 2016. An analysis of tribological performance on Cr/GLC film coupling with Si₃N₄, SiC, WC, Al₂O₃ and ZrO₂ in seawater. *Tribology International*, 96, pp.77-86.
69. Hatem, A., Lin, J., Wei, R., Torres, R.D., Laurindo, C. and Soares, P., 2017. Tribocorrosion behavior of DLC-coated Ti-6Al-4V alloy deposited by PIID and

- PEMS+ PIID techniques for biomedical applications. *Surface and Coatings Technology*, 332, pp.223-232.
70. Pagnoux, G., Fouvry, S., Peigney, M., Delattre, B. and Mermaz-Rollet, G., 2015. Influence of scratches on the wear behavior of DLC coatings. *Wear*, 330, pp.380-389.
71. Mobarak, H.M., Masjuki, H.H., Mohamad, E.N., Rahman, S.A., Al Mahmud, K.A.H., Habibullah, M. and Salauddin, S., 2014. Effect of DLC coating on tribological behavior of cylinder liner-piston ring material combination when lubricated with *Jatropha* oil. *Procedia Engineering*, 90, pp.733-739.
72. Benedetti, M., Fontanari, V., Torresani, E., Girardi, C. and Giordanino, L., 2017. Investigation of lubricated rolling sliding behaviour of WC/C, WC/C-CrN, DLC based coatings and plasma nitriding of steel for possible use in worm gearing. *Wear*, 378, pp.106-113.
73. Voevodin, A.A., Walck, S.D. and Zabinski, J.S., 1997. Architecture of multilayer nanocomposite coatings with super-hard diamond-like carbon layers for wear protection at high contact loads. *Wear*, 203, pp.516-527.
74. Robertson, J., 2002. Diamond-like amorphous carbon. *Materials science and engineering: R: Reports*, 37(4-6), pp.129-281.
75. Dalibón, E.L., Escalada, L., Simison, S., Forsich, C., Heim, D. and Brühl, S.P., 2017. Mechanical and corrosion behavior of thick and soft DLC coatings. *Surface and Coatings Technology*, 312, pp.101-109.
76. Tas, M.O., Banerji, A., Lou, M., Lukitsch, M.J. and Alpas, A.T., 2017. Roles of mirror-like surface finish and DLC coated piston rings on increasing scuffing resistance of cast iron cylinder liners. *Wear*, 376, pp.1558-1569.
77. Pillari, L.K., Umasankar, V., Sarma, A. and Gupta, M., 2017. DLC coating of magnesium nanocomposites using RF sputtering. *Materials Today: Proceedings*, 4(6), pp.6737-6742.
78. Sharma, N., Kumar, N., Dash, S., Das, C.R., Rao, R.S., Tyagi, A.K. and Raj, B., 2012. Scratch resistance and tribological properties of DLC coatings under dry and lubrication conditions. *Tribology International*, 56, pp.129-140.
79. Stallard, J., Mercs, D., Jarratt, M., Teer, D.G. and Shipway, P.H., 2004. A study of the tribological behaviour of three carbon-based coatings, tested in air, water and oil environments at high loads. *Surface and Coatings Technology*, 177, pp.545-551.

80. Solis, J., Zhao, H., Wang, C., Verduzco, J.A., Bueno, A.S. and Neville, A., 2016. Tribological performance of an H-DLC coating prepared by PECVD. *Applied Surface Science*, 383, pp.222-232.
81. Zhang, T.F., Xie, D., Huang, N. and Leng, Y., 2017. The effect of hydrogen on the tribological behavior of diamond like carbon (DLC) coatings sliding against Al₂O₃ in water environment. *Surface and coatings technology*, 320, pp.619-623.
82. Vitu, T., Escudeiro, A., Polcar, T. and Cavaleiro, A., 2014. Sliding properties of Zr-DLC coatings: The effect of tribolayer formation. *Surface and Coatings Technology*, 258, pp.734-745.
83. Zou, C.W., Wang, H.J., Feng, L. and Xue, S.W., 2013. Effects of Cr concentrations on the microstructure, hardness, and temperature-dependent tribological properties of Cr-DLC coatings. *Applied Surface Science*, 286, pp.137-141.
84. Müller, I.C., Sharp, J., Rainforth, W.M., Hovsepian, P. and Ehiasarian, A., 2017. Tribological response and characterization of Mo–W doped DLC coating. *Wear*, 376, pp.1622-1629.
85. Akaike, S., Kobayashi, D., Aono, Y., Hiratsuka, M., Hirata, A., Hayakawa, T. and Nakamura, Y., 2016. Relationship between static friction and surface wettability of orthodontic brackets coated with diamond-like carbon (DLC), fluorine-or silicone-doped DLC coatings. *Diamond and Related Materials*, 61, pp.109-114.
86. Zhang, T.F., Deng, Q.Y., Liu, B., Wu, B.J., Jing, F.J., Leng, Y.X. and Huang, N., 2015. Wear and corrosion properties of diamond like carbon (DLC) coating on stainless steel, CoCrMo and Ti6Al4V substrates. *Surface and Coatings Technology*, 273, pp.12-19.
87. Morita, T., Inoue, K., Ding, X., Usui, Y. and Ikenaga, M., 2016. Effect of hybrid surface treatment composed of nitriding and DLC coating on friction-wear properties and fatigue strength of alloy steel. *Materials Science and Engineering: A*, 661, pp.105-114.
88. Masami, I., Haruho, M., Tatsuya, M. and Junho, C., 2011. Low temperature Si-DLC coatings on fluoro rubber by a bipolar pulse type PBII system. *Surface and Coatings Technology*, 206(5), pp.999-1002.
89. Aboua, K.A.M., Umehara, N., Kousaka, H., Deng, X., Tasdemir, H.A., Mabuchi, Y., Higuchi, T. and Kawaguchi, M., 2017. Effect of carbon diffusion on friction and wear properties of diamond-like carbon in boundary base oil lubrication. *Tribology International*, 113, pp.389-398.

90. Schenkel, M., Martinez-Martinez, D., Pei, Y.T. and De Hosson, J.T.M., 2011. Tribological performance of DLC films deposited on ACM rubber by PACVD. *Surface and Coatings Technology*, 205(20), pp.4838-4843.
91. Hatipoglu, G., Kartal, M., Uysal, M., Cetinkaya, T. and Akbulut, H., 2016. The effect of sliding speed on the wear behavior of pulse electro Co-deposited Ni/MWCNT nanocomposite coatings. *Tribology International*, 98, pp.59-73.
92. Umeda, J., Fugetsu, B., Nishida, E., Miyaji, H. and Kondoh, K., 2015. Friction behavior of network-structured CNT coating on pure titanium plate. *Applied Surface Science*, 357, pp.721-727.
93. Li, Q.H., Savalani, M.M., Zhang, Q.M. and Huo, L., 2014. High temperature wear characteristics of TiC composite coatings formed by laser cladding with CNT additives. *Surface and Coatings Technology*, 239, pp.206-211.
94. Samad, M.A. and Sinha, S.K., 2011. Effects of counterface material and UV radiation on the tribological performance of a UHMWPE/CNT nanocomposite coating on steel substrates. *Wear*, 271(11-12), pp.2759-2765.
95. Lee, H.D., Penkov, O.V. and Kim, D.E., 2013. Tribological behavior of dual-layer electroless-plated Ag–carbon nanotube coatings. *Thin Solid Films*, 534, pp.410-416.
96. Samad, M.A. and Sinha, S.K., 2011. Dry sliding and boundary lubrication performance of a UHMWPE/CNTs nanocomposite coating on steel substrates at elevated temperatures. *Wear*, 270(5-6), pp.395-402.
97. Salah, N., Alshahrie, A., Iqbal, J., Hasan, P.M.Z. and Abdel-Wahab, M.S., 2016. Tribological behavior of diamond-like carbon thin films deposited by the pulse laser technique at different substrate temperatures. *Tribology International*, 103, pp.274-280.
98. Penkov, O.V., Pukha, V.E., Zubarev, E.N., Yoo, S.S. and Kim, D.E., 2013. Tribological properties of nanostructured DLC coatings deposited by C60 ion beam. *Tribology International*, 60, pp.127-135.
99. Karslioglu, R. and Akbulut, H., 2015. Comparison microstructure and sliding wear properties of nickel–cobalt/CNT composite coatings by DC, PC and PRC current electrodeposition. *Applied Surface Science*, 353, pp.615-627.
100. Pei, Y.T., Eivani, A.R., Zaharia, T., Kazantzis, A.V., van De Sanden, M.C.M. and De Hosson, J.T.M., 2014. High throughput deposition of hydrogenated amorphous carbon coatings on rubber with expanding thermal plasma. *Surface and Coatings Technology*, 245, pp.74-83.

101. Madej, M., 2014. The effect of TiN and CrN interlayers on the tribological behavior of DLC coatings. *Wear*, 317(1-2), pp.179-187.
102. Feng, X. and Xia, Y., 2012. Tribological properties of Ti-doped DLC coatings under ionic liquids lubricated conditions. *Applied surface science*, 258(7), pp.2433-2438.
103. Bayón, R., Igartua, A., González, J.J. and De Gopegui, U.R., 2015. Influence of the carbon content on the corrosion and tribocorrosion performance of Ti-DLC coatings for biomedical alloys. *Tribology international*, 88, pp.115-125.
104. Thirumalai, S., Hausberger, A., Lackner, J.M., Waldhauser, W. and Schwarz, T., 2016. Effect of the type of elastomeric substrate on the microstructural, surface and tribological characteristics of diamond-like carbon (DLC) coatings. *Surface and Coatings Technology*, 302, pp.244-254.
105. Van Der Pal, J.P., Martinez-Martinez, D., Pei, Y.T., Rudolf, P. and De Hosson, J.T.M., 2012. Microstructure and tribological performance of diamond-like carbon films deposited on hydrogenated rubber. *Thin Solid Films*, 524, pp.218-223.
106. Martinez-Martinez, D., Van der Pal, J.P., Schenkel, M., Shaha, K.P., Pei, Y.T. and De Hosson, J.T.M., 2012. On the nature of the coefficient of friction of diamond-like carbon films deposited on rubber. *Journal of Applied Physics*, 111(11), p.114902.
107. Bui, X.L., Pei, Y.T. and De Hosson, J.T.M., 2008. Magnetron reactively sputtered Ti-DLC coatings on HNBR rubber: The influence of substrate bias. *Surface and Coatings Technology*, 202(20), pp.4939-4944.
108. Aoki, Y. and Ohtake, N., 2004. Tribological properties of segment-structured diamond-like carbon films. *Tribology International*, 37(11-12), pp.941-947.
109. Bui, X.L., Pei, Y.T., Mulder, E.D.G. and De Hosson, J.T.M., 2009. Adhesion improvement of hydrogenated diamond-like carbon thin films by pre-deposition plasma treatment of rubber substrate. *Surface and Coatings Technology*, 203(14), pp.1964-1970.
110. Lubwama, M., Corcoran, B., Sayers, K., Kirabira, J.B., Sebbit, A., McDonnell, K.A. and Dowling, D., 2012. Adhesion and composite micro-hardness of DLC and Si-DLC films deposited on nitrile rubber. *Surface and Coatings Technology*, 206(23), pp.4881-4886.
111. Pei, Y.T., Bui, X.L., Zhou, X.B. and De Hosson, J.T.M., 2008. Microstructure and tribological behavior of tungsten-containing diamondlike carbon coated

- rubbers. *Journal of Vacuum Science & Technology A: Vacuum, Surfaces, and Films*, 26(4), pp.1085-1092.
112. Martinez, L., Nevshupa, R., Alvarez, L., Huttel, Y., Mendez, J., Roman, E., Mozas, E., Valdes, J.R., Jimenez, M.A., Gachon, Y. and Heau, C., 2009. Application of diamond-like carbon coatings to elastomers frictional surfaces. *Tribology International*, 42(4), pp.584-590.
 113. Lubwama, M., Corcoran, B., McDonnell, K.A., Dowling, D., Kirabira, J.B., Sebbit, A. and Sayers, K., 2014. Flexibility and frictional behaviour of DLC and Si-DLC films deposited on nitrile rubber. *Surface and Coatings Technology*, 239, pp.84-94.
 114. Lubwama, M., McDonnell, K.A., Kirabira, J.B., Sebbit, A., Sayers, K., Dowling, D. and Corcoran, B., 2012. Characteristics and tribological performance of DLC and Si-DLC films deposited on nitrile rubber. *Surface and Coatings Technology*, 206(22), pp.4585-4593.
 115. Pei, Y.T., Bui, X.L., Van der Pal, J.P., Martinez-Martinez, D. and De Hosson, J.T.M., 2013. Flexible diamond-like carbon film coated on rubber. *Progress in Organic Coatings*, 76(12), pp.1773-1778.
 116. Pei, Y.T., Bui, X.L., Zhou, X.B. and De Hosson, J.T.M., 2008. Tribological behavior of W-DLC coated rubber seals. *Surface and Coatings Technology*, 202(9), pp.1869-1875.
 117. Pei, Y.T., Bui, X.L. and De Hosson, J.T.M., 2010. Flexible protective diamond-like carbon film on rubber. *Scripta Materialia*, 63(6), pp.649-652.
 118. Pei, Y.T., Martinez-Martinez, D., Van Der Pal, J.P., Bui, X.L., Zhou, X.B. and De Hosson, J.T.M., 2012. Flexible diamond-like carbon films on rubber: Friction and the effect of viscoelastic deformation of rubber substrates. *Acta materialia*, 60(20), pp.7216-7225.
 119. Martinez-Martinez, D., Van Der Pal, J.P., Pei, Y.T. and De Hosson, J.T.M., 2011. Performance of diamond-like carbon-protected rubber under cyclic friction. I. Influence of substrate viscoelasticity on the depth evolution. *Journal of Applied Physics*, 110(12), p.124906.
 120. Martinez-Martinez, D., Schenkel, M., Pei, Y.T. and De Hosson, J.T.M., 2011. Microstructural and frictional control of diamond-like carbon films deposited on acrylic rubber by plasma assisted chemical vapor deposition. *Thin Solid Films*, 519(7), pp.2213-2217.

121. Pei, Y.T., Bui, X.L. and De Hosson, J.T.M., 2010. Deposition and characterization of hydrogenated diamond-like carbon thin films on rubber seals. *Thin Solid Films*, 518(21), pp.S42-S45.
122. Wang, J., Zhang, F.L., Zhang, T., Liu, W.G., Li, W.X. and Zhou, Y.M., 2018. Preparation of Ni-P-diamond coatings with dry friction characteristics and abrasive wear resistance. *International Journal of Refractory Metals and Hard Materials*, 70, pp.32-38.
123. Xu, H., Zang, J., Tian, P., Wang, Y., Yu, Y., Lu, J., Xu, X. and Zhang, P., 2018. Rapid grinding CVD diamond films using corundum grinding wheels containing iron. *International Journal of Refractory Metals and Hard Materials*, 71, pp.147-152.
124. Xiang, D., Feng, H., Guo, Z., Zhang, L. and Wu, B., 2018. Preparation technology and properties of microtexture diamond-coated tools. *International Journal of Refractory Metals and Hard Materials*, 76, pp.16-24.
125. Piazza, F., 2006. Hard-hydrogenated tetrahedral amorphous carbon films by distributed electron cyclotron resonance plasma. *International Journal of Refractory Metals and Hard Materials*, 24(1-2), pp.39-48.
126. Yehia, H.M., El-Kady, O. and Abu-Oqail, A., 2018. Effect of diamond additions on the microstructure, physical and mechanical properties of WC-TiC-Co/Ni Nanocomposite. *International Journal of Refractory Metals and Hard Materials*, 71, pp.198-205.
127. Chen, J., Mu, D., Liao, X., Huang, G., Huang, H., Xu, X. and Huang, H., 2018. Interfacial microstructure and mechanical properties of synthetic diamond brazed by Ni-Cr-P filler alloy. *International Journal of Refractory Metals and Hard Materials*, 74, pp.52-60.
128. Tyagi, A., Pandey, S.M., Murtaza, Q., Walia, R.S. and Tyagi, M., 2020. Tribological behavior of carbon coating for piston ring applications using Taguchi approach. *Materials Today: Proceedings*, 25, pp.759-764.
129. Tyagi, A., Pandey, S.M., Gupta, K., Walia, R.S., Murtaza, Q. and Krishen, K., 2019. Tribological behavior of sustainable carbon based composite coating for wear resistance applications. *Materials Research Express*, 6(12), p.125601..
130. Zabala, B., Igartua, A., Fernández, X., Priestner, C., Ofner, H., Knaus, O., Abramczuk, M., Tribotte, P., Girot, F., Roman, E. and Nevshupa, R., 2017. Friction and wear of a piston ring/cylinder liner at the top dead centre: Experimental study and modelling. *Tribology International*, 106, pp.23-33.

131. Agüero, A., Camón, F., García de Blas, J., Del Hoyo, J.C., Muelas, R., Santaballa, A., Ulargui, S. and Vallés, P., 2011. HVOF-deposited WCCoCr as replacement for hard Cr in landing gear actuators. *Journal of thermal spray technology*, 20(6), pp.1292-1309.
132. Peng, Y., Xu, Y., Geng, J., Dearn, K.D. and Hu, X., 2017. Tribological assessment of coated piston ring-cylinder liner contacts under bio-oil lubricated conditions. *Tribology International*, 107, pp.283-293.
133. Yao, Z. and Qian, Z., 2018. Thermal analysis of nano ceramic coated piston used in natural gas engine. *Journal of Alloys and Compounds*, 768, pp.441-450.
134. Yao, Z. and Li, W., 2020. Microstructure and thermal analysis of APS nano PYSZ coated aluminum alloy piston. *Journal of Alloys and Compounds*, 812, p.152162.
135. Dolatabadi, N., Forder, M., Morris, N., Rahmani, R., Rahnejat, H. and Howell-Smith, S., 2020. Influence of advanced cylinder coatings on vehicular fuel economy and emissions in piston compression ring conjunction. *Applied Energy*, 259, p.114129.
136. Bhosale, D.G., Rathod, W.S. and Rukhande, S.W., 2019. Sliding wear behavior of high velocity oxy-fuel sprayed WC-Cr₃C₂-Ni coating for automotive applications. *Materials Today: Proceedings*, 19, pp.339-343.
137. Picas, J.A., Forn, A. and Matthäus, G., 2006. HVOF coatings as an alternative to hard chrome for pistons and valves. *Wear*, 261(5-6), pp.477-484.
138. Tyagi, A., Pandey, S.M., Walia, R.S. and Murtaza, Q., 2019. Characterization and parametric optimization of tribological properties of Mo blend composite coating. *Materials Research Express*, 6(8), p.086428.
139. Bolelli, G., Berger, L.M., Börner, T., Koivuluoto, H., Lusvarghi, L., Lyphout, C., Markocsan, N., Matikainen, V., Nylén, P., Sassatelli, P. and Trache, R., 2015. Tribology of HVOF-and HVOF-sprayed WC-10Co4Cr hardmetal coatings: A comparative assessment. *Surface and Coatings Technology*, 265, pp.125-144.
140. Lee, C.W., Han, J.H., Yoon, J., Shin, M.C. and Kwun, S.I., 2010. A study on powder mixing for high fracture toughness and wear resistance of WC-Co-Cr coatings sprayed by HVOF. *Surface and coatings technology*, 204(14), pp.2223-2229.
141. Keshavamurthy, R., Sudhan, J.M., Kumar, A., Ranjan, V., Singh, P. and Singh, A., 2018. Wear behaviour of hard chrome and tungsten carbide-HVOF coatings. *Materials Today: Proceedings*, 5(11), pp.24587-24594.

142. Ramesh, C.S., Adarsha, H., Chaturvedi, A. and Nair, N., 2018. Investigations on the effect of molybdenum (Mo) and molybdenum silicon carbide (Mo-10% Sic) composite coatings on mild steel substrate using HVOF technique. *Materials Today: Proceedings*, 5(11), pp.24422-24427.
143. Pandey, S.M., Murtaza, Q. and Walia, R.S., 2018. Effect of NiCr on dry sliding wear of high carbon iron-molybdenum composite plasma spray coating. *International Journal of precision Technology*, 8(1), pp.1-23.
144. Picas, J.A., Punset, M., Teresa Baile, M., Martín, E. and Forn, A., 2011. Tribological evaluation of HVOF thermal-spray coatings as a hard chrome replacement. *Surface and interface analysis*, 43(10), pp.1346-1353.
145. Zhao, L., Maurer, M., Fischer, F., Dicks, R. and Lugscheider, E., 2004. Influence of spray parameters on the particle in-flight properties and the properties of HVOF coating of WC-CoCr. *Wear*, 257(1-2), pp.41-46.
146. Bolelli, G., Colella, A., Lusvarghi, L., Puddu, P., Rigon, R., Sassatelli, P. and Testa, V., 2019. Properties of HVOF-sprayed TiC-FeCrAl coatings. *Wear*, 418, pp.36-51.
147. Dave, D.P., Chauhan, K.V., Chavda, M.R. and Rawal, S.K., 2016. Study of tribological behavior for chromium based coatings deposited on conventional materials. *Procedia Technology*, 23, pp.91-97.
148. Wang, T. and Ye, F., 2018. The elevated-temperature wear behavior evolution of HVOF sprayed tungsten carbide coatings: Respond to heat treatment. *International Journal of Refractory Metals and Hard Materials*, 71, pp.92-100.
149. Venkatesh, L., Venkataraman, B., Tak, M., Sivakumar, G., Gundakaram, R.C., Joshi, S.V. and Samajdar, I., 2019. Room temperature and 600° C erosion behaviour of various chromium carbide composite coatings. *Wear*, 422, pp.44-53.
150. Gong, T., Yao, P., Zuo, X., Zhang, Z., Xiao, Y., Zhao, L., Zhou, H., Deng, M., Wang, Q. and Zhong, A., 2016. Influence of WC carbide particle size on the microstructure and abrasive wear behavior of WC-10Co-4Cr coatings for aircraft landing gear. *Wear*, 362, pp.135-145.
151. Venkateswarlu, K., Rajinikanth, V., Naveen, T., Sinha, D.P. and Ray, A.K., 2009. Abrasive wear behavior of thermally sprayed diamond reinforced composite coating deposited with both oxy-acetylene and HVOF techniques. *Wear*, 266(9-10), pp.995-1002.

152. Federici, M., Menapace, C., Moscatelli, A., Gialanella, S. and Straffelini, G., 2017. Pin-on-disc study of a friction material dry sliding against HVOF coated discs at room temperature and 300 C. *Tribology International*, 115, pp.89-99.
153. Zhang, W.C., Liu, L.B., Zhang, M.T., Huang, G.X., Liang, J.S., Xian, L.I. and Zhang, L.G., 2015. Comparison between WC–10Co–4Cr and Cr₃C₂–25NiCr coatings sprayed on H13 steel by HVOF. *Transactions of nonferrous metals society of china*, 25(11), pp.3700-3707.
154. Thiruvikraman, C., Balasubramanian, V. and Sridhar, K., 2014. Optimizing HVOF spray parameters to maximize bonding strength of WC-CrC-Ni coatings on AISI 304L stainless steel. *Journal of thermal spray technology*, 23(5), pp.860-875.
155. Żórawski, W. and Skrzypek, S.J., 2013. Tribological properties of plasma and HVOF-sprayed NiCrBSi–Fe₂O₃ composite coatings. *Surface and Coatings Technology*, 220, pp.282-289.
156. Pulsford, J., Venturi, F., Pala, Z., Kamnis, S. and Hussain, T., 2019. Application of HVOF WC-Co-Cr coatings on the internal surface of small cylinders: Effect of internal diameter on the wear resistance. *Wear*, 432, p.202965.
157. Das, P., Paul, S. and Bandyopadhyay, P.P., 2019. Tribological behaviour of HVOF sprayed diamond reinforced bronze coatings. *Diamond and Related Materials*, 93, pp.16-25.
158. Bolelli, G., Lusvarghi, L., Varis, T., Turunen, E., Leoni, M., Scardi, P., Azanza-Ricardo, C.L. and Barletta, M., 2008. Residual stresses in HVOF-sprayed ceramic coatings. *Surface and Coatings Technology*, 202(19), pp.4810-4819.
159. Du, J., Zhang, J., Xu, J. and Zhang, C., 2020. Cavitation-corrosion behaviors of HVOF sprayed WC-25WB-10Co-5NiCr and MoB-25NiCr coatings. *Ceramics International*, 46(13), pp.21707-21718.
160. Das, P., Paul, S. and Bandyopadhyay, P.P., 2019. Tribological behaviour of HVOF sprayed diamond reinforced bronze coatings. *Diamond and Related Materials*, 93, pp.16-25.
161. Hong, S., Wu, Y., Wu, J., Zheng, Y., Zhang, Y., Cheng, J., Li, J. and Lin, J., 2020. Effect of flow velocity on cavitation erosion behavior of HVOF sprayed WC-10Ni and WC-20Cr₃C₂–7Ni coatings. *International Journal of Refractory Metals and Hard Materials*, 92, p.105330.
162. Navinesh, B.C., Somasundaram, B. and Mamatha, M.P., 2020. Better wear resistance of HVOF coating CrC-NiCrFeSiBCoC (35%–65%) and CrC-

- NiCrFeSiBCoC (80%–20%) on SS316 steels. *Materials Today: Proceedings*, 20, pp.155-160.
163. Yeh, C.H., Jeyaprakash, N. and Yang, C.H., 2020. Temperature dependent elastic modulus of HVOF sprayed Ni-5% Al on 304 stainless steel using nondestructive laser ultrasound technique. *Surface and Coatings Technology*, 385, p.125404.
 164. Abbas, M., Smith, G.M. and Munroe, P.R., 2020. Microstructural evolution and bonding of HVOF sprayed Ni particles on both mild and stainless-steel substrates. *Surface and Coatings Technology*, 394, p.125909.
 165. Huang, Y., Ding, X., Yuan, C.Q., Yu, Z.K. and Ding, Z.X., 2020. Slurry erosion behaviour and mechanism of HVOF sprayed micro-nano structured WC-CoCr coatings in NaCl medium. *Tribology International*, 148, p.106315.
 166. Najib, A.Z.P., Kamdi, Z., Patar, M.A.A., Hatta, M.N.M., Yunus, M.Z. and Ainuddin, A.R., 2020. Corrosion behaviour of WC-Ni high velocity oxy-fuel (HVOF) coating with the influence of spraying parameter. *Materials Today: Proceedings*, 29, pp.100-103.
 167. Lin, J., Wei, R., Bitsis, D.C. and Lee, P.M., 2016. Development and evaluation of low friction TiSiCN nanocomposite coatings for piston ring applications. *Surface and Coatings Technology*, 298, pp.121-131.
 168. Ding, X., Huang, Y., Yuan, C. and Ding, Z., 2020. Deposition and cavitation erosion behavior of multimodal WC-10Co4Cr coatings sprayed by HVOF. *Surface and Coatings Technology*, 392, p.125757
 169. Abu-Warda, N., López, A.J., López, M.D. and Utrilla, M.V., 2020. Ni20Cr coating on T24 steel pipes by HVOF thermal spray for high temperature protection. *Surface and Coatings Technology*, 381, p.125133.
 170. Thakur, L. and Arora, N., 2020. An investigation on the development and wear performance of chromium-MWCNTs transformed HVOF sprayed nano-WC-CoCr coatings. *Surface and Coatings Technology*, 388, p.125610.
 171. Jayashree, P., Turani, S. and Straffelini, G., 2020. Dry sliding behavior of HVOF WC-CoCr coated counterface against Cu-Sn and SiC-graphite composite materials. *Surface and Coatings Technology*, 397, p.125977.
 172. Karaoglanli, A.C., Ozgurluk, Y. and Doleker, K.M., 2020. Comparison of microstructure and oxidation behavior of CoNiCrAlY coatings produced by APS, SSAPS, D-gun, HVOF and CGDS techniques. *Vacuum*, 180, p.109609.

173. Varis, T., Suhonen, T., Jokipii, M. and Vuoristo, P., 2020. Influence of powder properties on residual stresses formed in high-pressure liquid fuel HVOF sprayed WC-CoCr coatings. *Surface and Coatings Technology*, 388, p.125604.
174. Lima, C.R.C., Belém, M.J.X., Fals, H.D.C. and Della Rovere, C.A., 2020. Wear and corrosion performance of Stellite 6® coatings applied by HVOF spraying and GTAW hotwire cladding. *Journal of Materials Processing Technology*, 284, p.116734.
175. Shankar, R., Balasubramanian, K.R., Sivapirakasam, S.P. and Ravikumar, K., 2021. ANN and RSM models approach for optimization of HVOF coating. *Materials Today: Proceedings*, 46, pp.9201-9206.
176. Tian, Y., Zhang, H., Chen, X., McDonald, A., Wu, S., Xiao, T. and Li, H., 2020. Effect of cavitation on corrosion behavior of HVOF-sprayed WC-10Co4Cr coating with post-sealing in artificial seawater. *Surface and Coatings Technology*, 397, p.126012.
177. Muthu, S.M. and Arivarasu, M., 2020. Investigations of hot corrosion resistance of HVOF coated Fe based superalloy A-286 in simulated gas turbine environment. *Engineering Failure Analysis*, 107, p.104224.
178. Bansal, A., Goyal, D.K., Singh, P., Singla, A.K., Gupta, M.K., Bala, N., Kolte, J. and Setia, G., 2020. Erosive wear behaviour of HVOF-sprayed Ni-20Cr2O3 coating on pipeline materials. *International Journal of Refractory Metals and Hard Materials*, 92, p.105332.
179. Cheng, S., Geng, L., Liu, X. and Wang, Y., 2020. Laser ablation behavior and mechanism of C/SiC coated with ZrB₂-MoSi₂-SiC/Mo prepared by HVOF. *Ceramics International*, 46(11), pp.17752-17762.
180. Du, J., Zhang, J., Xu, J. and Zhang, C., 2020. Cavitation-corrosion behaviors of HVOF sprayed WC-25WB-10Co-5NiCr and MoB-25NiCr coatings. *Ceramics International*, 46(13), pp.21707-21718.
181. Somasundaram, B., Navinsh, B.C. and Mamatha, M.P., 2020. Wear behavior of HVOF sprayed WC-Co/NiCrAlYSi (35–65%) and WC-Co/NiCrAlYSi (80–20%) coatings on turbine SS316 steel. *Materials Today: Proceedings*, 20, pp.103-107.
182. Kumar, M., Singh, H. and Singh, N., 2020. Effect of increase in nano-particle addition on mechanical and microstructural behaviour of HVOF and cold-spray Ni-20Cr coatings on boiler steels. *Materials Today: Proceedings*, 21, pp.2035-2042.

183. Matikainen, V., Koivuluoto, H. and Vuoristo, P., 2020. A study of Cr₃C₂-based HVOF-and HVAF-sprayed coatings: abrasion, dry particle erosion and cavitation erosion resistance. *Wear*, 446, p.203188.
184. Tyagi, A., Chourasia, S., Murtaza, Q. and Walia, R.S., 2021. Evaluation of tribological, oxidation and corrosion behavior of HVOF sprayed sustainable temperature-dependent carbon coating. *Surface Topography: Metrology and Properties*, 9(4), p.045024.
185. Tyagi, A., Walia, R.S. and Murtaza, Q., 2019. Tribological behavior of temperature dependent environment friendly thermal CVD diamond coating. *Diamond and Related Materials*, 96, pp.148-159.
186. Manninen, N.K., Ribeiro, F., Escudeiro, A., Polcar, T., Carvalho, S. and Cavaleiro, A., 2013. Influence of Ag content on mechanical and tribological behavior of DLC coatings. *Surface and Coatings Technology*, 232, pp.440-446.
187. Casiraghi, C.F.A.R.J., Ferrari, A.C. and Robertson, J., 2005. Raman spectroscopy of hydrogenated amorphous carbons. *Physical review B*, 72(8), p.085401.
188. Matikainen, V., Koivuluoto, H., Vuoristo, P., Schubert, J. and Houdková, Š., 2018. Effect of nozzle geometry on the microstructure and properties of HVAF-sprayed WC-10Co4Cr and Cr₃C₂-25NiCr coatings. *Journal of Thermal Spray Technology*, 27(4), pp.680-694.
189. Hong, W.U., Lan, X.D., Yong, L.I.U., Fei, L.I., Zhang, W.D., Chen, Z.J., Zai, X.F. and Han, Z.E.N.G., 2016. Fabrication, tribological and corrosion behaviors of detonation gun sprayed Fe-based metallic glass coating. *Transactions of Nonferrous Metals Society of China*, 26(6), pp.1629-1637.
190. Tyagi, A., Walia, R.S. and Murtaza, Q., 2019. Tribological behavior of HVOF carbon coating for wear resistance applications. *Materials Research Express*, 6(12), p.125606.
191. Skordaris, G., Bouzakis, K.D., Charalampous, P., Kotsanis, T., Bouzakis, E. and Lemmer, O., 2016. Effect of structure and residual stresses of diamond coated cemented carbide tools on the film adhesion and developed wear mechanisms in milling. *CIRP Annals*, 65(1), pp.101-104.
192. Biberger, J. and Füller, H.J., 2017. Development of a test method for a realistic, single parameter-dependent analysis of piston ring versus cylinder liner contacts with a rotational tribometer. *Tribology International*, 113, pp.111-124.

193. Tyagi, A., Murtaza, Q. and Walia, R.S., 2021. Residual, Corrosion & Tribological Behavior of HVOF Sprayed Sustainable Temperature-Dependent Carbon-Based Hybrid Composite Coating. *Strojniski Vestnik/Journal of Mechanical Engineering*, 67(4).

RESEARCH PUBLICATIONS

International Journal

1. Ankit Tyagi, R S Walia, Qasim Murtaza, "Tribological behavior of HVOF carbon coating for wear resistance applications" Materials Research Express, Volume 6, Number 12. (SCI, IP 1.6).
2. Ankit Tyagi, R S Walia, Qasim Murtaza, "Residual, Corrosion & Tribological behavior of HVOF sprayed sustainable temperature dependent carbon based hybrid composite coating", Strojniški vestnik - Journal of Mechanical Engineering, 67(2021)4, 191-199 (SCI, IP 1.55)
3. Ankit Tyagi, RS Walia, Qasim Murtaza, "Evaluation of the residual stress of HVOF sprayed carbon coating after wear testing conditions using ANN coupled Taguchi approach", Surface Topography: Metrology and Properties 9 (3), 035027, (SCI, IP 2.03)
4. Ankit Tyagi, Shubhangi Chourasia, RS Walia, Qasim Murtaza, "Evaluation of Tribological, Oxidation and corrosion behavior of HVOF sprayed sustainable temperature-dependent carbon coating", Surface Topography: Metrology and Properties, 9 (2021) 045024 (SCI, IP 2.03).
5. Ankit Tyagi, RS Walia, Qasim Murtaza, Shailesh M. Pandey, Pawan K. Tyagi, Bharat Bajaj, 2018, "A critical review of Diamond like Carbon Coating for Wear Resistance Applications", International Journal of Refractory Metals and Hard Materials, 78 (2019) 107–122, (SCI, IP- 3.87).
6. Ankit Tyagi, Shailesh Mani Pandey, R.S. Walia, Qasim Murtaza, 2019, "Characterization and parametric optimization of tribological properties of Mo blend composite coating", Material Research Express, 6 (2019) 086428 (SCI, IP 1.6).
7. Ankit Tyagi, S M Pandey, Kalpana Gupta, R.S. Walia, Qasim Murtaza, Kumar Krishen, "Tribological behavior of sustainable Carbon based Composite coating for wear resistance applications" Materials Research Express, Volume 6, Number 12. (SCI, IP 1.6).
8. Ankit Tyagi, S M Pandey, R S Walia, Qasim Murtaza, "Characterization and parametric optimization of % change in residual stress of Mo composite coating using Taguchi approach" Materials Research Express, 6 (2019) 125623 (SCI, IP 1.6).
9. Ankit Tyagi, SM Pandey, Qasim Murtaza, R.S. Walia, Mohit Tyagi, "Tribological behavior of carbon coating for piston ring applications using Taguchi approach", Materials today proceeding, 759-764, Volume 25, Part 4, 2020.
10. Ankit Tyagi, SM Pandey, Qasim Murtaza, R.S. Walia, "Effect of temperature on the sliding wear behavior of HVOF sprayed Al₂O₃ composite coating", Advances in Materials and Mechanical Engineering, Lecture Notes in Mechanical engineering, ISBN 978-981-16-0673-1.

11. Ankit Tyagi, Jitendra Raj, Shubhangi Chourasia, SL Meena, SM Pandey, Qasim Murtaza, R.S. Walia, and Ajay Kumar, “Effect of sliding velocity on the wear behavior of HVOF sprayed Al₂O₃ coating”, Journal of Physics: Conference Series 1950 (2021) 012008.
12. Ankit Tyagi, Shubhangi Chourasia, Keshav Vats, Qasim Murtaza, R S Walia, Vikas Dhawan,” Tribological behavior of HVOF based Composite coatings for wear resistance applications”, Materials today proceeding, (Accepted In Press, Corrected Proof).

Conferences

1. Ankit Tyagi, SM Pandey, Qasim Murtaza, R.S. Walia, Mohit Tyagi, “Effect of temperature on the sliding wear behavior of HVOF sprayed Al₂O₃ composite coating”, 1st International Conference on Future Trends in Materials and Mechanical Engineering (ICFTMME)-2020
2. Ankit Tyagi, Qasim Murtaza, RS Walia, ““Effect of Reciprocating Frequency and Load on Wear Behaviour of Mo blend Composite Coating”, International conference of advance research and innovation (ICARI 2019), ISBN-978-93-5346-324-3
3. Ankit Tyagi, Qasim Murtaza, RS Walia, “Effect of high temperature (550⁰C) on tribological properties of Eco-friendly carbon based composite coating for piston ring application” International Thermal Spray Conference and Exposition - ITSC 2019 in Yokohama, Japan
4. Ankit Tyagi, SM Pandey, Qasim Murtaza, R.S. Walia, Mohit Tyagi, Tribological behavior of carbon coating for piston ring applications using Taguchi approach, 2nd International Conference on Computational & Experimental Methods in Mechanical Engineering (ICCEMME-2019).
5. Ankit Tyagi, S M Pandey, Qasim Murtaza, R.S. Walia, Effect of temperature on Mo-C blend Composite Coating for piston ring applications, 1st National conference on advances in Mechanical Engineering (NCAME)-2019